Universität Zürich
Medizinische Fakultät

Zentrum für Klinische Forschung (ZKF) / Center for Clinical Research (CCR)
Clinical Trials Center (CTC)

Program

15th Day of Clinical Research

Georg-Friedrich-Götz-Preisverleihung 2016

Zurich, March 31, 2016

UniversitätsSpital Zürich

Universität Zürich[UZH]

Assoziierte Kliniken
Kinderspital Zürich
Universitätsklinik Balgrist
Kinder- und Jugendpsychiatrischer Dienst des Kantons Zürich
Psychiatrische Universitätsklinik

Structure of the Center for Clinical Research/ Clinical Trials Center

Kuratorium
Prof. Dr. J-M. Fritschy (Stv. Dekan, ex officio)
Prof. Dr. Ch. Hock (Prorektor, ex officio)
Prof. Dr. J. Hodler
Prof. Dr. T. Lüscher
Prof. Dr. P.-A. Clavien
Prof. Dr. M. Pruschy
Prof. Dr. S. Gay
Prof. Dr. R. Nitsch
lic. oec. HSG R. Ziegler
Prof. Dr. B. Stieger
Prof. Dr. G. Zünd (Managing Director)

Direktorium
Prof. Dr. M. Weller
Prof. Dr. A. von Eckardstein (Co-Direktor)
Prof. Dr. A. Aguzzi (Co-Direktor)
Prof. Dr. G. A. Kullak-Ublick
Prof. Dr. H. Moch
Prof. Dr. G. Spinas
Prof. Dr. G. Zünd (Managing Director)
PD Dr. Paolo Cinelli
PD Dr. Mira Katan-Kahles

Geschäftsstelle ZKF
Robin Schneider, MBA
Geschäftsführer

Clinical Trials Center
PD Dr. G. Senti
Leitende Ärztin Clinical Trials Center

Biologisches Zentrallabor
Dr. Hugo Battaglia
Leiter Biologisches Zentrallabor

Forschungsgruppenleiterkonferenz
PD Dr. Paolo Cinelli
PD Dr. Mira Katan-Kahles
Scientific Research Group Leaders of the University Hospitals of Zurich (University Hospital, Children's Hospital, Balgrist University Clinic, Psychiatric University Hospital) and related institutions of the Faculty of Medicine

Table of contents

Bild Vorderseite: PD Dr. med. Paolo Cinelli & Nico Wick-Mazzarda, UniversitätsSpital Zürich

Programm

Donnerstag, 31. März 2016

Grosser Hörsaal Ost

08.15 **Eröffnung**
Prof. Dr. Gregor Zünd
Managing Director ZKF, Direktor Forschung und Lehre, UniversitätsSpital Zürich

08.20 **Begrüssung**
Rita Ziegler, lic. oec. HSG
Vorsitzende der Spitaldirektion

08.25 **Begrüssung**
Prof. Dr. Rainer Weber
Dekan der Medizinischen Fakultät der Universität Zürich

Session 1: Cardiovascular/Metabolics/Endocrinology

Chairpersons: Prof. Dr. Michele Genoni, Prof. Dr. Matthias Baumgartner

08.35 **Wissenschaftliches Hauptreferat**
"Vascular "glue" to cure sepsis?"
PD Dr. med. Reto Schüpbach, Leitender Arzt, Intensivmedizin, UniversitätsSpital Zürich

08.55 **A novel mouse model of methylmalonic aciduria circumvents neonatal lethality**
P. Forny, M. Mustedanagic, P. Burda, T. Hornemann, M. Baumgartner

09.05 **Impaired glucose tolerance in mice with β-cell specific deletion of *Pkbα***
M. Dietrich, R. Zuellig, M. Niessen, G. Spinas, O. Tschopp

09.15 **Obstructive Sleep Apnea in Ehlers-Danlos Syndrome. A prospective case-control study**
T. Gaisl, C. Giunta, K. Sutherland, D. Bratton, C. Schlatzer, N. Sievi, D. Franzen, P. Cistulli, M. Rohrbach, M. Kohler

09.25 **Mid-regional pro-adrenomedullin (MR-proADM) is an independent predictor of post stroke mortality**
C. Huber, J. Schneider, B. Mueller, M. Christ-Crain, M. Katan

09.35 Coffee Break

Session 2: Hematology/Oncology

Chairpersons: Prof. Dr. Markus Manz, Prof. Dr. Matthias Guckenberger

09.50 **Wissenschaftliches Hauptreferat**
"The landscape for early drug development in oncology: pitfalls and chances "
PD Dr. med. Roger von Moos, Leitender Arzt, Klinik & Poliklinik für Onkologie, UniversitätsSpital Zürich

10.10 **Aging-associated intrinsic and extrinsic factors control hematopoietic stem cell behavior**
L. Kovtonyuk, R. Ramin, H. Takizawa, M. Manz

10.20 **Blocking of the epigenetic repressor Ezh2 controls tumor escape upon IL-2cx immunotherapy**
N. Arenas-Ramirez, D. Zingg, R. Rosalia, A. Antunes, J. Haeusel, L. Sommer, O. Boyman

10.30 **Generation of a conditional transgenic mouse model of immunoglobulin light chain (AL) amyloidosis**
M. Nuvolone, S. Sorce, P. Pelczar, E. Rushing, F. Lavatelli, G. Palladini, G. Merlini, A. Aguzzi

10.40 **The NKG2D system mediates anti-tumor effects of chemotherapy and radiotherapy against glioblastoma**
T. Weiss, H. Schneider, M. Silginer, A. Steinle, M. Pruschy, M. Weller, P. Roth

Session 3: Stem Cell Research, Regenerative Medicine and Advanced Technologies

Chairpersons: Prof. Dr. Dr. Simon Hoerstrup, PD Dr. Oliver Gämperli

10.55 **Wissenschaftliches Hauptreferat**
"Translating basic research into clincially applicable skin"
Dr. Thomas Biedermann, PhD, Post Doc, Kinderspital Zürich, The Tissue Biology Research Unit

11.15 **Impact of solubilized muscle-specific urethral extracellular matrix on skeletal muscle differentiation for sphincter reconstruction**
I. Simões, D. Keller, P. Vale, J. Cabral, C. Da Silva, P. Baptista, T. Sulser, D. Eberli

11.25 **The Consent, Contact, and Community framework for Patient Reported Outcomes – Enhancing Apple's ResearchKit for iPhone Apps with FHIR**
P. Pfiffner, I. Pinyol, M. Natter, K. Mandl

11.35 **Maintenance of human hematopoiesis in in vivo engineered bone organs**
K. Fritsch, P. Bourgine, P. Bourgine, S. Pigeot, T. Schröder, I. Martin, H. Takizawa, H. Takizawa, M. Manz

11.45 **Drug Delivery device to support tendon rupture repair: biomechanical outcome of in vivo rabbit Achilles tendon full laceration experiments three weeks post-surgery**
O. Evrova, G. Meier Bürgisser, M. Calcagni, C. Scalera, E. Bachmann, J. Snedeker, P. Giovanoli, V. Vogel, J. Buschmann

11.55 Lunch/Poster viewing

Session 4: Infection/Immunity/Inflammation

Chairpersons: Prof. Dr. Janine Reichenbach, Prof. Dr. Roberto Speck

13.50 Wissenschaftliches Hauptreferat
"Cytokines: From Bench to Clinic"
Prof. Dr. med. Onur Boyman, Klinikdirektor, Klinik für Immunologie, UniversitätsSpital Zürich

14.10 **Stimulation of cytotoxic T cells by photosensitization-based Vaccination**
S. Freiberger, E. Varypataki, M. Hakerud, T. Kündig, P. Johansen

14.20 **Type II IL-4 receptor expression on neutrophils antagonizes their expansion and migration during infection and inflammation**
J. Woytschak, N. Keller, D. Impellizzieri, R. Thompson, T. Wynn, A. Zinkernagel, O. Boyman

14.30 **1-Deoxy-sphingolipids, novel biomarkers of diabetes, are cytotoxic for exocrine pancreatic cells**
R. Chen, T. Hornemann, W. Yu, S. Camargo, R. Graf, S. Sonda

14.40 **The impact of preconditioning by Sevoflurane after experimental mouse lung transplantation**
Y. Yamada, I. Laube, J. Jang, J. Bonvini, I. Inci, B. Beck Schimmer, W. Weder, W. Jungraithmayr

14.50 Coffee Break

Session 5: Neurosciences/Pharmacology

Chairpersons: Prof. Dr. Gerd-Achim Kullak-Ublick, Prof. Dr. Michael Weller

15.05 **Wissenschaftliches Hauptreferat**
"Sleep-wake disturbances following traumatic brain injury"
Prof. Dr. med. Christian Baumann, Leitender Arzt, Klinik für Neurologie, UniversitätsSpital Zürich

15.25 **The role of brain pericytes in the regulation of leukocyte trafficking and immune response under homeostatic and pathological conditions**
O. Török, B. Schreiner, A. Keller

15.35 **A neuroprotective role for microglia in prion diseases**
C. Zhu, U. Herrmann, J. Falsig, I. Abakumova, M. Nuvolone, P. Schwarz, E. Rushing, A. Aguzzi

15.45 **Inhibition of group I metabotropic glutamate receptors (mGluR1 and mGluR5) protects against prion-induced toxicity**
D. Goniotaki, L. Lakkaraju, A. Shrivastava, P. Bakirci, S. Sorce, P. Pelczar, F. Gasparini, A. Triller, A. Aguzzi

15.55 **Complete resection of contrast enhancing tumor volume is associated with improved survival in recurrent glioblastoma – results from the DIRECTOR trial**
H. Wirsching, J. Tonn, G. Tabatabai, C. Senft, P. Hau, M. Sabel, U. Herrlinger, R. Ketter, U. Schlegel, C. Marosi, G. Reifenberger, W. Wick, M. Weller, B. Suchorska

16.05 Coffee Break

Session 6: Klinische Forschungsschwerpunkte KFSP

16.20 **Präsentation**
Small RNA's
Prof. Dr. Adriano Aguzzi, Institutsdirektor, Institut für Neuropathologie, UniversitätsSpital Zürich

16.40 **Präsentation**
Molecular Imaging Network
Prof. Dr. phil. Bruno Weber, Lehrstuhl für Multimodale experimentelle Bildgebung,
Institut für Pharmakologie und Toxikologie, Universität Zürich

17.00 **Präsentation**
Zurich Primary HIV Infection Study
Dr. med. Dominique Braun, Oberarzt, Klinik für Infektionskrankheiten und Spitalhygiene,
UniversitätsSpital Zürich

17.25 **Posterpreis**

17.35 **Verleihung Georg Friedrich Götz-Preis 2016**

18.50 **Apéro**

Cardiovascular Diseases/Metabolics/Endocrinology

Basic Research

3447
G. Zhibo, G. Ting, H. Christian, K. Gerd
Farnesoid X receptor protects against kidney injury in uninephrectomized obese mice

3478
C. Schuoler, T. Haider, C. Leuenberger, L. Ostergaard, M. Gassmann, M. Kohler, L. Huber, M. Brock
Aquaporin 1 and Vascular Remodeling: a Novel Player in Hypoxia-Induced Pulmonary Hypertension

3519
M. Dietrich, R. Zuellig, M. Niessen, G. Spinas, O. Tschopp
Impaired glucose tolerance in mice with β-cell specific deletion of *Pkbα*

3533
L. Ahnen, S. Sanchez
Imaging Cerebral ischemia in preterm infants with sound and light

3584
L. Rigassi, E. Unterleutner, F. Barchiesi, B. Imthurn, R. Dubey
Role of microRNA-193a in mediating the protective action of Estradiol in vascular cells

3596
P. Forny, M. Mustedanagic, P. Burda, T. Hornemann, M. Baumgartner
A novel mouse model of methylmalonic aciduria circumvents neonatal lethality

Clinical Trials

3419
D. Benz, C. Gräni, F. Mikulicic, J. Vontobel, T. Fuchs, R. Buechel, P. Kaufmann
From Low-dose to Too-low-dose? Evaluating Two New Contrast Protocols for Coronary Computed Tomography Angiography on a Latest-generation 256-slice CT Scanner

3534
T. Gaisl, C. Giunta, K. Sutherland, D. Bratton, C. Schlatzer, N. Sievi, D. Franzen, P. Cistulli, M. Rohrbach, M. Kohler
Obstructive Sleep Apnea in Ehlers-Danlos Syndrome. A prospective case-control study

3548
C. Huber, J. Schneider, B. Mueller, M. Christ-Crain, M. Katan
Mid-regional pro-adrenomedullin (MR-proADM) is an independent predictor of post stroke mortality

3551
H. Rodriguez Cetina Biefer, S. Sündermann, M. Emmert, H. Alkadhi, M. Genoni, F. Maisano, A. Plass
Sternal healing in asymptomatic patients and potential influencing factors

3557
A. Plass, J. Barthelmes, K. Higashigaito, J. Sromicki, R. Manka, H. Rodriguez Cetina Biefer, H. Alkadhi, F. Maisano
Noninvasive ultra-low dose CT-image guided postoperative Quality Control of Coronary Artery Bypass Grafting

3558
D. Inderbitzin, M. Taramasso, F. Maisano, F. Eckstein, O. Reuthebuch
Magnetic Resonance Derived Blood-Flow Pattern after Off-Pump Aortic Valve Bypass Implantation

3559
D. Inderbitzin, D. Kalbermatten, M. Taramasso, F. Maisano, F. Eckstein, O. Reuthebuch
Severe Impairment of Parasternal Skin Perfusion after Pediculized Compared to Skeletonized LIMA-Harvesting Measured by Transcutaneous Duplex Sonographic Flow Mapping

Hematology/Oncology

Basic Research

3429
M. Nuvolone, S. Sorce, P. Pelczar, E. Rushing, F. Lavatelli, G. Palladini, G. Merlini, A. Aguzzi
Generation of a conditional transgenic mouse model of immunoglobulin light chain (AL) amyloidosis

3430
E. Bellini, N. Valtcheva, C. Stirnimann, M. Busquets Lopez, B. Bodenmiller, I. Frew, P. Wild
Identification of the molecular drivers of endometrial cancer progression

3434
O. Hasan Ali, R. Higgins, H. Cheng, F. Hartmann, S. Ring, L. French, A. Navarini, L. Flatz
Systematic Genomic Analysis for the Detection of Mutations in a Patient Suffering from Multiple Basal Cell Carcinomas and Palmoplantar Punctate Keratoderma

3458
M. Visentin, A. Torozi, C. Hiller, M. Töllke, B. Stieger, G. Kullak-Ublick
Deoxycholic acid (DCA) enhances the intracellular accumulation of potentially carcinogenic compounds

3472
M. Kiessling, S. Schuirer, M. Beibel, G. Rogler, G. Roma
Identification of oncogenic driver mutations by genome-wide CRISPR-Cas9 screening

3502
E. Saponara, G. Seleznik, R. Buzzi, F. Baschieri, H. Farhan, O. Pertz, I. Esposito, T. Reding, R. Graf, S. Sonda
Serotonin transporter inhibition prevents Rac1-dependent cytoskeletal remodeling and reduces pancreatic acinar-to-ductal metaplasia formation

3505
J. Kresoja-Rakic, E. Kapaklikaya, G. Ziltener, D. Dalcher, R. Santoro, B. Christensen, K. Johnson, B. Schwaller, W. Weder, R. Stahel, E. Felley-Bosco
Identification of cis- and trans-acting elements regulating calretinin expression in mesothelioma

3517
A. Kalyanov, C. Germanier, S. Sanchez Majos, M. Rudin, M. Wolf
Imaging of hypoxia in cancer by multispectral near-infrared tomography

3529
A. Bogdanova, A. Makhro, E. Seiler, N. Bogdanov, M. Gassmann, M. Manz, I. Hagemann, J. Goede
MemSID trial: first results of the Ca2+-lowering therapy in sickle cell disease patients

3537
T. Weiss, H. Schneider, M. Silginer, A. Steinle, M. Pruschy, M. Weller, P. Roth
The NKG2D system mediates anti-tumor effects of chemotherapy and radiotherapy against glioblastoma

3540
O. Riesterer, M. Nesteruk, R. Bundschuh, P. Veit-Haibach, M. Hüllner, G. Studer, S. Stieb, S. Glatz, M. Pruschy, M. Guckenberger, S. Lang
Radiomics in the CT perfusion maps – robustness study

3546
S. Freiberger, P. Cheng, R. Dummer, M. Levesque
Transcriptome Analysis to investigate Melanoma Heterogeneity and Drug Resistance

3549
A. Jöhl, M. Stäuble, M. Monn, M. Schmid Daners, S. Klöck, S. Lang
Modeling of a Robotic Treatment Couch to Improve the Control Performance

3560
U. Suessbier, H. Wong, A. Gomariz-Carillo, S. Isringhausen, T. Nagasawa, M. Manz, A. Müller, C. Nombela-Arrieta
Destruction and recovery of the bone marrow microenvironment following myeloablative treatment

3562
A. Rafiei, Y. Saito, M. Bühler, D. Soldini, M. Manz
Establishment of a Langerhans Cell Histiocytosis Model in Humanized Mice

3564
L. Kovtonyuk, R. Ramin, H. Takizawa, M. Manz
Aging-associated intrinsic and extrinsic factors control hematopoietic stem cell behavior

3566
N. Parrinello, M. Balabanov, C. Nombela-Arrieta, S. Isringhausen, S. Balabanov
Systems biology analysis of eIF5A function in eukaryotic cells

3570
M. Kirschner, B. Vrugt, M. Friess, M. Meerang, P. Wild, N. Van Zandwijk, G. Reid, W. Weder, I. Schmitt-Opitz
Evaluation of the novel prognostic miR-Score in a cohort of multimodality treated malignant pleural mesothelioma patients

3571
M. Meerang, B. Karima, E. Felley-Bosco, O. Lauk, B. Vrugt, A. Boss, A. Broggini-Tenzer, D. Kenkel, R. Stahel, S. Arni, W. Weder, I. Schmitt-Opitz
Antagonizing the Hedgehog Pathway with Vismodegib Impairs Malignant Pleural Mesothelioma Growth In Vivo by Affecting Stroma

3572
M. Meerang, B. Karima, M. Friess, B. Bitanihirwe, A. Soltermann, B. Vrugt, E. Felley-Bosco, R. Bueno, W. Richards, B. Seifert, R. Stahel, W. Weder, I. Schmitt-Opitz
Low Merlin Expression and High Survivin Staining Index are Indicators for Poor Prognosis of Malignant Pleural Mesothelioma Patients

3573
J. Jang, F. Janker, S. Arni, Y. Yamada, I. Gil-Bazo, I. De Meester, W. Weder, W. Jungraithmayr
Suppression of lung cancer in mice by the CD26/DPP4 inhibitor Vildagliptin

Translational Research

3446
M. Visentin, B. Van Rosmalen, C. Hiller, T. Van Gulik, G. Kullak-Ublick, B. Stieger
Organic Cation Transporters 1 and 3 (OCT1 and OCT3) as determinants of the intrahepatic uptake of the PET tracer 18F-fluorocholine

3484
K. Ikenberg, N. Valtcheva, M. Rechsteiner, S. Stieb, F. Singer, M. Prummer, D. Stekhoven, H. Moch, M. Guckenberger, G. Studer, O. Riesterer, P. Wild
Mapping the genomic landscape of head and neck squamous cell carcinoma for predicting the response to combined treatment with EGFR-blocking and radiation therapy

3503
S. Ehrbar, R. Perrin, M. Peroni, K. Bernatowicz, T. Parkel, I. Pytko, S. Klöck, M. Guckenberger, S. Lang, D. Weber, A. Lomax
Advanced respiratory motion management in radiation oncology - A phantom study

3518
N. Arenas-Ramirez, D. Zingg, R. Rosalia, A. Antunes, J. Haeusel, L. Sommer, O. Boyman
Blocking of the epigenetic repressor Ezh2 controls tumor escape upon IL-2cx immunotherapy

3543
D. Shinde, H. Ademi, J. Vogel, T. Gorr
Targeting vascularized and hypoxic compartments in solid malignancies: from basic research to dogs with cancer

3590
K. Nytko-Karouzakis, I. Grgic, M. Pruschy
The combined treatment modality of a hypoxia-activated prodrug (Evofosfamide) with ionizing radiation

3591
R. Myburgh, A. Müller, M. Van den Broek, B. Becher, M. Manz
Treatment of AML with CAR T cells

3595
R. Parrotta, A. Okonska, L. Penengo, E. Felley-Bosco
Alternative splicing in BAP1: implications in DNA damage response and drug sensitivity in mesothelioma

Clinical Trials

3481
I. Schmitt-Opitz, M. Friess, D. Nguyen-Kim, S. Hillinger, I. Inci, W. Weder
Correlation of CT san based tumor volume measurement to actual resected tumor weight in malignant pleural mesothelioma - a new T-factor?

3510
A. Mortezavi, S. Salemi, O. Gross, T. Sulser, D. Eberli
Inhibition of autophagy significantly increases the antitumor effect of Abiraterone in LnCap prostate cancer cells

3541
U. Rulle, R. Casanova, R. Stahel, W. Weder, A. Soltermann
External quality assessment of PTEN immunohistochemistry using computer-based image analysis compared to pathologist's scoring

3563
M. Schneider, D. Eshmuminov, R. Vonlanthen, P. Gertsch, K. Lehmann
Survival and Patterns of Recurrence after Cytoreductive Surgery (CRS) and Hyperthermic Intraperitoneal Chemotherapy (HIPEC) for colorectal and appendicular peritoneal malignancy – results of a 5-year monocentric experience

3574
I. Schmitt-Opitz, O. Lauk, M. Meerang, M. Friess, M. Kirschner, G. Wuilleret, C. Bommeli, A. Jetter, B. Aeschlimann, D. Günther, R. Stahel, W. Weder
Intracavitary Cisplatin-Fibrin Application following Resection of Mesothelioma

3575
I. Schmitt-Opitz, M. Friess, O. Lauk, T. Fraunfelder, T. Nguyen-Kim, I. Inci, S. Hillinger, D. Schneiter, B. Seifert, R. Stahel, W. Weder
A new prognostic score for treatment allocation for multimodality therapy for malignant pleural mesothelioma - an update

3576
I. Schmitt-Opitz, M. Friess, T. Nguyen-Kim, T. Fraunfelder, S. Hillinger, B. Seifert, I. Inci, W. Weder
Correlation of CT Scan based tumor volume measurement to actual resected tumor weight in malignant pleural mesothelioma - a new T-Factor?

Stem Cell Research/Regenerative Medicine/Advanced Technologies

Basic Research

3467
M. Langiewicz, A. Schlegel, B. Humar, R. Graf, P. Clavien
Molecular Mechanisms Underlying the Unprecedented Liver Regeneration Induced by ALPPS Surgery

3473
M. McLuckie, F. Robotti, D. Poulikakos, P. Giovanoli, A. Ferrari, N. Lindenblatt
Structured adipose-derived constructs influence the onset of neovascularization

3477
N. Sanchez Macedo, L. Zollinger, S. Eisenring, M. McLuckie, M. Kijanska, S. Bottan, A. Hegglin, F. Robotti, P. Giovanoli, D. Poulikakos, A. Ferrari, N. Lindenblatt
The dorsal skinfold chamber – the answer to difficult wound healing models?

3500
E. Malagola, E. Saponara, M. Bombardo Ayats, K. Grabliauskaite, T. Reding, R. Graf, S. Sonda
Role of thyroid hormone T3 in pancreatic acinar cells

3511
J. Smolar, M. Horsts, M. Ehrbar, D. Eberli
Co-culture of bladder-derived smooth muscle cells with smooth muscle-like adipose-derived stem cells leads to smooth muscle microtissue formation in 2D and 3D systems

3512
S. Salemi, D. Keller, M. Rottmar, T. Sulser
Multi-cell approach for successful bioengineering of functional smooth muscle layers

3514
S. Salemi, A. Mortezavi, T. Sulser, D. Eberli
Functional Smooth muscle cells differentiated from Adipose Derived Stem Cells: The importance of Authophagy

3527
E. Cambria, K. Renggli, C. Ahrens, C. Cook, C. Kroll, A. Krueger, B. Imperiali, L. Griffith
Sortase-mediated ligation of epidermal growth factor to pre-formed PEG hydrogels for in vitro tissue models

3553
D. Keller, C. Eberhardt, M. Rottmar, D. Haralampieva, T. Sulser, D. Eberli, A. Boss
Diffusion-Tensor-Imaging (DTI) for in vivo muscle regeneration after Cell therapy

3554
C. Eberhardt, D. Keller, M. Rottmar, D. Haralampieva, T. Sulser, D. Eberli, A. Boss
Magnetization transfer ratio (MTR) for in-vivo muscle regeneration after Cell therapy

3555
I. Simões, D. Keller, P. Vale, J. Cabral, C. Da Silva, P. Baptista, T. Sulser, D. Eberli
Impact of solubilized muscle-specific urethral extracellular matrix on skeletal muscle differentiation for sphincter reconstruction

3597
V. Chandrasekar, M. Einsiedler, U. Herrmann, S. Erni, H. Budka, A. Aguzzi
Elucidating the physiological function of cellular PrPC

3601
K. Fritsch, P. Bourgine, P. Bourgine, S. Pigeot, T. Schröder, I. Martin, H. Takizawa, H. Takizawa, M. Manz
Maintenance of human hematopoiesis in in vivo engineered bone organs

3604
E. Kachaylo, C. Tschuor, N. Borgeaud, N. Calo, P. Limani, M. Foti, R. Graf, B. Humar, P. Clavien
The regulation of liver volume gain and regeneration-associated steatosis through Pten

Translational Research

3426
D. Haralampieva, S. Salemi, I. Dinulovic, T. Sulser, S. Ametamey, C. Handschin, D. Eberli
Genetically modified human muscle precursor cells overexpressing PGC-1? support early myofiber formation in bioengineered muscle tissue

3448
J. Buschmann, E. Balli, S. Hess, W. Stark, P. Cinelli, S. Märsmann, M. Welti, W. Weder, W. Jungraithmayr
Adipose-derived stem cell seeded biominerizable nanocomposite for chest wall repair: Suppression of inflammatory cellular response in a murine model

3449
W. Baumgartner, M. Welti, N. Hild, S. Hess, W. Stark, G. Meier Bürgisser, P. Giovanoli, J. Buschmann
Tissue mechanics of piled critical size biomimetic and biominerizable nanocomposites: formation of bioreactor-induced stem cell gradients under perfusion and compression

3451
O. Evrova, G. Meier Bürgisser, M. Calcagni, C. Scalera, E. Bachmann, J. Snedeker, P. Giovanoli, V. Vogel, J. Buschmann
Drug Delivery device to support tendon rupture repair: biomechanical outcome of in vivo rabbit Achilles tendon full laceration experiments three weeks post-surgery

3454
F. Kivrak-Pfiffner, C. Waschkies, Y. Tian, M. Calcagni, P. Giovanoli, M. Rudin, J. Buschmann
SPIO-enhanced MRI as a nondestructive in vivo method to assess vascularization of 3D scaffolds planted on the Chorioallantoic Membrane of the Chick Embryo in ovo

3552
J. Günter, P. Wolint, J. Steiger, E. Cambria, A. Bopp, S. Hoerstrup, M. Emmert
Biobanking of 3D microtissues for future off-the-shelf regenerative therapies

3556
R. Schweizer, J. Schnider, W. Zhang, K. Marra, M. Solari, P. Rubin, V. Gorantla, J. Plock
Timing and Frequency of Immunomodulatory Cytotherapy with Adipose-derived Stem Cells Influences Graft Survival and Immunological Outcome in Vascularized Composite Allotransplantation

3568
J. Steiger, E. Cambria, J. Günter, P. Wolint, A. Bopp, S. Hoerstrup, M. Emmert
Generation of therapeutic multi-cellular three dimensional (3D) microtissues (MTs) for cardiac regeneration: Evaluation of the in vitro microenvironment of co-culture MTs

3594
C. Corro, A. Von Teichman, D. Vuong, C. Mittmann, H. Moch, M. Rechsteiner
Tumor heterogeneity and cancer stem cell properties in renal cancer

3605
P. Kron, A. Schlegel, O. De Rougemont, C. Oberkofler, P. Clavien, P. Dutkowski
Short, cool and well oxygenated – HOPE for Kidney Transplantation in a Rodent Model

Clinical Trials

3491
R. Reissner, G. Giesen, C. Calcagni
Mid term results of semiconstrained distal radioulnar joint arthroplasty

3516
P. Pfiffner, I. Pinyol, M. Natter, K. Mandl
The Consent, Contact, and Community framework for Patient Reported Outcomes – Enhancing Apple's ResearchKit for iPhone Apps with FHIR

Infection/Immunity/Inflammation

Basic Research

3421
M. Shilaih, A. Marzel, U. Scherrer, L. Braun, K. Darling, B. Battegay, H. Hoffmann, B. Bernasconi, H. Hirzel, H. Günthard, R. Kouyos
Dually Active HIV/HBV Antiretrovirals Protect Against Incident Hepatitis B Infections: Potential for Prophylaxis

3423
F. Rost, S. Schmidt, A. Atrott, G. Rogler, I. Frey-Wagner
Effects of NLRP3 on gut microbiota and murine colitis

3437
J. Woytschak, N. Keller, D. Impellizzieri, R. Thompson, T. Wynn, A. Zinkernagel, O. Boyman
Type II IL-4 receptor expression on neutrophils antagonizes their expansion and migration during infection and inflammation

3439
V. Strouvelle, V. Vongrad, K. Metzner, H. Günthard
Quantification of different HIV-1 genomic forms to characterize the viral reservoir

3441
D. Ignatova, Y. Chang, E. Contassot, T. Mehra, V. Mitev, R. Dummer, L. French, W. Hoetzenecker, A. Cozzio, E. Guenova
Expression of CD164 on malignant T cells in Sézary Syndrome

3445
V. Vongrad, C. Von Siebenthal, H. Günthard, K. Metzner
Highly sensitive droplet digital PCR to quantify the HIV-1 latent reservoir

3450
C. Leuenberger, C. Schuoler, H. Bye, C. Mignan, T. Rechsteiner, S. Hillinger, I. Opitz, B. Marsland, A. Faiz, P. Hiemstra, W. Timens, G. Camici, M. Kohler, L. Huber, M. Brock
microRNA-223 controls the expression of histone deacetylase 2: a novel axis in COPD

3456
M. Bombardo Ayats, E. Saponara, E. Malagola, G. Seleznik, T. Reding Graf, R. Graf, S. Sonda
Ms275 a Class I HDAC inhibitor, ameliorates pancreatic inflammation

3457
M. Rochat, D. Li, S. Ivic, A. Audige, E. Schlaepfer, M. Manz, R. Speck
Differential dynamics of HIV infection in MISTRG and MITRG mice

3460
J. Burgener, T. Skaria, G. Schoedon-Geiser
Inflammatory Wnt5A signaling in human macrophages is mediated by Caveolin-1 dependent internalization of Wnt5A/Fzd5 complexes

3468
N. Keller, J. Woytschak, S. Uchiyama, N. Leimer, O. Boyman, A. Zinkernagel
Plasmacytoid Dendritic Cell Migration in Response to Group a Streptococcus

3471
N. Keller, S. Uchiyama, E. Schläpfer, C. Grube, R. Schüpbach, R. Speck, A. Zinkernagel
Interferon-alpha induced properdin-enhanced clearance of Group a Streptococcus

3488
S. Freiberger, E. Varypataki, M. Hakerud, T. Kündig, P. Johansen
Stimulation of cytotoxic T cells by photosensitization-based Vaccination

3492
A. Marzel, M. Shilaih, W. Yang, J. Böni, S. Yerly, T. Klimkait, V. Aubert, H. Günthard, R. Kouyos, Swiss HIV Cohort Study
How to find HIV transmission and serosorting couples using follow-up visits dates

3504
D. Leuthard, S. Weiss, S. Freiberger, A. Duda, M. Heath, M. Skinner, M. Kramer, T. Kündig, P. Johansen
Microcrystalline tyrosine as an adjuvant in allergy immunotherapy: a mouse study

3530
R. Chen, T. Hornemann, W. Yu, S. Camargo, R. Graf, S. Sonda
1-Deoxy-sphingolipids, novel biomarkers of diabetes, are cytotoxic for exocrine pancreatic cells

3531
R. Chen, G. Mosca, M. Dietrich, E. Saponara, K. Grabliauskaite, R. Zuellig, O. Tschopp, R. Graf, S. Sonda
Akt1 regulates the development of inflammation and tissue regeneration during acute pancreatitis

3545
S. Isringhausen, N. Kraeutler, D. Stoycheva, U. Suessbier, P. Helbling, L. Kovtonyuk, H. Wong, M. Manz, A. Oxenius, C. Nombela-Arrieta
Dynamics of the bone-marrow microenvironment during viral infections

3547
A. Franchini, M. Ender, L. Vazquez Rojo, D. Heuberger, R. Schuepbach
Cleavage of protease activated receptor 2 (PAR2) by staphylococcal proteases

3561
R. Romao, E. Tejera Puente, K. Nytko, U. Siler, C. Münz, R. Reichenbach
Defective nuclear entry of hydrolases prevents NETosis in Chronic Granulomatous Disease

3582
R. Higgins, M. Theiler, A. Smith, R. Wälchli, L. Weibel, A. Navarini
Hunt for somatic mutations in Linear Localized Scleroderma

3583
S. Lukas, I. Jelcic, J. Hanson, K. Weber, K. Landau, M. Pless, A. Valavanis, A. Lutterotti, S. Schippling
Structural and functional outcomes in bilateral optic neuritis with MOG-antibodies

3586
D. Heuberger, A. Franchini, J. Madon, R. Schuepbach
Membrane-bound thrombomodulin mediates cleavage of protease-activated receptor 2 by thrombin

3588
U. Nüesch, A. Mauracher, B. Volkmer, A. Urwyler, S. Vavassori, J. Pachlopnik Schmid
The effect of dysfunctional mutation in Ttc7 on the haemtopoietic versus non-haemtopoietic system

3600
G. Wanner-Seleznik, T. Reding, L. Peter, A. Zabel, M. Heikenwalder, S. Sonda, R. Graf
Absence of p21 attenuates pancreatic inflammation but does not modulate the development of autoimmune pancreatitis

3603
Z. Song
Exogenous Melatonin Promotes Graft Regeneration

3607
Y. Yamada, I. Laube, J. Jang, J. Bonvini, I. Inci, B. Beck Schimmer, W. Weder, W. Jungraithmayr
The impact of preconditioning by Sevoflurane after experimental mouse lung transplantation

3608
Y. Yamada, D. Kenkel, J. Jang, C. Opelz, I. Inci, A. Boss, W. Weder, W. Jungraithmayr
Experimental chronic lung allograft rejection – which mouse model is reliable?

3609
Y. Yamada, I. Iskender, S. Arni, S. Hillinger, T. Cosgun, W. Jungraithmayr, W. Weder, I. Inci
Ex vivo treatment of donors with nebulized N-acetylcysteine partially improved post-transplant lung function

Translational Research

3422
N. Campbell, D. Seifert, C. Leemann, H. Kuster, D. Braun, R. Weber, H. Günthard, N. Beerenwinkel, K. Metzner
Characterization of HIV-1 in Transmission Pairs

3425
R. Bruckner, M. Spalinger, G. Rogler, M. Scharl
The role for T cells in the pathogenesis of Crohn's disease-associated fistulae

3474
C. Waschkies, T. Reding Graf, G. Seleznik, U. Ungethuem, R. Graf
Visceral Fat Volume and Within-Organ Signal Fat-Fraction as Magnetic Resonance Imaging-based Phenotypic Markers in a transgenic Mouse Model of Pancreatic Carcinogenesis

3489
C. Waschkies, C. Egger, T. Suter, R. Martin, M. Rudin
Magnetic Resonance Imaging Based Microstructural Phenotyping of Animal Models of MS and in Human Brain Tissue Samples

3497
S. Karlen, S. Kuster, E. Eschmann, S. Weiler, J. Blaser
Adherence to guidelines for therapeutic monitoring of glycopeptide and aminoglycoside antibiotics

3498
G. Petitjean, A. Fahrny, C. Mettling, F. Kirchhoff, R. Speck, M. Benkirane
Towards the development of a humanized mouse model for tracking, localizing and understanding HIV persistence in vivo

3526
E. Varypataki, S. Freiberger, T. Kündig, P. Johansen
PCI-based vaccination for improved in vivo stimulation of antigen-specific cytotoxic T cells

3589
I. Jelcic, B. Combaluzier, Il. Jelcic, W. Faigle, L. Senn, B. Reinhart, L. Ströh, R. Nitsch, T. Stehle, M. Sospedra, J. Grimm, R. Martin
Broadly Neutralizing Human Monoclonal JC Polyomavirus VP1-Specific Antibodies for the Treatment of Progressive Multifocal Leukoencephalopathy

Clinical Trials

3440
Y. Chang, M. Ziegler, D. Ignatova, K. Kerl, L. French, A. Cozzio, E. Guenova
Resistance to antibody-dependent cellular cytotoxicity impairs antitumor activity of Rituximab in a CD20+ mycosis fungoides

3459
P. Schreiber, H. Bischoff-Ferrari, K. Boggian, C. Van Delden, N. Enriquez, T. Fehr, C. Garzoni, H. Hirsch, C. Hirzel, O. Manuel, P. Meylan, L. Saleh, M. Weisser, N. Mueller, And. The Swiss Transplant Cohort Study
Vitamin D and its interplay with infections and rejections in kidney and liver recipients

3475
A. Scherrer, J. Böni, S. Yerly, T. Klimkait, V. Aubert, M. Cavassini, M. Battegay, C. Hauser, E. Bernasconi, H. Günthard
Failure Rate in NRTI-Free Treatment Is Higher in Two Compared to Three Class Regimens

3479
D. Lewandowska, B. Ruehe, P. Schreiber, O. Zagordi, F. Geissberger, M. Schuurmans, M. Greiner, A. Zbinden, J. Böni, C. Benden, N. Müller, A. Trkola, M. Huber
Identifying the etiology of previously undiagnosed respiratory infections in lung transplant recipients by unbiased metagenomic sequencing

3487
D. Braun, A. Marzel, D. Bircher, P. Schreiber, C. Grube, A. Scherrer, R. Kouyos, H. Günthard
High Rates of Asymptomatic STIs in Patients after Primary HIV-1 Infection

3495
M. Kälin, B. Ledergerber, B. Müllhaupt, A. Rauch, P. Schmid, F. Banderet, S. Giulieri, R. Weber, H. Kovari
Liver Fibrosis in HIV-monoinfected Persons with chronic elevated aminotransferase levels

3538
P. Beeler, S. Kuster, E. Eschmann, R. Weber, J. Blaser
Earlier Switching from Intravenous to Oral Antibiotics - Hospital-Wide Rollout of Electronic Reminders

3577
I. Jelcic, P. Ojer, M. Foege, R. Stenger, M. Kayser, J. Kessler, A. Müller, U. Schanz, J. Dudler, M. Sospedra, R. Martin
Individual Treatment Attempt of Progressive Multifocal Leukoencephalopathy (PML) with Adoptive Immunotherapy by Ex Vivo-Stimulated JC Polyoma Virus-Specific T cells

Neurosciences/Pharmacology

Basic Research

3428
M. Nuvolone, M. Hermann, S. Sorce, G. Russo, C. Tiberi, P. Schwarz, E. Minikel, D. Sanoudou, P. Pelczar, A. Aguzzi
Strictly co-isogenic C57BL/6J-Prnp knockout mice: a rigorous resource for prion science

3431
C. Zhu, U. Herrmann, J. Falsig, I. Abakumova, M. Nuvolone, P. Schwarz, E. Rushing, A. Aguzzi
A neuroprotective role for microglia in prion diseases

3432
D. Kirschenbaum, D. Laptev, O. Bichsel, J. Buhmann, A. Aguzzi
Crystal & Hits: a new methodology for whole-mount mouse brain imaging

3433
M. Pfaltz, T. Wingenbach, C. Mueller-Pfeiffer, K. Hassanpour, M. Plichta, M. Rufer, U. Schnyder
Emotion Recognition in Traumatized Individuals with and without Posttraumatic Stress Disorder: A Psychophysiological Study

3435
C. Röösli, S. Sim, I. Dobrev, F. Pfiffner, S. Stenfelt, A. Huber
Interaction between osseous and non-osseous vibratory stimulation of the human cadaveric head

3442
Y. Zarb, T. Jones, S. Dias, A. Keller
The role of oxidative stress in cerebral microvascular calcification

3443
M. Pfammatter, M. Andreasen, G. Meisl, J. Adamcik, R. Mezzenga, T. Knowles, A. Aguzzi, S. Hornemann
Digital amyloid amplification assay for the ultrasensitive quantification of amyloid aggregates

3452
A. Monge Naldi, C. Belfrage, N. Jain, E. Wei, B. Martorell, M. Gassmann, J. Vogel
Neuronal erythropoietin overexpression protects mice against age-related hearing loss (presbycusis)

3461
S. Sorce, M. Nuvolone, M. Labouesse, U. Stadlbauer, S. Giovanoli, C. Winter, G. Russo, A. Varol, C. Parkhurst, D. Littman, W. Gan, D. Sanoudou, L. Ozmen, J. Roeper, U. Meyer, A. Aguzzi
Cell-specific NURR1 overexpression in midbrain dopaminergic neurons improves affective and psychosis-related behavioral functions

3463
S. Sorce, M. Nuvolone, G. Russo, P. Schwarz, A. Aguzzi
Temporal transcriptional changes induced by prions in mice

3464
A. Lakkaraju, R. Marpakwar, E. Rushing, P. Liberski, A. Aguzzi
Identifying the determinants of spongiform phenotype in prion infections

3465
R. Reimann, A. Varol, L. Caflisch, M. Hermann, S. Hornemann, A. Senatore, V. Chandrasekar, M. Einsiedler, M. Nuvolone, B. Schneider, A. Aguzzi
Depicting the role of the FT functional domains in antiprion mediated neurodegeneration

3466
D. Ostojic, F. Scholkmann, M. Wolf
A new approach to calculate arterial oxygen saturation from blood volume pulsations measured on the human forehead using near-infrared spectroscopy NIRS

3469
F. Scholkmann, M. Wolf
A new approach to assess the complex coupling between cardiovascular activity and cerebral tissue oxygenation in preterm neonates: Multiscale convergent-cross mapping

3470
F. Scholkmann, U. Wolf
New insights into the physiological origin of fluctuations in fNIRS signals – A new analysis based on systemic physiology complemented (SPC) fNIRS brain imaging (SPC-fNIRS)

3501
B. Li, G. Meisl, C. Zhu, C. Tournaire, M. Zurbrügg, V. Eckhardt, M. Nuvolone, S. Sorce, T. Knowles, S. Hornemann, A. Aguzzi
Establishment of a homogenous-phase PrPSc-FRET for fully automated high-throughput prion detection

3507
T. Fedele, M. Van 't Klooster, S. Sergey, W. Zweiphenning, N. Van Klink, M. Zijlmans
Automatically detected residual fast ripples in the intraoperative corticogram predict epilepsy surgery out

3508
E. Boran, J. Sarnthein, G. Curio, J. Gotman, T. Fedele
Non-invasive detection of fast ripples in low-noise EEG recordings

3509
S. Burnos, T. Fedele, N. Krayenbühl, P. Hilfiker, K. König, T. Grunwald, J. Sarnthein
Relation of automatically detected High Frequency Oscillations (HFOs) with the SOZ and clinical outcome

3513
S. Burnos, B. Frauscher, R. Zelmann, C. Haegelen, J. Sarnthein, J. Gotman
The morphology of high frequency oscillations (HFO) does not improve delineating the epileptogenic zone

3515
M. Morawska, L. Imbach, A. Baumann, S. Masneuf, C. Baumann, D. Noain
Phenotypic characterisation of sleep-wake disturbances in VMAT2 deficient murine model of Parkinson's disease

3520
D. Noain, M. Morawska, F. Büchele, S. Schreglmann, Y. Gavrilov, M. Penner, L. Imbach, C. Baumann
Cognitive impairment, sleep-wake disturbances and diffuse axonal injury in a rat model of closed traumatic brain injury: Effect of sleep modulation on TBI-induced chronic symptoms

3523
C. Gonçalves-Moreira, M. Morawska, A. Baumann, S. Masneuf, D. Noain, C. Baumann
Inhibiting COMT in a mouse model of Parkinson's disease: a trial of Tolcapone in VMAT2-deficient mice

3525
T. Fleischmann, M. Arras, P. Jirkof
Paracetamol for pain relief after laparotomy for embryo-transfer in laboratory mice

3532
M. Widmer, N. Ziegler, J. Held, K. Lutz, A. Luft
Rewarding feedback promotes motor skill consolidation via striatal activity

3539
A. Senatore, C. Tiberi, G. Horny, N. George, T. Pietzonka, A. Aguzzi
Development of novel immunotherapeutics for genetic prion diseases

3542
O. Török, B. Schreiner, A. Keller
The role of brain pericytes in the regulation of leukocyte trafficking and immune response under homeostatic and pathological conditions

3580
D. Pease, M. Emmenegger, E. Schaper, V. Chandrasekar, V. Eckhardt, A. Hartung, S. Hornemann, A. Aguzzi
Discovery of Novel miRNA-Regulated PrPC Biosynthesis and PrPSc Conversion Pathways via a High-Throughput miRNA Screening Platform

3585
B. Li, M. Emmenegger, E. Schaper, M. Zurbrügg, V. Eckhardt, C. Zhu, N. Guex, P. Gribbon, S. Hornemann, I. Xenarios, A. Aguzzi
A genome-wide siRNA screen for genes controlling PrPC biosynthesis and prion propagation

3592
P. Manogaran, R. Opfer, T. Kepp, P. Suppa, L. Spies, C. Egger, S. Schippling
Assessing intra - and inter - scanner variability of automated brain volumetry using SPM12, SIENA, and SIENAX

3598
H. Leske, U. Herrmann, S. Hornemann, K. Wüthrich, A. Aguzzi
Removal of a single oxygen atom from the prion protein leads to significant reduction of proteinase K resistant PrP

3602
M. Wulf, M. Nuvolone, A. Aguzzi
Electrophysiological changes in prion protein ablated mice

3606
A. Vrana, K. Humphreys, M. Meier, S. Hotz-Boendermaker, F. Scholkmann
Hemodynamic responses in cortical sensorimotor areas to mechanosensory stimulations of the lower back measured by fNIRS

Translational Research

3420
E. Eschmann, S. Karlen, L. Perger, M. Schneemann, J. Blaser
Shifting Tasks from Nurses to Physicians: CDS Needed after Introduction of CPOE?

3455
P. Baumgartner, M. El-Amki, O. Bracko, A. Luft, S. Wegener
Manganese-enhanced MRI for the study of post-stroke cognitive impairment in a rodent stroke model

3476
J. Wagner, L. Regli, A. Keller
Early microvascular changes after subarachnoid hemorrhage in mice

3485
K. Frontzek, M. Lutz, A. Aguzzi, G. Kovacs, H. Budka
Cerebrovascular and brain amyloid-? pathology is frequent in iatrogenic Creutzfeldt-Jakob disease after dural grafting

3486
V. De Luca, A. Kündig, M. Hüser, M. Jaggi, E. Keller
Prediction of cerebral autoregulation capacity and intracranial pressure in neurointensive care patients using machine learning: a feasibility study

3490
V. De Luca, E. Keller
ICU-Cockpit: enabling multimodal monitoring and decision support in neurointensive care

3499
A. Jödicke, H. Dahmke, G. Kullak-Ublick, S. Weiler
Severe Injection Site Reactions after subcutaneous Administration of Sayana®: A qualitative post-marketing Analysis of Cases reported to the Regional Pharmacovigilance Centre Zurich

3528
D. Goniotaki, L. Lakkaraju, A. Shrivastava, P. Bakirci, S. Sorce, P. Pelczar, F. Gasparini, A. Triller, A. Aguzzi
Inhibition of group I metabotropic glutamate receptors (mGluR1 and mGluR5) protects against prion-induced toxicity

3587
K. Frontzek, M. Emmenegger, L. Saleh, R. Moos, E. Schaper, G. Meisl, D. Zimmermann, A. Von Eckardstein, H. Budka, S. Hornemann, A. Aguzzi
Prevalence of human autoantibodies against the prion protein in unselected USZ patients and in PRNP mutation carriers

3593
J. Hanson, S. Lukas, K. Landau, R. Martin, C. Gerth-Kahlert, S. Schippling
Evidence of functional retinal impairment in the absence of sustained structural damage following MS-related optic neuritis

Clinical Trials

3427
J. Sim, M. Alshamani, M. Chatzimichalis, C. Röösli, M. Huber
Experimental evaluation of new prostheses for tympanoplasty

3436
H. Wirsching, J. Tonn, G. Tabatabai, C. Senft, P. Hau, M. Sabel, U. Herrlinger, R. Ketter, U. Schlegel, C. Marosi, G. Reifenberger, W. Wick, M. Weller, B. Suchorska
Complete resection of contrast enhancing tumor volume is associated with improved survival in recurrent glioblastoma – results from the DIRECTOR trial

3438
D. Barthelmes, S. Zweifel, C. Böni, M. Marti
Treatment outcomes in eyes treated for choroidal neovascularization secondary to pathologic myopia using vascular endothelial growth factor inhibitors

3521
F. Wehrle, B. Latal, R. O'Gorman, C. Hagmann, R. Huber
EEG sleep slow wave activity as a potential marker of load-dependent deficits in executive functions in very preterm children and adolescents

3535
J. Deuel, D. Schaer, M. Cheetham, E. Battegay
Disease-disease-interactions determine in-hospital morbidity and mortality

3536
C. Naegeli, T. Zeffiro, M. Piccirelli, A. Jaillard, A. Weilenmann, K. Hassanpour, M. Schick, M. Rufer, S. Orr, C. Mueller-Pfeiffer
Cerebral networks underlying hypersensitivity to salient sounds in posttraumatic stress disorder

3544
Y. Valko, E. Werth, C. Baumann, D. Straumann, P. Valko, K. Weber
Positional nystagmus from BPPV in polysomnography of PD patients

3550
N. Vital, J. Malamud, J. Taeymans, C. Mueller-Pfeiffer
Functional impairment in posttraumatic stress disorder: a systematic review and meta-analysis

3567
N. Scherrer, Y. Devaux, F. Fays, O. Collignon, B. Mueller, A. Luft, M. Christ-Crain, M. Katan
MicroRNA-150 Adds Prognostic Information After Acute Ischemic Stroke

3578
T. Brodie, P. Ojer, M. Sospedra, R. Martin, A. Lutterotti
CD4+ T cell Reactivity to Myelin-Derived Autoantigens in the Cerebrospinal Fluid of Multiple Sclerosis Patients

3579
A. Lutterotti, M. Foege, C. Blumer, A. Zinganell, T. Berger, W. Faigle, M. Inglese, M. Sormani, M. Sospedra, R. Martin
Treatment of Clinically Isolated Syndrome and Relapsing Remitting Multiple Sclerosis with Sodium Chloride-based Nanoparticles (RNS60) Administered Intravenously – a Phase IIa Clinical Trial

3581
C. Egger, T. Kepp, L. Spies, R. Opfer, S. Schippling
Validation of automated versus manual T2-lesion segmentation in Multiple Sclerosis patients applied on FLAIR sequences

3419

D. Benz[1], C. Gräni[1], F. Mikulicic[1], J. Vontobel[1], T. Fuchs[1], R. Buechel[1], P. Kaufmann[1]

From Low-dose to Too-low-dose? Evaluating Two New Contrast Protocols for Coronary Computed Tomography Angiography on a Latest-generation 256-slice CT Scanner

Department of Nuclear Medicine, University Hospital Zürich, Zürich[1]

Introduction:
With the implementation of 256-slice CT scanners, single-beat acquisition of coronary CT angiography (CCTA) permits a reduction of contrast volume. The aim of the present study was to evaluate the impact of an ultra-low-dose (ULD) and a low-dose (LD) contrast protocol for CCTA on quantitative and qualitative image analysis.

Methods:
Prospectively, 120 consecutive patients referred for known or suspected coronary artery disease were scanned with a latest generation 256-slice scanner (Revolution CT, GE Healthcare) applying either an ULD (60 patients, 25-45 mL) or a LD (60 patients, 35-55 mL) BMI-adapted contrast protocol. For each patient, attenuation was measured by placing a region of interest in the aortic root and in each coronary segment, and vessel opacification was visually assessed on a 4-point scale. Attenuation and vessel opacification were compared to 20 consecutive patients scanned with a normal-dose (ND) contrast protocol previously validated for a state-of-the-art 64-slice CT scanner (VCT Lightspeed, GE Healthcare).

Results:
Baseline characteristics (61% male, 56±12 years, BMI of 25.8±4.6 kg/m^2) and scanning parameters (tube current 263±58 mA, tube voltage 101±9 kV, contrast flow 4.4±0.5 mL/s) did not significantly differ among study groups. By contrast, administered contrast volume increased significantly from the ULD (median volume 35 mL) over the LD (45 mL) and to the ND (70 mL) protocol ($p<0.001$). Attenuation in the aortic root (410±65 HU) and in the coronary segments (316±52 HU) was significantly lower for the ULD protocol compared to the LD (472±102 HU and 363±60 HU) and ND protocol (490±80 HU and 359±52 HU) ($p<0.001$), but with no significant differences between the LD and ND protocol. Visually assessed vessel opacification did not differ significantly among the protocols (i.e. 3.38±0.29, 3.48±0.20 and 3.43±0.28 for ULD, LD and ND, respectively).

Conclusion:
A LD contrast protocol with a median volume of 45 mL can be implemented for a latest-generation 256-slice CCTA without a decrease in vessel attenuation. By contrast, the median contrast volume of only 35 mL for the ULD protocol might be too low as vessel attenuation decreased significantly.

3420

E. Eschmann[1], S. Karlen[1], L. Perger[2], M. Schneemann[2], J. Blaser[1]

Shifting Tasks from Nurses to Physicians: CDS Needed after Introduction of CPOE?

Medical Informatics Research Centre, Directorate of Research and Education, University Hospital, Zurich[1], Division of Internal Medicine, University Hospital, Zurich[2]

Introduction:
Unintended effects can occur by introducing computerized physician order entry (CPOE) if responsibilities are shifted from nurses to physicians, e.g. regarding the specification of the duration of intravenous (IV) administrations. The purpose of this quality assessment was to determine the rate of IV prescriptions with too short durations, when the prescribers were not assisted by clinical decision support (CDS).

Methods:
All IV drug prescriptions for inpatients at the University Hospital Zurich (tertiary care, 850 beds) were included over a 25 month period following the introduction of CPOE. The prescribed durations of IV administrations were compared to the minimal duration defined by the Swiss drug knowledge base.

Results:
Analysis of the 100 most frequently ordered IV drugs showed that the duration of IV administrations was not defined in 112,594 of 247,255 orders (45.5%) and prescribed with too short durations in 13,640 orders (5.5%).

Conclusion:
Introduction of CPOE accompanied by a shift of tasks from nurses to physicians resulted in a high number of incomplete or erroneous IV medication orders. Patient safety might be improved by physicians' training complemented by CDS ensuring drug-specific default values for minimal durations of IV administration.

3421

M. Shilaih[1], A. Marzel[1], U. Scherrer[1], L. Braun[1], K. Darling[2], B. Battegay[3], H. Hoffmann[4], B. Bernasconi[5], H. Hirzel[6], H. Günthard[1], R. Kouyos[1]

Dually Active HIV/HBV Antiretrovirals Protect Against Incident Hepatitis B Infections: Potential for Prophylaxis

Universitätsspital Zürich[1], Lausanne University Hospital[2], Basel University Hospital, Basel[3], Infectious diseases department, St. Gallen Kantonal Hospital[4], Division of Infectious Diseases, Regional Hospital Lugano, Lugano[5], Department of Infectious Diseases, Inselspital, Bern University Hospital, University of Bern[6]

Introduction:
Hepatitis-B virus (HBV) and HIV have a detrimental effect on each other natural course, and HBV vaccination in HIV-infected individuals is less likely to elicit a protective immune response compared to the HIV-uninfected. We examine the protective effect of dually active antiretroviral therapy (DAART) for HIV/HBV (Tenofovir, Lamivudine, and Emtricitabine) in a large cohort encompassing heterosexuals, men who have sex with men (MSM), and intravenous drug users (IDU) HIV-infected individuals susceptible to HBV, with comprehensive follow-up data about risky behavior and immunological status

Methods:
An incident HBV infection was defined as the presence of any HBV serological marker (HBsAg, AntiHBc, or HBV-DNA) following a negative baseline test. We excluded patients who only developed positive AntiHBs response (indicating vaccination). Both univariate and multivariate Cox proportional-hazard-models were utilized, with an incident case of HBV infection as the outcome variable and the explanatory variable being the proportion of observation time on DAART.

Results:
We analyzed 1,716 eligible patients from the Swiss HIV Cohort Study with 177 incident HBV cases and 10,682 person observation years. DAART was negatively associated with incident HBV (hazard-ratio 0.4, 95%CI 0.2-0.6). This protective association was robust to adjustment (adjusted HR 0.3, 0.2-0.5) for condomless-sex, √CD4 cell count, drug use, and patients' demographics. Condomless-sex (1.9, 1.4-2.6), belonging to men who have sex with men (2.7, 1.7-4.2) or intravenous drug users (3.8, 2.4-6.1) transmission-groups were all associated with higher HBV hazard.

Conclusion:
Our study suggests that DAART, independently of CD4 count and risky behavior, has a potentially strong beneficial public health impact as pre-exposure prophylaxis for HBV co-infection.

3422

N. Campbell[1], D. Seifert[2], C. Leemann[1], H. Kuster[1], D. Braun[1], R. Weber[1], H. Günthard[1], N. Beerenwinkel[2], K. Metzner[1]

Characterization of HIV-1 in Transmission Pairs

Department of Infectious Diseases and Hospital Epidemiology, University Hospital of Zurich[1], Department of Biosystems Science and Engineering, ETH Zurich Basel[2]

Introduction:
Profiling the transmitted founder virus is yet a challenge in the HIV-1 field. This is due to the paucity of studies which analyze the relationship between the viral swarm of the transmitter and the recipient. Herein we aim to determine whether transmission of HIV-1 is a stochastic process via the reconstruction of HIV-1 haplotypes from Zürich Primary HIV Infection Study (ZPHI) and Swiss HIV Cohort Study (SHCS) individuals belonging to 8 transmission pairs.

Methods:
SHCS Drug Resistance Database HIV-1 pol genotypic resistance test sequences were used to determine whether individuals enrolled in the SHCS or ZPHI were possible transmitters for ZPHI individuals. Pairs were identified via phylogenetic clustering of sequences (distance < 1.5%) and validated with clinical data. Full-length sequencing of plasma viral RNA was performed using the Illumina MiSeq Reagent v2 500 cycles Kit at the time point nearest transmission. Statistical modeling and gene-wise haplotype reconstruction were performed (for genes: p24, gp120, and gp41) to determine the stochasticity.

Results:
Gene-wise haplotypes for the given pairs clustered together, when the Shannon entropy of the transmitter was >0.02 the recipient's haplotypes formed a cluster nested. Key regions of interest: the major haplotype was transmitted in 5/8 pairs for p24, 1/8 and 3/8 for gp120 and gp41 respectively - genes known to harbor a high degree of diversity.

Conclusion:
Here in we've successfully reconstructed the HIV-1 viral haplotypes of 8 transmission pairs. The monophyletic clustering of haplotypes further confirms the pairs. Modeling of the observed haplotypes in both pairs did not reveal any significant indication of stochasticity or selection.

3423

F. Rost[1], S. Schmidt[2], A. Atrott[1], G. Rogler[1], I. Frey-Wagner[1]

Effects of NLRP3 on gut microbiota and murine colitis

Gastroenterology and Hepatology, University Hospital Zurich, Zurich[1], Institute of Molecular Life Sciences, University of Zurich, Zurich[2]

Introduction:
Hypofunctional mutations in the NOD-like receptor pyrin domain containing 3 (*Nlrp3*) locus have been associated with inflammatory bowel disease. However, conflicting results about both a protective and aggravating nature of NLRP3 in experimental murine colitis have been published. We here investigate whether *Nlrp3*-induced changes in gut microbiota composition may be mediating differing colitis outcomes.

Methods:
Nlrp3$^{-/-}$ and wild-type (WT) littermates underwent dextran sodium sulphate (DSS)-induced acute (7 days, 2% DSS) or chronic colitis (4 x 7 days, 1.5% DSS). Colitis severity was evaluated by body weight change, murine endoscopic score of colitis (MEICS), mRNA and protein expression of key cytokines and histologic evaluation of colonic tissue sections. Gut microbiota composition was assessed by 16S rRNA amplicon sequencing of fecal samples collected in a longitudinal manner before colitis induction and from faecal samples and biopsies obtained after DSS-induced colitis.

Results:
Nlrp3$^{-/-}$ mice showed a trend to more severe colitis compared to WT littermates. Surprisingly, we found that mRNA expression of TNF-α and IFN-γ was downregulated in acutely inflamed *Nlrp3*$^{-/-}$ relative to WT mice. However, 16S metagenomics revealed that *Nlrp3*$^{-/-}$ and WT littermates also differed strongly in their gut microbiota composition before and after DSS-colitis.

Conclusion:
Gut microbiota composition and experimental colitis are affected by *NLRP3*. Our results suggest that the distinct gut microbiota of *Nlrp3*$^{-/-}$ mice may be a direct driver of inflammation, despite lower pro-inflammatory cytokine expression. Further experiments with microbiota transfer between genotypes and in animals with a limited defined microbiota will address a causal relationship between gut microbiota composition and colitis outcome. Data mining of the Swiss IBD cohort study (SIBDCS) for patients with differing *NLRP3* polymorphisms and determined gut microbiota composition is currently ongoing to compare and extend the relevance of our findings to the human pathology of inflammatory bowel disease (IBD).

3425

R. Bruckner[1], M. Spalinger[1], G. Rogler[1], M. Scharl[1]

The role for T cells in the pathogenesis of Crohn's disease-associated fistulae

Gastroenterology and Hepatology, University Hospital Zurich, Zurich[1]

Introduction:
Fistulae represent a frequent complication in Crohn's disease (CD). Surgical resection is often required, as medical treatment outcome with conventional drugs is often insufficient. We have previously demonstrated that epithelial-to-mesenchymal transition (EMT) plays a critical role for fistula development. The T cell cytokines tumor necrosis factor (TNF), interleukin (IL)-13, interferon (IFN) γ, IL-17A and IL-22 are highly expressed in transitional cells along fistula tracts in CD patients. Similar to transforming growth factor (TGF) b, TNF is able to induce EMT and the expression of molecules being associated with cell invasiveness and migration. IL-13 has no impact on epithelial cell morphology, but also induces expression of genes being associated with invasive cell growth, such as *SLUG* transcription factor and *b6-integrin*. Here, we analyzed the implication of the T cell-derived cytokines IFNγ, IL-17A and IL-22 in the event of EMT. Moreover, we investigated if there are differences in the composition of lymphocytes in the blood of CD patients suffering from fistulae compared to patients without fistulae or healthy controls.

Methods:
Three-dimensional intestinal epithelial cell (IEC) constructs (spheroids) were stimulated with IFNγ, IL-17A and IL-22 to investigate the effects on EMT development. Further, CD4+ and CD25+ T cells were isolated from fistulizing CD patients' blood or control blood samples and co-cultured together with HT29 cells. Afterwards, mRNA expression levels of EMT-associated genes were analyzed.

Results:
Treatment of the *in vitro* spheroid model with IFNγ resulted in a loss of the well-defined globular spheroid shape after day 7. We observed a clear separation of IECs, while mRNA levels for EMT-related transcription factors like *SNAIL-1* and *ETS-1* were not up-regulated. IL-17A and IL-22 had no effect on cell morphology suggesting that they do not induce EMT in our cell model. On a molecular level, both cytokines had no effect on the mRNA expression of EMT-associated genes, but prevented the TGFb-induced up-regulation of e.g. *SNAIL-1* or *ETS-1*.
The sorting of T cells isolated from blood of CD patients with fistulae revealed an elevated expression level of CD4+ and CD25+ T cells compared to healthy controls.

Conclusion:
Our data demonstrate that T cell derived cytokines may play a crucial role in the pathogenesis of CD-associated fistulae. Th1 cell-derived IFNγ may be involved in the event of EMT in IECs, however Th17 cell-derived cytokines IL-17A and IL-22 are likely not implicated in EMT onset, and may prevent EMT-associated effects of TGFb. This observation supports the hypothesis that Th17 cell-derived cytokines exert a pivotal role for maintaining intestinal homeostasis. The different lymphocyte composition in CD patients' blood represents a further hint for the importance of these cells in fistulae formation.

3426

D. Haralampieva[1], S. Salemi[1], I. Dinulovic[2], T. Sulser[1], S. Ametamey[3], C. Handschin[2], D. Eberli[1]

Genetically modified human muscle precursor cells overexpressing PGC-1? support early myofiber formation in bioengineered muscle tissue

Urology Clinic, University Hospital Zurich, Zurich, Switzerland[1], Biozentrum, Focal Area Growth and Development, University of Basel, Basel, Switzerland[2], ETH, Zurich, Institute of Pharmaceutical Sciences[3]

Introduction:
Muscle precursor cells (MPCs) are quiescent muscle cells capable of muscle fiber reconstruction. Therefore, autologous MPC transplantation is envisioned for the treatment of muscle diseases, many occurring in the aged population. However, density of MPCs, proliferation and differentiation potential gradually decline with age. The goal of this research was to explore the possibility of genetically modifying human MPCs to overexpress the peroxisome proliferator-activated receptor gamma co-activator (PGC-1α) in order to enhance skeletal muscle formation and quality.

Methods:
hMPCs were harvested from M. rectus abdominis of patients undergoing abdominal surgery. After genetically modifying the cells to overexpress PGC-1α (or GFP control), viability, proliferation and myogenic phenotype were evaluated in vitro. The expanded cells were suspended in a collagen carrier and s.c. injected bilaterally on the back of nude mice. One, two and four weeks later the bioengineered skeletal muscle tissues were harvested and further assessed by histology, WB and RTPCR.

Results:
We were able to confirm the sustained myogenic phenotype of the genetically modified hMPCs. Viability and proliferation potential were not significantly different compared to native cells in vitro. Fiber formation capacity and contractility were enhanced in PGC-1α modified hMPCs in vitro. Subcutaneously injected cell-collagen suspensions were harvested after 1, 2 and 4 weeks and histological analysis confirmed the earlier myotube formation in PGC-1α modified samples. Increased contractile protein levels were detected by WB.

Conclusion:
By genetically modifying hMPCs to overexpress PGC-1α we were able to enhance the early myotube formation in vitro and in vivo, thereby developing a novel strategy for improving skeletal muscle tissue engineering.

3427

J. Sim[1], M. Alshamani[1], M. Chatzimichalis[2], C. Röösli[1], M. Huber[1]

Experimental evaluation of new prostheses for tympanoplasty

Deptement of Otorhinolaryngology, Head and Neck Surgery, University of Zürich, Zürich, [1], ENT Department, Dorset County Hospital NHS Foundation Trust, Dorchester[2]

Introduction:
The middle-ear in human ear converts and transmits acoustically-induced sound stimuli to the inner ear. The middle-ear structures can be damaged by various middle-ear pathologies. The damaged middle-ear structures are frequently reconstructed by surgical procedures to rearrange or to replace the impaired middle-ear structures with an implantable prosthesis. Especially, the partial ossicular reconstruction prosthesis (PORP) and total ossicular reconstruction prosthesis (TORP) are used to provide direct connection between the tympanic membrane and the stapes. While such tympanoplasty surgeries are common these days, stable positioning of the prosthesis and reliable connection between the prosthesis and the remaining ossicular structure are still difficult to achieve. Recently, new prostheses have been introduced to provide for flexibility in the surgical procedures and to prevent the potential risk of postoperative dislocation.

Methods:
In this study, four newly-introduced prostheses for tympanoplasty were assessed in cadaveric temporal bones; two PORPs with a ball joint and a notch for placement under the malleus and two supplemental devices for TORP, Omega Connector and TotalOption Connector. All the prostheses were implanted to the temporal bones in sequence, and time for implantation was measured for each of the prostheses. With each of the prostheses implanted, motion of the stapes footplate and the volume displacement at the round window membrane were measured using a laser Doppler vibrometer (LDV). The measured quantities were assessed as the functional outcomes of the surgical reconstruction with the corresponding prosthesis, in comparison with sound transmission in normal ears.

Results:
Preliminary results indicate that middle-ear reconstructions with the newly-developed prostheses resulted in surgical outcomes comparative to normal middle-ear. Further, they provide relatively easy handling of the prostheses during the surgeries and relatively secure connection between the prostheses and the remaining middle-ear structures and thus relatively small risk of postoperative dislocation compared to current prostheses for tympanoplasty.

Conclusion:
The experimental assessments of the new prostheses in cadaveric temporal measurements provide objective ways to predict their functional outcomes and benefits prior to their clinical application.

3428

M. Nuvolone[1], M. Hermann[2], S. Sorce[1], G. Russo[3], C. Tiberi[1], P. Schwarz[1], E. Minikel[4], D. Sanoudou[5], P. Pelczar[6], A. Aguzzi[1]

Strictly co-isogenic C57BL/6J-Prnp knockout mice: a rigorous resource for prion science

Institute of Neuropathology, University Hospital of Zurich, Zurich, Switzerland[1], Institute of Laboratory Animal Science, University of Zurich, Zurich, Switzerland; Institute of Neuropathology, University Hospital of Zurich, Zurich, Switzerland[2], Functional Genomic Center Zürich, University Zurich/ETHZ, Switzerland[3], Prion Alliance, Cambridge, MA, USA; Broad Institute, Cambridge, MA, USA; Analytical and Translational Genetics Unit, Massachusetts General Hospital, Boston, MA, USA[4], 4th Department of Internal Medicine, Attikon Hospital, Medical School, University of Athens, Athens, Greece[5], Institute of Laboratory Animal Science, University of Zurich, Zurich, Switzerland[6]

Introduction:
While its involvement in prion replication and neurotoxicity during transmissible spongiform encephalopathies is undisputed, the physiological role of the cellular prion protein (PrP^C) remains enigmatic. A plethora of functions have been ascribed to PrP^C based on phenotypes of *Prnp*$^{-/-}$ mice. However, all currently available *Prnp*$^{-/-}$ lines were generated in embryonic stem cells from the 129 strain of the laboratory mouse and mostly crossed to non-129 strains. Therefore, *Prnp*-linked loci polymorphic between 129 and the backcrossing strain resulted in systematic genetic confounders and led to erroneous conclusions

Methods:
We used TALEN-mediated genome editing in fertilized mouse oocytes to create the Zurich-3 (ZH3) *Prnp*-ablated allele on a pure C57BL/6J genetic background.

Results:
Genomic, transcriptional, and phenotypic characterization of *Prnp*$^{ZH3/ZH3}$ mice failed to identify phenotypes previously described in non-coisogenic *Prnp*$^{-/-}$ mice. However, aged *Prnp*$^{ZH3/ZH3}$ mice developed a chronic demyelinating peripheral neuropathy, confirming the crucial involvement of PrP^C in peripheral myelin maintenance.

Conclusion:
This new line represents a rigorous genetic resource for studying the role of PrP^C in physiology and disease MN and MH contributed equally to this work.

3429

M. Nuvolone[1], S. Sorce[1], P. Pelczar[2], E. Rushing[1], F. Lavatelli[3], G. Palladini[3], G. Merlini[3], A. Aguzzi[1]

Generation of a conditional transgenic mouse model of immunoglobulin light chain (AL) amyloidosis

Institute of Neuropathology, University Hospital of Zurich, Zurich, Switzerland[1], Institute of Laboratory Animal Science, University of Zurich, Zurich, Switzerland[2], Amyloidosis Research and Treatment Center, Foundation Scientific Institute San Matteo, Department of Molecular Medicine, University of Pavia, Pavia[3]

Introduction:
Immunoglobulin light chain (AL) amyloidosis is a plasma cell dyscrasia characterized by the systemic deposition of monoclonal immunoglobulin light chains in form of amyloid fibrils, leading to tissue damage and organ dysfunction. The molecular mechanisms underlying AL amyloidosis remain elusive, in part due to the paucity of reliable animal models. Generation of transgenic mice overexpressing human amyloidogenic light chains (aLC) is technically hampered by the intrinsic toxicity of these proteins, which could result in embryolethality or selection against high expressor lines. To overcome this limitation, we aimed at generating a conditional transgenic mouse in which the expression of a human aLC can be regulated in a spatial and temporal manner using the Cre-loxP system.

Methods:
The cDNA encoding a human aLC was sub-cloned in the 3' region of an expression vector consisting (5'→3') of a ubiquitous promoter and a reporter gene-stop cassette flanked by two loxP sites. Transgenic mice obtained by pronuclear injection were crossed with mice expressing the Cre recombinase under the albumin promoter (Alb-cre) to activate the expression of aLC in hepatocytes.

Results:
Transgenic mice obtained by pronuclear injection showed ubiquitous expression of the reporter gene, but no expression of the human aLC, as expected. Crossing with Alb-cre resulted in the generation of mice with hepatocyte-restricted expression of aLC and detectable serum levels of aLC. Mice are in follow up for the identification of amyloid deposits and phenotypic abnormalities.

Conclusion:
We have generated a transgenic mouse in which the expression of aLC can be activated in a regulated manner. In mice with hepatocyte-restricted expression of aLC, all target organs (except the liver) are exposed to aLC coming only from the circulation, resembling the clinical situation. Additional cre transgenic lines, including tamoxifen-inducible ones, can be used to further manipulate the temporal and spatial pattern of human aLC expression. This newly developed conditional transgenic mouse could prove instrumental to deepen our current mechanistic understanding of AL amyloidosis.

3430

E. Bellini[1], N. Valtcheva[1], C. Stirnimann[2], M. Busquets Lopez[2], B. Bodenmiller[3], I. Frew[4], P. Wild[1]

Identification of the molecular drivers of endometrial cancer progression

Institut für Klinische Pathologie, UniversitätsSpital, Zürich[1], NEXUS Personalized Health Technologies, ETH Zürich, Zürich[2], Institut für Molekulare Biologie, Universität Zürich, Zürich[3], Physiologisches Institut, Universität Zürich, Zürich[4]

Introduction:
Endometrial carcinoma is the most common malignancy of the female genital tract. The characterization of tissue microarrays (TMAs) containing a very large cohort of human endometrial cancer tissues showed that, although PI3K-mTOR pathway activation and TP53 inactivation play different roles in the initiation of different endometrial cancer subtypes, co-occurring alterations in both signaling pathways represent a frequent unifying pathogenic feature of late stage tumors of all subtypes.

Methods:
Our aim is to identify and functionally assess the role of the proteins crucial for the survival of endometrial cancer cells with the aforementioned molecular signature. For this purpose, we designed a PI3K pathway-dependent synthetic lethality screen using RNAi technology and used TALEN (TAL-effector nuclease) genome editing tool to knock-out *PTEN* (an important inhibitor of the PI3K pathway) in *TP53*$^{-/-}$ endometrial carcinoma cell lines.

Results:
The signaling pathways of the identified targets will be further investigated in cell culture and in vivo experiments targeting the corresponding proteins. To confirm the aberrations critical for disease progression and assign them to each step of endometrial cancer development, we will further investigate the obtained results using the samples of our large human TMA cohort.

Conclusion:
Ultimately, this approach aims at using the knowledge gained from the cell culture model to decipher mechanisms commonly involved in the progression of the endometrial cancer of patients. The final goal is to characterize new prognostic and potentially predictive markers for improving personalized molecular diagnosis and treatment.

3431

C. Zhu[1], U. Herrmann[1], J. Falsig[1], I. Abakumova[1], M. Nuvolone[1], P. Schwarz[1], E. Rushing[1], A. Aguzzi[1]

A neuroprotective role for microglia in prion diseases

Institute of Neuropathology, University Hospital of Zurich, Zurich, Switzerland[1]

Introduction:
Prion diseases are progressive neurodegenerative disorders associated with striking microglial activation. Microglial activation occurs at an early stage of the disease and is found in areas of proteinase K-resistant prion protein (PrP^{Sc}) deposition. The presence of high prion infectivity in microglia suggests that microglia may disseminate prions within the central nervous system. In addition, the cytokines produced by activated microglia may contribute to progression of the disease. In contrast, microglia are also professional phagocytes and can engulf and degrade PrP^{Sc}. Indeed, microglial depletion from RML6-infected CD11b-HSVTK cerebellar organotypic cultured slices (COCS) results in increased deposition of PrP^{Sc} and augmented prion titers, indicating that microglia play an important role in prion clearance. Nevertheless, due to the dearth of appropriate animal models, the exact role of microglia in prion pathogenesis remains unknown.

Methods:
We first pharmacogenetically ablated microglia ex vivo by ganciclovir (GCV) treatment on tga20/CD11b-HSVTK COCS and examined prion-induced neurotoxicity. We also assessed prion pathogenesis in tga20/CD11b-HSVTK mice after GCV-mediated microglia depletion in vivo. Additionally, we applied an independent genetic model $IL34^{-/-}$ mice, which have a reduced number of microglia, to determine the effect of prion deficiency on prion pathogenesis.

Results:
We found that GCV-mediated microglia ablation on tga20/CD11b-HSVTK drastically enhanced the neurotoxicity of prions ex vivo and shortened the lifespan of prion infected mice. In $IL34^{-/-}$ mice, we found enhanced PrP^{Sc} deposition and accelerated prion progression compared to wild-type littermates.

Conclusion:
These results indicate that microglia play an overall protective rather than deleterious role in prion disease.

3432

D. Kirschenbaum[1], D. Laptev[2], O. Bichsel[1], J. Buhmann[2], A. Aguzzi[1]

CRYSTAL & HITS: a new methodology for whole-mount mouse brain imaging

Institute of Neuropathology, University Hospital Zürich[1], Institute of Machine Learning, Department of Comupter Science, ETH Zurich[2]

Introduction:
Morphological information from biological tissue at cellular resolution was based on classical histology in the past 150 years, until recently. Classical histology refers to a series of methods by which tissue is fixed, processed, embedded, sliced and stained, followed by microscopic detection. The backbone of this approach is slicing; this is because tissue is not transparent and as such not accessible to microscopy past a shallow depth. This problem is addressed by tissue clearing, which by homogenizing the refractive indices between cell membranes and water, transparentizes tissue. This process enables deep imaging without slicing. Recently, multiple methods arose providing tissue clearing approaches. Clearing techniques either require a long time, quench fluorescence, or are difficult to implement. A further challenge is to achieve a uniform and specific molecular labelling in whole-mount tissue.

Methods:
We developed a clearing technique of unprecedented rapidity and user-friendliness based on the CLARITY method, which we termed CRYSTAL. We further developed a technology for rapid staining of whole-mount tissue, which we termed HITS.

Results:
These two combined methods allowed us to transparentize and stain whole mouse brains within a matter of hours. Later, we imaged cleared whole brains with light-sheet microscopy within minutes. Here we show the power of this method by rapidly clearing and staining the brains of APP/PS1 transgenic mice. These mice develop β-amyloid plaques (AβP), resembling one of the pathologic hallmarks of Alzheimer's disease (AD). By clearing and staining these brains we were able to count the total amount of AβP with a custom-designed computer algorithm. Additionally, we segmented the images into microanatomical regions and provided exact numbers of AβP frequencies in various brain regions.

Conclusion:
In summary, we present a combined methodology for high-throughput whole-mount tissue clearing, staining and imaging.

3433

M. Pfaltz[1], T. Wingenbach[2], C. Mueller-Pfeiffer[1], K. Hassanpour[1], M. Plichta[1], M. Rufer[1], U. Schnyder[1]

Emotion Recognition in Traumatized Individuals with and without Posttraumatic Stress Disorder: A Psychophysiological Study

Department of Psychiatry and Psychotherapy, University Hospital Zurich, Zurich[1], Department of Psychology, University of Bath, United Kingdom[2]

Introduction:
Previous research has shown that individuals with posttraumatic stress disorder (PTSD) have difficulties recognizing facial emotional expressions. We aimed at replicating these previous findings. Moreover, we assessed if dissociative symptoms and suppression of one's facial expressions (expressive suppression, ES) affect the hypothesized emotion recognition (ER) deficits in PTSD.

Methods:
Participants with PTSD, non-traumatized healthy controls (HC) and traumatized healthy controls (TC) were watching 300 one-second movies showing emotional facial expressions and indicated which of 10 emotions were presented in each movie. ES during this task was assessed by the emotion regulation questionnaire (Gross & John, 2003) and by facial electromyography (EMG). Dissociative symptoms and potentially associated, autonomic changes occurring during the task were assessed by questionnaires (e.g., Dissociation Tension Scale – acute, Stiglmayr et al., 2009) and by changes in heart rate, respiratory sinus arrhythmia, and electrodermal activity.

Results:
Unexpectedly, preliminary analyses (PTSD: n=29; HC: n=28; TC: n=34) showed no ER deficits in individuals with PTSD. Yet, we found a significant number of experienced trauma types (0, 1-2, 3+) x emotions (pos vs. neg) interaction ($F=3.7$, $p=.028$): Across study groups, higher numbers of traumas were related to better recognition of neg emotions (anger, fear, disgust, contempt) and poorer recognition of pos emotions (happiness, pride). Reaction times to the presented movies were longer in participants reporting high vs. low rates of childhood physical abuse ($F=5.4$, $p = .022$) and in participants reporting high vs. low rates of emotional neglect ($F=11.6$, $p=.001$). These effects were unaffected by study group. PTSD patients tended to show more pronounced ES than the control groups. This was, however, only the case for self-report but not for EMG data (i.e., facial mimicry as assessed by EMG was comparable between study groups), and both self-reported and facial mimicry measures of ES were unrelated to ER. Self-reported dissociative symptoms were unrelated to autonomic changes and to ER abilities.

Conclusion:
Processing and recognition of emotional expressions may thus be related to (childhood) trauma, rather than to diagnoses of PTSD and trauma history may differentially impact recognition of pos vs. neg emotions. Previous self-reports of ES in PTSD could not be objectified by physiological measures. We will discuss clinical and methodological implications.

3434

O. Hasan Ali[1], R. Higgins[2], H. Cheng[3], F. Hartmann[3], S. Ring[3], L. French[2], A. Navarini[2], L. Flatz[1]

Systematic Genomic Analysis for the Detection of Mutations in a Patient Suffering from Multiple Basal Cell Carcinomas and Palmoplantar Punctate Keratoderma

Department of Dermatology and Allergology, Cantonal Hospital of St. Gallen, St. Gallen[1], Dermatology, University Hospital, Zurich[2], Institute of Immunobiology, Cantonal Hospital Hospital St.Gallen, St.Gallen[3]

Introduction:
Basal cell carcinoma (BCC) is a slow-growing skin tumor and considered the most common overall tumor. The most important external risk factor is cumulative sun exposure. Risk groups are Caucasians, the elderly (>60y) and fair skin types (Fitzpatrick's classification I and II). Incidences in younger people should prompt further investigation for a genetic predisposition, e.g. Nevoid Basal Cell Carcinoma Syndrome (NBCCS).
We present a 58-year-old patient with skin type II (Fitzpatrick) who is regularly seen in our clinic for BCC excision on sun and non-sun exposed sites. The first BCC appeared in his 40s. Family history is positive for multiple BCCs (brother). A skin exam showed palmoplantar punctate hyperkeratosis. His medical history revealed odontogenic cysts in the past. Both punctate hyperkeratosis and odontogenic cysts also affect some of his siblings.
Due to the symptoms mentioned above, we suspect a hereditary mutation predisposing him and possibly his siblings to BCC formation. This suspicion prompted us to conduct a genetic investigation.

Methods:
We extracted DNA from Peripheral Mononuclear Blood Cells (PBMCs) from our patient and his siblings as well as from a BCC-tissue sample from our patient. DNA sequencing is performed via Whole Exome Sequencing (WES, unbiased approach). Additionally, we carry out Sanger sequencing on validated BCC-associated genes, such as PTCH and WNT (directed approach). Validated reference sequences are being obtained via publicly accessible databases, such as NCBI and COSMIC. Geneious genomics software is being used for sequence analysis. Additional software, e.g. CEQer for copy number recognition, may be employed at a later stage.

Results:
Unlike conventional Sanger Sequencing, Whole Exome Sequencing permitted us to analyze not only specific, but all exons. We present the new genetic mutations in our index case and compare it with his own tumor sample and siblings. We confirm the mutations using Sanger sequencing.

Conclusion:
These data are of particular interest as BCCs have been described to be the most mutated tumors known so far. Past and recent studies strongly suggest that mutated genes in the hedgehog pathway play a crucial role in BCC genesis, and genes other than PTCH can be involved, such as SUFU and GLI. Also, genes on other loci, e.g. p53, are have been described to play an important role. Yet, PTCH is the most common candidate and was the first to be identified as a cause for NBCCS in 1996. PTCH protein inhibits Smoothened protein (SMO). If PTCH is dysfunctional, SMO is constantly active, which downstream can induce BCC formation.
The variety of PTCH-mutations is very high and if one limits the investigation to mutations found only in BCC tissue and not PBMCs it is not possible to discern an inherited from a somatic mutation. To avoid this pitfall we are comparing the DNA from the patient's tumor (highly mutated), his own DNA and that of his siblings we can single out inherited mutations. Inherited mutations can act as a first hit in Knudsens two hit hypothesis and, when genes in the Hedgehog pathway are affected, render one prone to BCC development. Describing and listing inherited mutations leading to BCCs may, in future, aid genetic risk screening assays and improve our understanding of the role of those mutations in BCC genesis.

3435

C. Röösli[1], S. Sim[1], I. Dobrev[1], F. Pfiffner[1], S. Stenfelt[2], A. Huber[1]

Interaction between osseous and non-osseous vibratory stimulation of the human cadaveric head

Department of Otorhinolaryngology, Head and Neck Surgery, University Hospital Zurich[1], Department of Clinical and Experimental Medicine, Linköping University, Linköping, Sweden[2]

Introduction:
Bone conduction (BC) is an alternative way to stimulate the cochlea. It can be applied by vibration to the bony or skin covered skull (osseous BC), or on soft tissue such as the neck (non-osseous BC). The interaction between osseous and non-osseous bone conduction pathways is assessed in this study.

Methods:
The relation between bone vibrations measured at the cochlear promontory with a Laser Doppler Vibrometer (LDV) and the intracranial sound pressure measured with a hydrophone for stimulation directly on the dura and for stimulation at the mastoid between 0.2 – 10 kHz was compared. The coupling force at the dura for the BC vibrator was varied. The measurements were performed with intracranial fluid absent or present.

Results:
First, for stimulation on the dura, varying the static coupling force of the BC transducer on the dura had only a small effect on promontory vibration. Second, the presence or absence of intracranial fluid did not affect promontory vibration for stimulation on the dura. Third, stimulation on the mastoid elicited both promontory vibration and intracranial sound pressure. Stimulation on the dura caused intracranial sound pressure to a similar extent above 0.5 kHz compared to stimulation on the mastoid, while promontory vibration was less by 20-40 dB.

Conclusion:
From these findings, we conclude that intracranial sound pressure (non-osseous BC) only marginally affects bone vibrations measured on the promontory (osseous BC), whereas skull vibrations affect intracranial sound pressure.

3436

H. Wirsching[1], J. Tonn[2], G. Tabatabai[1], C. Senft[3], P. Hau[4], M. Sabel[5], U. Herrlinger[6], R. Ketter[7], U. Schlegel[8], C. Marosi[9], G. Reifenberger[10], W. Wick[11], M. Weller[1], B. Suchorska[2]

Complete resection of contrast enhancing tumor volume is associated with improved survival in recurrent glioblastoma – results from the DIRECTOR trial

Dept. of Neurology, University Hospital Zurich, Switzerland[1], Dept. of Neurosurgery, Ludwig-Maximilians University Munich, Germany[2], Dept. of Neurosurgery, University Hospital Frankfurt am Main, Germany[3], Dept. of Neurology, University Hospital Regensburg, Germany[4], Dept. of Neurosurgery, University Hospital Duesseldorf, Germany[5], Dept. of Neurology, University Hospital Bonn, Germany[6], Dept. of Neurosurgery, University Hospital Saarland, Homburg/Saar, Germany[7], Dept. of Neurology, Knappschaftskrankenhaus Bochum, Germany[8], Dept. of Oncology, Vienna General Hospital, Austria[9], Institute of Neuropathology, University Hospital Duesseldorf, Germany[10], Dept. of Neurology, University Hospital Heidelberg, Germany[11]

Introduction:
The role of reoperation for recurrent glioblastoma remains unclear. Prospective studies are lacking. Here, we studied the association of clinical outcome with extent of resection upon surgery for recurrent glioblastoma in the patient cohort of DIRECTOR, a prospective randomized multicenter trial comparing two dose-intensified temozolomide (TMZ) regimens at first recurrence of glioblastoma.

Methods:
We analyzed prospectively collected clinical, molecular and imaging data from the DIRECTOR cohort (N=105). Volumetric analysis was performed on gadolinium (Gd)-enhanced as well as FLAIR/T2 MRI and correlated with progression-free survival after initial progression (PFS_2) and post recurrence-survival (PRS). Quality of life (QoL) was monitored by EORTC QLQ-C30 and QLQ-BN20 in 8-weekly intervals.

Results:
Seventy-one patients received surgery at first recurrence. Prognostic factors were balanced between patients with and without reoperation, including age (p=0.495), O6-methylguanine-DNA-methyltransferase (*MGMT)* promoter methylation (p=0.965), time to first progression (PFS_1, p=0.366), tumor volume at recurrence (p=0.234), Karnofsky performance score (KPS) (p=0.880) and steroid intake (p=0.797) at study entry. Outcome in patients with versus without surgery at recurrence was similar for PFS_2 (2.0 months versus 1.9 months, p=0.360) and PRS (11.4 months versus 9.8 months, p=0.633). Among patients who underwent reoperation, post-surgery imaging was available in 59 cases. In these patients, complete resection of Gd-enhanced tumor (N=40) versus residual detection of Gd-enhancement (N=19) was associated with improved PRS (12.9 months [95% CI 11.5-18.2] versus 6.5 months [95% CI 3.6-9.9], p<0.001) and better QoL. Incomplete tumor resection was associated with inferior PRS compared to patients who did not undergo surgery (6.5 versus 9.8 months, p=0.052). QoL was similar in these two groups.

Conclusion:
Surgery at first recurrence of glioblastoma improves outcome if complete resection of Gd-enhanced tumor is achieved.

Reference:
Bogdana Suchorska, Michael Weller, Ghazaleh Tabatabai, Christian Senft, Peter Hau, Michael C. Sabel, Ulrich Herrlinger, Ralf Ketter, Uwe Schlegel, Christine Marosi, Guido Reifenberger, Wolfgang Wick, Jörg C. Tonn, Hans-Georg Wirsching for the DIRECTOR study group. Neuro-Oncology (2016), in press

3437

J. Woytschak[2], N. Keller[3], D. Impellizzieri[2], R. Thompson[1], T. Wynn[1], A. Zinkernagel[3], O. Boyman[2]

Type II IL-4 receptor expression on neutrophils antagonizes their expansion and migration during infection and inflammation

Laboratory of Parasitic Diseases, National Institutes of Health, Bethesda[1], Department of Immunology, University Hospital Zurich, Zurich[2], Department of Infectious Diseases, University Hospital Zurich, Zurich[3]

Introduction:
Neutrophils are the first immune cells recruited to sites of inflammation and infection. This is a multistep process including vigorous *de novo* generation, proliferation and maturation of neutrophil precursors in the bone marrow, followed by their release as mature neutrophils to the bloodstream. However, patients with allergic disorders such as atopic dermatitis show a paucity of skin neutrophils and are prone to bacterial skin infections, suggesting that allergic 'type-2' inflammation might curtail neutrophil responses. Given that interleukin (IL)-4 is instrumental in initiating, polarizing and maintaining type-2 immunity, these findings beg the question whether IL-4 signals directly affect neutrophil expansion, migration or function.

Methods:
Mice were infected either systemically with 10^5 cfu *Listeria monocytogenes* or subcutaneously with $3x10^7$ cfu Group A *Streptococcus* M1 and analyzed for bacterial load in different organs or their survival. Animals received PBS, cytokine/anti-cytokine monoclonal antibody (mAb) complexes of granulocyte colony-stimulating factor (G-CSF) or IL-4, or neutralizing mAb against G-CSF or IL-4 prior infection. $CD11b^+$ $Ly6G^+$ neutrophils, isolated from skin, bone marrow, spleen and blood, were analyzed for their frequencies and receptor expression by multicolor flow cytometric analysis. This technique was further used to assess STAT6 or p38 MAPK phosphorylation in neutrophils upon IL-4 stimulation. Neutrophil migration was evaluated *in vitro* by using a transwell migration assay and *in vivo* in an airpouch model.

Results:
We show that the type-2 signature cytokine IL-4 hampers neutrophil expansion and migration by antagonizing G-CSF and chemokine receptor-mediated signals. Cutaneous bacterial infection in mice was exacerbated by IL-4 signaling and improved when IL-4 was blocked, with each outcome inversely correlating with neutrophil migration to skin. Likewise, systemic bacterial infection was worsened by heightened IL-4 activity, with IL-4 restricting G-CSF-induced neutrophil expansion in and migration from bone marrow to tissues by disrupting CXCR2–CXCR4 chemokine signaling in neutrophils. These effects were dependent on IL-4 acting through type II IL-4 receptors (consisting of IL-4Ralpha and IL-13Ralpha1) on neutrophils, inducing thereby p38 MAPK phosphorylation.

Conclusion:
By showing a direct action of IL-4 on neutrophils via type II IL-4Rs we extend the range of target cells of IL-4 and also demonstrate that type II IL-4Rs can become very prominent on immune cells and potently affect their responses during immunity and immunopathology.
The therapeutic implications are manifold and could find relevance in various allergic disorders. For example, skin of patients with atopic dermatitis contains more IL-4 and lower counts of neutrophils and is more susceptible to bacterial infections that are usually contained by neutrophils. Thus, therapeutic approaches targeting IL-4Ralpha, IL-13Ralpha1 or p38 MAPK might lower the risk of recurrent bacterial infections.

3438

D. Barthelmes[1], S. Zweifel[1], C. Böni[1], M. Marti[1]

Treatment outcomes in eyes treated for choroidal neovascularization secondary to pathologic myopia using vascular endothelial growth factor inhibitors

Department of Ophthalmology, University Hospital, Zurich[1]

Introduction:
To report 12 month treatment outcomes in eyes treated for choroidal neovascularization secondary to pathologic myopia (mCNV) using ranibizumab or bevacizumab.

Methods:
Observational longitudinal study using anonymized data from patients treated for mCNV. Visual acuity (VA) was recorded at each visit using the logarithm of the Minimum Angle of Resolution (logMAR) letter score. For each treated eye an index visit was defined as the visit when treatment for mCNV was commenced. Visual acuity, mCNV lesion activity and treatment given were recorded for each follow-up visit. Decision to treat was made by the treating physician, thus reflecting daily clinical practice. Eyes included were treatment naïve and were required to have at least 12 months of follow-up and no concomitant conditions. VA at the index visit was compared with 12 months after start of treatment. Treatment intensity during 12 months as well as state of mCNV lesion activity at 12 months were analyzed.

Results:
A total of 34 eyes were included. In 22 eyes ranibizumab was used, in 12 eyes bevacizumab. Index VA in all eyes was 50.1±18.5 logMAR letters. About 64.7% were female. During 12 months 4.1±2.4 treatments were administered. Mean VA improved to 59.8±22.1 logMAR letters, representing a +9.7 letter change. Twelve months after start of treatment, 17% still had active mCNV requiring ongoing treatments.

Conclusion:
Treatment of mCNV in clinical practice using vascular endothelial growth factor inhibitors results in favorable outcomes.

3439

V. Strouvelle[1], V. Vongrad[1], K. Metzner[1], H. Günthard[1]

Quantification of different HIV-1 genomic forms to characterize the viral reservoir

Infectious Diseases and Hospital Epidemiology, University Hospital Zurich, Zurich[1]

Introduction:
The HIV-1 latent reservoir is a major barrier to eliminating HIV-1 as it is responsible for the persistence of HIV-1 in patients on effective antiretroviral treatment (ART). Thus, patients have to remain on ART life-long. For this reason, characterization of the viral reservoir is necessary as important questions still need to be answered, such as, is there low level replication ongoing in patients on ART? And can the reservoir be altered with the addition of different treatments?

Methods:
To assess the stages of HIV-1 replication in patients on ART, qPCR assays for various forms of the HIV-1 genome were established to measure a broad spectrum of HIV-1 DNAs and RNAs including proviral DNA, non-integrated DNA, unspliced, multiple- and singularly spliced mRNAs, all of them markers for different stages of the HIV-1 life cycle. An all-in-one standard was generated including all those viral genome forms and nominators (CCR5 and GAPDH) on one DNA fragment, eliminating the need for multiple standards and consequential higher variances.

Results:
The qPCR assays have a detection limit of 10 HIV-1 DNA/cDNA copies/reaction, with a linear dynamic range of >6 logs. The assays were validated with a time course experiment using HIV-1 infected cell cultures. As expected, multiple spliced RNA forms emerged first, followed by the other genomic forms. Proviral DNA and 2-LTR circular DNA could both be detected in the expected ratio as well.

Conclusion:
This elaborated panel of quantifiable HIV-1 genomic forms will allow us to characterize the latent reservoir in patients.

3440

Y. Chang[1], M. Ziegler[1], D. Ignatova[1], K. Kerl[1], L. French[1], A. Cozzio[1], E. Guenova[1]

Resistance to antibody-dependent cellular cytotoxicity impairs antitumor activity of Rituximab in a CD20+ mycosis fungoides

Department of Dermatology, UniversitätsSpital Zurich[1]

Introduction:
Anti-CD20 antibodies are well established in the treatment of CD20 positive B cell malignancies, antibody dependent cellular cytotoxicity being a major mode of action. Based on these observations, we initiated an anti-CD20 targeted systemic therapy with Rituximab in a highly aggressive, resistant to treatment $CD4^{-}CD20^{+}$ tumor stage mycosis fungoides.

Methods:
A standard therapeutic regiment of Rituximab, as established for the treatment of B cell lymphoma was chosen, and a total of 4 treatment cycles were initially planned.

Results:
Against our expectations, no clinical response could be observed, but rather further progression of the mycosis fungoides with enlargement of the preexisting and development of new mycosis fungoides lesions. Reevaluation after the third cycle Rituximab revealed complete loss of the aberrant CD20 expression on the malignant T cells, and the treatment was discontinued. Moreover, laboratory analysis showed impaired antibody-dependent cellular cytotoxicity not only in the rituximab-treated $CD20^{+}$ mycosis fungoides, but in patients with advanced leukemic CTCL disease in general. After a short follow-up period and additional treatment with liposomal doxorubicin, the patient deceased.

Conclusion:
Our result suggests that CD20 has no therapeutic implication when aberrantly expressed by neoplastic T cell in mycosis fungoides.

3441

D. Ignatova[1], Y. Chang[1], E. Contassot[1], T. Mehra[2], V. Mitev[3], R. Dummer[1], L. French[1], W. Hoetzenecker[1], A. Cozzio[1], E. Guenova[1]

Expression of CD164 on malignant T cells in Sézary Syndrome

Department of Dermatology, University Hospital of Zurich, Zurich[1], Medical Directorate, University Hospital of Zürich, Zurich[2], Department of Medical Chemistry and Biochemistry, Medical University, Sofia[3]

Introduction:
Sézary syndrome is a primary cutaneous T cell lymphoma characterized by pruritic erythroderma, peripheral lymphadenopathy, and the presence of malignant T cells in the blood. Unequivocal detection of malignant cells in Sézary Syndrome patients is of important diagnostic, prognostic and therapeutic value and is essential for disease monitoring under treatment. However, a single Sézary syndrome specific cell surface marker has not yet been identified.

Methods:
Flow cytometry: Peripheral blood mononuclear cells (PBMC) were isolated by Ficoll centrifugation. Analysis of T cells was performed using monoclonal antibodies against human CD3 (clone BW264/56, label PerCP; Miltenyi Biotec #130-096-910), CD4 (Clone VIT4; label APC-Vio770; Miltenyi Biotec # 130-098-153), CD26 (Clone BA5b, label PE-Cy7, # 302714, BioLegend) and CD164 (clone N6B6; label FITC; BD Biosciences #551297). Isotype-matched negative control antibodies were used to set the gates for positive staining. Vβ clonal T cell population was assessed by flow cytometry using the IOtest Beta Mark TCR Vβ Repertoire kit (Beckman Coulter). Analysis was performed on Becton Dickinson FACSCanto instruments and data were analyzed using FCS Express 5 Flow Cytometry RUO and Origin Pro 9.1G Software.

Results:
In a cohort of Sézary syndrome patients, CD164 expression on total $CD4^+$ lymphocytes was significantly upregulated compared to healthy controls. CD164 expression was in most cases limited to $CD4^+CD26^-$ malignant T lymphocytes, unequivocally flow-cytometrically identified by the expression of a specific Vβ clone for each patient.

Conclusion:
Increased expression of CD164 may be a promising diagnostic parameter and a potential target for a CD164-linked therapeutic approach in Sézary syndrome.

3442

Y. Zarb[1], T. Jones[1], S. Dias[1], A. Keller[1]

The role of oxidative stress in cerebral microvascular calcification

Department of Neurosurgery, University Hospital Zurich, Switzerland [1]

Introduction:
Primary familial brain calcification (PFBC) is a rare neurodegenerative disease in humans, which exhibits an autosomal dominant inheritance. Clinical manifestations are variable (e.g. parkinsonism, dementia), however, all patients present with bilateral brain calcifications. The pathogenic mechanism of PFBC is unknown, but several autopsy studies point to microvascular insufficiency. Although PFBC is a rare disease, brain calcifications are a common CT finding, and vascular dysfunction is the second cause of dementia after Alzheimer's disease. Thus insights into PFBC will aid in better understanding vessel-associated calcification in the brain. Loss of function of platelet-derived growth factor-B (PDGFB) and its receptor PDGFRβ, are associated with PFBC. Moreover, mouse hypomorphic PDGFB mutants develop brain calcifications similar to human PFBC patients, making it a good PFBC mouse model. Oxidative stress is caused by elevated levels of reactive oxygen species (ROS), which can be caused by normal physiological function but has also been implicated in various pathologies, such as inflammation, cancer and ageing. Nicotinamide adenine dinucleotide phosphate (NADPH) oxidase (NOX) proteins are generators of ROS. There are four isoforms; NOX 1, 2, 3, 4 and these proteins have been implicated in the process of atherosclerosis, the calcification of vascular smooth muscle cells. PDGF-BB signaling has been linked to oxidative stress, although studies are in conflict over its role. In addition, transcriptional data from isolated brain microvessels from PDGFB hypomorphs and controls provide evidence that genes implicated in redox balance have a deregulated expression. Given this, we are investigating the role of oxidative stress in a PFBC mouse model to better understand the underlying mechanism.

Methods:
In this study, we employ mouse hypomorphic PDGFB mutants and NOX2 null mice, to investigate the role oxidative stress plays in cerebral microvascular calcification. We also investigate protein, lipid and DNA damage in these transgenic mice using immunohistochemical and Western blot analysis.

Results:
Our preliminary results indicate that changes in oxidative stress levels modulate the formation of vessel-associated calcifications in the brain.

Conclusion:
These insights provide a better understanding of the mechanism underlying vessel-associated brain calcifications and pave the way to future experiments exploring potential therapeutic strategies.

3443

M. Pfammatter[1], M. Andreasen[2], G. Meisl[2], J. Adamcik[3], R. Mezzenga[3], T. Knowles[2], A. Aguzzi[1], S. Hornemann[1]

Digital amyloid amplification assay for the ultrasensitive quantification of amyloid aggregates

Institute of Neuropathology, University Hospital of Zurich, Zurich, Switzerland[1], Department of Chemistry, University of Cambridge, Cambridge, United Kingdom[2], Department of Health Sciences and Technology, ETH Zurich, Zurich, Switzerland[3]

Introduction:
The peptide hormone insulin which can be recombinantly produced as therapeutic protein for the treatment of Diabetes patients is prone to aggregation. Its tendency to aggregate raises major problems in pharmaceutical production and drug formulation which can lead to both high production costs and complications in patients. Validation assays for the sensitive detection of early aggregated states in recombinant insulin preparations are therefore of high interest to guarantee high product quality and stability. To address this need, we have developed an innovative, digital amyloid amplification assay for the ultrasensitive detection and quantification of early aggregated states of insulin.

Methods:
We exploit the property of amyloid fibrils to propagate their fibrillar conformation to monomeric proteins for the establishment of a conversion assay, in which selective amplification of preformed amyloid fibrils allows to sensitively detect minute quantities of fibrils. Therefore, monomeric substrate protein is mixed with the sample to be analysed for the number of “propagons” (defined as the minimal propagating unit of amyloid fibrils) and partitioned into several parallel reactions for propagon-catalysed amplification. Endpoint amplification in every reaction leads to *de novo* formation of aggregates in the propagon-containing reactions, which can be followed by Thioflavin T fluorescence. Fluorescence positive and negative reactions are counted. By performing serial limiting dilutions of the test sample and applying Poisson statistics the absolute number of propagons present in the test sample is quantified.

Results:
In a first step, we established the assay in a bulk 384-well microplate format. We performed an intense experimental condition screen to identify conditions that promote propagon-catalysed aggregation while suppressing spontaneous aggregation of insulin monomers. Under the identified optimal conditions the assay is capable to detect single propagating units of insulin fibrils, which allowed us to precisely quantify the absolute number of propagons in the test sample. To improve the precision and accuracy of the assay, we transferred the assay to a microfluidics platform to miniaturize the assay to nanoliter volumes and to run several 1000 of parallel reactions. We found similar assay sensitivity and precision as for the bulk assay, but a significant reduction in false-positive, spontaneously aggregating reactions. Both assays show a good correlation, revealing a similar number of propagons present in a test sample. Moreover, we could demonstrate that the number of propagons determined by their biological activity correlates well with the number of propagons determined by quantitative atomic force microscopy, suggesting that almost each aggregate in our test sample is biologically active.

Conclusion:
Our newly developed digital amyloid amplification assays allow for the highly sensitive amplification and detection of minimal amounts of aggregates, thereby reaching a sensitivity of detecting single propagating amyloid units. Due to similarities in the aggregation mechanism of insulin and other amyloidogenic proteins involved in protein misfolding and aggregation diseases, such as Alzheimer’s, Parkinson or prion disease, the assay raises the hope for the development of a highly sensitive and accurate diagnostic test for these diseases.

3445

V. Vongrad[1], C. Von Siebenthal[1], H. Günthard[1], K. Metzner[1]

Highly sensitive droplet digital PCR to quantify the HIV-1 latent reservoir

Division of Infectious Diseases and Hospital Epidemiology, University Hospital of Zurich, Zurich[1]

Introduction:
The latent reservoir of the human immunodeficiency virus type 1 (HIV-1) is the major hurdle in curing HIV-1. It is established early after infection and maintained by the integration of viral DNA that mostly stays transcriptionally silent in long-lived cells on antiretroviral therapy (ART). The measurement of the HIV-1 latent reservoir in human peripheral blood mononuclear cells (PBMCs) in patients on ART is challenging, since the reservoir is relatively small.

Methods:
We developed a highly sensitive assay for the measurement of total intracellular HIV-1 DNA based on the RainDrop digital PCR system, which allows absolute quantification of genomic DNA by separating one sample into a large number of picoliter-sized droplets and carrying out a PCR reaction within each droplet. We established and validated a multiplex PCR protocol by measuring HIV-1 pol in a highly conserved region and CCR5, a single copy gene to determine the input cell number. The optimization procedures included comparisons of different DNA extraction protocols, PCR conditions, primer and fluorescent probes design variations.

Results:
Finally, we achieved a very sensitive limit of detection of 20 HIV-1 DNA copies per 10^6 million genomic equivalents for the evaluation of 3 µg DNA per reaction (~450,000 cells). Furthermore, in comparison with a well established qPCR HIV-1 DNA assay the droplet digital PCR assay shows similar accuracy and higher sensitivity.

Conclusion:
Thus, droplet digital PCR is an attractive tool to measure HIV-1 DNA with high sensitivity that will improve monitoring of patients on ART.

3446

M. Visentin[1], B. Van Rosmalen[2], C. Hiller[1], T. Van Gulik[2], G. Kullak-Ublick[1], B. Stieger[1]

Organic Cation Transporters 1 and 3 (OCT1 and OCT3) as determinants of the intrahepatic uptake of the PET tracer 18F-fluorocholine

Department of Clinical Pharmacology and Toxicology, University Hospital, Zurich[1], Department of Surgery, Academic Medical Center, University of Amsterdam, Amsterdam[2]

Introduction:
Magnetic resonance (MR) and computer tomography (CT) imaging are the noninvasive methods of choice for the detection and characterization of focal liver lesions. However, atypical lesions can complicate the diagnosis, especially for the distinction between focal nodular hyperplasia (FNH) and other hypervascular hepatic lesions such as hepatocellular adenoma (HCA) and hepatocellular carcinoma (HCC). FNH is a benign lesion and does not need any therapeutic intervention whereas HCA carries a substantial risk of bleeding and malignant transformation. Hence, differentiation of these two entities is crucial to decide on the appropriate management. The introduction of hepatobiliary contrast agents improved the accuracy of MR imaging for the assessment of liver focal lesions. The differential accumulation of these contrast agents in different focal lesions often depends on an altered expression of the main hepatic membrane transporters. Likewise, the coupling of CT with the PET tracer [^{18}F]fluorocholine enhances the sensitivity for the detection of HCC and for the differentiation of HCA and FNH. HCA tend to accumulate less [^{18}F]fluorocholine than the surrounding normal tissue whereas FNH is more avid than the normal liver to [^{18}F]fluorocholine. [^{18}F]fluorocholine variable accumulation between different types of hypervascular liver lesions might be due to heterogeneous expression levels of relevant membrane transporters.

Methods:
We combined a functional transport study with tritiated ([^{3}H]) fluorocholine to identify the transporters expressed in the liver mediating the uptake of fluorocholine with a retrospective analysis of their mRNA expression pattern in patients with different types of liver lesions. Subsequently we investigated whether changes of transporter expression correlated with the intrahepatic [^{18}F]fluorocholine accumulation at the PET scan analysis.

Results:
[^{3}H]fluorocholine was transported by OCT1 and OCT3 but not by OCTN1 and OCTN2. After 30 minute incubation with [^{3}H]fluorocholine at the extracellular concentration of 10 mM the intracellular [^{3}H]fluorocholine was 30% higher in the OCT1-HEK293 cells than in the WT-HEK293 cells (79.7 ± 8.8 vs 59.9 ± 6.1 pmol/mg of protein, P=0.04). Transport mediated by OCT3 was detectable even at a lower concentration than that mediated by OCT1. The uptake of [^{3}H]fluorocholine at the extracellular concentration of 1 mM in cells expressing OCT3 was ~ 3-fold higher compared with that in the WT-HEK293 cells (slope 0.88 ± 0.27 vs 0.34 ± 0.13 min^{-1}, P=0.01). Interestingly, in the same experimental conditions, OCT3 could not transport [^{14}C]choline, the endogenous analogue of fluorocholine. The relative expression of the different target genes was correlated to the tumor:normal ratio of the Standardized Uptake Values (SUV) obtained from the PET/CT scans. One HCC and 4 HCA were analyzed. The HCC and 3 out of 4 HCA were ipo-chromatic than the respective surrounding normal tissues to [^{18}F]fluorocholine. One HCA and the respective normal tissue were iso-avid for [^{18}F]fluorocholine. When the 4 HCA were considered, an interesting pattern emerged. OCT1 and OCT3 were downregulated in the 3 ipo-chromatic HCA. In the iso-avid HCA OCT1 remained downregulated but OCT3 was upregulated.

Conclusion:
OCT1 and OCT3 might play an important role in the hepatic uptake of the PET tracer [^{18}F]fluorocholine. Since OCT1 and OCT3 expression is often altered in HCC, this finding might explain the abnormal uptake of [^{18}F]fluorocholine in intrahepatic lesions.

3447

G. Zhibo[1], G. Ting[2], H. Christian[1], K. Gerd[1]

Farnesoid X receptor protects against kidney injury in uninephrectomized obese mice

University Hospital Zurich, University of Zurich, Switzerland[1], University Hospital Bern, Switzerland[2]

Introduction:
Activation of the farnesoid X receptor (FXR) has indicated a therapeutic potential for this nuclear bile acid receptor in the prevention of diabetic nephropathy and obesity-induced renal damage. Here, we investigated the protective role of FXR against kidney damage induced by obesity in mice that had undergone uninephrectomy, a model resembling the clinical situation of kidney donation by obese individuals.

Methods:
Mice fed a high-fat diet developed the core features of metabolic syndrome, with subsequent renal lipid accumulation and renal injury, including glomerulosclerosis, interstitial fibrosis, and albuminuria.

Results:
The effects were accentuated by uninephrectomy. In human renal biopsies, staining of 4-hydroxynonenal (4-HNE), glucose-regulated protein 78 (GRP78) and C/EBP-homologous protein (CHOP), markers of ER stress, was more prominent in the proximal tubules of 15 obese compared with 16 non-obese patients. In mice treated with the FXR agonist obeticholic acid (OCA), renal injury, renal lipid accumulation, apoptosis and changes in lipid peroxidation were attenuated. Moreover, disturbed mitochondrial function was ameliorated and the mitochondrial respiratory chain recovered following OCA treatment. Culturing renal proximal tubular cells with free fatty acid (FFA) and FXR agonists showed that FXR activation protected cells from FFA-induced oxidative stress and ER stress, as denoted by a reduction in the level of ROS staining and Grp78 immunostaining, respectively. Several genes involved in glutathione metabolism were induced by FXR activation in the remnant kidney, which was consistent with a decreased glutathione disulfide / glutathione ratio.

Conclusion:
In summary, FXR activation maintains endogenous glutathione homeostasis and protects the kidney in uninephrectomized mice from obesity-induced injury.

3448

J. Buschmann[1], E. Balli[1], S. Hess[2], W. Stark[2], P. Cinelli[3], S. Märsmann[1], M. Welti[1], W. Weder[4], W. Jungraithmayr[4]

Adipose-derived stem cell seeded biominerizable nanocomposite for chest wall repair: Suppression of inflammatory cellular response in a murine model

Plastic and Hand Surgery, University Hospital Zurich[1], Institute for Chemical and Bioengineering, Department of Chemistry and Applied Biosciences, ETH Zurich, CH-8093 Zurich, Switzerland[2], Division of Trauma Surgery, University Hospital Zurich, Switzerland[3], Division of Thoracic Surgery, University Hospital Zurich, Switzerland[4]

Introduction:
Defects to the chest wall can occur after tumor resections or trauma caused by accidents, and appropriate chest wall reconstruction is therefore needed. Stability and integrity of the repaired chest wall should reach similarity to natural physiology. Addressing the treatment of critical size full-thickness chest wall defects, the ideal graft should be stable, fluid- and air-tight, biocompatible inducing no inflammatory reactions, biodegradable during the healing with non- toxic degradation products as well as rapidly integrating into the surrounding tissue. Here, we present the implantation of a biocompatible, biodegradable and easily vascularizable nanocomposite seeded with adipose-derived stem cells (ASCs) as a chest wall graft in a murine model. The cellular response towards this graft is compared to the cell-free graft.

Methods:
An electrospun poly(lactic-co-glycolide)/amorphous calcium phosphate (PLGA/aCaP) nanocomposite was seeded on both sides with murine ASCs and cultivated for two weeks before implantation as a chest wall graft. In addition, a cell-free analogous PLGA/aCaP scaffold was implanted on top of the cell-seeded scaffold towards the skin in order to be able to study not only direct cell-to-cell contact-based effects, but also to address paracrine effects caused by ASCs (control: cell-free scaffold alone). Histomorphometric analysis was performed 4 and 8 weeks, respectively, to assess cell density of macrophages, lymphocytes and foreign body giant cells.

Results:
Inflammatory response towards the graft material was significantly reduced for macrophages, lymphocytes and foreign body giant cells in the presence of ASCs compared to cell-free scaffolds. Moreover, this anti-inflammatory action caused by ASCs was not only found on the side where direct cell-to-cell contact between seeded ASCs and local cell population was enabled and studied, but also on the scaffold side where only diffusible factors secreted by ASCs were active (no cell-to-cell contact due to physical separation by the electrospun mesh of the scaffold).

Conclusion:
In clinics, the state of the art of repairing critical size chest wall defects is to use inert materials such as Goretex® which are not easily vascularizable and not biodegradable. Here, we present a biocompatible, biodegradable and well vascularizable nanocomposite for chest wall repair. In order to enhance integration of this graft material and accelerate wound healing, ASCs were seeded. A beneficial effect of these ASCs was that the inflammatory response towards the implant was significantly reduced. Therefore, such cell-seeded nanocomposites may be applied in clinics in the future.

3449

W. Baumgartner[1], M. Welti[1], N. Hild[2], S. Hess[2], W. Stark[2], G. Meier Bürgisser[1], P. Giovanoli[1], J. Buschmann[1]

Tissue mechanics of piled critical size biomimetic and biominerizable nanocomposites: formation of bioreactor-induced stem cell gradients under perfusion and compression

Plastic and Hand Surgery, University Hospital Zurich[1], Institute for Chemical and Bioengineering, Department of Chemistry and Applied Biosciences, ETH Zurich, CH-8093 Zurich, Switzerland[2]

Introduction:
Perfusion bioreactors are used to solve problems in bone tissue engineering with respect to sufficient nutrient and oxygen supply especially in critical size bone grafts. Biominerizable and biocompatible nanocomposite materials are attractive and suitable scaffold materials for bone tissue engineering because they offer mineral components in organic carriers. Human adipose derived stem cells (ASCs) can potentially be used to increase bone healing, especially when seeded onto a porous electrospun scaffold.

Methods:
Electrospun nanocomposite disks of poly-lactic-co-glycolic acid and amorphous calcium phosphate nanoparticles (PLGA/a-CaP) were seeded with ASCs and eight disks were stacked in a bioreactor running with normal culture medium (no differentiation supplements). Under continuous perfusion and uniaxial cyclic compression, load-displacement curves as a function of time were assessed during 9 days. Stiffness and energy dissipation were recorded. Moreover, stem cell densities in the layers of the piled scaffold were determined as well as their morphologies and differentiation status (endothelial cell differentiation, chondrogenesis and osteogenesis).

Results:
While the stiffness of the cell free constructs increased over time based on the transformation of the a-CaP nanoparticles into flake-like apatite, ASC-seeded constructs showed a constant stiffness. Stem cell density gradients were histologically determined with a linear increase from the bottom to the top of the pile ($r^2 > 0.95$) [1]. Cell morphology was influenced by the flow rate, with stem cells getting more roundish at higher flow rates. Some osteogenesis was found upon osteopontin immunostaining, while no endothelial cell differentiation and no chondrogenesis was triggered.

Conclusion:
The fabrication of a critical size bone graft is presented based on a biominerizable bone-biomimetic nanocomposite with preserved stiffness when seeded with ASCs. The cell densities of ASCs inside the piled construct varied with a linear gradient. Beginning osteogenesis was triggered by the dynamic culture conditions including perfusion and compression.

[1] Baumgartner, W. et al. Tissue mechanics of piled critical size biomimetic and biominerizable nanocomposites: Formation of bioreactor-induced stem cell gradients under perfusion and compression. J. Mech. Behav. Biomed. Mater. **47**, 124-134, (2015).

3450

C. Leuenberger[1], C. Schuoler[1], H. Bye[1], C. Mignan[1], T. Rechsteiner[1], S. Hillinger[2], I. Opitz[2], B. Marsland[3], A. Faiz[4], P. Hiemstra[5], W. Timens[6], G. Camici[7], M. Kohler[1], L. Huber[1], M. Brock[1]

microRNA-223 controls the expression of histone deacetylase 2: a novel axis in COPD

Division of Pulmonology University Hospital Zurich, University of Zurich, Zurich, Switzerland[1], Division of Thoracic Surgery, University Hospital Zurich, University of Zurich, Zurich, Switzerland[2], Faculty of Biology and Medicine, University of Lausanne, Service de Pneumologie, Centre Hospitalier Universitaire Vaudois (CHUV), Lausanne, Switzerland[3], Department of Pulmonary Diseases, University Medical Center Groningen, University of Groningen, Groningen, The Netherlands[4], Department of Pulmonary Diseases, Leiden University Medical Center, Leiden, The Netherlands[5], Department of Pathology and Medical Biology, University Medical Center Groningen, University of Groningen, Groningen, the Netherlands[6], Center for Molecular Cardiology, Division of Cardiology, University Hospital of Zurich, University of Zurich, Zurich, Switzerland[7]

Introduction:
Histone Deacetylase 2 (HDAC2) is a key epigenetic modifier with reduced expression and activity in patients with chronic obstructive pulmonary disease (COPD). MicroRNAs (miRNAs) are a group of small, non-coding RNA molecules that have emerged as gene silencers. We hypothesized that miRNAs are involved in the regulation of HDAC2.

Methods:
Levels of miRNA and mRNA were quantified by quantitative PCR. Protein expression and activity of HDAC2 were measured by HDAC-Glo assay. Manipulation of miRNA levels in human pulmonary endothelial cells (HPAEC) was achieved by using electroporation with either miRNA inhibitors or miRNA mimics. Interaction between miRNA-223 and HDAC2 promoter was assessed with a reporter gene assay.

Results:
Prediction software (miRWalk ®) identified miRNA-223 as a potential repressor of HDAC2. Stimulation experiments with inflammatory cytokines involved in the pathogenesis of COPD (e.g. IL-1βand TNF-α) induced the expression of miRNA-223 in HPAEC. Subsequent functional experiments demonstrated that overexpression of miRNA-223 decreased both HDAC2 expression levels and its activity in HPAEC. Direct miRNA-target interaction was confirmed by reporter gene assay. Reduced expression of HDAC2 was found to increase the levels of the chemokine Fractalkine (CX_3CL1). *In vivo* studies confirmed elevated expression levels of miR-223 in mice exposed to cigarette smoke and in emphysematous lung tissue from LPS treated mice. Moreover, a significant inverse correlation of miR-223 and HDAC2 expression was found in two independent cohorts of COPD patients.

Conclusion:
miR-223 was recently found to be upregulated in COPD patients. Our data here demonstrate that miRNA-223 controls expression and activity of HDAC2 in pulmonary cells. This pathway provides a novel pathogenetic link between dysregulated miRNA expression and epigenetic activity in COPD.

3451

O. Evrova[1], G. Meier Bürgisser[1], M. Calcagni[1], C. Scalera[2], E. Bachmann[3], J. Snedeker[3], P. Giovanoli[1], V. Vogel[4], J. Buschmann[1]

Drug Delivery device to support tendon rupture repair: biomechanical outcome of in vivo rabbit Achilles tendon full laceration experiments three weeks post-surgery

Plastic and Hand Surgery, University Hospital Zurich[1], ab medica, Via Nerviano 31, Lainate (Milan), Italy[2], Uniklinik Balgrist, Department of Orthopedics, Forchstrasse 340, 8008 Zurich, Switzerland[3], Laboratory of Applied Mechanobiology, ETH Zürich Vladimir-Prelog-Weg 1-5/10, 8093 Zürich, Switzerland [4]

Introduction:
Healing of tendon ruptures represents a major challenge in musculoskeletal injuries and combinations of biomaterials with biological factors are suggested to improve healing. Major problems in tendon healing are adhesion to the surrounding tissue and re-rupture. We developed an electrospun polymer tube acting as a drug delivery device to release a growth factor in a sustained manner [1]. In addition to a conventional suture such tubes were applied in fully transsected rabbit Achilles tendons. Biomechanical outcome was assessed three weeks post-operation.

Methods:
An elastic type of DegraPol® (DP), a polyester urethane as a delivery device for platelet-derived growth factor – BB (PDGF-BB) was used. Emulsion electrospun DP tubes carrying PDGF-BB were implanted around a fully transsected rabbit Achilles tendon (control: DP tubes without PDGF-BB). The tube had two layers; the one facing the wound site released the PDGF-BB, while the one facing the surrounding tissue had no growth factor. Three weeks post-operation, the tendons were extracted and tensile testing of the specimen was performed. Load until failure, failure stress, stiffness and elastic modulus were measured.

Results:
The application of growth-factor loaded DP tubes around the transsected tendons led to significantly enhanced biomechanical properties three weeks post-surgery.

Conclusion:
The sustained release of PDGF-BB to the wound site significantly improves the biomechanical stability of the tendon. Such DP tubes applied in clinics, for example after flexor tendon ruptures, may help the patient to find his way back to a normal motion pattern at earlier time points during regeneration.

[1] Buschmann, J. *et al.* Synthesis, characterization and histomorphometric analysis of cellular response to a new elastic DegraPol (R) polymer for rabbit Achilles tendon rupture repair. *Journal of Tissue Engineering and Regenerative Medicine* **9**, 584-594, doi:10.1002/term.1624 (2015).

3452

A. Monge Naldi[1], C. Belfrage[1], N. Jain[3], E. Wei[3], B. Martorell[2], M. Gassmann[4], J. Vogel[2]

Neuronal erythropoietin overexpression protects mice against age-related hearing loss (presbycusis)

Clinic for Otolaryngology, Head and Neck Surgery[1], Institute of Veterinary Physiology, University Zürich, Zürich[2], Department of Biomedicine, University Hospital Basel and Clinic for Otolaryngology, Head and Neck Surgery, University of Basel[3], Institute of Veterinary Physiology, University of Zurich and Zurich Center for Integrative Human Physiology (ZIHP), Zurich, Switzerland[4]

Introduction:
So far typical causes of age-related hearing loss (presbycusis) such as degeneration of hair cells and / or primary auditory (spiral ganglion) neurons cannot be treated. Because erythropoietin's (Epo) anti-apoptotic and neuroprotective potential has been shown previously we hypothesized that Epo might inhibit development of presbycusis.

Methods:
We determined hearing thresholds of juvenile (19-21 weeks) and aged (43-45 weeks) mice overexpressing Epo solely in neuronal tissues and age-matched C57BL6 control mice using behavioral audiometry and click auditory-evoked brainstem response measurements. In addition, the density of spiral ganglion cells was determined and the organs of Corti were inspected and analyzed as to the presence of inner and outer hair cells.

Results:
Behavioral audiometry revealed, in contrast to 19-21 weeks of age, that 43-45 weeks old Epo-transgenic mice had up to 35 dB lower hearing thresholds between 1.4 and 32kHz. Of note, at the highest frequencies (50-80kHz) thresholds could be obtained in aged Epo-transgenic only but not anymore in old C57BL6 control mice. Click-evoked auditory brainstem response showed similar results. Numbers of spiral ganglion neurons in aged C57BL6 but not Epo-transgenic mice were dramatically reduced mainly in the basal turn, the location of high frequencies. In addition, there was a tendency to better preservation of inner and outer hair cells in Epo-transgenic mice.

Conclusion:
In summary, Epo's known anti-apoptotic and neuroprotective actions effectively suppress the loss of spiral ganglion cells and probably also hair cells and, thus, development of presbycusis in mice.

3454

F. Kivrak-Pfiffner[1], C. Waschkies[2], Y. Tian[2], M. Calcagni[1], P. Giovanoli[1], M. Rudin[3], J. Buschmann[1]

SPIO-enhanced MRI as a nondestructive in vivo method to assess vascularization of 3D scaffolds planted on the Chorioallantoic Membrane of the Chick Embryo in ovo

Plastic and Hand Surgery, University Hospital Zurich[1], Division of Visceral and Transplantation Surgery, University Hospital Zurich, Switzerland[2], Institute for Biomedical Engineering, ETH and University of Zurich, Switzerland[3]

Introduction:
We recently presented Magnetic Resonance Imaging (MRI) as a nondestructive in vivo readout to report perfusion capacity in biomaterials planted on the chorioallantoic membrane (CAM) in the living chick embryo in ovo [1]. Perfusion capacity was assessed in various scaffold materials through changes in T1 pre and post injection of Gd-DOTA (Dotarem®, Guerbet S.A.). Hence local contrast agent concentration was dependent on perfusion, vascular permeability and extravascular compartment size. In the present study we explore intravascular SPIO particles of 30-40 nm size (Viscover™, Miltenyi Biotec, Germany) that stay in the vasculature to deliver a direct measure of functional vascularization.

Methods:
Fertilized Lohman white LSL chick eggs were incubated at 37°C and 65% relative humidity. After 3.5 days a hole was excised into the eggshell and on incubation day (ID) 7 collagen or DegraPol® scaffolds were placed onto the CAM. MRI was conducted on ID 14. The chick embryos were sedated with 0.3 mg/kg medetomidine. T1- and T2-weighted MR images were collected from a sagittal slice through the scaffold (0.2 x 0.2 x 1mm^3, RARE sequence of variable TR and TE) pre and 8 to 140 min post i.v. injection of SPIOs at a dose of 80 umol Fe /kg BW of the chick embryo.

Results:
MR images devoid of motion artifacts were obtained and the scaffold was clearly and reproducibly depicted in all MRI sessions, indicating that our medetomidine anesthesia protocol [2] offered proper sedation of the chick embryo. No signal change was observed within the egg yolk, consistent with the SPIO remaining in the vasculature. Consequently, T1 positive signal enhancement (reduction in T1) and T2 negative contrast (reduction in T2) were observed only in the vasculature and hence were restricted mainly to the surface of the CAM. Effect upon T2 was stronger than in T1. Interestingly, no change in contrast was observed inside the scaffold, which might relate to our observation that the slightly viscous contrast agent did not distribute easily but rather slowly within the finer segments of the vasculature, like in the scaffold. Consistent with this notion is the observation that T1 as well as T2 reduction was more prominently seen at 140 min than 8 min post injection of the SPIO.

Conclusion:
The results demonstrate that SPIO-enhanced MRI is feasible in and well-tolerated by the chick embryo. For future experiments, however, smaller (10-20 nm) SPIOs may be better suited due to their stronger (positive) T1 effect.

References:
[1] Kivrak Pfiffner, F. et al. A new in vivo MRI method to non-invasively monitor and quantify the perfusion capacity of 3D-biomaterials grown on the chorioallantoic membrane of chick embryos. Tissue Eng. Part C-Methods **21**, 1-8 (2014).

[2] Waschkies, C., Nicholls, F. & Buschmann, J. Comparison of medetomidine, thiopental and ketamine/midazolam anaesthesia in chick embryos for in ovo Magnetic Resonance Imaging free of motion artefacts. *Scientific Reports* **5**, 15536 (2015).

3455

P. Baumgartner[1], M. El-Amki[1], O. Bracko[1], A. Luft[1], S. Wegener[1]

Manganese-enhanced MRI for the study of post-stroke cognitive impairment in a rodent stroke model

Department of Neurology, University Hospital Zurich[1]

Introduction:
Cognitive impairment is a serious consequence of stroke in the middle cerebral artery (MCA) territory. However, cognitive symptoms affecting episodic memory are not easily explained by the stroke lesion itself, which usually does not affect hippocampal or parahippocampal areas. Our goal was to reveal an anatomical and/ or functional link between the sensorimotor and the hippocampal network in a rodent stroke model using manganese (Mn^{2+}) enhanced MRI (MEMRI). The metal ion Manganese Mn^{2+} has strong paramagnetic properties. It has the unique capability to enter neurons through similar channels as Ca^{2+} and can travel anterogradely along neuronal pathways that are electrically active. This technique allows to trace neuronal connections and to image functionally active brain regions independently of the hemodynamic state. Furthermore, the effect of a motor rehabilitation algorithm on cognitive symptoms after stroke was investigated.

Methods:
Adult Sprague-Dawley rats were subjected to 60 minutes of intraluminal MCAO or sham surgery. Sensorimotor and cognitive deficits were assessed during a 4 week period using a neurological score (18 points), the sticky-tape test and the Novel Object Recognition Test (NORT). After 28 days, we performed structural (T1/T2-w, Flash 3D) MRI in all animals on a 4.7T rodent MRI system (BZL). Afterwards, $MnCl_2$ was stereotactically injected into the entorhinal cortex (EC) and MRI repeated directly and 1 day after the injection to follow distribution of the Mn-signal. In a subset of rats, motor rehabilitation for the affected (right) side was performed using the pellet-reaching apparatus between days 5 and 12 after MCAO.

Results:
Stroke rats showed sensorimotor deficits on days 1 and 7 after MCAO, which correlated to lesion size. NORT performance was reduced on day 7, independent of direct hippocampal affection or lesion size. MEMRI revealed a targeted distribution of the tracer within the hippocampal network including connections to the septal nuclei in sham animals. A disturbed Mn signal pattern including thalamic enhancement was found after MCAO. While sensorimotor deficits were correlated with T2 lesion volume, NORT performance was not. Involvement of the hippocampus (38%) or perirhinal cortex (57%) was more common than anticipated. However, these regions were not more often affected in rats with cognitive deficits beyond day 7 after MCAO. Motor rehabilitation of the affected forelimb in the pellet-reaching task from day 5-12 after MCAO did not improve cognitive deficits. There was, however, a tendency for faster improvement of sensorimotor deficits in the sticky tape test between day 7 and 14 after MCAO in the rehabilitation group.

Conclusion:
Alterations of the hippocampal network after MCAO can be detected by MEMRI, indicating that thalamic structures are involved in post-stroke cognitive impairment. Further MRI and histological characterization and studies of training effects on this phenomenon are under way.

3456

M. Bombardo Ayats[1], E. Saponara[1], E. Malagola[1], G. Seleznik[1], T. Reding Graf[1], R. Graf[1], S. Sonda[1]

Ms275 a Class I HDAC inhibitor, ameliorates pancreatic inflammation

Swiss HPB Center, Visceral & Transplantation Surgery, University Hospital Zurich[1]

Introduction:
Epigenetic mechanisms regulated by the activity of histone deacetylases (HDACs) have been suggested that contribute to the pathology of many inflammatory diseases. The role of HDAC during the development of pancreatitis has not yet been investigated. Thus, in this study we analyzed whether HDAC-mediated epigenetic mechanisms are activated during pancreatitis and whether pharmacological inhibition of HDACs has a beneficial effect during this pancreatic disease.

Methods:
Acute pancreatitis was induced by serial cerulein injections in wild type C57BL/6 and MRL/MpJ mouse strains, characterized by a mild and strong inflammation phenotype, respectively. Class I HDAC activity was inhibited *in vivo* with daily injections of the selective inhibitor Ms275. Analyses of HDAC expression and activity, acetylation levels, as well as pancreatic inflammation were evaluated over a period of 72h following pancreatitis.

Results:
Induction of pancreatitis resulted in increased expression of class I HDACs, increased nuclear HDAC activity and a decreased acetylation of nuclear proteins. Inhibition of class I HDAC with Ms275 significantly reduced the migration of neutrophils and macrophages in the pancreas. In addition, histological analyses revealed that Ms275 treatment limited the severe acinar cell damage and formation of acinar-to-ductal metaplasia normally observed in MRL/MpJ mice following pancreatitis.

Conclusion:
Our results indicate that class I HDACs' activity is up-regulated during the development of pancreatitis and it promotes the infiltration of inflammatory cells in the organ with consequent exacerbation of tissue damage. These data suggest that blockage of class I HDAC may be a useful treatment to ameliorate the outcome of pancreatitis.

3457

M. Rochat[1], D. Li[1], S. Ivic[1], A. Audige[1], E. Schlaepfer[1], M. Manz[2], R. Speck[1]

Differential dynamics of HIV infection in MISTRG and MITRG mice

Infectiology, UniversitatsSpital Zurich[1], Hematology, University Hospital Zürich[2]

Introduction:
Humanized mice (hu-mice) are a valuable tool to study HIV pathogenesis. MI(S)TRG mice, which harbor human versions of four cytokines important for innate immune cell development with or without the human SIRPα transgene, develop a human lymphoid system supporting the development of monocytes, macrophages and NK cells as compared to previous hu-mouse models. We aim to explore the impact of the improved innate immune cell compartment on the dynamics of HIV infection.

Methods:
MI(S)TRG newborn mice were transplanted intra-hepatically with cord-blood-derived CD34+ cells. Human immune cell reconstitution was assessed after 9 weeks, followed by intra-peritoneal HIV infection with the R5 strain YU2. Plasma viral load (determined by RT-PCR), frequencies of cell subsets (analyzed by flow cytometry), and cytokine secretion (measured by multiplexed particle-based flow cytometry) were monitored up to 12 weeks post-infection (p.i.).

Results:
HIV infection in MISTRG mice was characterized by a fulminant viremia, which rapidly declined. Human blood engraftment drastically decreased during the first 4 weeks p.i., which was associated with a disappearance of myeloid cells (CD33+, CD14+ and CD14+CD16+ cells), while T cells steadily increased over the time of infection. Plasma levels of IFN-γ and IL-12p70 peaked at around 4 weeks p.i.. In contrast, HIV infection in MITRG mice was characterized by a slow progression, an expansion of myeloid cells and the secretion of IL-6 and TNF-α.T cell frequencies were much lower throughout the infection than in MISTRG mice.

Conclusion:
In conclusion, the dynamics of HIV infection, myeloid cell frequencies and cytokine profiles were different between MISTRG and MITRG mice. Early control of viral replication in the MISTRG mice might be explained by a transient Th-1 response. Future experiments will assess the impact of each myeloid cell subset on HIV infection though cell-specific depletion protocols.

3458

M. Visentin[1], A. Torozi[1], C. Hiller[1], M. Töllke[1], B. Stieger[1], G. Kullak-Ublick[1]

Deoxycholic acid (DCA) enhances the intracellular accumulation of potentially carcinogenic compounds

Department of Clinical Pharmacology and Toxicology, University Hospital, Zurich[1]

Introduction:
Extensive epidemiological studies have revealed that there is a strong link between obesity and some cancers. The exact molecular mechanisms linking obesity and cancer are not fully understood yet but the growing hypothesis suggests that abnormal plasma deoxycholic acid (DCA) pool in obesity might induce carcinogenesis. DCA is a secondary bile salt produced by microbiota metabolism in the intestinal lumen. Obese mice had 3-4 times higher plasma level of DCA than the lean mice but did not show any higher incidence in cancer development compared with the normal mice. When the same mice were exposed to some oncogenic compounds, all the obese mice developed hepatocellular carcinoma and other types of cancer (i.e. lung) compared with only the 5% of the lean mice. The present work shows that the intracellular accumulation of oncogenic compounds such as estrogens and prostaglandins is dramatically increased in presence of DCA.

Methods:
The nature of the enhanced intracellular accumulation of different radiolabeled oncogenic compounds by co-incubation with non-labeled DCA was assessed in different mammalian cells lines by rapid uptake determination.

Results:
The intracellular level of different radiolabeled compounds in CHO cells was measured after 10 min co-incubation with 400 µM DCA. The transport of 1 µM [^{3}H]Estrone-3-Sulfate ([^{3}H]E3S) in presence of DCA was 10 times higher than that in the control (22.16 ± 4.18 vs 2.59 ± 1.45, pmol/ mg of protein, $P<0.01$). [^{3}H]Prostaglandin 2 ([^{3}H]PGE2) uptake in presence of DCA was 2.5 times that in the control (21.09 ± 2.15 vs 8.96 ± 1.10, pmol/mg of protein). Similarly, [^{3}H]17-β-estradiolglucuronide ([^{3}H]E17βG) showed higher intracellular levels when co-incubated with DCA as compared with the control (14.37 ± 0.07 vs 2.82 ± 0.12, pmol/mg of protein). DCA stimulation was observed, to different extent, also in PC3 and HeLa cells. To study the nature of the stimulatory effect of DCA on the transport of [^{3}H]E3S, an influx kinetics was performed in CHO cells in presence of DCA at the extracellular concentration of 50 µM. The kinetics showed saturability and, based upon a nonlinear regression analysis of the data, the K_m and the V_{max} values were calculated to be 21.18 ± 1.78 µM and 136.10 ± 21.18 pmol/mg of protein, respectively. When the ratio of the initial substrate concentration [S] to the reaction velocity V is plotted against [S] (Hanes–Woolf plot) a straight line could be drawn, suggesting a first order kinetics. To study whether the stimulation of [^{3}H]E3S by DCA was Na^+-dependent, the uptake experiment was performed with or without Na^+ in the transport buffer. The intracellular level of radiolabeled E3S were similar in presence or absence of Na^+ (12.39 ± 1.57 vs 10.10 ± 3.08, P=NS), suggesting that the stimulatory effect of DCA was Na^+-independent.

Conclusion:
DCA can stimulate the cellular accumulation of potentially carcinogenic compounds such as prostaglandins and estrogens. The influx kinetic data indicated that a single carrier-mediated system was involved. The stimulatory effect was rapid suggesting that DCA altered the functionality of the transporter rather than the expression. This transporter might belong to the Organic Anion Transporting Polypeptide (OATP) family because the pattern of substrates stimulated by DCA and the Na^+-independence of transport support an involvement of OATP transporters.

3459

P. Schreiber[1], H. Bischoff-Ferrari[10], K. Boggian[2], C. Van Delden[3], N. Enriquez[3], T. Fehr[4], C. Garzoni[5], H. Hirsch[6], C. Hirzel[5], O. Manuel[7], P. Meylan[7], L. Saleh[8], M. Weisser[6], N. Mueller[1], And. The Swiss Transplant Cohort Study[9]

Vitamin D and its interplay with infections and rejections in kidney and liver recipients

University Hospital Zurich, Division of Infectious Diseases and Hospital Epidemiology, Zurich[1], Cantonal Hospital St. Gallen, Division of Infectious Diseases, St. Gallen[2], University Hospitals Geneva, Service of Transplantation, Department of Surgery, Geneva[3], Cantonal Hospital Graubünden, Department of Internal Medicine, Chur, Switzerland [4], University Hospital Bern, Division of Infectious Diseases and Hospital Epidemiology, Bern[5], University Hospital Basel, Division of Infectious Diseases and Hospital Epidemiology, Basel[6], University Hospital (CHUV) and University of Lausanne, Infectious Diseases Service, Lausanne[7], University Hospital Zurich, Institute of Clinical Chemistry, Zurich[8], Swiss Transplant Cohort Study[9], University Hospital Zurich, Department of Geriatrics, Zurich[10]

Introduction:
Inadequate vitamin D levels are highly prevalent in patients with end-stage organ failure. Beside its role for bone health an impact on additional outcome measures (e.g. infections, rejections) has been implicated.

Methods:
This study utilized prospectively collected samples and data derived from 70 kidney and 70 liver recipients within the STCS. Standardized, centralized measurement of 25-OH vitamin D (25OHD), 1,25-OH vitamin D (1,25OHD) and bone markers was performed. 25OHD levels were classified as severe deficiency (<30nmol/l), deficiency (>30&<50nmol/l), suboptimal (>50&<75nmol/l) and adequate (>75nmol/l).

Results:
Peri-transplant and at 6 months post-transplant the majority of kidney recipients had severely deficient 25OHD levels (45.7% resp. 31.4%). 27.1% resp. 34.3% had deficient levels, whereas a low proportion had suboptimal (15.7% resp. 30%) or adequate (11.4% resp. 2.9%) levels. 25OHD levels did not differ peri- and post-transplant, whereas 1,25OHD was significantly higher at 6 months post-transplant ($p<0.001$), resulting in an increased ratio of 1,25OHD/25OHD ($p<0.001$).
Comparably, at time of transplantation as well as 6 months post-transplant the majority of liver transplant recipients showed severe deficiency (51.4% resp. 45.7%) or deficiency (24.3% resp. 25.7%), only 12.9% resp. 14.3% had suboptimal and 11.4% resp. 2.9% optimal 25OHD levels. No significant change was recorded in 25OHD and 1,25OHD over time.
In kidney recipients no association between vitamin D and infections was detectable. In contrast, in liver graft recipients 25-OH vitamin D values of less than 50nmol/l were independently associated with incidence of at least one infectious disease event (composite of bacterial, viral, fungal and parasitic infections) within the first 6 months post-transplant.
In kidney recipients vitamin D levels < 50nmol/l were associated with a lower incidence of acute cellular rejections compared to kidney recipients with vitamin D levels of > 50nmol/l. We were not able to identify an impact of vitamin D on rejections in liver recipients.

Conclusion:
Vitamin D deficiency is highly prevalent at time of transplantation and remains common at 6 months post-transplant in both kidney and liver recipients. The association with infections in liver recipients and with rejections in kidney recipients may suggest a role for vitamin D in the immune response.

3460

J. Burgener[1], T. Skaria[1], G. Schoedon-Geiser[1]

Inflammatory Wnt5A signaling in human macrophages is mediated by Caveolin-1 dependent internalization of Wnt5A/Fzd5 complexes

Inflammation Research Unit, Department of Medicine, University Hospital of Zurich, Switzerland[1]

Introduction:
Sepsis is still a major healthcare problem with high mortality rates and increased morbidity upon survival. The pathophysiology is highly complex, and satisfactory therapeutic strategies are still scant. Macrophages are crucially involved as a source of and target for an array of inflammatory mediators. However, therapeutic antagonists of the most abundant inflammatory mediators IL-1 and TNFalpha were not successful in the past suggesting that other, yet unknown, factors might be involved in this fatal systemic inflammatory condition.
Recently, we identified Wnt5A/CamKII as a crucial part of macrophage inflammatory signaling upon TLR-dependent activation. Wnt5A is secreted by TLR-activated macrophages and can signal both auto-and parakrinically. Wnt5A is present in high amounts in sera of patients with severe systemic inflammation and septic shock. Therefore, we investigated the yet scarcely understood autokrine Wnt5A/CaMKII pathway in primary human macrophages.

Methods:
Using a genome-wide differential expression approach we analysed the whole genome transcriptome of primary human macrophages in response to Wnt5A. Expression of novel target genes was verified on the transcriptional and protein level. Ligand/receptor interactions were investigated using specific antibodies to Wnt5A (R&D systems), Frizzled-5 (Fzd5), Calmodulin, and Caveolin-1 (all from Abcam). For immunofluorescent labeling, red (AlexaFluor 568) and green (AlexaFluor 488) fluorescent secondary antibodies (all from Invitrogen) were used. Specimen were analysed microscopically using Zeiss Axiovision Software 4.8.2. with Zeiss Axioskope2 MOT. Zeiss ZEN 2012 software with AxioObserver.Z1,was used for 3D deconvolution (Carl Zeiss AG, Feldbach, Switzerland).

Results:
Analysis of the transcriptome response revealed both, genes and pathways of immune response signaling, and cytoskeleton remodeling as most significantly regulated in human macrophages in response to Wnt5A. Besides the already known, and hereby confirmed expression of inflammatory response factors such as IL-1, TNFalpha, IL-6, and IFNgamma, factors regulating actin cytoskeleton, cell motily, and adhesion, were among the top up-regulated genes. Most interestingly, specific mediators of endocytosis such as ZO-2 and Caveolin-1 were also significantly up-regulated. Immunofluorescence staining of Wnt5A-treated macrophages for 10, 30, and 60 minutes, respectively, revealed formation, internalization, and intermediary sequestration of Wnt5A/Fzd5/Calmodulin complexes. Formation and internalization of those complexes was comletely inhibited by monensin, indicating the involvement of an active trafficking process. Caveolin-1, known as factor responsible for endocytosis, and being significantly induced by Wnt5A, might be involved in the internalization of the Wnt5A/Fzd5 complex. Further investigation of receptor–ligand internalization targeting Caveolin-1 revealed endosomal co-localization of Caveolin-1/Wnt5A/Fzd5 complexes in Wnt5A treated macrophages. The Frizzled receptor antagonist sFRP1, known to inhibit inflammatory Wnt5A signaling in human macrophages, almost completely suppressed Caveolin-1 mediated internalization of Wnt5A/Fzd5 complexes.

Conclusion:
The present study shows for the first time that inflammatory Wnt5A/Fzd5 signaling in human macrophages involves Caveolin-1 to form an internalization complex of Wnt5A/Fzd5/Calmodulin, that is transiently sequestered into endosomal signalosomes. Factors interfering with Wnt5A/Fzd interaction like sFRP1 abrogate Caveolin-1 mediated Wnt5A internalization. Our finding sheds new light on the mechanism of inflammatory macrophage activation and might provide novel targets for the development of innovative strategies for therapeutic interventions in severe systemic inflammation and septic shock.

3461

S. Sorce[2], M. Nuvolone[2], M. Labouesse[3], U. Stadlbauer[3], S. Giovanoli[3], C. Winter[1], G. Russo[4], A. Varol[2], C. Parkhurst[5], D. Littman[6], W. Gan[5], D. Sanoudou[7], L. Ozmen[8], J. Roeper[9], U. Meyer[10], A. Aguzzi[2]

Cell-specific NURR1 overexpression in midbrain dopaminergic neurons improves affective and psychosis-related behavioral functions

Department of Psychiatry, Technical University Dresden, Dresden, Germany[1], Institute of Neuropathology, University Hospital of Zurich, Zurich, Switzerland[2], Physiology and Behaviour Laboratory, ETH Zurich, Switzerland[3], Functional Genomics Center Zürich, University of Zurich, Zurich, Switzerland[4], Department of Neuroscience and Physiology, New York University School of Medicine, New York, USA[5], Department of Pathology and Howard Hughes Medical Institute, New York University School of Medicine, New York, USA; [6], Department of Pharmacology, Medical School, University of Athens, Athens, Greece[7], F Hoffmann-La Roche AG, Basel, Switzerland[8], Institute of Neurophysiology, Goethe University, Frankfurt, German[9], Physiology and Behaviour Laboratory, ETH Zurich, Switzerland and Institute of Pharmacology and Toxicology, University of Zurich – Vetsuisse, Zurich, Switzerland[10]

Introduction:
The orphan nuclear receptor NURR1 (NR4A2) is best known for its essential role in the differentiation and maintenance of midbrain dopamine neurons. Converging evidence suggest that NURR1 deficiency is involved in the etiology of various neuropsychiatric and neurological disorders that are characterized by dysfunctions of the dopaminergic neurotransmission. The restoration or augmentation of NURR1 signaling has been thus suggested as a strategy to improve such abnormalities. We sought to specifically characterize the effect of NURR1 overexpression on the dopaminergic system by developing a new conditional transgenic mouse model.

Methods:
In order to generate a line allowing for cell-type specific NURR1 overexpression we used the CAG–loxP–CAT–loxP vector. Breeding of the CAG-CAT-NURR1 mice with the dopamine transporter DAT-cre line or the chemokine receptor CX_3CR1-cre line was performed to overexpress NURR1 in dopaminergic neurons or in microglia, respectively. Immunohistochemistry, neurochemical, transcriptional, electrophysiological and behavioral analyses were performed to characterize these new models. The effects of pharmacologically induced NURR1 activation were also evaluated.

Results:
We show that cell-type specific NURR1 overexpression in midbrain dopamine neurons leads to increased dopamine release in striatal output regions, specific electrophysiological patterns and altered transcriptional profiles. This genetic manipulation also led to reduction in despair-like behavior, enhancement of sociability and central information processing, and attenuation of the sensitivity to the psychostimulant drug amphetamine. Cell-specific NURR1 overexpression in microglia cells did not induce similar phenotypes, suggesting that the behavioral effects of NURR1 are specifically related to its overexpression in dopamine neurons. Pharmacological activation of NURR1 in wild-type mice recapitulated the behavioral effects induced by cell-specific NURR1 overexpression in midbrain dopaminergic neurons.

Conclusion:
Our findings corroborate the important role of NURR1 in regulating midbrain dopamine functions and highlight the consequences of its overexpression. Such insights are relevant in light of the clinical potential of inducing the NURR1 signaling pathway in the treatment of brain disorders characterized by abnormalities in dopamine circuitries. The newly generated mouse model can also represent a tool to investigate specific NURR1 overexpression in other brain areas and peripheral tissues where an involvement of NURR1 has been demonstrated.

3463

S. Sorce*[1], M. Nuvolone*[1], G. Russo[2], P. Schwarz[1], A. Aguzzi[1]

Temporal transcriptional changes induced by prions in mice

Institute of Neuropathology, University Hospital of Zurich, Zurich, Switzerland[1], Functional Genomics Center Zürich, University of Zurich, Zurich, Switzerland[2]

Introduction:
Transmissible Spongiform Encephalopathies (TSEs) are a group of neurodegenerative diseases caused by the accumulation of infectious prion deposits and characterized by the presence of spongiform vacuoles in affected brain regions. Although some of the molecular mechanisms underlying prion neurotoxicity have been identified, so far it is not possible to definitively arrest the course of the disease. Therapeutic treatment of TSEs remains therefore challenging; but clarifying all the components involved in prion neurotoxicity can be instrumental for novel possible therapeutic approaches.

Methods:
In order to better understand the toxicity pathways related to prion replication and accumulation in the brain, we have performed a transcriptional profile analysis by RNA-sequencing of mouse brain samples collected at different time points during prion disease incubation. Mice challenged with prions or normal brain homogenate have been sacrificed at different time points after injection and RNA extracted from different brain areas.

Results:
As expected, the results show a temporal pattern of changes linked to the exacerbation of the disease, and mainly related to neuroinflammatory reactions. However, certain disease-related molecular changes could be detected already at the earliest time points, despite the known absence of obvious neuropathological or neurological hallmarks. In addition, we have noticed that these alterations in gene expression largely overlap with changes induced by the normal aging process: the brain of a 2.5 month-old mouse injected with prions presents features of the brain of an 8 month-old control mouse. Further analyses are ongoing to corroborate these results, identify the underlying molecular mechanisms and validate the clinical relevance of this process.

Conclusion:
These findings uncover a completely different perspective to understand and analyze the progression of prion diseases since they would implicate a premature, accelerated aging effect on the brain of young individuals in the presence of small amounts of seed prion aggregates. In light of the similarities with other common neurodegenerative diseases, it could be then imagined that such an early aging process could occur in the brain of young individuals that will eventually develop neurodegeneration in advanced age. Understanding this premature brain aging process during the initial disease stages would therefore mean that novel targets of early diagnosis and intervention could be identified in order to prevent/delay neurodegeneration.

*equal contribution

3464

A. Lakkaraju[1], R. Marpakwar[1], E. Rushing[1], P. Liberski[2], A. Aguzzi[1]

Identifying the determinants of spongiform phenotype in prion infections

Institute for Neuropathology, Universitatsspital Zurich, Switzerland[1], Medical University of Lodz, Lodz, Poland[2]

Introduction:
Prion disease is a protein misfolding and aggregating disorder (PMA) implicated in Creutzfeldt-Jakob disease (CJD) and several transmissible spongiform encephalopathies of humans and animals. It is characterized by the accumulation and deposition of an abnormal conformer (PrP^{Sc}) of the endogenous prion protein (PrP^{C}). In addition to generic neuropathological changes (astrogliosis, neuronal loss, deposition of amyloid plaques), prion-infected brains feature a characteristic "spongiosis" which is caused by the accumulation of intraneuronal/intraneuritic vacuoles containing membrane fragments and, sometimes, degenerating organelles which are of uncertain biogenesis and content. The etiology of such pathology is still unclear, but vacuolation is spatiotemporally concurrent with the accumulation and deposition of PrP^{Sc}, an aggregated, proteinase K-resistant conformer of the cellular prion protein PrP^{C}. Previous studies have documented the accumulation of PrP^{Sc} in multivesicular bodies after prion infection, suggesting impairment of the endo/lysosomal machinery. Depletion of PIKfyve and FIG4, which are involved in synthesis of phospholipid PI(3,5)P2 a key cog of endo/lysosomal machinery, induces vacuolation similar to spongiosis. We therefore decided to investigate whether the breakdown of the endolysosomal fusion machinery is the cause of spongiosis in prion infections.

Methods:
To address mechanistic details of spongiosis, we plan to use animal models (mice), organotypic slice cultures and cell lines. Techniques such as immunohiostochemistry, electron microscopy and *in vitro* biochemical assays will be utilized in all these model systems to identify determinants of vacuolation. Rescue experiments will be performed using osmotic minipumps to deliver a water-soluble version of PI(3,5)P2 to the brains of prion-infected mice and we will monitor the survival and evaluate the neuropathology of brain.

Results:
We monitored the protein levels of PIKfyve and FIG4 in the brains of prion-infected *tga20* mice (overexpressing PrP^{C}) infected with Rocky Mountain Laboratory strain 6 (RML6) of prion. PIKfyve was significantly depleted at 90 days post-infection and profoundly depleted in terminally sick mice, whereas no change was observed in FIG4 levels. The mRNA levels of PIKfyve were unaltered, suggesting that posttranslational events led to destabilization. PIKfyve levels were also downregulated in cerebellar organotypic cultured slices (COCS) treated with anti-PrP^{C} antibody POM1, which induces pathologies reminiscent of prion infections. ER stress plays an important role in the toxicity in prion infections and time course analyses in N2A neuroblastoma cells revealed PIKfyve depletion upon ER stress induction. Treatment with GSK2606414, which alleviates the ER stress induced via the PERK pathway, restored PIKfyve levels. Our time-course studies in *tga20* mice infected with RML6 prions showed that ER stress precedes the downregulation of PIKfyve.

Conclusion:
Our preliminary data suggests that spongiform change may directly result from the suppression of the PIKfyve kinase, resulting in the impairment of endolysosomal machinery and formation of progressively larger vacuoles. In our study, activation of ER stress preceded the depletion of PIKfyve, which was rescued by ER stress inhibitors. We propose to dissect the events leading to PIKfyve downregulation and investigate their importance for prion toxicity in a variety of models. Furthermore, the possibility that PIKfyve-dependent events may play a causative role in additional neurodegenerative disorders exhibiting vacuolation will be investigated.

3465

R. Reimann[1], A. Varol[1], L. Caflisch[1], M. Hermann[1], S. Hornemann[1], A. Senatore[1], V. Chandrasekar[1], M. Einsiedler[1], M. Nuvolone[1], B. Schneider[2], A. Aguzzi[1]

Depicting the role of the FT functional domains in antiprion mediated neurodegeneration

Neuropathology, University Hospital of Zurich, Zurich[1], Brain Mind Institute, Ecole Polytechnique Fédéral de Lausanne, Lausanne[2]

Introduction:
Neurodegeneration is one of the central pathological hallmarks of fatal transmissible spongiform encephalopathy (TSE) affecting humans and animals. Prions represent the causative infectious agent in TSE, which are associated with PrP^{SC} a pathological conformer of the cellular prion protein (PrP^{C}). The expression of the normal ubiquitously expressed PrP^{C} is a prerequisite for prion induced neurodegeneration (*1, 2*) and for the propagation of PrP^{SC} (*3, 4*). Therefore one of the first-line targets towards the development of a curative treatment is PrP^{C}, which is encoded by *Prnp* and structurally consist of a globular domain (GD) hinged to an amino-proximal tail (FT, amino-acids 23-125) (*5*). Neurotoxicity induced by antiprion antibodies is triggering converging pathways as in bona fide TSE (*6*) and enabled the identification of the FT as the mediator of neurotoxicity (*7*). In order to identify well-defined therapeutic targets, we now address the relation between the known functional domains of the FT and its pathological function.

Methods:
Cerebellar organotypic slice cultures (COCS) from PrP deficient mice ($Prnp^{ZH3/ZH3}$) are infected at day zero in culture with Adeno Associated Virus (AAV), resulting in a transient expression of a bicistronic construct. Different constructs under the synapsin promoter were assembled with Golden Gate cloning (*8*). By the use of a 2A side (*9*) the fluorescent reporter NeonGreen is simultaneously expressed with unaltered or mutated PrP^{C} (synthetic DNA). After two weeks in culture neurotoxicity is induced with the Fab fragment of the antiprion antibody POM19 (FabPOM19, binding the GD). The read out is based on NeonGreen morphometry.

Results:
In order to investigate the role of the different FT's functional domains in the mediation of neurotoxicity, we assembled bicistronic constructs allowing for the expression of unaltered or differently selectively point-mutated PrP^{C}. Avoiding the generation of new transgenic mice in the first round of experiments, we decided to use a transient transduction system by the use of AAV. COCS were utilized as they represent the best-established tool to investigate neurotoxicity in the antiprion antibody model and in prion infection ex vivo. We found that the infection of COCS from PrP deficient mice ($Prnp^{ZH3/ZH3}$) with the generated AAV vectors allows for the expression of NeonGreen simultaneously with unaltered or mutated PrP^{C} selectively in Purkinje cells. While PrP deficient mice are resistant towards antiprion antibody mediated neurotoxicity, we could monitor a loss of NeonGreen over time in Purkinje cells transfected with the unaltered PrP^{C} when treated with the neurotoxic FabPOM19. This effect was blocked when FabPOM19 was pre-incubated with molar excesses of its cognate antigen.

Conclusion:
Antibody mediated neurotoxicity is restored in Purkinje cells of PrP deficient COCS when infected with an AAV vector to express the normal cellular prion protein under the synapsin promoter. Using a bicistronic construct we could utilize the expression of NeonGreen as a surrogate for cell loss. While these findings represent prove of concept for our experimental system, currently further optimizations steps of the read-out are required before we will test all point-mutated PrP^{C}.

1.) S. Brandner et al. Nature, 1996.; 2.) G. Mallucci et al. Science, 2003. 3.) H. R. Büeler et al. Cell, 1993. 4.) A. Aguzzi, A. M. Calella. Physiol Rev, 2009. 5.) R. Riek et al.. FEBS Lett, 1997. 6.) U. Hermann et al. PLOS Pathogens, 2015. 7.) T. Sonati et al. Nature, 2013. 8) T. Cermak et al. Nucleic Acids Res, 2011. 9.) M. L. Donnelly et al. J Gen Virol, 2001.

3466

D. Ostojic[1], F. Scholkmann[1], M. Wolf[1]

A new approach to calculate arterial oxygen saturation from blood volume pulsations measured on the human forehead using near-infrared spectroscopy NIRS

Department of Neonatology, University Hospital Zurich, Zürich[1]

Introduction:
Near-infrared spectroscopy (NIRS) is an technology offering the possibility for clinical monitoring of changes in arterial and tissue oxygenation (SpO2 and StO2), key health status parameters in neonatal intensive care units [1].
Using multiple sensors to measure StO2 and SpO2 is not an optimal option given the small size of the neonate's body.
The aim of the present work was to develop an algorithm that allows measurement of SpO2 on the head with a sensor originally built to measure only StO2.

Methods:
The new algorithm, SED-ATOD (Spectrogram and Edge-Detection based Arterial Oxygenation Determination), comprises three main signal processing steps:
1.Detection of the frequency band related to heart activity employing a short-time Fourier transform on the [O2Hb] and [HHb] signals.
2.Finding the instantaneous frequency of the heart activity by applying the "Canny Edge Detection" algorithm
3.Calculating SpO2 according to: $SpO2= A[O2Hb]_{HR}/(A[O2Hb]_{HR}+A[HHb]_{HR})$, with $A[x]_{HR}$ the instantaneous amplitude (A) of the signal x in the heart rate (HR) frequency band.

Results:
The newly developed algorithm was tested with signals measured on the forehead of an adult healthy volunteer (see Fig. 2 and Fig. 3).
The usefulness of the algorithm could be proven.

Conclusion:
We developed and evaluated a novel signal processing technique to determine SpO2.
Further validations are ongoing.
The algorithm will be freely available for fNIRS researchers and the inclusion in diverse fNIRS signal processing packages is planned.

3467

M. Langiewicz[1], A. Schlegel[1], B. Humar[1], R. Graf[1], P. Clavien[1]

Molecular Mechanisms Underlying the Unprecedented Liver Regeneration Induced by ALPPS Surgery

Visceral and Transplantation Surgery, Universitatsspital Zurich[1]

Introduction:
In many patients with liver cancer, the tumor is too advanced to permit a curative resection. The surgical approach, ALPPS (combining PVL with transection), may be used for unresectable disease due to its ability to induce massive acceleration of liver regeneration. Using the ALPPS mouse model, we aim to elucidate the molecular mechanisms underlying this unprecedented liver growth.

Methods:
Plasma samples were collected 30 minutes after ALPPS and confirmed for protein activity by protein enrichment and injection into mice treated with PVL only. Plasma proteins were identified by HRM proteomics analysis with data-independent acquisition on the Q-Exactive HF mass spectrometer. Liver tissue was collected at early time points post ALPPS surgery and analysed by RNA Deep Sequencing on the Illumina 2500 System. Metacore and Oncofinder were used for pathway analysis.

Results:
Plasma proteins have been identified as necessary contributors to the accelerated liver growth underlying ALPPS surgery. Proteomics analysis elucidated two protein candidates that are unique to ALPPS and Transection. 8 hours after ALPPS, the accelerated liver growth occurs by hyperplasia as seen by increased levels of Cyclin D and E mRNA, and a downregulation of p21. Genomics analysis shows differential gene expression occurring as early as 4 hours after ALPPS. Unique ALPPS-specific pathways have been identified through Oncofinder analysis and need to be validated.

Conclusion:
ALPPS is conducive to accelerated liver regeneration through the proteins that are regulated in the plasma 30 minutes after ALPPS. By introducing liver injury, transection induces the plasma proteins necessary to induce the accelerated liver regeneration. We aim to elucidate the mechanisms connecting the early upregulated plasma proteins and the later differentially expressed genes in liver tissue as those that underlie the unprecedented liver growth in ALPPS.

3468

N. Keller[1], J. Woytschak[2], S. Uchiyama[1], N. Leimer[1], O. Boyman[2], A. Zinkernagel[1]

Plasmacytoid Dendritic Cell Migration in Response to Group a Streptococcus

Infectious Diseases and Hospital Epidemiology, University Hospital Zurich, Zurich[1], Division of Immunology, University Hospital Zürich, Zürich[2]

Introduction:
The human pathogen Group A Streptococcus (GAS) causes both mild infections as well as severe, life-threatening infections. Disease severity is influenced by virulence factors that allow GAS to circumvent recognition and elimination by the human immune system. One important virulence factor is the streptococcal nuclease Sda1, which interferes with neutrophil extracellular trap mediated killing[1]. In addition, Sda1 reduces TLR9-mediated recognition through DNA degradation[2]. TLR9 and TLR7 are highly expressed on plasmacytoid dendritic cells (pDCs), a subtype of dendritic cells. TLR-mediated pDC activation followed by type I interferon production is important to fight viral infections, however, their role during bacterial infections is less defined.
We hypothesized that pDCs are able to sense bacterial DNA and/or RNA in a TLR-dependent manner and migrate to the site of infection. Further we postulated that streptococcal Sda1 degrades nucleotides to evade immune recognition by pDCs.

Methods:
We used murine pDCs, primary human pDCs isolated from buffy coats by using a pDC isolation kit (Milteny) as well as the pDC cell line PMDC05 originating from a patient with pDC-derived acute leukemia[3].
In vivo pDC migration towards bacterial infection was analyzed by FACS whereas in the *in vitro* model, pDC migration was assessed in transmigration wells with various bacterial stimuli. Synthetic TLR9 agonist (ODN2216) and antagonist (ODN-G) served as control. To study the importance of streptococcal nuclease, either RNA/DNA or live GAS wildtype M1T1 5448 and its isogenic mutant Δ*sda1* were used[4].

Results:
We found that human as well as murine pDCs migrated towards streptococcal RNA and DNA or live bacteria. Blocking of TLR9-signaling abolished human pDC migration, whereas a TLR9 agonist enhanced migration thus confirming a TLR9-dependency. In addition, GAS nuclease Sda1 not only degraded streptococcal DNA but also RNA. Hence, the presence of Sda1 reduced pDC migration towards streptococcal RNA.

Conclusion:
We showed that murine as well as human pDCs, known to be activated during viral infections, had the capacity to migrate towards a bacterial stimulus. Streptococcal Sda1, an important GAS virulence factor, abolished the observed TLR-dependent pDC migration *in vivo* as well as *in vitro*.

References:
[1] M.J. Walker et al., 2007, Nature Medicine. / [2] S. Uchiyama et al., 2012, PLoS Pathogen.
[3] M. Narita et al., 2009, Leukemia Research. / [4] J.T. Buchanan et al., 2006, Current Biology.

3469

F. Scholkmann[1], M. Wolf[1]

A new approach to assess the complex coupling between cardiovascular activity and cerebral tissue oxygenation in preterm neonates: Multiscale convergent-cross mapping

Biomedical Optics Research Laboratory, Department of Neonatology, University Hospital Zurich, University of Zurich, 8091 Zurich, Switzerland[1]

Introduction:
The coupling between cerebral tissue oxygenation and cardiovascular activity (reflecting the cerebral autoregulatory state) is potentially a significantly important clinical biomarker in preterm neonates. The aim of the present study was to test a novel signal analysis method that is able to analyze and characterize the coupling.

Methods:
Cerebral tissue oxygenation (StO_2) and the heart rate (HR) were measured on four preterm neonates for several hours. In addition, the fractional tissue oxygenation extraction (FTOE) was calculated. To characterize the coupling between StO_2 and HR as well as HR and FTOE the novel multiscale convergent-cross mapping (MCCM) method was employed.

Results:
We found that (i) each neonate showed individual coupling characteristics, (ii) the coupling characteristics between StO_2 and HR as well as HR and FTOE was specific for each neonate and showed a specific feature for a neonate with a reduced health status, possibly indicating an impaired cerebral autoregulation.

Conclusion:
In conclusion, our data analysis framework enabled novel insights into the characteristics of spontaneous hemodynamic and oxygenation changes in preterm infants. This is the first application of MCCM to human StO_2 data measured with near-infrared spectroscopy (NIRS).

3470

F. Scholkmann[1], U. Wolf[1,2]

New insights into the physiological origin of fluctuations in fNIRS signals – A new analysis based on systemic physiology complemented (SPC) fNIRS brain imaging (SPC-fNIRS)

Biomedical Optics Research Laboratory, Department of Neonatology, University Hospital Zurich, University of Zurich, 8091 Zurich, Switzerland[1], University of Bern, Institute of Complementary Medicine IKOM, 3012 Bern, Switzerland[2]

Introduction:
It is a well-known fact that signals measured with functional near-infrared (fNIRS) contain different physiological fluctuations. Their origin is not completely investigated and understood yet. The present work aimed to add to the understanding of the physiological origin by reporting of newly multimodal measurement and presenting result from novel analyses.

Methods:
For the analysis, a novel data set was used comprising systemic physiology complemented (SPC) fNIRS brain imaging (SPC-fNIRS) data from a light-exposure study (13 healthy subjects, 35.4±10.5 years, 3 different types of light exposure). Each measurement lasted 33 min. Cerebral hemodynamics/oxygenation (HD/OX) were measured bilaterally over the prefrontal and visual cortex by a multi-channel frequency-domain NIRS system. Systemic physiology parameters recorded and analyzed were: pulse-respiration quotient (PRQ), end-tidal CO_2 ($P_{ET}CO_2$) and continuous mean arterial blood pressure (MAP).
The coupling between HD/OX and the systemic physiological signals was analyzed by multiscale convergent cross mapping (MCCM), a novel signal-processing method for non-linear dynamical systems.

Results:
The analysis revealed that (i) all systemic physiological signals have an influence on HD/OX, whereas (ii) the strength and sign of the correlation depends on the type of correlated signals and the individual measured subject. Furthermore, the analysis revealed that (iii) the quantification of the correlation and phase-couplings between the signals, as well as the causal inference is possible using MCCM. An overview of the results (single subject level and group level) will presented.

Conclusion:
Multiscale convergent cross mapping is a promising new method to investigate the coupling of physiological signals measured by systemic physiology complemented fNIRS brain imaging.

3471

N. Keller[1], S. Uchiyama[1], E. Schläpfer[1], C. Grube[1], R. Schüpbach[2], R. Speck[1], A. Zinkernagel[1]

Interferon-alpha induced properdin-enhanced clearance of Group a Streptococcus

Infectious Diseases and Hospital Epidemiology, University Hospital Zurich, Zurich[1], Surgical Intensive Care Unit, University Hospital Zurich, Switzerland[2]

Introduction:
Patients suffering from neutropenia due to chemotherapy are at higher risk for succumbing to bacterial infection. However, interferon-α (IFN-α) induced neutropenia seems not to follow this pattern. IFN-α plays an important role during viral infections and contradictory observations have been made for its function during bacterial infections. Pegylated IFN-α regulates a variety of genes including properdin, an activator of the alternative complement pathway. Pathogen elimination through complement factors in the blood alone or in combination with phagocytic killing by macrophages and neutrophils is an important part of the host immune system.
Group A Streptococcus (GAS) is a human pathogen causing a high variety of infections ranging from mild, non-invasive (pharyngitis, impetigo) to more severe and invasive infections (necrotizing fasciitis, sepsis, streptococcal toxic shock syndrome).
We hypothesized that IFN-α per se could boost innate immune cells by inducing properdin and therefore supporting bacterial clearance despite the IFN-α-induced neutropenia.

Methods:
To investigate the influence of IFN-α on killing of the model pathogen GAS, GAS killing by whole blood from patients' pre, during and post IFN-α therapy was assessed *ex vivo*. Further, the role of properdin during GAS infections was elucidated by using patients' plasma or recombinant properdin and GAS survival was evaluated. In a next step, we investigated the efficiency of human monocytes to kill GAS after pre-opsonization with properdin-enriched serum.

Results:
We found that the presence of IFN-α positively influenced GAS killing in whole blood *ex vivo*. This was associated with increased production of properdin by both professional as well as non-professional phagocytic cells as observed in serum. In addition, monocytes killed GAS more efficiently when they were opsonized with serum containing high levels of properdin.

Conclusion:
These findings showed that properdin is up-regulated during IFN-α therapy resulting in enhanced GAS killing by monocytes. This helps to explain the preserved anti-bacterial innate immune defences in patients receiving IFN-α despite often pronounced neutropenia.

3472

M. Kiessling[1], S. Schuirer[2], M. Beibel[2], G. Rogler[1], G. Roma[2]

Identification of oncogenic driver mutations by genome-wide CRISPR-Cas9 screening

Universitätsspital Zürich[1], Novartis Pharma AG, Basel, Switzerland[2]

Introduction:
Genome-wide CRISPR-Cas9 screening is a powerful tool for positive selection or resistance screening. Initial deletion screens using CRISPR-Cas9 found that many genes essential for survival and involved in fundamental cellular processes are depleted during the screening. So far, however, it is not yet clear whether driver mutations can be detected throughout all depleted survival genes.

Methods:
Depletion screen: $30x10^6$ HCC-827 and CHP-212 cells were transduced with lentiviral whole genome library. Cells were treated with 1ug/ul puromycin and harvested after 14, 21, and 28 days in duplicates for genomic DNA extraction and analysis.
Genomic DNA sequencing: Frozen cell pellets were thawed and genomic DNA was extracted with a Blood & Cell Culture Maxi kit (Qiagen). PCR was performed in two steps to achieve 350X coverage over the sgRNA library. The resulting amplicons were sequenced using a HiSeq 2500 (Illumina).
Data processing and initial analysis: The reads of the raw FASTQ files were aligned, calculated and normalized to the 75 percentile of the mean of the samples in the data set. Log2 fold changes were then computed by taking the logarithm of the counts.

Results:
Here we report that the driving mutation EGFR was one of the highest-ranking candidates in the EGFR mutated HCC-827 cell line. Likewise, RAF-1 and MAP2K1 (MEK1), downstream kinases of mutant NRAS, were identified among the top hits of the NRAS mutated cell line CHP-212. Depletion of these sgRNAs strongly correlated with sensitivity to respective kinase inhibitors of the EGFR or RAS pathway.

Conclusion:
Our data suggest that whole genome CRISPR screens allow the identification of essential genes for survival that are suitable for drug targeting.

3473

M. McLuckie[1], F. Robotti[2], D. Poulikakos[2], P. Giovanoli[1], A. Ferrari[2], N. Lindenblatt[1]

Structured adipose-derived constructs influence the onset of neovascularization

University Hospital Zurich, Division of Plastic Surgery Research[1], ETH Zurich, Laboratory of Thermodynamic in Emerging Technologies[2]

Introduction:
Both *in vitro* and *in vivo* studies have shown that surface structure has an influence on cell mobility and guidance. Additionally, in tissue injury, it is essential that vasculogenesis occurs in a timely manner in order to supply oxygen and nutrients and therefore circumvent cellular necrosis. However, larger defects or a lack of healthy tissue to transplant have generated an increase in engineered constructs in recent years in effort to overcome this. These constructs generally consist of a scaffold material, cells, and growth factors, which due to their thickness may still not allow vasculature to grow into it in due time, therefore resulting in failure. Consequently, a persisting challenge in tissue engineering is therefore the ability to successfully integrate vasculature into the construct prior to implantation. As adipose tissue contains mesenchymal stem cells (MSCs), liposuction serves as a valuable source of beneficial autologously derived material with the potential to promote rapid and stable angiogenesis.

Methods:
Male B6 mouse fractioned adipose was characterised in regards to morphology and viability, in comparison to human liposuction. Using a polydimethylsiloxane (PDMS) mold, it was possible to create basic implantable constructs. Circular constructs with a 6mm radius and 0.4mm thickness were generated and implanted into the dorsal skinfold chamber (DSC) of four groups of male B6 mice (n=5) as follows: (I) unstructured empty control, (II) unstructured basic construct (BC), (III) 5µm gridded BC, and (IV) 50µm gridded BC. Intravital microscopy (IVM) was used to observe the onset of neovascularization, and histological stainings were performed after for to observe integration.

Results:
Although *in vitro* human and mouse adipose derivatives were shown to survive after several days under various conditions, fresh samples were used for experimentation. In groups (II) and (III), neovascularisation occurred as early as day 3. An intense angiogenic reaction began to peak around day 3 for group (III) and immediately normalise after, whereas group (II) only reached its peak reaction on day 10. Group (IV) had a delayed onset of angiogenesis marked by day 7, followed by delayed stabilization, indicating that larger structures did not promote rapid vascularization. H&E and Masson's Trichrome histology stainings confirmed these results.

Conclusion:
The use of a 5µm structured construct may not only help organise the drive of vessel growth, but also promote surrounding cell migration into the defect site. Using such constructs may serve as a simple and promising vascularization strategy for patients that lack tissue to transplant. As adipose tissue contains MSCs, which have the potential to differentiate into a variety of cells under appropriate environments, it may be useful for several different organs.

3474

C. Waschkies[1], T. Reding Graf[1], G. Seleznik[1], U. Ungethuem[1], R. Graf[1]

Visceral Fat Volume and Within-Organ Signal Fat-Fraction as Magnetic Resonance Imaging-based Phenotypic Markers in a transgenic Mouse Model of Pancreatic Carcinogenesis

Division of Visceral and Transplant Surgery, University Hospital, Zurich[1]

Introduction:
Pancreatic inflammation is a risk factor for pancreatic ductal adenocarcinoma development and overexpression of lymphotoxin (LT) α and β in acinar cells of the pancreas of transgenic tg(Ela1-Ltαβ) mice, referred to as LT mice here, has been shown to lead to chronic pancreatitis and reproduced key features of human autoimmune pancreatitis. In the present study we explore visceral fat volume and organ signal fat fraction as potential MRI based non-invasive in vivo phenotypic markers, based on incidental observations that LT mice presented more visceral fat upon visual inspection at organ harvest in these mice. It will be of interest to use such gross imaging markers that are accessible with standard preclinical MRI equipment, to characterize the development of phenotypic changes over time in this mouse model.

Methods:
MR imaging was performed on a 4.7T/20 cm Bruker PharmaScan unit equipped with transmit/receive a 40 mm bird-cage resonator. Five LT mice (1 male 36.6g, 4 female, 32.3±2.8g, 9 months) and three wildtype (wt) littermates (1 male, 33g; 2 females, 27.5±0.5g) underwent abdominal MRI. Motion-triggered T1-weighted images (FLASH, TE_{ip}/TE_{op}/TR 2.9/2.2/200ms, flip angle 50°, 12 slices, NA 8) for water/fat in-phase and out-of-phase acquisitions and T2-weighted images with and w/o fat supression (TurboRARE, TE/TR 30/2500ms, 24 slices, NA 6) were acquired with a spatial resolution of $234x234um^2$ (FOV 3.4x3 cm, MTX 145x128) and a 0.7/1.0 mm slice thickness/gap. Visceral fat volume was determined from intensity-based image segmentation in all axial slices comprising both kidneys and normalized to the abdominal volume in each animal. Wihtin-organ signal fat-fraction was calculated in three regions of interest, pancreas, liver and kidney cortex as control regions, from ip/op FLASH and TurboRARE images with and w/o fat suppression.

Results:
Abdominal T1- and T2-weighted images were obtained from all animals with water and fat signal in-phase/out-of-phase and with and w/o fat suppression, respectively, to obtain measures of visceral fat volume and signal fat fraction in selected organs. No striking difference in visceral fat volume was apparent upon visual inspection between LT and wt mice in anatomical images w/o fat signal suppression. Quantitative analysis of gross fat volume, however, revealed a somewhat higher, however not significant, visceral fat volume and bodyweight in LT as compared to wt animals. Quantitative analysis of signal fat-fraction obtained in ROIs placed inside the pancreas, liver and kidney cortex (as control regions) revealed a slightly lower, also not significant, signal fat-fraction in pancreas of LT as compared to wt mice. No difference was observed in liver and kidney cortex.

Conclusion:
Though small increase in visceral fat volume and decrease in pancreatic signal fat-fraction were observed in the small animal cohort studied, both measures do not seem to deliver sufficiently robust quantitative phenotypic markers to differentiate LT and wt mice based on MRI.

3475

A. Scherrer[2], J. Böni[1], S. Yerly[3], T. Klimkait[4], V. Aubert[8], M. Cavassini[9], M. Battegay[5], C. Hauser[6], E. Bernasconi[7], H. Günthard[2]

Failure Rate in NRTI-Free Treatment Is Higher in Two Compared to Three Class Regimens

National Center for Retroviruses, University of Zürich[1], Division of Infectious Diseases and Hospital Epidemiology, University Hospital Zürich[2], Central Laboratory of Virology, Division of Infectious Diseases, Geneva University Hospitals, Faculty of Medicine, University of Geneva[3], Department Biomedicine, Haus Petersplatz, University of Basel[4], Division of Infectious Diseases and Hospital Epidemiology, University Hospital Basel[5], Department of Infectious Diseases, Berne University Hospital and University of Berne[6], Division of Infectious Diseases, Regional Hospital Lugano[7], Division of Immunology and Allergy, University Hospital Lausanne[8], Division of Infectious Diseases, University Hospital Lausanne[9]

Introduction:
Little knowledge exists about the optimal drug combination in nuclesoside/tide (NRTI)-free antiretroviral treatment (ART). We studied the effectiveness of NRTI-free ART containing two compared to three drug classes.

Methods:
We studied time to virological failure (VF) in 503 NRTI-free treatment episodes from 342 patients participating in the Swiss HIV Cohort Study (ART start after 01/01/2007). VF was defined as two consecutive viral loads (VL) >50 copies/mL or 1 VL>50 copies/mL followed by a treatment change or interruption after 180 days of continuous treatment or previous viral suppression. Cox proportional hazards models with robust standard errors to account for intra-patient correlation were performed. The following variables were considered as potential confounders: VL before start of NRTI-free ART, CD4 cell count, gender, risk group, age, previously reported non-adherence, previously experienced VF, year of first ART initiation, genotypic sensitivity score of NRTI-free ART (Stanford algorithm version 7.0) and presence of major drug resistance mutations (IAS-USA list 2014). In the multivariable model, all variables with a p-value <0.2 were included.

Results:
A comparable number of NRTI-free episodes included two and three drug classes, 252 (50.1%) and 251 (49.9%), respectively. Most patients were ART-experienced (99%) and in 65% of patients VL was <50 copies/mL when starting the NRTI-free episode. Overall, 7% of patients experienced a treatment failure. Patients treated with two drug classes had a higher risk for ART failure, the multivariable hazard ratio (mHR) was 3.0 (95% CI: 1.4-6.6, p=0.007). Another important risk factor for VF was the VL level before NRTI-free ART initiation. The mHR was 3.2 (95% CI: 1.1-9.1, p=0.032) and 6.7 (95% CI: 2.6-17.7, p<0.001) for VL 50-10,000 and >10,000 copies/mL, respectively (reference <50 copies/mL). In addition, we found that male participants were more likely to fail NRTI-free ART (mHR: 3.0, 95% CI: 1.1-8.0). No other factor was significantly associated with VF.

Conclusion:
NRTI-free ART with three drug classes was more effective compared to two drug classes. Thus, NRTI-free ART with two classes should be prescribed very cautiously, if at all, especially for patients with a detectable VL before starting NRTI-free treatment.

3476

J. Wagner[1], L. Regli[1], A. Keller[1]

Early microvascular changes after subarachnoid hemorrhage in mice

Department of Neurosurgery, University Hospital Zurich, Zurich[1]

Introduction:
Subarachnoid hemorrhage (SAH) is mainly caused on ruptured intracranial aneurysms, leading to extravasation of blood into the subarachnoid space. Patients might develop an ischemic neurological damage but the pathomechanism of this complication is not clear.
Several studies suggest that microvascular dysfunction e.g. (blood-brain barrier breakdown, microthrombosis, and vasoconstriction) is one of the early pathological changes in brain parenchyma after SAH, however, the changes in the blood-brain barrier are poorly understood.

Methods:
In order to characterize spatial and temporal changes in microvascular permeability and integrity, we use the filament perforation model to induce experimental SAH in mice and at the meantime monitor vital parameters (intracranial pressure, blood pressure and respiration). Hypoxic areas and blood-brain barrier alterations are analyzed using immunohistochemistry and tracer injection studies. Whole brain clearing and imaging is used in order to gain insights into vascular permeability after SAH. The temporal course of edema formation and ischemia, as well as the distribution and volume of the subarachnoid blood, are analyzed using magnetic resonance imaging.

Results:
The MRI results show a variability of pathological changes on day 1 and 2 after SAH. We detect a formation of vasogenic edema, a variability in blood extravasation and ischemic lesions in SAH operated animals which are absent in sham operated animals. Hypoxic areas can be detected in paraformaldehyde fixed brain sections around the bleeding side of SAH. We also observe a pathological permeability of the blood brain barrier after SAH. A strong extravasation of tracer (70 kDa dextran) can be seen near the lesion side of the subarachnoid bleeding.

Conclusion:
Subarachnoid hemorrhage causes microvascular deficiency in the brain parenchyma shortly after bleeding which manifests in the dysfunction of the blood-brain barrier and tissue hypoxia. Further studies will be directed towards elucidating the cellular and molecular mechanism that leads to these pathological changes.

3477

N. Sanchez Macedo[1], L. Zollinger[1], S. Eisenring[1], M. McLuckie[1], M. Kijanska[1], S. Bottan[2], A. Hegglin[1], F. Robotti[2], P. Giovanoli[1], D. Poulikakos[2], A. Ferrari[2], N. Lindenblatt[1]

The dorsal skinfold chamber – the answer to difficult wound healing models?

Universitätsspital Zürich, Division of Plastic and Reconstructive Surgery[1], Laboratory of Thermodynamics in Emerging Technologies, ETH Zürich[2]

Introduction:
Skin wound healing is one of the most complicated biological processes. When impaired, it can cause mortality in several pathologies such as diabetes mellitus and cancer. There are increasing efforts being done to understand the wound repair process and to develop novel therapies that promote it. However, as wound repair cannot be reproduced *in vitro*, it requires the use of animal models.
The mouse excisional wound splint model is commonly used to investigate therapeutic applications that allow for wound healing – whether cells or biomaterials. The splint is needed in order to avoid skin contraction and to mimic human wound healing. Nevertheless, the model presents several problems as it is very difficult to ensure that both the splint and the biomaterial stay in place on the back of an active rodent. Additionally, the placement of the splint causes variability in the results. Here we tested two variations of the splint model and a modified version of the dorsal skinfold chamber (DSC) model. Our results showed that the DSC can be a reliable and reproducible wound healing model.

Methods:
Excisional wound splint models: We tested the effect of polydimethylsiloxane (PDMS) in wound healing with two different splint models: (i) 6-week old BL6 mice (n = 20) with 6 mm diameter full-thickness skin punches in the upper back. The wounds were surrounded with 1.2 mm silicone splint, which was fixed with 10 sutures and Super Glue. (ii) PDMS integrated into the silicone splint to allow a better contact of the biomaterial with the wound bed (n = 12). The splints were fixed only with a clinical dermatological skin glue.
Dorsal skinfold chamber: Unlike the classical DSC, with a 10 mm full-thickness excision, we performed 6-mm cuts. This allowed wound closure and healing without skin contraction. In addition, we tested the efficacy of the DSC by testing materials that promote wound healing and angiogenesis. The following biomaterials were inserted in the DSC: bacterial cellulose (n = 10 BL6 mice), polyurethane (PU, n = 15) and the SERI® Silk Surgical Scaffold (n = 20).

Results:
Both excisional splint models showed negative and unreproducible results. In both versions of the model we observed skin contraction and inflammation. The latter was caused by the glues and the sutures used to fix the splints. In addition, the animals were able to reach the splints and tried to detach them, therefore hurting themselves. This happened despite of the daily health checks. Due to these problems, we were unable to see the effects of PDMS in wound healing.
On the other hand, the DSC showed to be a suitable model for wound healing. The animal was unable to reach the chamber. Furthermore, the chamber protected the wounds from contamination and allowed the tested biomaterials to be in close contact with the wound bed. Finally, PU, SERIâ and cellulose nicely promoted angiogenesis, and healing or regeneration of full-thickness wound excisions.

Conclusion:
The DSC serves as a viable alternative to excisional splint wound models. The rodent has no access to the material within it, the chamber does not allow skin contraction to occur, it can be easily monitored, and is highly reproducible. The model can be easily adapted based on the experiment, and the wound can also be measured for closure statistics.

3478

C. Schuoler[2], T. Haider[1], C. Leuenberger[2], L. Ostergaard[1], M. Gassmann[1], M. Kohler[2], L. Huber[2], M. Brock[2]

Aquaporin 1 and Vascular Remodeling: a Novel Player in Hypoxia-Induced Pulmonary Hypertension

Institute of Veterinary Physiology, Vetsuisse Faculty, University of Zurich, Switzerland[1], Division of Pulmonology, University Hospital Zurich, Switzerland[2]

Introduction:
Vascular remodeling in the context of hypoxia-induced pulmonary hypertension (PH) is characterized by excessive proliferation and migration of pulmonary artery smooth muscle and endothelial cells. Exposure to hypoxia (Hx) also results in upregulation of aquaporin 1 (AQP1), an integral membrane water channel protein involved in various physiological processes including cell migration, proliferation and angiogenesis. Here, we investigated the interplay between AQP1, Hx and PH.

Methods:
The hypoxic mouse model (10% O_2 for 5 weeks) was used for experimental PH *in vivo*. Mice were treated by intraperitoneal injections of antisense locked nucleic acid (LNA) modified oligonucleotides targeting AQP1 (GapmeR AQP1) or scrambled control GapmeR. Hemodynamic assessment was evaluated by right heart catheterization performed at the end of *in vivo* experiments. For *in vitro* experiments, human pulmonary artery smooth muscle (HPASMC) and endothelial cells (HPAEC) were exposed to Hx (1% O_2). Quantitative expression of AQP1 in lung tissue and cell lysates were analysed by qPCR and Western blotting. Functional analyses (migration, proliferation and apoptosis) after GapmeR transfection were assessed by wound healing, BrdU incorporation and caspase assays. The coding sequence of AQP1 was cloned into the pcDNA 3.1(+) vector to perform overexpression studies in HPASMC.

Results:
In mice, both mRNA and protein levels of AQP1 were significantly increased upon exposure to Hx and right ventricular pressure (RVP) was found to be elevated in these animals compared to normoxic control mice. Treatment with GapmeR targeting AQP1 abated the hypoxia-induced upregulation of AQP1 on mRNA ($p<0.01$) and protein levels. Moreover, treatment resulted in normalization of RVP to the level of normoxic control animals ($p<0.05$). No difference in AQP1 expression levels (mRNA and protein) was observed between HPASMC and HPAEC. Long-term exposure to Hx increased AQP1 protein expression in HPASMC, with a significant upregulation after 48h of oxygen deprivation. Upon transfection of HPASMC with GapmeR AQP1, migration and proliferation rates were significantly reduced. In addition, apoptosis was increased compared to GapmeR negative controls ($p<0.001$). Conversely, the proliferative response of HPASMC overexpressing AQP1 was significantly increased compared to control transfected cells.

Conclusion:
These findings emphasize that AQP1 controls a pro-proliferative and migratory phenotype of HPASMC. Experimental inhibition of AQP1 through GapmeR technology decreased the migratory and proliferative response while increasing apoptosis. Our data suggest an important functional role of AQP1 in the development of pulmonary vascular remodeling in hypoxia-induced PH.

3479

D. Lewandowska[3], B. Ruehe[3], P. Schreiber[1], O. Zagordi[3], F. Geissberger[3], M. Schuurmans[2], M. Greiner[1], A. Zbinden[3], J. Böni[3], C. Benden[2], N. Müller[1], A. Trkola[3], M. Huber[3]

Identifying the etiology of previously undiagnosed respiratory infections in lung transplant recipients by unbiased metagenomic sequencing

University Hospital Zurich, Division of Infectious Diseases, Zurich[1], University Hospital Zurich, Division of Pulmonary Medicine, Zurich[2], Institute of Medical Virology, University of Zurich, Zurich[3]

Introduction:
Lung transplant patients are a vulnerable group of immunocompromised individuals prone to respiratory infections. Early diagnosis and specific treatment of infections post-transplantation potentially reduces respiratory complications and allograft dysfunction. Despite routine testing for the most common respiratory viruses and bacteria, a considerable number of post-transplant infections with respiratory symptoms remain of unknown etiology. We re-analyzed respiratory samples from lung transplant patients presenting with symptoms suggestive of an airway infection for which no viral or microbial etiology could be found by routine diagnostic methods. We used an open metagenomic approach to identify potential pathogenic viruses responsible for the respiratory symptoms.

Methods:
For metagenomic sequencing, virus particles were enriched from respiratory swabs, total nucleic acids extracted and amplified randomly. Sequencing libraries were prepared with NexteraXT and sequenced on a MiSeq Illumina (1 x 150 bp). Quality filtered reads were cleaned from non-viral reads by an in-house bioinformatics pipeline and blasted against a database containing > 40'000 viral sequences.

Results:
Among 71 participating individuals, 22 (31%) showed no respiratory symptoms up to 15 months after lung transplantation; 49 (69%) developed a total of 55 episodes of respiratory disease of which 27 were of viral and 3 of bacterial origin. In 26 (47%) episodes, no microbial or viral etiology of infection could be determined by routine diagnostics.
When we analyzed 24 throat swabs of individuals with unknown etiology the metagenomic approach identified a viral etiology in 4 patients: Rhinovirus A (n=2), Rhinovirus B (n=1) and Coronavirus HKU (n=1). Of note, in 2 cases these viruses showed evidence of late amplification in routine PCR but did not fulfil the criteria for positivity. In 6 of the 24 samples we detected HHV-7 reads that may have contributed to the observed disease patterns. Using a sensitive real-time PCR, 17 of 24 samples proved positive for HHV-7. Of note, HHV-7 viral loads increased between transplantation and the first routine visit (after 4 - 6 weeks) in 6 out of 7 patients studied longitudinally. In addition, we frequently found Torque Teno virus and bacteriophage reads but no other potentially disease related viruses were found in the remaining symptomatic lung transplant patients leaving their exact etiology of symptoms unclear. Reads from *Streptococcus* phage suggested colonization with *Streptococcus* spp., which was supported by reads from *Streptococcus pneumoniae.*

Conclusion:
Our metagenomic approach was able to identify diverse microbial and viral pathogens in a single analysis. In 4 of 24 samples with unknown etiology we detected low-level infections with respiratory viruses that were not picked up in routine screening.
We additionally identified several cases of HHV-7 infection. HHV-7 virus loads increased under immunosuppressive therapy in the early post transplantation phase. The presence of HHV-7 is intriguing and should be investigated in more detail to understand its role in pathogenesis.
Overall our study highlights the potential of metagenomic sequencing in complex diagnostic situations such as immunocompromised hosts and underlines the need to incorporate this technology in the diagnostic repertoire.

3481

I. Opitz[1], M. Friess[1], D. Nguyen-Kim[2], S. Hillinger[1], I. Inci[1], W. Weder[1]

Correlation of CT san based tumor volume measurement to actual resected tumor weight in malignant pleural mesothelioma - a new T-factor?

Division of Thoracic Surgery, University Hospital Zurich, Zurich[1], Institute of Diagnostic and Interventional Radiology, University Hospital Zurich, Zurich[2]

Introduction:
Tumor volume has been reported several times to be a valuable prognosticator for malignant pleural mesothelioma (MPM) survival. We wanted to assess the precision of CT scan based preoperatively measured tumor volume when correlated to the actual resected tumor weight during macroscopic complete resection and their impact on overall survival.

Methods:
From October 2012 until November 2015 the tumor weight of surgery specimens was measured in 27 patients undergoing macroscopic complete resection. 26 patients were male (96%), 25 MPM showed epithelioid type (96%) and the median age at surgery was 66 years (range 41-77). Twenty-two patients underwent induction chemotherapy prior to surgery. In all 27 patients tumor volume was measured in the CT or PET-CT scans performed before surgery as described previously. Tumor weight and volume were compared using the Pearson correlation. Tumor volume and tumor weight were also tested for association with pT stage using Kruskal-Wallis test. Association with overall survival (OS) was evaluated with the Kaplan-Meier method.

Results:
The median tumor volume assessed by CT scan was 79 ml and the median tumor weight 520 g. The analysis revealed a correlation between tumor volume and weight ($r=0.529$, $p=0.005$). There was also a significant association of tumor volume ($p=0.016$) as well as tumor weight ($p=0.005$) with the pT-stage (Figure 1). Association of tumor volume and weight with OS could not be evaluated as 82% of the cases were censored.

Conclusion:
The preoperative assessed tumor volume in CT scan seems to be a valuable descriptor of actual tumor volume to be resected and might be a reliable future T-descriptor.

3484

K. Ikenberg[1], N. Valtcheva[1], M. Rechsteiner[1], S. Stieb[2], F. Singer[3], M. Prummer[3], D. Stekhoven[3], H. Moch[1], M. Guckenberger[2], G. Studer[2], O. Riesterer[2], P. Wild[1]

Mapping the genomic landscape of head and neck squamous cell carcinoma for predicting the response to combined treatment with EGFR-blocking and radiation therapy

Institute of Surgical Pathology, Department of Pathology, University Hospital Zurich, Switzerland[1], Radiooncology, University Hospital Zurich, Zurich[2], NEXUS Personalized Health Technologies, ETH Zürich, Zürich[3]

Introduction:
Head and neck squamous cell cancer (HNSCC) is the sixth most common cancer worldwide. Despite advances in diagnostics, more than 60% of patients present with an already advanced stage of the disease. Unfortunately, advanced cancer patients do have a high risk of metastasis and recurrence. Therefore, a combined therapy approach is the standard of care. However, prediction of response to these intense treatment modalities is still insufficient.

Methods:
A defined cohort of 11 patients with primary advanced HNSCC, who responded well to a combined treatment of radiation and targeted anti-EGFR therapy (Cetuximab), was compared with 12 non-responder patients. For the latter set of patients, primary cancer specimens and matching recurrent tumors were analyzed. We used the Ion Torrent Platform and a customdesigned panel for re-sequencing of genes commonly mutated in HNSCC as reported in exome sequencing studies. Additionally, we screened the cohort for copy number variation using Affymetrix OncoScan arrays, optimized for formalin-fixed, paraffin-embedded (FFPE) samples.

Results:
Tumors of these two patient groups (responder vs. non-responder) showed a differential mutational landscape. Moreover, in the non-responder group we found three groups of variants: i) variants not affected by the therapy, ii) variants found in the primary tumor but not detectable after the therapy, and iii) variants absent in the primary tumor but emerging in the relapse samples. We are especially interested in the alterations that accumulate after therapy, since they provide information on the clonal selection advantage due to treatment. A phylogenetic analysis on the aberrations identified in the primary and recurrent tumor was performed.

Conclusion:
The confirmed mutations and copy number changes are potential new predictive biomarkers and might also represent novel drug targets. After validation analyses by Sanger sequencing, we will screen the confirmed genes in a larger patient cohort.

3485

K. Frontzek[1], M. Lutz[2], A. Aguzzi[1], G. Kovacs[2], H. Budka[1]

Cerebrovascular and brain amyloid-? pathology is frequent in iatrogenic Creutzfeldt-Jakob disease after dural grafting

Institute of Neuropathology, University Hospital Zürich, Switzerland[1], Institute of Neurology, Medical University Vienna, Austria[2]

Introduction:
Recently Jaunmuktane et al. (Nature 2015; 525(7568):247-50) reported Alzheimer-type gray matter and vascular amyloid-β (Aβ) pathology in four of eight brains of individuals with iatrogenic Creutzfeldt-Jakob disease (iCJD) after treatment with human cadaveric growth hormone (hGH) preparations. With one exception (Preusser *et al.*, J Neurol Neurosurg Psychiatry 2006;77(3):413-6), data on development of Aβ pathology in iCJD after dural transplantation have not been reported.

Methods:
By immunohistochemistry for Aβ, we studied brains of seven individuals with autopsy-confirmed iCJD (age range 28-63) after dural grafting, including two cases previously reported (Preusser *et al., op. cit.*; and Frontzek et al., Prion 2015; 9(6):444-8). Dural transplants (Lyodura, Braun-Melsungen, whenever specified) had been applied by neurosurgery between 11 and 25 years before death. Each iCJD case was age-matched to three cases of sporadic CJD (sCJD) from the Swiss or Austrian National Reference Centres for Human Prion Diseases (40-63 years). At least three different cortical and other brain regions were investigated. Moreover, Aβ was studied in 81 sCJD cases of usual age range (55-85) from Vienna.

Results:
Aβ was detectable in meningeal vessels as cerebral amyloid angiopathy (CAA) and in brain gray matter of five of seven iCJD brains (71%, age 28, 33, 47, 52, 63), but only in one as CAA (5%, age 55) and in five as parenchymal deposits (24%, age 49, 51, 62, 62, 63) of the 21 age-matched sCJD controls. Moreover, all five iCJD brains with Aβ pathology showed combined presence of CAA and brain Aβ depositions, while age-matched sCJD cases showed either CAA or parenchymal Aβ. The larger sCJD series showed CAA in 9/81 (11%), brain Aβ deposits in 9/81 other cases, and both in one more case. Statistically, CAA was significantly more frequent in iCJD than in age-matched sCJD ($p<0{\cdot}01$) and sCJD ($p<0{\cdot}001$); brain parenchymal deposits were significantly more frequent in iCJD than in sCJD ($p<0{\cdot}01$); and their combination was significantly more frequent in iCJD than in both age-matched sCJD and sCJD ($p<0{\cdot}001$).

Conclusion:
We conclude that CAA and brain parenchymal Aβ pathology are frequent in iCJD after dural grafting, even in young individuals. As previously reported (Jaunmuktane et al., op.cit.), there was no conspicuous tau pathology in iCJD. The presence of Aβ pathology in young individuals who do not present with a family history of early-onset dementia is highly unusual and suggests a causal relationship to the dural grafts. Further studies will be needed to elucidate whether such pathology resulted from the seeding of Aβ aggregates from the grafts to host tissues.

3486

V. De Luca[1], A. Kündig[1], M. Hüser[4], M. Jaggi[3], E. Keller[2]

Prediction of cerebral autoregulation capacity and intracranial pressure in neurointensive care patients using machine learning: a feasibility study

ETH Zurich, Computer Vision Laboratory[1], Neurochirurgie, Universitätsspital, Zürich[2], ETH Zurich, Data Analytics Lab[3], ETH Zurich, Mobile Health System Laboratory[4]

Introduction:
Monitoring of intracranial pressure is vital in severely brain-injured patients. Intracranial hypertension and failures of cerebral autoregulation are important risk factors of secondary brain injury. Cerebral autoregulation could be summarized by indices derived from arterial blood pressure (ABP), ventilation, and intracranial pressure (ICP), which are continuously monitored. An example of cerebral autoregulation index is the Pressure-reactivity index (PRx). Critical conditions are currently identified by prospective evidence. Yet a pro-active approach in which the future status of patient is forecasted is desirable. In this work, we proposed a data-driven prediction model for forecasting the mean ICP, ABP and PRx values up to 2 hours in advance.

Methods:
We considered a subset of the publicly-available MIMIC II dataset (http://physionet.org/), which consisted of 26 ICU patients, where ICP, ABP, heart rate, respiratory frequency, and blood oxygenation were monitored over a total amount of 50 days. Out of these signals, we computed auto-regulation indices, statistical summaries, and Fourier, wavelet and other non-linear transformations of the data. We then trained a regularized regression model using stochastic gradient descent. We predicted the 30-second mean ICP and ABP, and the 10-minute PRx in up to 2 hours in the future. The PRx was computed as the Pearson correlation coefficient of 10-second mean ICP and ABP over the previous 10 minutes and directly predicted by the model.

Results:
Based on a leave-one-patient-out cross validation scheme, we evaluated our model against a baseline model assuming no change in the predicted targets. We achieved a mean absolute prediction error of [1.1, 1.6, 2.1] mmHg for ICP, [2.8, 4.8, 7.2] mmHg for ABP and [0.1, 0.3, 0.3] for PRx, with prediction horizons [5, 30, 120] min, respectively. These results showed an improvement of [4, 9, 11] % for ICP, [4, 5, 7] % for ABP and [2, 15, 19] % for PRx with respect to baseline.

Conclusion:
The proposed feasibility study showed that it is possible to reliably predict ICP and the cerebral autoregulation status, based on physiological measurements up to 2 hours in advance. Future work aims at validating our model on a larger set of clinical data and conditions, and including patient data from the Neurointensive Care Unit of the Universtity Hospital Zurich. This work represents a valuable step towards the development of intelligent forecasting systems for pro-active decision-making in intensive care.

3487

D. Braun[1], A. Marzel[1], D. Bircher[1], P. Schreiber[1], C. Grube[1], A. Scherrer[1], R. Kouyos[1], H. Günthard[1]

High Rates of Asymptomatic STIs in Patients after Primary HIV-1 Infection

Infectious Diseases and Hospital Epidemiology, University Hospital Zurich, Zurich[1]

Introduction:
The Prevalence of asymptomatic sexually transmitted infections (STIs) in patients who presented with a primary HIV-1 infection and received early antiretroviral therapy is unknown.

Methods:
Between June 1st and August 31th 2015 we offered STI screening to all patients from the Zurich Primary HIV-1 Infection Study who attended a clinical visit. Patients were tested for gonorrhea, chlamydia and herpes simplex virus (HSV) by polymerase chain reaction (PCR) and for syphilis by serological assay. In addition, patients presenting with elevated liver enzymes were tested for acute hepatitis C virus (HCV) infection by HCV PCR. All patients were asked to give a first-catch urine specimen and a blood sample. Additional specimens were taken from the throat, rectum and vagina from patients who reported having had receptive oral, anal or vaginal sex. Patients were asked to complete a supplementary questionnaire about sexual behaviour in the preceding three months.

Results:
Within three months a total of 173 patients attended a clinical visit. Most patients were male (95%), were men who have sex with men (MSM) (85%) and had a suppressed HIV viral load to <50 HIV-1 RNA copies/ml of plasma (90%) at the time-point of STI screening. Of all 173 patients, 45 patients (26%) denied STI screening. Heterosexuals refused STI screening significantly more often compared to MSM (49% versus 20%; p= 0.001). Most frequently self-reported reason for refusing screening was having no sexual contact in the preceding three months (33/45, 73%). Out of all 128 tested patients, 30 (23%) were affected by a STI; 22 patients (73%) being asymptomatic (Table 1). The detected STIs included chlamydia trachomatis (n=17, 52%), gonorrhoea (9, 27%), syphilis (4, 12%), acute HCV infection (2, 6%), and HSV (1, 3%). Three persons had >1 STI. Number of occasional sex-partners, reporting sexual risk behaviour and being MSM was associated with a significant increased risk for acquisition of a STI (Table 1). The favoured anatomical site of asymptomatic presentation was the rectum (n= 13). The number needed to screen to detect one STI in MSM was 4 compared to 19 in heterosexuals.

	No STI (% or IQR)	**STI** (% or IQR)	**p-value**
Number	98 (77)	30 (23)	
Age, median	42 (35, 49)	38 (32, 43)	0.07[a]
Male	93 (95)	29 (97)	1[b]
Female	5 (5)	1 (3)	
Protected sex with occasional partner	77 (79)	16 (3)	**0.013**[c]
Unprotected sex with occasional partner	21 (21)	14 (46)	
Number of occasional partners, median	2 (1, 4)	4 (2, 7)	**0.002**[a]
Men who have sex with men	80 (82)	29 (97%)	**0.044**[b]
Heterosexuals	18 (18)	1 (3)	
Stable partnership	39 (40)	18 (60)	0.1[c]
No stable partnership	58 (59)	12 (40)	
Prior syphilis	24 (25)	10 (33)	0.5[c]
CD4+ cell count cells/µl, median	647 (512, 864)	635 (468, 743)	0.3[a]
Suppressed HIV viral load (<50copies/ml)	88 (90)	27 (90)	0.7[b]
Symptomatic STI	-	8 (27)	0.07b
Asymptomatic STI	-	22 (73)	

Conclusion:
A high rate of STIs was diagnosed in MSM who initially presented with a primary HIV-1 infection and received early antiretroviral therapy. The majority presented asymptomatically. Thus, a regular STI screening including asymptomatic individuals should strongly be considered in MSM who report having changing partners or practicing sexually risky behaviour.

3488

S. Freiberger[1], E. Varypataki[1], M. Håkerud[1], T. Kündig[2], P. Johansen[1]

Stimulation of cytotoxic T cells by photosensitization-based Vaccination

Department of Dermatology, University of Zurich, Zurich[1], Department of Dermatology, University Hospital Zurich, Zurich[2]

Introduction:
Photochemical internalization (PCI) is a new method to facilitate endosomal uptake of drugs or vaccines into cells for release into the cytosol. After administration, the photosensitizer incorporates into the membrane of antigen-presenting cells (APCs). Upon endocytosis, co-administered drugs or vaccines are internalized, and subsequent light exposure leads to the activation of the photosensitizer which causes disruption of the endosome and releases of the endosomal content. We are using PCI to develop a novel vaccination method for stimulation of cytotoxic T cells.

Methods:
Typically, mice were vaccinated intradermally with di-sulfonated tetraphenyl chlorin (TPCS2a) photosensitizer and ovalbumin (OVA). Eighteen hours later, the mice were exposed to light using a standardized illumination tool and scheme for activation of the photosensitizer. Blood and spleen cells were harvested at different time points and analyzed for proliferation and function of OVA-specific CD8 T cells by FACS and ELISA. Moreover, vaccinated mice were challenged with OVA-expressing B16 tumor cells for functional analysis of the effect of PCI-based vaccination on tumor growth.

Results:
PCI-based vaccination with OVA protein led to activation of OVA-specific CD8 T cells in both blood and spleen. The observed immunological effects, such as proliferation and cytokine secretion, were dependent on CD11c expression on APCs, but not on Langerin (CD207) expression. Furthermore, tumor growth was prevented by PCI-based vaccination, whereas vaccination with OVA protein alone had no effect on tumor development.

Conclusion:
PCI-based vaccination is a powerful tool to stimulate cytotoxic T cell responses in vivo. Using this technique, the growth of B16 melanoma could be prevented in mice. Furthermore, we show that CD11c expressing cells are playing an important role in the mechanism of PCI-based antigen presentation.

3489

C. Waschkies[1], C. Egger[2], T. Suter[2], R. Martin[2], M. Rudin[1]

Magnetic Resonance Imaging Based Microstructural Phenotyping of Animal Models of MS and in Human Brain Tissue Samples

Institute for Biomedical Engineering, ETH and University of Zurich, Zurich[1], Neuroimmunology and MS Research, University Hospital Zurich, Zurich[2]

Introduction:
In the present study we exploit Magnetic Resonance Imaging (MRI) in animal models of MS and in human brain tissue samples to investigate to what extent different MS disease courses are characterized by specific structural phenotypes, and whether multi-parametric MRI delivers unique fingerprints to resolve these phenotypes.
The objectives of the present study are to establish in animal models of MS and in human brain tissue samples quantitative MRI readouts of improved specificity and sensitivity with regards to underlying pathological processes. The ultimate goal is to apply such multi-parametric quantitative MRI at high spatial resolution to human brain tissue samples to characterize and dissect different MS subtypes by establishing unique structural fingerprints that relate to differential pathomorphological changes in these phenotypes ('microstructural phenotyping').

Methods:
The most commonly used EAE mouse model, C57BL/6 mice immunized with MOG35-55 peptide, is studied as a 'chronic-remitting' model associated with demyelination and axonal loss. Quantitative MRI assays were collected on a Bruker Pharmascan 4.7T system, equipped with a quadrature surface CryoProbe™, at three times during the course of the disease. Respective structural readouts include T2 and T2* maps to detect edema and quantify myelin water fraction and determine lesion load, T2' as a measure for the paramagnetic effects of iron and the diamagnetic effects of myelin, contrast-enhanced MRI to characterize lesions (differentiate between enhancing and non-enhancing lesions under i.v. injection of Gd-complex Dotarem®), DTI (Diffusion Tensor Imaging) to assess structural (axonal and myelin) integrity through measures of fractional anisotropy and axial and radial diffusivity, MTC (Magnetization Transfer Contrast) to assess changes in myelination/macromolecular content, and whenever possible (within time constrains) ^{1}H-MRS (Magnetic Resonance Spectroscopy) to assess underlying neurochemical/metabolic changes. Furthermore, resting-state fMRI was used to access alterations in functional connectivity as an early marker for disease-related functional reorganization. Comparative histology has been performed in selected samples. Human tissue samples were characterized with similar structural readouts at high spatial resolution on a Bruker Biospec 7T system.

Results:
Data from our ongoing study reveal in lumbar spinal cord and brain changes in markers of neuronal and myelin integrity, consistent with earlier pathological and commensurate histological findings. Trends towards reduced T2 and ADC and small increase in MT in brain however, are inconclusive in the animal cohorts studied so far, but may point towards accummulation of myelin breakdown products. It is of note that consistency/sensitivity of our assessments is particularly hampered by disease heterogeneity, which may be tackled by including an intra-subject baseline and longitudinal measurements into future studies. Moreover, MRI protocols were translated for MRI histology to comprehensively phenotype brain tissue samples obtained from the UK MS Society Tissue Bank. The two samples obtained, however, did not contain visible lesions and are not sufficient to describe more diffuse changes in normal appearing gray and white matter at present.

Conclusion:
With the small cohort of EAE mice and human tissue samples studied no conclusions can be drawn as yet with regards to defining more subtype-specific disease markers and the sensitivity of MR imaging-based phenotypization of MS phenotypes. However, with collecting more data we aim to develop classification criteria based on these signatures for stratified and personalized medicine.

3490

V. De Luca[1], E. Keller[2]

ICU-Cockpit: enabling multimodal monitoring and decision support in neurointensive care

ETH Zurich, Computer Vision Laboratory[1], Neurointensive Care Unit, Department of Neurosurgery, University Hospital Zurich[2]

Introduction:
In neurocritical care, patient monitoring is based not only on standard intensive care monitoring, but also on numerous data obtained from very complex pathophysiological changes in the human brain. Examples are recordings from electrocardiography, artificial ventilation, electroencephalography, hemodynamics, metabolism and imaging. It is extremely difficult for clinicians to integrate the huge amount of clinical data continuously generated by different devices. The lack of data integration and usability is one of the major reasons why only a small part of the knowledge that physicians use in this field is evidence based. The growth of knowledge in medicine, as well as personalized medicine including genotype data is no longer manageable for physicians alone in daily clinical practice.
We introduced the first prototype of ICU-Cockpit, an integrated platform for patient monitoring, automatic data analysis and therapy support for neurointensive care units (neuroICUs).

Methods:
We acquire data from four bed units of the neuroICU of the University Hospital Zurich, which are equipped with the CNS 220 Monitor (Moberg Research, USA). This device is connected to and receives data and alarms from several monitoring devices in use at the ICU, e.g. Draeger Infinity, Pulsion PiCCO2, Covidien BIS and Iscus Flex. In addition, its user interface can be customized, to have the optimal multimodal visualization of the patient. Video recordings of the bed area are also used. The data are acquired only after written consent of the patients or their relatives, and the study was approved by the Swiss Ethics Committees on research involving humans.
ICU-Cockpit consists of several parts: (1) a data aggregation phase; (2) data streaming, using IBM InfoSphere Streams (IBM Research); (3) data archiving; (4) data analysis; (5) user-friendly and customizable data visualization, developed by Supercomputing Systems, Zurich. In (4), we firstly filter the data, and use video information to automatically detect and remove motion-driven false alarms. Artifact-free data are then used to develop and validate data mining algorithms. These analysis tools include exploratory data correlation, detection of delayed cerebral ischemia and temporal prediction of intracranial hypertension.

Results:
Four bed units of the neuroICU are currently part of the proposed system. Yet experiments on data streaming and analysis were conducted off-line using prospective data from up to 20 patients. Using streaming analytics, we achieved real-time data transfer and analysis. Results of the motion-based false alarm detection showed a reduction of at least 20% of false alarms, without mislabeling any real alarm. Preliminary results on the prediction of inracranial hypertension offsets showed an accuracy of 80% (AUROC score) for prediction horizons up to 20 minutes.
Finally we enabled the visualization of integrated, multimodal patient data, which has been and is tested by clinicians of the neuroICU in every-day clinical practice.

Conclusion:
ICU-Cockpit can trigger a fundamental change in the safety culture and standard operating procedures in daily emergency and intensive care medicine. The accessibility of full patient recordings, diagnostic and treatment information allow the development of data mining tools that can help medical personnel. ICU-Cockpit can open up enormous potentials for personalized medicine, future clinical studies and scientific evidence.

3491

R. Reissner[1], G. Giesen[1], C. Calcagni[1]

Mid term results of semiconstrained distal radioulnar joint arthroplasty

Division of Plastic Surgery and Hand Surgery, University Hospital Zurich / Switzerland[1]

Introduction:
Range of motion and stability are important outcome parameters to assess function of the distal radioulnar joint (DRUJ), in particular pronation, supination and weight lifting capacity. The aim of the study was to investigate the subjective, clinical and radiographic results in ten patients after primary implantation of the semiconstrained distal radioulnar joint arthroplasty following DRUJ derangement and painful instability with and average follow-up of three years.

Methods:
Between July 2010 and December 2013, 10 patients with osteoarthritis and/or instability of the DRUJ were surgically treated with the semiconstrained distal radioulnar joint prosthesis. 8 patients had already multiple surgical procedures at the same wrist. Standardised preoperative and postoperative evaluation included assessment of pain by a visual analogue scale, radiographic examination, range of motion measurements, lifting capacity and grip strength. The patient-perceived function was investigated using clinical score charts.

Results:
Compared to the preoperative status range of motion showed little change, whilst grip strength, lifting capacity, pain score, and patient-perceived functions improved significantly.

Conclusion:
In this study arthroplasty of the DRUJ using the semiconstrained distal radioulnar joint arthroplasty was found to result in satisfactory oucome.

3492

A. Marzel[1], M. Shilaih[1], W. Yang[1], J. Böni[5], S. Yerly[2], T. Klimkait[3], V. Aubert[4], H. Günthard[1], R. Kouyos[1], Swiss HIV Cohort Study[1]

How to find HIV transmission and serosorting couples using follow-up visits dates

Division of Infectious Diseases and Hospital Epidemiology, University Hospital Zurich, Zurich, Switzerland[1], Geneva University Hospital, Laboratory of Virology, Geneva, Switzerland[2], University of Basel, Molecular Virology, Department of Biomedicine–Petersplatz, Basel, Switzerland[3], University Hospital Lausanne, Division of Immunology and Allergy, Lausanne, Switzerland[4], Institute of Medical Virology, Swiss National Center for Retroviruses, Zurich, Switzerland[5]

Introduction:
Identifying and characterizing steady, as opposed to occasional, HIV transmission pairs can facilitate targeted prevention efforts on the population level and illuminate host-pathogen interactions and microevolution on the biological level. We hypothesize that some steady couples can be identified in cohort studies since they frequently attend together to the follow-up and laboratory test visits at the outpatient clinics.

Methods:
We analyzed 16,139 Swiss HIV Cohort Study patients, who accounted for a total of 434,432 visits, 1990 to 2014. Background probabilities for sharing visits by chance were obtained by shuffling the visits within each quarter and 108 flagged pairs were further evaluated.

Results:
Thirty-five putative transmission pairs with a high number of shared visits (median 15) were successfully validated using a large phylogenetic tree with 19,893 Swiss and 116,408 Los Alamos sequences, self-reported steady HIV positive partnership and risk group affiliation. Nine steady serosorting pairs were detected as well. Notably, twelve transmission pairs (34%, 12/35) were of a mixed ethnicity with a large median age gap (19 years, IQR 15.5-23) and predominantly non-B subtypes, alluding to imported infections.

Conclusion:
We propose and validate a simple concept for identification of steady transmission and serosorting pairs, alongside with the illumination of privacy hazards which are inherent to large, detailed and prospective anonymized datasets.

3495

M. Kälin[2], B. Ledergerber[2], B. Müllhaupt[1], A. Rauch[3], P. Schmid[4], F. Banderet[5], S. Giulieri[6], R. Weber[2], H. Kovari[2]

Liver Fibrosis in HIV-monoinfected Persons with chronic elevated aminotransferase levels

Division of Gastroenterology and Hepatology, University Hospital of Zurich, Zurich, Switzerland[1], Division of Infectious Diseases and Hospital Epidemiology, University Hospital of Zurich, Zurich, Switzerland[2], University Clinic of Infectious Diseases, University Hospital Berne and University of Berne, Berne, Switzerland[3], Division of Infectious Diseases, Cantonal Hospital, St. Gall, Switzerland[4], Division of Infectious Diseases and Hospital Epidemiology, University Hospital, Basle, Switzerland[5], Division of Infectious Diseases, University Hospital, Lausanne, Switzerland[6]

Introduction:
Chronic alanine aminotransferase elevation (LEE) is frequent among HIV-infected persons without hepatitis B and C coinfection. However, little is known about its clinical significance. We studied the association of LEE and significant liver fibrosis in HIV-monoinfected patients.

Methods:
A case control study was performed including patients with LEE without chronic viral hepatitis and matched controls of the Swiss HIV Cohort Study (SHCS). Matching criteria were similar duration of HIV infection and follow-up. Chronic LEE was defined as ALT >50/>35 U/L (males/females) at ≥2 consecutive semi-annual visits. All participants underwent transient elastography (TE) and the two non-invasive fibrosis biomarkers, APRI and FIB-4, were calculated. Significant liver fibrosis was defined as Metavir ≥F2 in TE.

Results:
In 94 case patients and 101 controls valid TE, APRI and FIB-4 results were available. Baseline characteristics of cases and controls were as follows: median age 48(cases)/48(controls) yrs (p=0.68); male 72/80% (p=0.20); median CD4 cell count 615/524/µL (p=0.03); on antiretroviral therapy (ART) 98/95% (p=0.64); median ART duration 9.6/8.7 yrs (p=0.17); median BMI 26.1/24.3 kg/m^2 (p=0.01). The median TE score was 5.05 kPa (IQR 4.0-7.3 kPa) in cases and 4.6 kPa (3.7-5.8 kPa) in controls. Significant liver fibrosis was present in 24 (25.5%) of cases, and 8 (7.9%) of controls, including cirrhosis (Metavir F4) in 6 (6.4%) cases, and 2 (2.0%) controls. Adjusted logistic regression analyses showed an independent association between LEE and liver fibrosis (OR 3.84 [95% CI 1.57-9.42]). There was a trend but no significant association between liver fibrosis and older age (40-50 yrs 2.00 [0.38-10.54], >50 yrs 2.23 [0.41-12.13], versus <40 yrs), duration of ART exposure (5-9 yrs 1.86 [0.55-6.29], 10-14 yrs 1.05 [0.28-3.96], ≥15 yrs 2.49 [0.66-9.38] versus <5 yrs), obesity (1.87 [0.64-5.45]), and moderate/severe alcohol consumption (1.09 [0.19-6.21]). APRI and FIB-4 correlated with TE with Spearman's rho of 0.357 (p<0.001) and 0.240 (p<0.001), respectively.

Conclusion:
HIV-monoinfected persons with LEE had a high rate of significant liver fibrosis and cirrhosis. LEE was independently associated with liver fibrosis.

3497

S. Karlen[1], S. Kuster[2], E. Eschmann[1], S. Weiler[3], J. Blaser[1]

Adherence to guidelines for therapeutic monitoring of glycopeptide and aminoglycoside antibiotics

Medical Informatics Research Centre, Directorate of Research and Education, University Hospital of Zurich, Zurich[1], Division of Infectious Diseases and Hospital Epidemiology, University Hospital of Zurich, Zurich[2], Division of Clinical Pharmacology and Toxicology, University Hospital of Zurich, Zurich[3]

Introduction:
Guidelines for therapeutic drug monitoring (TDM) have been established for glycopeptide and aminoglycoside antibiotics due to their narrow therapeutic windows to ensure therapeutic efficacy and to avoid toxic overdosing with nephro- or ototoxicity. The purpose of this quality control study was to determine the adherence to TDM guidelines for the aminoglycoside gentamicin (G) and the glycopeptides vancomycin (V) and teicoplanin (T) in order to assess the need for improvements.

Methods:
We included all inpatients admitted to the University Hospital Zurich over a 3-year-period from 01/01/2012 to 31/12/2014. All electronic orders of intravenously administered G, V, and T and the corresponding TDM-lab-orders were analyzed retrospectively. Medication orders during intensive care stays were not electronically available and were therefore excluded.
Institutional guidelines released 2011 provided recommendations for initial monitoring no later than 72 h for G, 60 h for V and 96 h for T, respectively. Shorter initial TDM intervals have been advised for patients with impaired renal function and for thrice in contrast to once daily dosing of G. Guidelines released 2014 propose shorter intervals for G and T. In this analysis, however, these shortened intervals have not been considered.
Drug therapies may be prescribed as single or multiple subsequent orders (e.g. for dose adjustments). Therefore, subsequent prescriptions being separated by ≤ 24h were considered as single continuous therapies. To analyze the adherence to guidelines we measured the time period between the start of drug therapy and the initial TDM.

Results:
Drug therapies administered to 115’509 inpatients were analyzed, including 470 G therapies consisting of 1’045 orders, 2’396 V therapies with 6’168 orders and 807 T therapies with 2’184 orders.
Therapies were administered for less than 72 h in 40% (188/470) of G, 41% (985/2’396) of V and 26% (209/807) of T.
Therapies lasting ≥ 72 h were monitored according to guidelines for G in 72% (203/282), for V in 67% (939/1411) and for T in 63% (379/598).
Therapies of ≥ 96 h, were monitored within 72 h for G in 74% (178/241), for V in 74% (907/1’224), and for T in 50% (275/552).
Therapies of ≥ 120 h were not monitored at all for G in 7% (14/208), for V in 7% (68/1046), and for T in 13% (66/512), respectively.

Conclusion:
Physicians’ adherence to TDM guidelines was only 72% or below, with the best compliance for G. Overall TDM adherence offers room for improvement and quality assurance actions have to be considered. Educational programs require a continuous effort. As a complementary measure computerized decision support might be implemented. Automated reminders could be displayed in the medical record whenever TDM is overdue. The same algorithms might also be applied to other therapies that have to be monitored according to guidelines. Studies are needed to evaluate the impact of these concepts on patients’ safety, treatment efficacy and physicians’ over-alerting.

3498

G. Petitjean[1], A. Fahrny[2], C. Mettling[3], F. Kirchhoff[4], R. Speck[2], M. Benkirane[1]

Towards the development of a humanized mouse model for tracking, localizing and understanding HIV persistence in vivo

Molecular Virology Laboratory, Institute of Human Genetics CNRS UPR1142, Montpellier[1], Department of Infectious Diseases and Hospital Epidemiology, University Hospital Zurich, Zurich[2], Homing, Immune activation and Infection, Institute of Human Genetics CNRS UPR1142, Montpellier[3], Institute of Molecular Virology, Ulm University Medical Center, Ulm[4]

Introduction:
Efforts toward the development of therapies aimed at targeting the HIV reservoir are complicated by the evidence that HIV persistence is the result of persistent productive and non-productive infection in a number of cell types and mediated by a variety of mechanisms. *In vitro* models of HIV persistence in different cellular reservoirs have been key in advancing our knowledge in this area of research, however they are limited by their inability to recapitulate the extremely complex virus-cell interactions occurring *in vivo*. Understanding the complex interaction between HIV, its host and therapeutic tools is required to achieve HIV cure. Therefore, developing a latency and persistence model of HIV-1 enabling the identification and testing of therapeutic strategies is needed. For this purpose we developed an animal model to study viral persistence in which tracking, localizing, sorting and validating identified targets is possible.

Methods:
We designed a dual color infection-reporter transgene able to express fluorescent proteins in productively and/or latently-infected cells. We used this transgene in humanized NOD-*scid* IL2R?^{null} (NSG) mice, which were then infected with a recombinant HIV-1 strain. Once disseminated HIV infection was confirmed by qPCR, flow cytometry was employed to evaluate the reporter system. To characterize the tissues and cell types involved in HIV-1 in mouse model, an 8-color staining panel was implemented, including CD45RA, HLA-DR and CCR7.

Results:
Despite low frequencies, GFP+RFP+ CD4+ T cells could be detected by flow cytometry in the spleens, lymph nodes and bone marrows of humanize mice, with highest frequency being found in the spleens. This cell population could not be detected in PBMCs, most likely due to the low amount of cells that could be collected from the mice. High viral loads resulted in greater numbers of infected lymphocytes found in each compartment.

Conclusion:
Such an animal model will bring answers to key questions in the field of viral persistence such as: 1) What is the source of viral rebound after ART interruption? 2) Where do HIV-infected persistent cells localize *in vivo*? 3) What are the cellular factors and the mechanisms involved in the establishment and maintenance of transcriptionally latent provirus *in vivo*. 4) Do latently infected cells express a specific marker differentiating them from their non-infected counterparts?

3499

A. Jödicke[1], H. Dahmke[1], G. Kullak-Ublick[1], S. Weiler[1]

Severe Injection Site Reactions after subcutaneous Administration of Sayana®: A qualitative post-marketing Analysis of Cases reported to the Regional Pharmacovigilance Centre Zurich

Regional pharmacovigilance Centre Zurich, Department of Clinical Pharmacology and Toxicology, University Hospital Zurich and University of Zurich, Switzerland[1]

Introduction:
Sayana® was introduced into the market as the first depot-medroxyprogesteron acetate containing contraceptive that is administered via subcutaneous injection every 3 months. In 2014 and 2015 the regional pharmacovigilance centre of Zurich (RPVC Zurich) received 11 anonymised reports of severe local reactions after Sayana® administration. The injection site reactions were classified as lipodystrophies, atrophies or persisting indurations. In this case series individual case safety reports (ICSRs) concerning this adverse drug reaction (ADR) were analysed.

Methods:
International, national and regional ICSRs during Sayana® administration were analysed. Data on ADRs were retrieved from the WHO Global Database VigiBase™. Additional demographic data, drug administration information, duration of Sayana® treatment, latency time of the ADR, its course, severity and outcome were collected and analysed.

Results:
Worldwide 396 ICSRs (351 (88.6%) serious vs. 45 (11.4%) non-serious) after Sayana® were registered in the database until 2015-11-01. Overall in 325 (82%) cases injection site reactions were coded. In Switzerland 78 ICSRs (68 (87.2%) serious vs. 10 (12.8%) non-serious) were registered and 11 cases were reported by physicians to the RPVC Zurich, all categorized as serious ADRs. In all of these 11 patients lipoatrophy or -dystrophy, persisting atrophy or induration at the injection site occurred. In 9 of 11 patients, the indication for the use of Sayana® was contraception, in 1 patient hypermenorrhoea (in 1 patient not reported). In all patients Sayana® was administered subcutaneously. In the majority of patients (n=7, 63.6%) the latency between the application of Sayana® and the development of the lipodystrophy was 2-4 months. In 6 patients (54.5%) further administration of Sayana® led to another dystrophic area. In 3 patients (27.3%) the rechallenge was negative. Most of the reactions were irreversible (n=9, 81.8%) and caused major distress to the affected patients. One patient even underwent plastic surgery for cosmetic improvement of the lesion.

Conclusion:
Administration site reactions during Sayana® treatment occur frequently. Serious adverse drug reactions include lipodystrophy and persistent atrophy at the injection site. These reactions were recently integrated in the Swiss product information of Sayana®. Patients should be informed and advised about these recently labelled and potentially irreversible adverse drug reactions at the injection site.

3500

E. Malagola[1], E. Saponara[1], M. Bombardo Ayats[1], K. Grabliauskaite[1], T. Reding[1], R. Graf[1], S. Sonda[1]

Role of thyroid hormone T3 in pancreatic acinar cells

Visceral and Transplantaion Surgery Department, University Hospital Zürich, Zürich[1]

Introduction:
Acute pancreatitis is a debilitating inflammation of the pancreas, which leads to exocrine dysfunction. In this pathological condition, acinar cells enter a regenerative response of transient dedifferentiation and proliferation. The aim of this study is to investigate the molecular mechanisms that govern induction of acinar cell proliferation, with emphasis on thyroid hormone T3, which has been shown to act as a potent mitogenic stimulus.

Methods:
Wild type C57BL/6 mice were injected with cerulean to induce pancreatitis, T3 or a combination of the two molecules. Levels of cell proliferation, inflammation and fibrosis were investigated through immunohistochemistry as well as gene expression analysis. Signalling cascade activation was quantified through biochemical analyses.

Results:
Analysis of gene expression at early stages of acute pancreatitis revealed a specific activation of T3 pathway within the pancreatic tissue. T3 supplementation in combination with cerulein stimulated proliferation only of pancreatic acinar cells, while no mitogenic activity was found in islet or ductal cells. Furthermore we detected activation of β-catenin as well as AKT pathway following T3 supplementation.

Conclusion:
The evidence of a regulation of thyroid hormone pathway during pancreatitis highlights a putative patho-physiological role of endogenous T3 in pancreatic regeneration. T3 robustly promotes cell cycle progression of acinar cells in both normal and injured pancreas. Our data point out a putative correlation between T3 and AKT and β-catenin pathways, which are already known to regulate pancreatic regeneration. Thus, T3 administration may have a therapeutic role to improve the outcome of this severe disease.

3501

B. Li[1], G. Meisl[2], C. Zhu[1], C. Tournaire[1], M. Zurbrügg[1], V. Eckhardt[1], M. Nuvolone[1], S. Sorce[1], T. Knowles[2], S. Hornemann[1], A. Aguzzi[1]

Establishment of a homogenous-phase PrPSc-FRET for fully automated high-throughput prion detection

Institute of Neuropathology, University Hospital Zurich, Switzerland[1], Department of Chemistry, University of Cambridge, UK[2]

Introduction:
Prion diseases are a group of fatal neurodegenerative disorders that are characterized by deposition of scrapie prion protein (PrP^{Sc}), a misfolded and aggregated isoform of the host-encoded cellular prion protein (PrP^{C}), within the central nervous system (CNS) and other organs. Prion diseases are unique among neurodegenerative conditions because of their transmissibility between individuals. The infectious agent consists of PrP^{Sc}, which acts as a propagon capable of seeding a self-perpetuating reaction of templated nucleation.
So far, several key questions of prion replication and subsequent neurodegeneration have not been answered yet, including the genes and proteins that regulate the endogenous PrP^{C}, the machinery of PrP^{C} to PrP^{Sc} conversion, and the molecules affecting susceptibility to prion infection and cell-to-cell spread of prions. This is mainly because the conventional methods for PrP^{C} and PrP^{Sc} measurement and prion infectivity titration have inherent limitations in applicability to high-throughput research, leading to the dearth of high-throughput technology that can be used to identify the mechanisms.

Methods:
To measure prion proteins in a fast, sensitive, and automatable manner, we developed homogeneous-phase fluorescent resonance energy transfer (HPFRET) assays for quantification of either PrP^{C} or PrP^{Sc}. In the assay version aimed at detecting PrP^{Sc} in homogeneous phase (PrP^{Sc}-HPFRET), test samples were homogenized and treated with a lysis/digestion buffer containing detergents and proteinase K (PK). Any cellular PrP^{C} present in samples is fully degraded by PK, whereas PrP^{Sc} aggregates indicative of prion infection are PK-resistant and therefore preserved. After PK inactivation by PMSF, concentrated sodium hydroxide was added to disassemble PrP^{Sc} aggregates into monomers, followed by phosphate buffer for pH neutralization. Detection of residual PrP was accomplished by adding a mixture of two monoclonal antibodies directed against two non-overlapping epitopes of PrP and labeled with Europium (Eu^{3+}) and allophycocyanin (APC), respectively. By bridging the two antibodies, any PrP present in the sample enabled concentration-dependent FRET, thereby providing a homogeneous-phase readout with extremely little background, a broad linear dynamic range, and sufficient sensitivity.
We ported the PrP^{Sc}-HPFRET to a Perkin-Elmer Janus liquid handling platform integrated with a FRET reader and an automated incubator capable of hosting forty-four 384-well microplates. The fully automated assay including three elements: 1) cell lysis and proteolysis of PrP^{C}, 2) disaggregation of PrP^{Sc}, 3) detection of residual PrP by a FRET antibody pair. Under typical production conditions, this translated into a throughput of 15360 wells/24 hours, enabling sufficient throughput for large-scale HTS applications.

Results:
We established PrP^{Sc}-HPFRET which allowed us 1) to assess PrP^{Sc} level in various prion-infected mouse brain regions at different time points; 2) to establish a cell-based prion infectivity bioassay; 3) to detect RNAi-mediated gene silencing and block of prion replication.

Conclusion:
The PrP^{Sc}-HPFRET is highly adapted to high-throughput screening platforms for basic and applied prion research, including e.g. high-throughput screens for the identification of chemicals interfering with prion secretion, prion infection, and/or prion replication, and genome-wide RNAi or CRISPR/Cas9 screens aimed at understanding the mechanisms of prion transmissibility and replication.

3502

E. Saponara*[1], G. Seleznik[1], R. Buzzi[1], F. Baschieri[2], H. Farhan[2], O. Pertz[3], I. Esposito[4], T. Reding[1], R. Graf[1], S. Sonda[1]

Serotonin transporter inhibition prevents Rac1-dependent cytoskeletal remodeling and reduces pancreatic acinar-to-ductal metaplasia formation

Swiss HPB Center, Visceral & Transplantation Surgery, Switzerland[1], Department of Biology University of Konstanz Biotechnology Institute Thurgau, Switzerland[2], Department of Biomedicine University of Basel, Switzerland[3], Institute of Pathology Medical University of Innsbruck, Austria[4]

Introduction:
Acinar-to-ductal metaplasias (ADMs) are considered a prerequisite for pancreatic intraepithelial neoplasia (PanIN) development. Importantly, ADM formation depends on cytoskeletal remodeling promoted by the activity of the small GTPase Rac1. We recently demonstrated that intracellular serotonin (i5-HT) induces actin remodeling in pancreatic acini. We aim now to investigate whether pharmacological inhibition of 5-HT uptake prevents the formation of ADM and PanIN lesions.

Methods:
Murine and human pancreatic cancer cell lines, in vitro 3D culture models of ADM formation and genetically modified mice were utilized to identify the molecular mechanisms at the base of 5-HT-dependent cytoskeletal remodeling. The therapeutic potential of selective 5-HT transporter inhibitors (SERTi) was evaluated both in vitro and in vivo using transgenic mice harboring KrasG12D mutation, which spontaneously induces ADM and PanIN lesions.

Results:
Biochemical and imaging assays showed that reduced levels of 5-HT prevented Rac1 activation both in vitro and in vivo. Inhibition of 5-HT uptake completely abolished ADM formation in 3D culture-system and significantly reduced pancreatic cancer cell migration, without affecting cell viability. Importantly, pharmacological treatment of KrasG12D mice with SERTi significantly reduced ADM and PanIN lesion formation without apparent drug toxicity.

Conclusion:
Our data indicate that cytoskeletal remodeling, dependent on i5-HT, is critical for the formation of ADM lesions and cancer cell migration likely through Rac1 activation. Given the aggressive nature of pancreatic ductal adenocarcinoma (PDAC), we are currently investigating the potential of SERTi as a novel therapeutic strategy to target cancer development and invasiveness.

3503

S. Ehrbar[1], R. Perrin[2], M. Peroni[2], K. Bernatowicz[2], T. Parkel[3], I. Pytko[1], S. Klöck[1], M. Guckenberger[1], S. Lang[1], D. Weber[2], A. Lomax[2]

Advanced respiratory motion management in radiation oncology - A phantom study

Radiation Oncology, University Hospital Zurich, Zurich[1], Center for Proton Therapy, Paul Scherrer Institute, Villigen[2], Centre Suisse d'Electronique et de Microtechnique, Landquart[3]

Introduction:
Radiotherapy treatment of lung tumors is affected by respiratory tumor motion, which enlarges the tumor position uncertainty during the treatment. These uncertainties result in increased treatment volumes (PTV) and hence higher radiation dose to nearby organs at risk (OAR). The following four motion-management techniques (MMT) can be applied to deal with this respiratory tumor motion: The internal target volume (ITV) concept with a PTV enclosing the whole tumor motion, the mid-ventilation (MidV) principle with probabilistic tumor margins, respiratory gating of the irradiation beam at steady tumor position, or dynamic treatment couch tracking with real-time compensation of the tumor motion. Dosimetric performances of these four techniques were investigated with film measurements in a sophisticated lung-tumor phantom

Methods:
The anthropomorphic and dynamic lung phantom LuCa (CSEM and PSI) was operated with 5 different respiration patterns with 10 to 20 mm internal tumor motion amplitude. Individual radiotherapy treatments were prepared, adapting the PTV to the four MMT (ITV, MidV, gating, tracking). A radiation dose of 8x6 Gy was prescribed to the PTV using VMAT stereotactic treatment planning. The phantom was irradiated with all individual treatment plans using the corresponding respiration pattern and MMT, together with static measurements. The internal tumor motion of the phantom was monitored with Calypso (Varian) for gating and tracking, and compensated with the PerfectPitch couch (Varian) for tracking. The radiation dose delivered the moving tumor was measured with Gafchromic EBT2 (ISP) films inside the tumor. These measured dose distributions were compared to the planned dose with gamma agreement scores using a 3%/3mm criterion ($GS_{3\%/3mm}$), and the film areas receiving more than the planned minimum dose ($A_{>Dmin}$) were calculated to report on tumor dose coverage. To report on dose sparing of OARs, their doses from the treatment plans were compared.

Results:
The results for each MMT are summarized in Table 1. All techniques achieved a good coverage of the tumor. Median values for $A_{>Dmin}$ were above 99% for all techniques and ITV and MidV concepts showed lower gamma agreement scores (median: 88.9% and 87.7%) compared to gating and tracking (94.2% and 94.8%). Gating and tracking were able to reduce OAR dose in all cases, when compared to ITV concept.

Table 1: Evaluated parameters from film measurements inside the tumor and OAR doses

	GS3%/3mm (%)	A>Dmin (%)	Lung Dmean (Gy)	Lung V20Gy (%)	Heart Dmean (Gy)	Spinal cord Dmax (Gy)
ITV	88.9 (82.3-95.7) [97.9]	99.8 (99.6-99.9) [99.5]	8.3 (7.9-8.9)	14.1 (13.0-15.5)	1.4 (1.3-1.5)	11.1 (10.9-11.7)
MidV	87.7 (74.5-91.5) [97.0]	99.1 (96.9-99.5) [100]	7.9 (7.2-8.0)	12.8 (11.3-13.4)	1.1 (1.1-1.3)	10.4 (10.2-10.4)
Gating	94.2 (93.2-96.4) [96.5]	99.9 (99.4-99.9) [99.0]	7.2 (7.1-7.3)	11.6 (11.3-11.8)	0.8 (0.6-0.9)	10.2 (9.5-10.8)
Tracking	94.8 (91.7-96.0) [96.7]	100 (99.9-100) [99.8]	7.2 (7.2-7.2)	12.1 (11.9-12.2)	1.0 (1.0-1.1)	9.8 (9.7-9.8)

Values: Median, (q_{25}-q_{75}), [static], pp: percentage points

Conclusion:
Tracking and gating showed a superior agreement with the planned dose distribution and were able to reduce the dose to OAR in comparison to the passive motion management techniques. These techniques should therefore be considered when treating lung tumor patients with pronounced respiratory tumor motion.

3504

D. Leuthard[1], S. Weiss[1], S. Freiberger[1], A. Duda[1], M. Heath[2], M. Skinner[2], M. Kramer[2], T. Kündig[1], P. Johansen[1]

Microcrystalline tyrosine as an adjuvant in allergy immunotherapy: a mouse study

Departement of Dermatology, University Hospital Zurich[1], Allergy Therapeutics Ltd., Worthing, United Kingdom[2]

Introduction:
Adjuvants in vaccines and allergen-specific immunotherapy (AIT) facilitate immune responses. The most commonly used adjuvant is aluminium hydroxide (alum). However, Alum has major limitations. It is not biodegradable, has potential toxic effects, and it mediates T-helper type 2 (Th2) immune response, which is associated with pathological rather than therapeutic pathways in allergy. Hence, new and improved adjuvants are being developed. Co-precipitates of L-tyrosine (microcrystalline tyrosine; MCT) with allergens/allergoids, and especially formulations also containing MPLA have been described as suitable adjuvants in AIT that facilitate short-course therapy. This ongoing study aims to assess the potential of MCT in AIT as well as to further elucidate action mechanisms of the adjuvant.

Methods:
A murine model for immunisation and AIT was applied. Typically, mice were immunised subcutaneously or sensitised intraperitoneally with ovalbumin (OVA) and MCT or OVA and alum. Immune responses were assessed by OVA-specific ELISA for IgG, IgG1, IgG2a, IgG2b, IgG3 and IgE. T-cell analysis was done by OVA-specific cytokine-ELISA after in vitro restimulation of spleen cells. The clinical effect was examined by measuring the change in body temperature after a systemic challenge with OVA. Possible mechanisms of action of MCT as an adjuvant were studied both in vitro and in vivo. Here, the role of MCT in activating inflammasomes and Toll-like receptors was investigated.

Results:
After three fortnightly immunisations, the levels of IgG antibodies in mice treated with MCT-based vaccines were comparable to those in mice treated with alum-based vaccines. The IgE production was slightly higher in the alum-treated mice, whereas the MCT-treated group showed slightly stronger IFN-γ response. The potential sensitisation risk by multiple injections with therapeutic allergens was slightly lower with MCT than with alum, and a challenge of sensitised mice with OVA-MCT showed less systemic anaphylaxis than a challenge with OVA-alum. Concerning the action mechanisms, results from in vitro experiments with antigen-presenting cells suggested that MCT is able to induce inflammasome-dependent IL-1β secretion. Moreover, immunisation with OVA-MCT in MyD88-deficient mice showed decreased immune responses compared to wild type mice.

Conclusion:
MCT and alum are comparable adjuvants with regards to the immunogenicity potential of allergens in mice. Due to the better safety profile, MCT represents a suitable adjuvant alternative to alum in AIT.

3505

J. Kresoja-Rakic[1], E. Kapaklikaya[1], G. Ziltener[1], D. Dalcher[2], R. Santoro[2], B. Christensen[3], K. Johnson[3], B. Schwaller[4], W. Weder[1], R. Stahel[5], E. Felley-Bosco[1]

Identification of cis- and trans-acting elements regulating calretinin expression in mesothelioma

Universität Zürich, Klinik für Thoraxchirurgie[1], Universität Zürich[2], Departments of Epidemiology, Pharmacology and Toxicology and Community and Family[3], University of Fribourg, Department of Medicine, Anatomy, Fribourg, Switzerland [4], Clinic of Oncology, University Hospital Zurich, Switzerland[5]

Introduction:
Calretinin *(CALB2)* is a diagnostic marker for epithelioid mesothelioma. It is also a prognostic marker since patients with tumors expressing high calretinin levels have better overall survival. Silencing of calretinin decreases viability of epithelioid mesothelioma cells. Our aim was to elucidate mechanisms regulating calretinin expression in mesothelioma.

Methods:
To investigate human calretinin *(CALB2*) promoter, ?1kb of genomic sequence surrounding the transcription start site (TSS) +1 was analyzed using luciferase reporter pGL3-basic vector. Transcriptional activity of 5'-deletion *CALB2* promoter constructs in mesothelioma cells was measured via dual luciferase assay. Mutant constructs were created by site-directed mutagenesis. Electrophoretic mobility shift (EMSA) assay and chromatin immunoprecipitation (ChIP) assay were used to show binding of functional transcription factors (TF). To demonstrate cell-cycle regulated calretinin expression, mesothelioma cells were synchronized using double thymidine treatment followed by nocodazole treatment.

Results:
Analysis of calretinin transcript and protein suggested a control at the mRNA level. Treatment with 5-aza-2'-deoxycytidine and analysis of TCGA data indicated that promoter methylation is not likely to be involved. Therefore, we investigated *CALB2* promoter by analyzing ?1kb of genomic sequence surrounding the transcription start site (TSS) +1 using promoter reporter assay. Deletion analysis of *CALB2* proximal promoter showed that sequence spanning the -161/+80bp region sustained transcriptional activity. Site-directed analysis identified important cis-regulatory elements within this -161/+80bp *CALB2* promoter. EMSA and ChIP assays confirmed binding of NRF-1 and E2F2 to the *CALB2* promoter and siRNA knockdown of NRF-1 led to decreased expression of calretinin. Cell synchronization experiment showed that calretinin expression was cell cycle regulated with a peak of expression at G1/S Phase.

Conclusion:
Our study identified the transcription factors NRF-1 and E2F2 to bind to the human *CALB2* promoter and we demonstrated cell cycle-dependent regulation of calretinin expression in mesothelioma cells providing the first insight into the regulation of *CALB2* expression in mesothelioma cells.

3507

T. Fedele[1], M. Van 't Klooster[2], S. Sergey[1], W. Zweiphenning[2], N. Van Klink[2], M. Zijlmans[2]

Automatically detected residual fast ripples in the intraoperative corticogram predict epilepsy surgery out

Universitätsspital Zürich[1], University Medical Center, Utrecht, Netherlands[2]

Introduction:
Fast ripple (FR) High Frequency Oscillations (HFOs) in the post-resection ECoG have recently been shown to be highly specific predictors of surgical outcome. However, FR visual marking is time consuming and depends on the expert observer. We propose here a time-frequency based automatic HFO detector .

Methods:
Presurgical ECoG (N=14 patients) with visually marked HFOs were used to calibrate the detector's parameters defining baseline and threshold. Then the calibrated detector was applied on a larger post-resection ECoG dataset (N=54), and compared with visual marking and clinical outcome. The analysis was conducted separately for ripples (80-250 Hz) and FRs (250-500 Hz).

Results:
Automatically detected FRs were predictive of clinical outcome with positive predictive value PPV = 100% and negative predictive value NPV = 62%. Channel-wise comparison showed a high association between automatic detection and visual marking ($p<0.001$).

Conclusion:
Our automatic and fully unsupervised detection of HFO events emulated the expert observer's performance in both event selection and outcome prediction. It provides a standardized definition of clinically relevant HFOs, which may spread its use in clinical application.

3508

E. Boran[1], J. Sarnthein[1], G. Curio[2], J. Gotman[3], T. Fedele[1]

Non-invasive detection of fast ripples in low-noise EEG recordings

Neurosurgery Department, University Hospital Zürich, Zürich[1], Neurophysics Group, Department of Neurology, Campus Benjamin Franklin, Charite, Berlin, Germany[2], Montreal Neurological Institute and Hospital, Montreal, Quebec, Canada[3]

Introduction:
Ripples (80-250 Hz) and fast ripples (FRs, 250-500 Hz) are characterized by poor signal-to-noise ratio (SNR), which reduces their visibility in non-invasive recordings. While ripples could be observed in scalp EEG, FR detection has been restricted only to invasive recordings. We report here on FRs detection in the scalp EEG of epilepsy patients, recorded with low-noise technology.

Methods:
One hour scalp EEG was recorded in two patients with focal epilepsy exhibiting interictal spikes and one non-epileptic patient. We used a custom-made low-noise 8-channel amplifier, with noise level 2.3 nV/√Hz. Electrodes were placed on both hemispheres with impedances below 2 kΩ. Segments of artifact-free bipolar traces, filtered in the FR band, were selected for analysis. FR rates were obtained semi-automatically by combining entropy based amplitude threshold computation and single event visual validation.

Results:
For patient 1 (spikes on left side), FR rates averaged across channels were 0.495/min on the left and 0.046/min the right side. For patient 2 (spikes predominantly on the right side), rates were 1.365/min on the left and 1.262/min the right side. For patient 3 (absence of spikes), rates were 0.057/min. The mean FR peak-to-peak amplitude was 3.23 ± 2.79 µV. The amplitude threshold was 0.51 ± 0.08 µV across all channels.

Conclusion:
FRs in scalp EEG could be detected using optimized low-noise technology. FRs were more frequent in the more epileptogenic regions and may therefore represent epileptic activity. The opportunity to access FRs non-invasively represents a critical step towards the non-invasive investigation of fast neural dynamics.

3509

S. Burnos[2], T. Fedele[1], N. Krayenbühl[1], P. Hilfiker[3], K. König[3], T. Grunwald[3], J. Sarnthein[1]

Relation of automatically detected High Frequency Oscillations (HFOs) with the SOZ and clinical outcome

Neurosurgery Department, University Hospital Zurich, Zurich, Switzerland[1], Institute of Neuroinformatics, ETH Zurich, Zurich, Switzerland[2], Swiss Epilepsy Centre, Zurich, Switzerland [3]

Introduction:
While HFOs are gaining acceptance as biomarkers of the epileptogenic zone, their standardized detection is still debated.

Methods:
Preoperative invasive recordings were collected during sleep in 10 epilepsy patients, 6 implanted with medial temporal depth electrodes and 4 with neocortical electrodes. Recordings were analyzed with two automatic detectors, based on instantaneous spectral estimation. Both detectors have previously been validated independently on two different visually marked datasets. Analyses were conducted separately for ripple (80-250Hz) and fast ripple (FR, 250-500Hz) frequency ranges. Areas with the highest HFO rates were related to the seizure onset zone (SOZ) as determined by invasive ictal recordings and clinical outcome.

Results:
In patients with depth electrodes, we observed both ripples and FRs, while FRs were detected less frequently in cortical signals. With respect to the SOZ, FRs were more specific than ripples and correctly identified the SOZ in 5 patients, with a partial overlay in 2 more patients. In patients with good outcome (4 patients), we observed a high specificity of FRs. Ripples were more sparsely distributed, and we observed possibly physiological ripples outside the SOZ. In patients with poor outcome (4 patients), ripples and FRs occurred in contacts showing epileptiform potentials and were present also in non-resected non-SOZ areas.

Conclusion:
The time-frequency based automatic ripple and FR detection provides a rapid assessment of the potential contribution of HFOs. Fast ripples were more specific than ripples in identification of the epileptogenic tissue. The clinical relevance of HFOs was evaluated with fully automatic detectors, which standardize the definition of an HFO.

3510

A. Mortezavi[1], S. Salemi[1], O. Gross[1], T. Sulser[1], D. Eberli[1]

Inhibition of autophagy significantly increases the antitumor effect of Abiraterone in LnCap prostate cancer cells

Urology Clinic, University Hospital Zurich, Zurich, Switzerland[1]

Introduction:
Abiraterone (Abi) is an approved treatment for men with metastatic castration resistant prostate cancer. Abi is an inhibitor of CYP171A, a key enzyme of the androgen synthesis. Recent data implicates, that Abi does not only lead to a further decrease of circulating testosterone levels, it also has inhibitory effects on the intratumoral synthesis of active androgens, which plays a significant role in gaining resistance against conventional androgen deprivation therapies. An additional mechanism of survival in prostate cancer cells during extracellular androgen deprivation is autophagy; a conserved lysosomal degradation pathway, which can ensure cellular survival during stress and starvation. We hypothesized that inhibition of intracellular androgen synthesis with Abi may lead to a more excessive up-regulation of autophagy. Furthermore we investigated, if a combination of Abi with autophagy inhibition could further increase the antitumor activity.

Methods:
To mimic androgen deprivation, human prostate cancer LnCap cell lines were cultured in steroid-free medium. Simultaneously cells were treated with Abi (10 µM), with the autophagy inhibitors 3-methyladenine (3MA, 5 mM) or chloroquine (CHQ, 20 µM). In a second step cells were treated with a combination of Abi and 3MA or Abi and CHQ. Ethidium Bromide, Annexin V and Propidium Iodide were used to assess cell viability and apotosis by performing flow cytometry on the 4th day after initiation of treatment. Autophagy was monitored by western blotting; lysates were analyzed by protein staining for expression of ATG5, Beclin 1, LC3-I, LC3-II and P62. LnCap cells were stained for ATG5, LC3-II, Beclin 1 and Autodot for microscopic analysis.

Results:
Abi treatment in LnCap cells lead to an 8.1% reduction of cell viability and an 11.4% increase of apoptosis compared to control on day 4. Inhibition of autophagy through 3MA and CHQ also reduced cell viability (12.6% and 3.3%) and increased apoptosis (14.8% and 17.7%). When autophagy was inhibited in abi treated cells, a further significant reduction of cell viability (26.46%, p=0.02) and significant increase of apoptosis rates (27.3%, p=0.03) could be observed. Assessment of autophagy levels of Abi treated cells by Western blot revealed enhanced up-regulation of Atg5 and LC3-II with a reduction of P62 protein expression. No changes in Beclin 1 expression could be noticed. Immunocytochemistry revealed significantly increased autophagy levels in abi treated cells indicated through high reactivity for ATG5 and pronounced LC3-II punctuation. Same increased autophagosomes punctuation pattern was observed using Autodot staining.

Conclusion:
Taken together, this data demonstrates that Abiraterone treatment leads to increased autophagy levels in LnCap cells and a combination with autophagy inhibition significantly increases its antitumor effect providing a new therapeutic approach potentially translatable to patients.

3511

J. Smolar[1], M. Horsts[2], M. Ehrbar[3], D. Eberli[1]

Co-culture of bladder-derived smooth muscle cells with smooth muscle-like adipose-derived stem cells leads to smooth muscle microtissue formation in 2D and 3D systems

Urology Clinic, University Hospital Zurich, Zurich, Switzerland[1], Children's University Hospital, Department of Urology, Steinwiesstrasse 75, CH-8032 Zürich[2], Obstretrical Research Unit, Department of Obstetrics and Gynecology, University Hospital Zurich, Zurich[3]

Introduction:
Neuropathic bladder often leads to the development of severe bladder dysfunction, recurrent urinary tract infections, stone formation, vesicoureteral reflux and kidney failure. Although enterocystoplasty provides some functional improvement it is associated with long-term complications, such as metabolic abnormalities and malignancies. Therefore, there is a strong clinical need for an alternative approach for these reconstructive procedures. Our ultimate goal is to bioengineer contractile bladder tissue using co-culture of bladder-derived smooth muscle cells (SMCs) and pre-differentiated smooth muscle-like adipose-derived stem cells (pADSCs) in an optimized hydrogel scaffold and to further improve vascularization and innervation of the regenerating bladder tissue.

Methods:
We have isolated and characterized SMCs and pADSCs using immunofluorescence and flow cytometry. Further, we have mixed the SMCs and pADSCs in different ratios and co-cultured them in 2D and 3D systems using PEG hydrogel scaffold. Cells were analyzed morphologically and for the expression of SMC-markers calponin, MyH11 and smoothelin by immunostaining, as well as by viability measurement and proliferation assay.

Results:
All co-cultured conditions of SMCs and pADSCs in ratios 1:1, 1:3 and 1:5 (SMCs:pADSCs) showed an improved cell proliferation after 4 days. However, the 1:1 and 1:3 ratios showed significantly better results after 8 days, compared to 1:5 ratio and single cell cultures. Additionally, cells in 1:1 and 1:3 ratios showed a stable expression of all SMC-markers at a similar level as native SMCs. After 2 weeks of 2D co-culture the 1:1 and 1:3 ratios formed large microtissues positive for all SMC markers, whereas the 1:5 ratio showed only minimal microtissue formation and lower smoothelin expression.
Poor cell survival and no microtissue formation were observed when SMCs and pADSCs were cultured in 2% PEG hydrogel for 2 weeks. However, upon co-cultured at the ratios 1:1, 1:2 and 1:3 (SMCs:pADSCs), cells showed correct morphology and microtissue formation was detected already after 1 week. After 3 weeks of co-culture, formed microtissues showed increased cellular interconnectivity and strong expression of all SMC-markers.

Conclusion:
We have shown that both 2D and 3D co-cultures of SMCs and pADSCs exhibit a beneficial effect on cell proliferation, phenotype stability, microtissue formation and faster cell-cell network development compared to single cell cultures. This effect may help to engineer functional bladder tissue by solving some of the main issues of tissue engineering, namely poor cell survival, proliferation and phenotypic instability.

3512

S. Salemi[1], D. Keller[1], M. Rottmar[1], T. Sulser[1]

Multi-cell approach for successful bioengineering of functional smooth muscle layers

Urology Clinic, University Hospital Zurich, Zurich, Switzerland[1]

Introduction:
Engineered tissues for bladder augmentation or substitution would allow circumventing the side effects of using bowel tissue for reconstruction. Tissue engineering using a combination of cells may provide novel approach for functional reconstruction. Adipose derived stem cells (ADSC) might be a key instrument to bioengineer contractile bladder tissue when differentiated to smooth muscle cells (SMC). However, it is uncertain whether these cells maintain their cell fate long term in vivo. It is our aim to evaluate different combinations of cells to improve the bladder tissue formation, by improving the microenvironment and cell-to-cell interactions.

Methods:
We have characterised rat ADSCs and optimally differentiated them to SMC (3 weeks) prior to subcutaneous injection into nude mice. Cells were injected in different combinations (ADSC, ADSC + differentiated ADSC, SMC, differentiated ADSC + SMC). The tissue formation was followed by MRI and PKH labelling. The formed tissue was analysed for contractile proteins measuring gene and protein expression by using RT-qPCR, western blot and immunohistochemistry.

Results:
In all experimental conditions, the PKH positive cells could be detected after 4 weeks, indicating the presence and survival of engineered tissues in vivo. MRI was able to visualize the engineered SM tissue over the study period. Collagen without cells showed no signal and was absorbed quickly. The tissue size differed between the experimental conditions with tissues grown from cells with 3 week ex vivo differentiation showing the largest constructs with good correlation in histology. Differentiated ADSC showed positive upregulation of smooth muscle makers (Calponin, Smoothelin, MYH11 and αSMA) similar to bladder derived SMC.

Conclusion:
The presented research offers key information on survival and functionality of bioengineered smooth muscle tissue grown using differentiated ADSC in combination with differentiated cells. This approach could help to engineering contractile bladder tissue for future clinical application.

3513

S. Burnos[2], B. Frauscher[3], R. Zelmann[3], C. Haegelen[4], J. Sarnthein[1], J. Gotman[3]

The morphology of high frequency oscillations (HFO) does not improve delineating the epileptogenic zone

Neurosurgery Department, University Hospital Zurich, Zurich, Switzerland[1], Institute of Neuroinformatics, ETH Zurich, Zurich, Switzerland[2], Montreal Neurological Institute and Hospital, Montreal, Quebec, Canada[3], MediCIS, INSERM, Faculté de Médecine, University of Rennes, Rennes, France[4]

Introduction:
We hypothesized that high frequency oscillations (HFOs) with irregular amplitude and frequency more specifically reflect epileptogenicity than HFOs with stable amplitude and frequency.

Methods:
We developed a fully automatic algorithm to detect HFOs and classify them based on their morphology, with types defined according to regularity in amplitude and frequency: type 1 with regular amplitude and frequency; type 2 with irregular amplitude, which could result from filtering of sharp spikes; type 3 with irregular frequency; and type 4 with irregular amplitude and frequency. We investigated the association of different HFO types with the seizure onset zone (SOZ), resected area and surgical outcome.

Results:
HFO rates of all types were significantly higher inside the SOZ than outside. HFO types 1 and 2 were strongly correlated to each other and showed the highest rates among all HFOs. Their occurrence was highly associated with the SOZ, resected area and surgical outcome. The automatic detection emulated visual markings with 93% true positives and 57% false detections.

Conclusion:
HFO types 1 and 2 similarly reflect epileptogenicity. For clinical application, it may not be necessary to separate real HFOs from “false oscillations” produced by the filter effect of sharp spikes. Also for automatically detected HFOs, surgical outcome is better when locations with higher HFO rates are included in the resection.

3514

S. Salemi[1], A. Mortezavi[1], T. Sulser[1], D. Eberli[1]

Functional Smooth muscle cells differentiated from Adipose Derived Stem Cells: The importance of Authophagy

Urology Clinic, University Hospital Zurich, Zurich, Switzerland[1]

Introduction:
Tissue engineering using smooth muscle cells may provide a treatment option for diseases with smooth muscle pathology such as bladder dysfunction, urinary incontinence, and erectile dysfunction. As autologous smooth muscle cells (SMC) should not be harvested from organs with end-stage disease and tissue regeneration requires large amount of functional SMCs, there is a need for other cell sources. Adipose derived stem cells (ADSC) can be harvested easily and differentiated into SM tissue. We have shown that autophagy, a conserved lysosomal degradation pathway, is required for cell survival and differentiation of human blood and skin SC. Therefore, we investigated the functional role of autophagy during differentiation and remodeling of ADSCs to SMC in vitro.

Methods:
Human and rat ADSC were characterized and induced towards SMC using induction medium for 1 to 6 weeks. The changes in gene and protein expression levels for SMC specific markers: calponin, smoothelin, α-SMA, MyH11; and autophagy genes: LC3, Atg5, Beclin1, were investigated by qPCR, immunocytochemistry (ICC) and WB.

Results:
Upon induction, up regulation of Atg5 and beclin1 was observed during 1 - 3 weeks at both mRNA and protein levels. This was supported by an increased autophagosomes formation in the cells and conversion of cytosolic LC3-I to LC3-II protein. At the same time the contractile proteins calponin, MyH11 and smoothelin were up regulated during 1 - 3 weeks and decreased after 5 - 6 weeks of differentiation detected by WB and ICC. After the treatment with 3-MA, LC3 punctuation and the transformation of LC3 I to LC3II significantly decreased confirming the role of autophagy during differentiation.

Conclusion:
Our study demonstrates that autophagy plays an important role in ADSC differentiation to SMC. This finding might lead to novel supporting strategies for ADSC use in clinics, since autophagy can be easily influenced by FDA approved drugs.

3515

M. Morawska[1], L. Imbach[1], A. Baumann[1], S. Masneuf[1], C. Baumann[1], D. Noain[1]

Phenotypic characterisation of sleep-wake disturbances in VMAT2 deficient murine model of Parkinson's disease

University Hospital Zurich, Department of Neurology, Zurich[1]

Introduction:
Parkinson's disease (PD) is second most common neurodegenerative disease. Sleep-wake disturbances (SWD) belong to the most frequent non-motor symptoms of PD, often preceding the onset of other symptoms. SWD affect up to 90% of PD patients, greatly reducing quality of life and increasing the appearance of comorbidities. Prevalent SWD in PD are insomnia, sleep instability and low sleep efficiency, among others. Despite substantial progress in treatment of motor symptoms, current therapeutic approaches do not fully alleviate sleep disturbances. In recent years, there has been growing interest in studying SWD in context of PD to underpin the pathophysiology behind them and eventually design better treatment alternatives. However, appropriate rodent models closely mimicking PD-related SWD symptoms and mechanisms are missing. Here, we present a phenotypic description of SWD in the VMAT2 deficient mouse model of PD.

Methods:
We conducted monthly electroencephalogram/electromyogram (EEG/EMG) recordings in female VMAT2 deficient mice (KO, n=6) and wild-type (WT, n=7) littermates from age 5 to 7 months. The acquired traces were visually scored and time spent in each vigilance state was determined. Additionally, we performed spectral power analysis to determine possible changes in EEG characteristics.

Results:
Our analyses show that the VMAT2 deficient mice present with SWD and EEG changes similar to those seen in PD, namely: increased arousal, decreased time spent in NREM and REM sleep, decreased sleep efficiency, higher sleep fragmentation, higher delta power and slowing of oscillatory activity.

Conclusion:
Taken together these results suggest that VMAT2 deficient mice can be a useful tool for studying the mechanisms underlying SWD in PD, enabling future therapeutic approaches aimed at developing tailored treatments for these symptoms.

3516

P. Pfiffner[1], I. Pinyol[2], M. Natter[2], K. Mandl[2]

The Consent, Contact, and Community framework for Patient Reported Outcomes – Enhancing Apple's ResearchKit for iPhone Apps with FHIR

Forschungszentrum Medizininformatik, Direktion Forschung und Lehre, UniversitätsSpital Zürich[1], Computational Health Informatics Program, Boston Children's Hospital, Harvard Medical School[2]

Introduction:
Smartphones have become an interesting tool for patients to participate in a clinical trial from the comfort of their homes. A year ago, Apple Inc. announced *ResearchKit*, an open source programming framework that greatly simplifies creation of iPhone research apps. This first iteration of ResearchKit helps guiding participants through an easily comprehensible consent process, collecting their signature on-screen, administers surveys for patient-reported outcome (PRO) collection, and collects data from the phone's built-in sensors and the *HealthKit* health data storage.
We intended to collect research data from completely anonymous subjects, via their iOS-based smartphones, and delivering this data to our research infrastructure for a study about the impact of hepatitis C on patients' daily lives. For this purpose we extended ResearchKit with *C3-PRO*: the **C**onsent, **C**ontact, and **C**ommunity framework for **P**atient **R**eported **O**utcomes. C3-PRO is a set of tools that connects any ResearchKit app to a widely-used clinical research database called *i2b2*.

Methods:
First, to alleviate ResearchKit's need for programmatically creating informed consent and participant surveys, we chose to represent these tasks in files stored with the emerging HL7 *Fast Healthcare Interoperability Resources* (FHIR) standard. Survey responses, but also device-collected activity data, are likewise represented in the FHIR format. All transmissions to the research backend are encrypted on device.
Second, we built three server-side tools: a publicly hosted "receiver", capable to be deployed to well-known hosting services such as Amazon Web Services for scalability; a "consumer" part that lives on the research server behind the firewall and continuously reads data authenticated by the receiver; and an i2b2 "cell", a plug-in component for i2b2 that receives FHIR data and stores it in its research database.

Results:
With our additions, ResearchKit is capable to display interactive informed consent and research surveys by reading data from file. This removes the need to create those tasks programmatically.
By design, a random identifier serves as identifier of study participants. After consenting, a PDF file is generated on the iPhone, containing participant name, signature and date. This file however is never sent off the device to preserve anonymity. We instead transmit a FHIR resource, which includes the random participant identifier, to indicate participant consent to the researchers.
Responses to surveys are complemented by activity data, obtained from devices' built-in sensors and data stored to HealthKit by activity trackers. This information is converted to the FHIR format, encrypted using public key cryptography and securely sent to the C3-PRO receiver server, which authenticates incoming data using OAuth2. Authenticated resources are sent to the consumer service, which proceeds with decryption of the resources.
Finally, our i2b2 cell receives those decrypted resources and stores them in the i2b2 research database. This allows analysis of research data collected via C3-PRO in the same fashion as other research data stored to i2b2, such as electronic medical record data.

Conclusion:
For researchers wanting to use ResearchKit as part of a clinical trial, C3-PRO provides a secure, open source, end-to-end solution. Work to enable data-linkage to already known participants, for example patients in an existing cohort, is underway. Additionally, an Android version called *ResearchStack* is in development and adaptation to C3-PRO is planned.

3517

A. Kalyanov[2], C. Germanier[1], S. Sanchez Majos[2], M. Rudin[1], M. Wolf[2]

Imaging of hypoxia in cancer by multispectral near-infrared tomography

Institute for Biomedical Engineering, ETH and University of Zurich, Switzerland[1], Biomedical Optics Research Laboratory (BORL), Division of Neonatology, University Hospital Zurich, Switzerland[2]

Introduction:
Tumor oxygenation is one of the most important diagnostic indicators of the aggressiveness of the tumor. Tumor hypoxia presents a significant risk for patients with survival rates reduced by factor of 2 to 3 after 5 years compared to higher oxygenated tumors. Information about tumor oxygenation would not only be crucial for prognosis, but also in choosing the appropriate treatment strategy. Despite the high relevance of tumor oxygenation it is not routinely measured *in vivo*, because there is currently no technique available. Therefore the aim of this project is to develop such a method. Our approach is based on near-infrared light, because this light penetrates deep into the tissue, is harmless and enable to determine the oxygen saturation of hemoglobin.

Methods:
In this work we present a continuous wave multispectral near-infrared optical tomography (mNIROT) technique for determining the oxygenation state of tissue in small animals.
The mNIROT was used for quantitative measurements of tissue oxygen saturation (StO_2) in hypoxic tumors in laboratory mice. The study was carried out in BALB/c nude, female mice. Two separate batches of experiments were performed. Batch 1 included 3 mice at the age of 6 weeks, and batch 2 included 5 mice at the age of 10 weeks in the beginning of the experiments. Tumor cells DLD-1 wt n°6 HRE-iRFP were injected subcutaneously. Measurements were performed approximately twice per week starting from the second week after the injection. The duration of the experiments was limited by the health status of the mice according to recommendations of Catonal Veterinary Office of Zurich, which determine when an animal has to be sacrificed. The first batch lived for 37 days and the second one for 52 days.
Images were recorded with a modified homemade fluorescence tomography instrument, which included a novel light source to enable mNIROT. The 3D surface of the mice was scanned as well. The image reconstructions were processed by extensively adapted NIRFAST software (open source package for MATLAB). The wavelength normalization approach was employed to improve reconstruction stability and resolution. The modified NIRFAST was also integrated with 3D-scanning algorithms, so the geometry of objects was taken into account.

Results:
The StO_2 values decreased significantly with time, reaching very low values of 23±7%. This indicates that the oxygenation of the tumor decreases its growth.
In addition periodic oscillations of the StO_2 values were revealed. The period of these oscillations was ~10 days and similar for both batches despite on the original difference in age between them. Another longer period of 30 days was identified. There is a local minimum at the 15^{th} day and another one around the 45^{th} day, and a maximum at the 29^{th} day of measurements.

Conclusion:
The cancer developing in a body and tumour oxygen level was tracked with mNIROT *in vivo* during a long-term study. The dynamic of StO_2 in tumors as expected a decrease over time and substantial periodic fluctuations. The latter may be of high relevance for therapy. E.g. the effectiveness of radiation therapy could be substantially increased by targeting tumors, when their oxygenation is high, because the kill rate of radiation depends strongly on the oxygenation of tumors.

3518

N. Arenas-Ramirez[1], D. Zingg[2], R. Rosalia[1], A. Antunes[2], J. Haeusel[2], L. Sommer[2], O. Boyman[1]

Blocking of the epigenetic repressor Ezh2 controls tumor escape upon IL-2cx immunotherapy

Department of Immunology, University Hospital Zurich, University of Zurich[1], Cell and Developmental Biology, Institute of Anatomy, University of Zurich[2]

Introduction:
Interleukin (IL)-2/anti-IL-2 antibody complexes (IL-2cx) have been previously shown to lead to vigorous activation of effector immune cells generating potent anti-tumor effects in mice. However, despite initial control the tumor usually relapses. The molecular processes of tumor escape from immune surveillance remain poorly understood. In order to investigate them, we considered rewiring of epigenetic landscape focusing on the enhancer of zeste homologue 2 (Ezh2), a prominent epigenetic modifier catalysing the trimethylation of lysine 27 in histone 3 (H3K27me3) and being associated with unfavourable progression of different types of cancer.

Methods:
We checked Ezh2 expression levels performing immunofluorescence stainings and western blots in the tumors of wild-type (WT) mice bearing melanoma cells (B16-F10 or RIM-3) treated with PBS, IL-2cx, Ezh2 blockade or the combination. In order to identify the target genes of Ezh2 we performed chromatin immunoprecipitation assays for Ezh2 and H3K27me3 in the tumor site of those mice and checked at their expression levels by RT-qPCR. We then treated *WT* mice bearing B16-F10 tumors with PBS, IL-2cx, Ezh2 blockade or the combination. We analyzed the cellular immune composition within the tumors and tumor draining lymph nodes of the different groups by FACS. In order to confirm which cells and mechanisms were essential for the anti-tumor response obtained, we used the combination therapy for the treatment of *Tcrbd*$^{-/-}$, Rag1$^{-/-}$, Ifng$^{-/-}$, Tnfa$^{-/-}$ and Wt mice depleted of CD4^{+} or CD8^{+} T cells bearing B16-F10 tumor cells.

Results:
Ezh2 was found to be up-regulated upon IL-2cx immunotherapy resulting in melanoma dedifferentiation, loss of immunogenicity and upregulation of the PD-1/PD-L1 axis. These mechanisms favor tumor cell immune escape through exhaustion of cytotoxic CD8^{+} T cells. In line with this, the combination of Ezh2 blockade and IL-2cx immunotherapy lead to a more potent and prolong tumor control of WT mice bearing B16-F10 tumors, correlating with favorable ratios of effector CD8^{+} T cells over immune suppressive cells. Tcrbd$^{-/-}$, Rag1$^{-/-,}$ Ifng$^{-/-}$ or Wt *mice depleted of CD8*$^{+}$ T cells did not respond to the combination therapy showing that the effect of Ezh2 inhibition and IL-2x immunotherapy depends on IFN-gamma-producing CD8^{+} T cells.

Conclusion:
The anti-tumor properties obtained with IL-2 cx immunotherapy can be enhanced by Ezh2 blockade keeping tumor cells immunogenic and facilitating efficient CD8^{+} T cell-mediated anti-tumor responses. Targeting Ezh2 remains an attractive strategy to combine with IL-2cx immunotherapy.

3519

M. Dietrich[1], R. Zuellig[1], M. Niessen[1], G. Spinas[1], O. Tschopp[1]

Impaired glucose tolerance in mice with β-cell specific deletion of *Pkbα*

Division of Endocrinology, Diabetes & Clinical Nutrition, University Hospital Zurich, Zurich, Switzerland[1]

Introduction:
Protein kinase B (PKB)/Akt is considered an important target downstream of insulin receptor substrate 2 (IRS2) in the regulation of pancreatic β-cell mass. There exist three isoforms of PKB, i.e. PKBα/Akt1, PKBβ/Akt2, and PKBγ/Akt3, which are all expressed in pancreatic β-cells. It is, however unclear, whether these isoforms exert differential effects with regard to functional β-cell mass. The aim of this study was to investigate in mice the effect of β-cell specific deletion of *Pkbα* (*βpkbαKO*) on glucose homeostasis, β-cell function, and β-cell mass.

Methods:
Mice were rendered insulin resistant by feeding a high-fat diet (HFD) and characterized metabolically by intraperitoneal glucose and insulin tolerance tests. In addition, glucose-stimulated insulin secretion (GSIS) was assessed in isolated islets *in vitro.* Islet morphology was studied in pancreatic tissue sections.

Results:
Western blot analysis showed that PKBα was normally expressed in control mice, but absent in β-cells from *βpkbαKO* mice. PKBβ and PKBγ expression was not affected in those mice. In contrast, PKBα expression was similar in metabolic relevant tissue (skeletal muscle, different fat depots, liver and brain) between *βpkbαKO* mice and controls. Under normal chow diet male *βpkbαKO* mice exhibited reduced glucose tolerance with significantly increased AUC (+22.6% ± 6.5%; $p \leq 0.05$) only later in adult live at the age of 26 weeks. HFD accelerated the onset of impaired glucose tolerance with significantly increased AUC (+10.06% ± 3.6%; $p \leq 0.05$) already at age of 12 weeks (6 weeks on HFD). Plasma insulin levels during GTT were reduced in HFD-fed *βpkbαKO* mice. Additionally, random fed plasma insulin levels were decreased (4.2 ng/mL ± 0.58 ng/mL) compared to control littermates (6.31 ng/mL ± 0.97 ng/mL). However, GSIS was not decreased in islets from chow or HFD-fed *βpkbαKO* mice. Analyses of pancreas morphology suggests a 50% decrease of β-cell area in *βpkbαKO* mice under chow and HFD as compared to control littermates.

Conclusion:
This study shows for the first time that β-cell specific loss of *Pkbα* results in impaired glucose tolerance, potentially due to reduced β-cell mass. Whether the reduced β-cell mass in adulthood is the result of islet loss or of a failure to form new islets, or even caused by impaired embryonic development is currently under investigation.

3520

D. Noain[1], M. Morawska[1], F. Büchele[1], S. Schreglmann[1], Y. Gavrilov[1], M. Penner[1], L. Imbach[1], C. Baumann[1]

Cognitive impairment, sleep-wake disturbances and diffuse axonal injury in a rat model of closed traumatic brain injury: Effect of sleep modulation on TBI-induced chronic symptoms

Neurology department, University Hospital Zurich, Switzerland[1]

Introduction:
Traumatic brain injury (TBI) is one of the major causes of death and disability worldwide. Memory impairment and sleep-wake disturbances (SWD) are some of the most significant and persistent residual deficits following TBI, lasting several years post-injury. The nature and pathophysiology of chronic post-TBI symptoms remains largely unknown and there is lack of effective and specific treatment options for at least some of the symptoms. In the past, sleep manipulations have been shown to alleviate outcomes of certain neurological conditions, such as stroke. Thus, in this study we aim at characterizing a novel weigh drop-induced TBI model in terms of SWD, cognition and histological trauma outcome. In addition, we assay an alternative treatment strategy by modulation of sleep in the acute phase after trauma.

Methods:
We developed a novel rat model of closed TBI compatible with the implantation of electrodes for electroencephalography/electromyography (EEG/EMG). We examined posttraumatic sleep-wake patterns by EEG/EMG recordings and their histopathological correlates by immunohistochemistry and stereological methods, determined the presence of cognitive impairment by the novel object recognition test (NORT), and quantified chronic axonal accumulation of amyloid precursor protein (APP), a marker of diffuse axonal injury, by immunofluorescence in SHAM-operated and TBI rats.
Following, we aimed at evaluating whether 5 days of sleep modulation consisting of sleep induction (SI) by administration of Xyrem (Sodium Oxybate, ~400mg/kg, i.p.) and sleep restriction (SR) by gentle handling immediately after trauma induction could be a possible treatment option for at least some of the TBI-induced impairments.

Results:
Our sleep analysis revealed a chronic increase in the sleep need/24h after TBI as compared to SHAM animals. In addition, sleep stability was increased particularly in the dark phase in the TBI group compared to baseline measurements. A decrease in the number of histamine immunoreactive cells in the tuberomammillary nucleus, a wake-promoting hypothalamic centre, was found to be significantly correlated with the amount of sleep. Memory deficits were observed in the TBI group, which presented a reduced recognition index of a familiar object in the NORT. APP accumulation in the axons appeared increased in the TBI animals compared to the SHAM controls in the chronic stage after trauma.
Sleep modulation both by means of SI and SR with sleep rebound resulted in memory preservation and reduced accumulation of axonal APP after trauma.

Conclusion:
In summary, our rat TBI model replicates some of the sleep and behavioural deficits observed in human TBI patients. Histaminergic deficits appear correlated to the posttraumatic hypersomnia phenotype. Finally, sleep modulation by different means could be a promising potential treatment for the cognitive impairment and diffuse axonal injury associated with TBI.

3521

F. Wehrle[1], B. Latal[2], R. O'Gorman[3], C. Hagmann[1], R. Huber[2]

EEG sleep slow wave activity as a potential marker of load-dependent deficits in executive functions in very preterm children and adolescents

Department of Neonatology, University Hospital Zurich, Zürich[1], Child Development Center, University Children's Hospital Zurich, Zurich[2], Center for MR Research, University Children's Hospital, Zürich[3]

Introduction:
Many children born very preterm (<32 weeks of gestation) experience difficulties in executive functions, *e.g.*, planning, with the deficits often only becoming evident when the cognitive load is high. Sleep slow wave activity (SWA, 1-4.5 Hz EEG power), the key characteristic of deep non-rapid eye movement sleep, reflects the degree of synaptic strength and network synchrony. It has been shown to be locally increased after the intense use of a certain cortical region, *e.g.*, after an intensive cognitive training. This study investigated whether sleep SWA is an electrophysiological marker of local alterations in executive function networks in very preterm children and adolescents.

Methods:
A group of 38 very preterm children and adolescents without any severe neonatal brain injuries (age at assessment [M± SD] 12.9 ± 1.7 years) and 43 health term-born peers [13.1 ± 2.0 years] were assessed with a comprehensive battery of executive function measures. A composite score was calculated to reflect the ability to cope with increasing load. All-night high-density sleep EEG (128 electrodes) was recorded in all participants. SWA averaged across the first hour of NREM sleep was obtained and correlated with the composite score.

Results:
Sleep efficiency was high in both groups (approximately 90%). The architecture and quality of sleep were not significantly different between the groups (all $p > .41$). Very preterm participants had significantly lower abilities to cope with increasing load ($p < .001$). Looking at all participants, the composite score was positively correlated with SWA in a cluster of 14 electrodes over frontal brain regions ($r = .32 \pm .06$, $p < .05$). Within this cluster, SWA was higher in those participants with better coping abilities than in those with worse coping abilities ($p < .05$). Additionally, comparing the two groups, very preterm participants showed higher SWA compared to term-born participants when the level of task demands was taken into account ($p < .05$).

Conclusion:
The local increase of SWA in very preterm children and adolescents compared to similarly performing term-born peers may reflect the more intense use of neuronal networks underlying executive functions to achieve normal performance. However, if demands are highest, this compensatory mechanism may fail and lead to the load-dependent executive function deficits often reported in very preterm children and adolescents. This study shows that sleep SWA may represent a marker for load-dependent alterations in brain networks known to be involved in executive functioning.

3523

C. Gonçalves-Moreira[1], M. Morawska[1], A. Baumann[1], S. Masneuf[1], D. Noain[1], C. Baumann[1]

Inhibiting COMT in a mouse model of Parkinson's disease: a trial of Tolcapone in VMAT2-deficient mice

Neurology Department, University Hospital Zurich, Zurich, Switzerland[1]

Introduction:
In patients with Parkinson's disease, the progressive loss of dopamine-producing cells in the substantia nigra pars compacta leads to a neurochemical imbalance in the basal ganglia and finally to bradykinesia, rigidity and tremor. Symptoms reminiscent of these motor dysfunctions, as well as of non-motor signs of Parkinson's disease, were revealed in transgenic mice with 5% expression of vesicular monoamine transporter 2 (VMAT2-deficient mice). PD is typically treated with dopaminergic drugs, in particular L-DOPA. Because methylation of L-DOPA by catechol-O-methyltransferase (COMT) leads to increased concentration of homocysteine, which is a known risk factor of vascular events and cognitive impairment, dopamine replacement may accelerate neuronal dysfunction and neurodegeneration. Previous attempts to restore striatal dopamine apart from L-DOPA and provide neuroprotection remained unsuccessful. We hypothesized that Tolcapone, a COMT inhibitor drug, may not only inhibit the degradation of L-DOPA but further improve PD treatment by increasing and stabilizing serum dopamine concentrations, and ultimately, show in prospective manner whether pharmacological inhibition of COMT offers long-term benefits in Parkinson's disease context by reducing risk of vascular events and cognitive decline, and exerts neuroprotective effect.

Methods:
We investigate possible independent effects of Tolcapone on behavioral functions, and on biochemical markers of neurodegeneration and homocysteine metabolism in brain tissue and peripheral blood, respectively, in VMAT2-deficient mice under chronic L-DOPA treatment.

Results:
So far, the mutant mice do not seem to positively respond to chronic L-DOPA, Tolcapone or L-DOPA + Tolcapone interventions when behaviorally tested during *off*-periods. treatment.

Conclusion:
Our preliminary behavioral results reveal no signs of disease modifying effect of COMT inhibition, nor alone or in combination with DA replacement. off-periods. treatment.

3525

T. Fleischmann[1], M. Arras[1], P. Jirkof[1]

Paracetamol for pain relief after laparotomy for embryo-transfer in laboratory mice

Division of Surgical Research, University Hospital, Zurich[1]

Introduction:
The generation of genetically modified (GM) mouse models usually requires surgery for transferring founder embryos after in-vitro manipulation of their genome into recipient female mice, i.e. foster mothers. Providing post-operative analgesia in foster mothers with oral self-administration of pain killers has several advantages but is mostly dismissed because of the uncertainty of voluntary ingestion of the drug and possible negative influence on embryo viability and development. Therefore, the impact of the analgesic paracetamol on the outcome of the procedure was determined by comparing offspring after embryo transfer (ET) with and without paracetamol treatment of their foster mothers. In addition, we investigated whether voluntary paracetamol uptake with the drinking water is sufficient enough as to effectively cover the post-operative analgesic requirements.

Methods:
Water consumption was measured in foster mothers (from ET onwards for 48 h) and in naïve female mice. Drinking water was either untreated or contained paracetamol (Dafalgan® Children Sirup, 30 mg/ml, Bristol-Myers Squibb SA, Steinhausen, Switzerland) in a dosage calculated to provide the mice with approximately 200 mg/kg paracetamol per day (dosage taken from textbooks). In naïve mice, serum concentration of paracetamol was measured at 6, 11 and 24 h during which treated water was offered (n=8 per time point).
Fifteen mice were used as foster mothers. After ascertaining pseudo-pregnancy embryo recipients were randomly allocated either to the untreated (n=8) or the paracetamol treated group (n=7). Paracetamol containing water was provided at 6 h before ET and continued for 2 days. Each foster mother received 12 embryos; litters were closely monitored until weaning.

Results:
ET was successful with all foster mothers of the untreated group, they delivered litters of 2 to 6 pups.
In the paracetamol treated group, one foster mother was detected not to be pregnant at day 12 of gestation. This negative result was included for calculations and analysis. The remaining 6 foster mothers of the paracetamol treated group delivered litters of 3 to 8 pups. Since the treated foster mothers delivered in average slightly more pups per litter, the final success of the ET was marginally better in the treated group compared to the untreated group. The body weight of the newborns was not significant different between both groups. No dead or injured pups were found at the time of birth and all pups were reared, i.e. no losses were noticed until weaning. In summary, our results provided no evidence for adverse effects of paracetamol treatment on overall outcome of ET.
Water consumption increased if paracetamol was added to the drinking water with similar amounts consumed by naïve mice and foster mothers. Serum concentration of paracetamol reached a sufficient level at 6 h (at the time point where ET is performed) and increased further in the post-operative phase, i.e. at 11 h and 24 h.

Conclusion:
In conclusion paracetamol in drinking water was voluntarily consumed by female mice after surgery in an amount and regularity that allow the assumption of constant sufficient post-operative pain treatment. Relevant side-effects on the outcome of embryo transfer were not detected therefore administering paracetamol in drinking water is suggested as a feasible and efficient method for providing pain relief in mice during generation of GM lines.

3526

E. Varypataki[1], S. Freiberger[1], T. Kündig[1], P. Johansen[1]

PCI-based vaccination for improved in vivo stimulation of antigen-specific cytotoxic T cells

Department of Dermatology, University of Zurich[1]

Introduction:
Cytotoxic $CD8^+$ T cells are key players of adoptive cellular immunity, crucial for the fight against cancer and chronic infectious diseases. Hence, the design of therapeutic vaccines focuses on ways to induce strong cytotoxic immune responses. Current vaccines activate only weak antigen-specific $CD8^+$ T cells, mainly due to the default processing of exogenous antigens via the MHC class II pathway leading to the activation of $CD4^+$ helper and not $CD8^+$ T cells. Photochemical internalization (PCI) is a new concept of intracellular delivery that is able to circumvent this MHC II processing. Briefly, after antigen and photosensitiser uptake in endosomes of antigen presenting cells (APCs), light activation of the photosensitiser cause disruption of endosomal membrane and the release of antigen into the cytosol, resulting in stimulation of MHC class I-restricted $CD8^+$ T cell responses. While the proof-of-concept of PCI-based vaccination has recently been demonstrated, we here attempt to unravel its potential action mechanisms.

Methods:
Wildtype, as well as MHC class II, MyD88, TRIF, and TLR4 deficient mice were immunized intradermally with ovalbumin (OVA) protein and the photosensitizer (TPCS2a), followed by visible light exposure after 18h in order for the photosensitizer to be activated. The effectiveness of the PCI-method to stimulate $CD8^+$ T cells was analysed by measuring antigen-specific T cells in blood and spleens and assessing their functionality by cytokine production and *in vivo* cytotoxicity.

Results:
Wildtype mice vaccinated by the PCI method, showed improved *in vivo* activation of OVA-specific $CD8^+$ T cells in blood, compared to mice immunised with OVA without PCI. *Ex vivo* restimulation of blood or splenocytes also showed improved functions in terms of production of IFN-γ cytokine, while mice vaccinated by the PCI method performed a strong cytotoxic capacity. The $CD8^+$ T-cell effector functions were not impaired in MHC class II deficient mice, suggesting that the PCI-mediated endosomal escape and MHC class I antigen processing and presentation is independent of the presence of the MHC class II and $CD4^+$ T helper cells. Experiments with the TLR-associated mouse strains are still ongoing.

Conclusion:
Our data demonstrate the potential of PCI–based vaccination for the stimulation of functional cytotoxic $CD8^+$ T cells, making PCI a strong tool for the design of effective therapeutic vaccines against cancer and infectious conditions.

3527

E. Cambria[1], K. Renggli[1], C. Ahrens[2], C. Cook[3], C. Kroll[4], A. Krueger[4], B. Imperiali[5], L. Griffith[1]

Sortase-mediated ligation of epidermal growth factor to pre-formed PEG hydrogels for in vitro tissue models

Department of Biological Engineering, Massachusetts Institute of Technology, Cambridge, Massachusetts United States[1], Department of Chemical Engineering, Massachusetts Institute of Technology, Cambridge, Massachusetts United States[2], Center for Gynepathology Research, Massachusetts Institute of Technology, Cambridge, Massachusetts United States[3], Department of Chemistry, Massachusetts Institute of Technology, Cambridge, Massachusetts United States[4], Department of Biology, Massachusetts Institute of Technology, Cambridge, Massachusetts United States[5]

Introduction:
Synthetic extracellular matrices are widely used in regenerative medicine and as tools in building in vitro physiological culture models. Synthetic hydrogels display advantageous physical properties, but are challenging to modify with large peptides or proteins. In this study, a facile, mild, enzymatic postgrafting approach is presented. We aimed at: (i) tethering human epidermal growth factor (EGF) to pre-formed poly(ethylene glycol) (PEG) hydrogels and releasing it on demand via sortase-mediated ligation; (ii) characterizing the reaction and the hydrogel system and (iii) validating the system and the biological activity of the tethered EGF with biological applications using human primary epithelial cells.

Methods:
Hydrogels were formed through Michael-type addition by cross-linking acrylate-terminated 8-arm PEG, thiol-terminated 4-arm PEG and thiol-containing peptides (a cell-adhesive peptide and the sortase LPRTG substrate). Sortase-mediated ligation was then used to conjugate a model human growth factor in solution (EGF) fused to a GGG ligation motif (GGG-EGF) to the pre-formed hydrogels containing the sortase LPRTG substrate. After ligation, the reversibility of the sortase reaction was also exploited to cleave tethered EGF from the hydrogels for analysis. A compendium of techniques were used for the analysis of the reaction supernatant and the postligation hydrogels. Sandwich ELISA was used for the quantification of GGG-EGF in solution after tethering and after cleavage. LPRTG consumption in hydrogel was quantified through fluorescence reading and tethered GGG-EGF was detected on hydrogel with direct ELISA. The hydrogel system and the EGF bioactivity were validated with a DNA synthesis assay (EdU) with primary human hepatocytes and endometrial epithelial cells (EECs).

Results:
Analyses showed that the amount of tethered EGF increased with increasing LPRTG in the hydrogel or GGG-EGF in solution. Sortase-tethered EGF was biologically active, as demonstrated by enhanced stimulation of DNA synthesis in primary human hepatocytes and EECs compared to unmodified hydrogels or soluble human EGF.

Conclusion:
As a conclusion, the simplicity, specificity, and reversibility of sortase-mediated ligation and cleavage reactions make it an attractive approach for modification of hydrogels with large proteins, thus improving culture systems for in vitro models.

3528

D. Goniotaki[1], L. Lakkaraju[1], A. Shrivastava[2], P. Bakirci[1], S. Sorce[1], P. Pelczar[3], F. Gasparini[4], A. Triller[2], A. Aguzzi[1]

Inhibition of group I metabotropic glutamate receptors (mGluR1 and mGluR5) protects against prion-induced toxicity

Institute of Neuropathology, University Hospital of Zurich, Zurich, Switzerland[1], École Normale Supérieure, Institut de Biologie de l'ENS (IBENS) INSERM CNRS PSL Research University, Paris, France[2], Institute of Laboratory Animal Science, University of Zurich, Zurich, Switzerland[3], Novartis Institutes for Biomedical Research, Basel, Switzerland[4]

Introduction:
Prion infections cause inexorable, progressive neurological dysfunction and neurodegeneration. Expression of the cellular prion protein PrP^C by target cells is required for toxicity, suggesting the existence of deleterious PrP^C-dependent signaling cascades. Because the Group-I metabotropic glutamate receptors (mGluR1 and mGluR5) can form complexes with the cellular prion protein (PrP^C), we investigated the impact of mGluR1 and mGluR5 inhibition on prion toxicity *ex vivo* and *in vivo*. We tested the hypothesis that selective inhibition of group I mGluRs can be protective against prion protein-induced toxicity.

Methods:
Several biochemical (immunoprecipitation assays, western blot) and imaging (confocal, PALM/STORM microscopy) approaches, multiple prion toxicity models [prion infection (RML6 strain) and treatment with toxic prion-mimetic compounds], rotarod performance behavioral testing, immunohistochemistry, primary hippocampal cultures, organotypic brain slice cultures and Grm5ko mice were utilized so as to identify the role of group I mGluRs in prion toxicity. The therapeutic potential of selective mGluR1 and mGluR5 inhibitors (YM202074 and MPEP) was evaluated *ex vivo* and *in vivo* in prion infected wt mice.

Results:
In our study, we focused on the role of group I mGluR-PrP^C coupling in prion disease. We found that toxic prion-mimetic compounds increase mGluR5 clustering and accumulation at dendritic spines. Also, pharmacological inhibition of mGluR1 and mGluR5, as well as genetic ablation of the *Grm5* gene encoding mGluR5, protects organotypic slice cultures against the toxicity of prions and of prion-mimetic compounds. Furthermore, pharmacological inhibition of mGluR5 improved the neurological status and, to some extent, the survival of prion-infected mice.

Conclusion:
Our results indicate a significant role of group I mGluRs in prion toxicity. Although Group-I mGluR inhibition was not curative, these results suggest that it may have the potential to alleviate – at least temporarily – the neurological dysfunctions induced by prion diseases.

3529

A. Bogdanova[1], A. Makhro[1], E. Seiler[1], N. Bogdanov[1], M. Gassmann[1], M. Manz[2], I. Hagemann[2], J. Goede[1]

MemSID trial: first results of the Ca2+-lowering therapy in sickle cell disease patients

Institute of Veterinary Physiology, Vetsuisse Faculty, University of Zurich, Zurich, Switzerland[1], Division of Haematology, University Hospital Zurich, Zurich, Switzerland [2]

Introduction:
The MemSID trial was designed to test the efficacy of the N-methyl D-aspartate receptor (NMDAR) antagonist memantine for treatment of a small cohort of sickle cell disease patients observed at the Division of Hematology, University Hospital Zurich. Memantine was earlier on shown to decrease intracellular Ca^{2+} levels in red blood cells (RBCs) of these patients ex vivo. As Ca^{2+} overload regulates multiple processes in RBCs. Ca^{2+} overload is associated with facilitated appearance of clearance markers (oxidative stress, proteolysis, band 3 clustering, phosphatidylserine exposure and dehydration), increased fragility and abnormally high adherence. By blocking Ca^{2+} uptake via the NMDARs we wanted to hit multiple targets and reduce or prevent vaso-occlusive pain crises and haemolysis.

Methods:
MemSID is a phase II open label single center trial in which memantine is given daily at a dose from 5 mg to 20 mg (up-scaling of the dose within the first month of treatment). Assessed are the changes in blood cytology and biochemistry, as well as Ca^{2+} handling and Ca^{2+}-dependent parameters (cell volume and density, metabolism and redox state as well as RBC age and integrity and adherence) in three patients at different stages (2, 3 or 4 months) of treatment.

Results:
After the onset of treatment none of the patients was presented with in-hospital pain crises despite several events involving inflammation and hypoxia. Reduction in the intracellular Ca^{2+} was particularly prominent in patient with most severe form of disease. New population of RBCs produced in response to medication had stabilized membranes and were less adherent. The overhydrated and terminally dehydrated and “sickling” cells were less abundant. The produced red blood cells under therapy were less oxidised and more metabolically active. Along with increase in band 3 abundance at the membrane surface all these changes suggest an increase in longevity of patients RBCs. This suggestion was further confirmed by the decrease of reticulocytes production and a tendency to increase haemoglobin, haematocrit within the first months of treatment.

Conclusion:
These findings indicate that Ca^{2+} lowering therapy may be a promising therapeutic strategy for supportive long term treatment of symptomatic sickle cell disease.

3530

R. Chen[1], T. Hornemann[2], W. Yu[2], S. Camargo[3], R. Graf[1], S. Sonda[1]

1-Deoxy-sphingolipids, novel biomarkers of diabetes, are cytotoxic for exocrine pancreatic cells

Department of Visceral & Transplantation Surgery, University Hospital of Zurich, Switzerland[1], Institut of Clinical Chemistry, University Hospital, Zurich[2], Institute of Physiology, University of Zurich, Switzerland[3]

Introduction:
Exocrine pancreatic insufficiency and dysfunctions are frequently associated with diabetes mellitus (DM), further aggravating the management of the disease. In addition, DM also constitutes a risk factor to develop pancreatitis. The molecular mechanisms at the base of pancreatic dysfunctions following DM are not completely elucidated. In this context, we recently discovered that deoxy-sphingolipids (1-deoxySLs), the levels of which increase during DM and metabolic syndrome, are cytotoxic for beta cells. Knowing the anatomical and functional relationships between endocrine and exocrine pancreatic tissues, we hypothesize that elevated 1-deoxySLs levels observed in DM directly damage the pancreatic exocrine compartment, thus increasing its predisposition to develop exocrine pancreatic diseases.

Methods:
The research took advantage of in vivo mouse models of streptozocin-induced diabetes and cerulein-induced pancreatitis. Reduction of 1-deoxySLs synthesis was obtained by oral L-serine supplementation. Disease severity was evaluated with biochemical and immunohistochemical methods. Levels of mRNA and composition of sphingolipid species were quantified by real-time PCR and mass spectrometry, respectively. 1-deoxySLs-dependent toxicity was evaluated in vitro on pancreatic acinar cell line AR42J and primary pancreatic fibroblasts.

Results:
Induction of pancreatitis resulted in more severe damage of exocrine tissue in mice with DM compared with control mice, indicating that DM increases not only the predisposition but also the severity of pancreatitis. 1-deoxySL levels were elevated in mice with DM in combination with pancreatitis but not in mice with pancreatitis only. Reduction of 1-deoxySL synthesis by oral L-Serine supplementation in mice with DM ameliorated the damage and inflammation of the exocrine pancreatic tissue, without restoring insulin production in beta cells. This suggests that elevated 1-deoxySLs rather than deficiency of insulin contribute to the exocrine damage in DM. In vitro studies showed that treatment with 1-deoxysphinganine at low micromolar concentration reduced cell replication and promoted cytotoxicity in pancreatic acinar cells AR42J and pancreatic primary fibroblast.

Conclusion:
Our work revealed that 1-deoxySL are cytotoxic for exocrine pancreatic cells, suggesting a role for these lipids in the exocrine dysfunctions observed following DM. Oral L-Serine supplementation could be an option for ameliorating exocrine pancreatic diseases in diabetic patients.

3531

R. Chen[1], G. Mosca[1], M. Dietrich[2], E. Saponara[1], K. Grabliauskaite[1], R. Zuellig[2], O. Tschopp[2], R. Graf[1], S. Sonda[1]

Akt1 regulates the development of inflammation and tissue regeneration during acute pancreatitis

Department of Visceral & Transplantation Surgery, University Hospital of Zurich, Switzerland[1], Division of Endocrinology, Diabetes and Clinical Nutrition, University Hospital of Zurich, Switzerland[2]

Introduction:
The serine/threonine kinase Akt/PKB plays a key role in the conserved phosphoinositide 3-kinase signaling pathway. In mammals, activation of Akt is implicated in the regulation of divergent cellular processes, including proliferation, survival and cell size. Recently, Akt has also been implicated in the regulation of inflammation through activation of the NF-kB pathway. Three Akt isoforms (Akt1, Akt2, and Akt3) are found in mammals and, despite being highly related and sharing the same structural organization, they show non-redundant physiological functions. In this study, we analyzed the role of Akt1 during the development of acute pancreatitis, a debilitating and potentially lethal disease.

Methods:
Acute pancreatitis was induced by multiple cerulein injections in mice, an experimental model that mimics human edematous pancreatitis. The severity of disease onset and progression were evaluated by biochemical and immunohistochemical methods in wild type and in $Akt1^{-/-}$ animals.

Results:
Western blot analyses revealed that only the Akt1 and Akt2 isoforms are expressed in the exocrine pancreas. A different protein composition was detected in pancreatic islets, liver and brain, indicating a tissue-specific distribution of Akt isoforms. Upon pancreatitis induction, release of amylase into the blood, the most sensitive parameter to determine the initial acinar cell damage, was comparable in the two strains. However, during the disease progression, $Akt1^{-/-}$ mice showed reduced inflammatory cell infiltration, acinar cell proliferation and de-differentiation into acinar-to-ductal metaplasia.

Conclusion:
Our results revealed that Akt1 signaling does not mediate the initial acinar cell damage observed at the onset of acute pancreatitis. However, Akt1 signaling promotes both the inflammatory response and the regeneration of the pancreatic tissue. Collectively, our data contribute to expand our knowledge on the pathophysiological roles of Akt1. In addition, these findings provide novel insights into the molecular pathways governing pancreatic inflammation and tissue regeneration, with potential therapeutic implications.

3532

M. Widmer[1], N. Ziegler[3], J. Held[1], K. Lutz[2], A. Luft[1]

Rewarding feedback promotes motor skill consolidation via striatal activity

Department of Neurology, University Hospital of Zurich, Zurich[1], Cereneo, Center for Neurology and Rehabilitation, Vitznau[2], Institute of Human Movement Sciences and Sport, ETH Zurich, Zurich[3]

Introduction:
Knowledge of performance (KP) can activate the striatum, a key region of the reward system and highly relevant for motivated behaviour. This activation further increases, if KP informs about a monetary gain (i.e. increases the extrinsic subjective value). Via midbrain dopaminergic pathways to the motor cortex, such rewarding stimuli are hypothesized to influence motor skill learning by altering long term potentiation (LTP) and thus synaptic plasticity. This is of great clinical interest, as plasticity is also essential for recovery/rehabilitation after brain injury (e.g., stroke) and plasticity promoting interventions might therefore increase the efficacy of rehabilitative training.

Methods:
Using functional magnetic resonance imaging (fMRI), striatal activity linked to KP was measured during the training of an arc-pointing task (APT). KP included a numeric score and was given after a random selection of trials (KP_R) or after relatively good performance (KP_{GP}). For a third group, the score, delivered after good performance, represented a monetary reward (KP_{GP}+MR). Performance was assessed before, right after and 24 hours after the training of the APT without providing additional terminal feedback in these testing sessions. In turn, learning, measured as relative change of error from pre- to post- (online learning) and from post- to 24 hours post-training (consolidation), was hypothesized to be facilitated under conditions that more efficiently activate the striatum during feedback presentation.

Results:
fMRI: The reward condition (main effect “group”) significantly influenced the relative signal increase in the ventral striatum ($F=5.04$, $p=0.0220$), but less clearly in the dorsal striatum ($F=2.56$, $p=0.179$). In the ventral striatum, KP_{GP}+MR experienced significantly higher activation compared to the KP_{GP} control condition ($t=2.98$, $p=0.0093$).
Behavioural: While all groups profited similarly from APT training, only KP_R and KP_{GP}+MR could consolidate their performance overnight. KP_{GP}’s performance, on the other hand, decreased significantly ($t=3.39$, $p=0.0008$) and this worsening was significantly larger compared to the very stable consolidation performance of KP_{GP}+MR ($t=2.42$, $p=0.0324$).

Conclusion:
Indeed, our results demonstrate an influence of the feedback condition on motor skill learning. If a score presented after good performance signified monetary outcome (KP_{GP}+MR vs. KP_{GP}) task consolidation was improved. Likewise, ventral striatal response to KP during training was increased under monetary reward conditions. Notably, both groups showing a significant response of the ventral striatum to feedback during training, i.e., KP_R and KP_{GP}+MR, could retain their performance from the first day at the 24 hours post-training test. A lack of ventral striatal response to KP, on the other hand, comes along with significant offline forgetting, as observed in KP_{GP}. We conclude that increasing ventral striatal activity during acquisition of a motor skill by using appropriate reward improves consolidation of the acquired skill. In turn, rewarding feedback during rehabilitative training possibly improves therapy outcome.

3533

L. Ahnen[1], S. Sanchez[1]

Imaging Cerebral ischemia in preterm infants with sound and light

Neonatologie, UniversitätsSpital, Zürich[1]

Introduction:
Approximately, 800 preterm infants between 23 and 32 weeks of gestation are born each year in Switzerland. Despite improved survival of these extremely preterm infants, long term neurodevelopmental problems such as cognitive, motor and behavioral impairment remain constant. Cerebral ischemia (low blood perfusion) is a key initiating factor for Periventricular diffuse white matter injury, the most common pathology behind these problems. Its early detection would be of outmost importance to determine infants at highest risk and to treat ischemia. Ultimately, this will reduce the high incidence of neurodevelopmental impairments.

Methods:
Opto-acustic imaging is a hybrid modality, combining the high contrast and spectroscopic-based specificity of optical with the high spatial resolution of US imaging. We have developed a first stage of an instrument that combines the strengths of opto-acustics and near infrared optical tomography to detect local hypoxia in the brain of preterm infants on the bed side and non-invasively. The sensor is based on highly flexible optical fibers to deliver and measure light to a ring like frame located around the fontanel and will incorporate in the future an ultrasound probe placed in the center of the ring whose angular position will be variable.

Results:
We present first results on silicone phantoms of the instrument. We also describe a new algorithm that makes use of small blood vessels in the brain as virtual light detectors, allowing imaging of deeper structures at higher spatial resolution. Ratios of absorbed energy at different wavelengths are obtained by measuring the change in the transient acoustic signal, generated during the rapid expansion of the blood vessels as a response to light pulses with a conventional ultrasound probe located in the fontanel area. We define the mathematical structure of an inverse problem where chromophore concentrations for bulk brain tissue, inhomogeneities and blood vessels are obtained simultaneously, giving a precise map of cerebral oxygenation.

Conclusion:
The results acquired with the first stage of the instrument and the algorithms developed and validated in simulations to use blood vessels as virtual detectors of relative fluences define a very powerful tool for early detection of Cerebral ischemia.

3534

T. Gaisl[1], C. Giunta[2], K. Sutherland[3], D. Bratton[1], C. Schlatzer[1], N. Sievi[1], D. Franzen[1], P. Cistulli[3], M. Rohrbach[2], M. Kohler[1]

Obstructive Sleep Apnea in Ehlers-Danlos Syndrome. A prospective case-control study

Department of Pulmonology, University Hospital Zurich, Zurich[1], Division of Metabolism, Children´s Hospital Zurich, Zurich[2], Department of Respiratory and Sleep Medicine, Royal North Shore Hospital, Sydney[3]

Introduction:
The Ehlers-Danlos syndrome (EDS) is an inherited heterogeneous group of connective tissue disorders, affecting tissue fragility, blood vessels, and other organs. EDS patients are known to suffer from significant sleep problems and excessive daytime sleepiness. EDS-features such as increased pharyngeal collapsibility have been proposed to cause obstructive sleep apnea (OSA). However, data about the actual prevalence of OSA and its consequences in EDS do not exist.

Methods:
In this prospective case-control study, we included 100 EDS patients (46% hypermobility type, 35% classical type, 19% other subtypes) which were one-to-one matched to 100 healthy controls according to sex, age, weight, and height. Participants underwent structured interviews (including validated questionnaires for daytime sleepiness and quality of life) and level-III respiratory polygraphy. EDS was diagnosed according to the Villefranche diagnostic criteria and OSA-syndrome was diagnosed according to the criteria of the International Classification of Sleep Disorders 2014. Aortic stiffness assessment was conducted in a subgroup of patients. Conditional logistic regression with random effects (within pairs) was used to compare the two groups in a confounder-adjusted analysis.

Results:
The study population was predominantly female (82%) and young (39.9±12.6 years). The apnea-hypopnea-index was higher in patients with EDS than in controls (2.9/h [1.3-7.6] vs. 0.5/h [0.2-1.5], $p<0.001$) and EDS patients had a higher prevalence of symptomatic OSA (23% vs. 3%, difference +20, 95% confidence interval +11 to +28, $p<0.001$) when compared to controls. Subgroup analysis revealed no differences in apnea-hypopnea index among EDS subtypes (global t-test, $p=0.241$). Generally, EDS patients reported lower quality of life ($p<0.001$), had a higher resting and night-time heart rate ($p<0.001$), and a higher aortic augmentation index (22.4 ± 11.0 vs. 14.8 ± 14.0, $p=0.02$) compared to controls. In EDS patients, symptomatic OSA was associated with lower quality of life, higher night-time heart rate, and excessive daytime sleepiness (all $p<0.05$).

Conclusion:
This is the first study to suggest that patients with EDS are disproportionally affected by sleep disordered breathing when compared to a matched non-EDS control population. In EDS, the high prevalence of OSA might contribute to clinically significant problems such as daytime sleepiness, lower quality of life, and autonomic dysfunction. Future randomized controlled trials are warranted to assess effectivity and clinical consequences of OSA-treatment in patients with EDS.

3535

J. Deuel[1], D. Schaer[1], M. Cheetham[1], E. Battegay[1]

Disease-disease-interactions determine in-hospital morbidity and mortality

Department of Internal Medicine, University Hospital of Zurich;[1]

Introduction:
Multimorbidity (MM), defined as the concurrent presence of more than one active or chronic disease in a single patient, is highly prevalent in hospital patients and the elderly. Until now MM has been understood as the sum of a patient's diagnoses. However, disease-disease-interactions in the framework of MM may be a main determinant of in-hospital morbidity and mortality of multimorbid patients. In this study we have quantified the influence of disease-disease-interactions on morbidity and mortality and identified clusters of diagnoses with a high potential for interactions.

Methods:
We have retrospectively analyzed all 38'793 patients hospitalized in our hospital during 2014. Anonymized data included in the analysis were the ICD-10 coded diagnoses of each individual, all medications given during hospitalization and the basic demographic characteristics of the patients. The analysis did neither include individual chart review nor the consideration of unorganized or unsystematic data. Diagnoses were grouped by affected organ system, and organ impairment was scored. Medications were classified by ATC-code and quantified by frequency of application and cumulative dose. Multimorbid patients were identified by cluster analysis in dependence of affected organ systems and applied medications. The extent of burden of morbidity was estimated from the duration of hospitalization, and in-hospital mortality was determined.

Results:
The number of diagnoses strongly correlated with increased mortality and morbidity. Intrestingly, this increment was not linear but exponential, suggesting that the presence of disease-disease-interactions and other variables may contribute to morbidity and mortality in multimorbid patients. We then used cluster analysis to identify and characterize specific multimorbidity clusters. The variance of multimorbid patients was much larger than the variance of oligo- or even monomorbid patients, multimorbid patient clustered in a large number of small clusters (containing a low number of patients each) while the oligo- and monomorbid patients clusterd in only a few very large clusters.

Conclusion:
The number of diagnoses correlated exponentially with burden of morbidity and mortality of in-patients. Cluster analysis and identification of specific multimorbidity clusters can easily be automated and would allow to identify and score multimorbidity in individual patients in real-time, and to identify and improve care of these patients.
By assessing the interaction potential for all diagnoses within a patient we have established a tool to quantify the burden of multimorbidity on in-hospital morbidity and mortality.

3536

C. Naegeli[1], T. Zeffiro[2], M. Piccirelli[3], A. Jaillard[4], A. Weilenmann[1], K. Hassanpour[1], M. Schick[1], M. Rufer[1], S. Orr[5], C. Mueller-Pfeiffer[1]

Cerebral networks underlying hypersensitivity to salient sounds in posttraumatic stress disorder

Department of Psychiatry and Psychotherapy, University Hospital Zurich, Zurich[1], Neural Systems Group, Massachusetts General Hospital, Boston, MA[2], Department of Neuroradiology, University Hospital Zurich, Zurich[3], Unité IRM 3T – Recherche, Pôle Recherche - CHU de Grenoble, Grenoble[4], Department of Psychiatry, Massachusetts General Hospital and Harvard Medical School, Boston, MA[5]

Introduction:
The ability to accurately detect potentially meaningful environmental events is essential for survival. Patients with posttraumatic stress disorder (PTSD) are often overly sensitive and responsive to unexpected or potentially threatening stimuli in the environment. This is evidenced by observations of autonomic hyper-responsiveness to brief, 95 dB pure tones in PTSD in psychophysiological studies. We have investigated whether hyper-responsiveness to unexpected sounds in PTSD is mediated by alterations in attention, salience, or auditory networks.

Methods:
PTSD (n=26) and trauma-exposed healthy participants (Non-PTSD, n=23) listened to 500 msec, 95 dB pure tone or white noise stimuli presented every 30 sec during concurrent fMRI and psychophysiological recording. Outside the scanner, the subjects evaluated the relative loudness and valence of the stimuli by magnitude estimation.

Results:
PTSD participants perceived sounds as similarly loud, but more aversive, than did Non-PTSD participants ($p=0.051$). Heart rate, skin conductance and pupil size responses to white noise, relative to pure tones, were larger in PTSD, compared to Non-PTSD subjects (p'*s* ≤ 0.019). As expected, both PTSD and Non-PTSD participants showed neural responses to sounds in the 1) auditory network in thalamus and superior temporal gyrus, 2) salience network, including anterior insula and dorsal anterior cingulate cortex, and 3) attention network including frontal eye fields, intraparietal sulcus, superior parietal lobule, temporoparietal junction, and middle frontal gyrus, and 4) premotor network (t'*s* ≥ 4.64, p'*s* ≤ 0.05, FWE-corrected). PTSD, compared to Non-PTSD, participants exhibited larger neural responses to pure tones in left precentral gyrus and to white noise in bilateral precentral gyrus and right intraparietal sulcus (t'*s* ≥ 4.18, p'*s* < 0.05, FWE-corrected). PTSD participants also exhibited larger neural responses to white noise, compared to pure tones, in left temporoparietal junction ($t \geq 4.20$, $p < 0.05$, FWE-corrected). Sound-related neural responses were similar between groups in the salience and auditory networks.

Conclusion:
Hypersensitivity to unexpected, salient sounds in PTSD seems mediated by altered cerebral attention mechanisms rather than altered auditory perception or salience detection. The stronger neural responses generated by white noise make these stimuli more suitable for investigating autonomic hyper-responsiveness in PTSD in the noisy fMRI environment, compared to the pure tone stimuli that have commonly been used in the quieter psychophysiological laboratory.

3537

T. Weiss[1], H. Schneider[1], M. Silginer[1], A. Steinle[2], M. Pruschy[3], M. Weller[1], P. Roth[1]

The NKG2D system mediates anti-tumor effects of chemotherapy and radiotherapy against glioblastoma

Department of Neurology and Brain Tumor Center, University Hospital Zurich and University of Zurich, Zurich[1], Institute for Molecular Medicine, University of Frankfurt, Frankfurt[2], Department of Radiation Oncology, University Hospital Zurich and University of Zurich, Zurich[3]

Introduction:
Glioblastoma is the most common primary malignant brain tumor in adults and almost exclusively lethal. The current treatment standard comprises surgery followed by radiotherapy and chemotherapy with temozolomide (TMZ). Recent studies investigate immunotherapy as another treatment strategy because glioma cells express molecules that allow the interaction with immune cells. Remarkable representatives are ligands that bind to the natural-killer group 2 member D (NKG2D) receptor because these ligands enable for the interaction with cells of the innate as well as the adpative immune system. Furthermore, these NKG2D ligands (NKG2DL) are inducible by conditions that lead to cellular stress, like chemotherapy or radiotherapy. However, the effect of these treatment modalities on NKG2DL expression in glioma cells has been only scarcely investigated and the functional relevance is unknown.

Methods:
We used a variety of human and mouse glioma models including glioma-initiating cell lines. For *in vitro* studies, these cells were treated with different concentrations of TMZ or with different doses of γ-irradiation. The expression of different human and mouse NKG2DL was determined on mRNA level by real-time PCR as well as on protein level by flow cytometry. For functional immunological studies, we used a flow-cytometry based cytotoxicity assay. For *in vivo* studies, we engineered mouse glioma cell lines syngeneic to C57BL/6 and VM/Dk mice to stably express near-infrared fluorescent proteins which allows the detection of these cells by flow cytometry. Orthotopic tumor-bearing mice received a single dose of local irradiation or were treated with TMZ per oral gavage for five days and cell surface NKG2DL protein expression was assessed *ex vivo*. To asssess the impact of NKG2D on the survival benefit gained with irradiation and TMZ, we blocked the NKG2D system *in vivo* with a blocking but non-depleting anti-NKG2D antibody.

Results:
TMZ or irradiation led to an upregulation of NKG2DL on mRNA as well as on protein level in human and mouse glioma cells including glioma-initiating cell lines. This effect was independent from cytotoxic and growth inhibitory effects. The clinically relevevant expression of O^6-methylguanine-DNA-methyltransferase (MGMT) affected only the TMZ-mediated NKG2DL induction. We assessed the mediating pathway and demonstrated that the ataxia telangiectasia mutated (ATM)-dependent DNA damage response was required for NKG2DL induction upon both, TMZ exposure and irradiation. On a functional level, the TMZ- or irradiation-mediated NKG2DL induction promoted immune-cell mediated cytolysis of glioma cells in a NKG2D-dependent manner. *In vivo,* we confirmed the upregulation of NKG2DL cell surface expression by TMZ and irradiation. The survival benefit gained with TMZ or irrdiation in immunocompetent, SMA-560 glioma-bearing VM/Dk mice was attenuated when signaling through the NKG2D system was abrogated.

Conclusion:
We elucidate a new NKG2D-dependent anti-glioma effect of TMZ and irradiation. These findings could provide a rationale for therapeutic strategies combining radiochemotherapy and immunotherapy against glioblastoma.

3538

P. Beeler[1], S. Kuster[2], E. Eschmann[1], R. Weber[2], J. Blaser[1]

Earlier Switching from Intravenous to Oral Antibiotics - Hospital-Wide Rollout of Electronic Reminders

Research Center for Medical Informatics, University Hospital Zurich and University of Zurich[1], Division of Infectious Diseases and Hospital Epidemiology, University Hospital Zurich and University of Zurich[2]

Introduction:
Paper-based interventions have been shown to stimulate switching from intravenous (i.v.) to oral (p.o.) antibiotic therapies. Shorter i.v. durations are associated with a lower risk of iatrogenic infections as well as reduced workload and costs. The purpose of this study was to determine whether automated electronic reminders are able to promote earlier switching.

Methods:
In this controlled before-and-after study conducted at the University Hospital Zurich, an algorithm identified patients who were eligible for i.v.-to-p.o. switch 60 h after starting i.v. antimicrobials. Reminders offering guidance on the re-assessment of initial i.v. therapy were displayed within the electronic health records in 12 units (28% of hospitalized patients) during the intervention period (year 2012). In contrast, no reminders were visible during the baseline period (2011) and in the control group (17 units; 72% of hospitalized patients).

Results:
A total of 22 863 i.v. antibiotic therapies were analysed; 6082 (26.6%) were switched to p.o. therapy. In the intervention group, 757 courses of i.v. antibiotics were administered for a mean ± standard deviation duration of 5.4±8.1 days before switching to p.o. antibiotics in the baseline period, and 794 courses for 4.5±5.5 days in the intervention period (P=0.004), corresponding to a 17.5% reduction of i.v. administration time. In contrast, in the control group the duration increased; 2240 i.v. antibiotics were administered for a mean duration of 4.0±5.9 days in the baseline period, and 2291 for 4.3±5.8 days in the intervention period (P=0.03).

Table: Change of the mean IV duration from the baseline (2011) to the intervention period (2012) of the top 5 antibiotics according to the weighted change in the intervention group.

		2011				2012						
	Antibiotic	Mean IV duration [days]	SD	n	%	Mean IV duration [days]	SD	n	%	Change of mean duration [days] (change percentage)		**Weighted change[1)] [days]**
Intervention group	Piperacillin/ tazobactam	7.56	13.20	163	21.5	5.26	5.29	170	21.4	-2.30	(-30.4%)	-383.0
	Imipenem/ cilastatin	12.12	7.98	8	1.1	6.75	7.25	8	1.0	-5.37	(-44.3%)	-43.0
	Vancomycin	7.63	9.14	16	2.1	5.77	6.74	23	2.9	-1.86	(-24.4%)	-36.3
	Teicoplanin	14.34	12.48	14	1.8	11.30	11.96	5	0.6	-3.04	(-21.2%)	-28.9
	Amoxicillin	9.31	6.06	6	0.8	6.28	5.40	6	0.8	-3.03	(-32.6%)	-18.2
	Overall	5.42	8.15	757	100	4.47	5.49	794	100	-0.95	(-17.5%)	-736.7

SD: Standard deviation.

[1)] Estimated mean reduction of IV days per year, defined as follows: Weighted change = change of mean duration * ((n_{2011} + n_{2012}) / 2).

Conclusion:
Electronic reminders fostered earlier i.v.-to-p.o. switches, thereby reducing the duration of initial i.v. therapies by nearly a day. So far, savings of 737 days of i.v. antibiotic therapy per year were calculated. However, the electronic reminders were introduced in the control group on 4th of January 2016 and have now the potential to additionally benefit 72% of the hospitalized patients in the University Hospital Zurich.

3539

A. Senatore[1], C. Tiberi[1], G. Horny[2], N. George[2], T. Pietzonka[2], A. Aguzzi[1]

Development of novel immunotherapeutics for genetic prion diseases

Institute of Neuropathology, University Hospital Zürich, Zurich[1], Novartis Institutes for BioMedical Research, Novartis Pharma, Basel[2]

Introduction:
Familial prion diseases, which account for about 15% of prion diseases in humans, are rare neurodegenerative disorders with no known therapy. They are caused by dominant inherited germ line mutations in the *PRNP* gene encoding for the cellular prion protein, PrP^C, a glycosylphosphatidyl-inositol (GPI)-anchored membrane protein, highly abundant in the nervous system and conserved among species. PrP^C consists of two moieties: the C-terminal globular domain (GD) and the N-terminal flexible tail (FT), which includes the octapeptide repeat (OR) region, two regions enriched in positively charged residues (CC1 and CC2) and a hydrophobic core. Similar to infectious prions, pathogenic mutations produce a misfolded version of the protein which is abnormally deposited in the brain and toxic to neurons.
Whether antibody-based therapy for prion diseases is a valuable strategy has been highly debated. By testing our own series of monoclonal antibodies (mAb) for toxicity in vitro and in vivo, we recently demonstrated that the biological effect of anti-PrP antibodies strongly depends on the targeted PrP epitope: binding of the FT was always innocuous, whereas binding of epitopes within the GD was toxic.
Thus, in-depth structural and molecular studies are needed to identify epitopes of PrP that can be pursued for a safe immunotherapy.

Methods:
With the goal to establish a preclinical pipeline for discovering therapeutic anti-PrP mAbs, we executed a high-throughput screen for saturation coverage of the PrP surface in collaboration with Novartis Institute for Biomedical Research. Specifically, novel anti-PrP Fabs have been generated by using phage display technology coupled with Next Generation Sequencing (NGS) analysis of the panning output pools. This enables to identify rare, otherwise invisible epitopes in complement to the classical ELISA screening technique. A synthetic human Fab phage display library has been selected by sequential biopanning rounds to identify a broad range of Fabs binding to PrP in different regions. These Fabs are subcloned into expression vectors for production and purification and have been characterized by surface plasmon resonance (SPR), ELISA and flow cytometry.

Results:
We have selected 80 anti-PrP Fabs with CDRs and framework regions completely sequenced, and definite binding profile: CC1, OR, CC2 and GD binders. Additional clones with diverse epitopes have been rescued by PCR from the output pools, based on the HCDR3 sequence frequency in NGS, to retrieve candidates with interesting binding profiles to the different PrP domains. Epitope mapping at amino acid level has been determined by competition ELISA experiments using 12-mer PrP sequential peptides spanning the entire FT. The binding affinity, as determined by SPR, is within the nM as order of magnitude and analysis by flow cytometry indicated the ability of most of the Fabs to detect native PrP on the surface of neuronal cells.

Conclusion:
We have provided a more exhaustive anti-PrP antibody repertoire based on a rational design for the discovery of effective immunotherapeutics against familial prion diseases.

3540

O. Riesterer[1], M. Nesteruk[1], R. Bundschuh[2], P. Veit-Haibach[3], M. Hüllner[4], G. Studer[1], S. Stieb[1], S. Glatz[1], M. Pruschy[1], M. Guckenberger[1], S. Lang[1]

Radiomics in the CT perfusion maps – robustness study

Department of Radiation Oncology, University Hospital Zurich[1], Department of Nuclear Medicine, University Hospital Bonn[2], Department of Nuclear Medicine and Department of Diagnostic and Interventional Radiology, University Hospital Zurich[3], Department of Nuclear Medicine, University Hospital Zurich[4]

Introduction:
Prediction of therapy outcome using radiomics has been a growing field of research in the last few years. The aim of this study was to identify a set of stable texture features computed on CT perfusion (CTP) maps with respect to CTP calculation parameters and image discretization.

Methods:
11 patients with head and neck (HN) cancer and 11 patients with lung cancer who underwent CTP before treatment were included in the study. Software for texture features calculation was developed based on 3D definitions of first-order statistical parameters (n = 5), the Gray-Level Co-Occurrence Matrix (n = 14), the Neighborhood Gray Tone Difference Matrix (NGTDM) (n = 4), the Gray Level Size Zone Matrix (n = 11) and fractal dimension. Together 35 texture parameters were computed for three perfusion maps: blood volume (BV), blood flow (BF) and mean transit time (MTT) and their 3D wavelet transforms (n = 8). First the variability of texture parameters with respect to the image discretization method (set number of bins in comparison to set intervals) was studied using intraclass correlation ICC two-way mixed model. Second the correlations of texture parameters with tumor volume were investigated using Spearman correlation. To further examine the stability of texture parameters the ICC was calculated for factors influencing the perfusion maps determination (Table 1). The stability was first analyzed according to tumor site and only features stable for both sites were included in the final set. Finally, the parameters were grouped according to inter-parameters Spearman correlations and only the parameter with the highest ICC was chosen. The acceptance level for ICC was 0.9 and for Spearman correlation 0.7.

Results:
Texture parameters were computed in the three perfusion maps and their 3D wavelet transforms, which resulted in 945 texture features defined for each of the two tumor sites. The discretization of images using set number of bins and set intervals gave the similar number of stable texture parameters. 40 parameters were correlated with tumor volume. Potentially standardizable factors introduced more variability into texture features than non-standardizable. The highest variability was observed for pixel size. It caused instability in around 80% of parameters for both HN and lung tumors. Ten parameters were found to be stable in both HN and lung for potentially non-standardizable factors after the correction for inter-parameters correlations:

- BF: entropy, sum entropy, LHH low gray-level size emphasis
- MTT: long size low gray-level emphasis
- BV: difference entropy, coarseness, long size high gray-level emphasis, HLH information measure of correlation 2, LLL covariance, LLL average.

Conclusion:
The set of stable texture parameters in CTP was identified. Pixel size, image discretization and HU intervals have to be standardized to build reliable prediction models based on CTP texture analysis.

3541

U. Rulle[1], R. Casanova[1], R. Stahel[2], W. Weder[3], A. Soltermann[1]

External quality assessment of PTEN immunohistochemistry using computer-based image analysis compared to pathologist's scoring

Institute of Surgical Pathology, University Hospital Zurich[1], Clinic of Oncology, University Hospital Zurich, Switzerland[2], Division of Thoracic Surgery, University Hospital Zurich[3]

Introduction:
PTEN (phosphatase and tensin homolog) is a major tumor suppressor and may serve as surrogate marker for a hyper-activated PI3K-Akt pathway. Thereby, tumors more responsive to PI3K inhibitors may be identified. Loss of total protein expression is likely to be most important parameter in this setting, but an optimal immunohistochemistry (IHC) protocol for assessing this molecule on formalin-fixed paraffin-embedded tissue is still lacking. We set up a European-wide external quality assessment in order to validate PTEN IHC.

Methods:
Ten human tumors of various origin and 2 cell lines (5+1 each PTEN positive and negative) were stained on whole sections in Zurich with 3 different anti-PTEN antibodies, including clones SP218 (Spring Bioscience), 138G6 (Cell Signaling Technology) and 6H2.1 (DAKO). Scanned IHC stainings were assembled into a webbook. A tissue microarray (TMA) was manufactured from the same cases and all 16 centers of the European Thoracic Oncology Platform (ETOP) performed a local IHC using SP218 on automated IHC platforms. Both webbook and TMA stainings were H-scored by the ETOP pathologists as well as by the computer using 50 frames analyzed on ImageJ.

Results:
Robust immunoreactivity was achieved with all 3 anti-PTEN clones on either Ventana Benchmark or Leica Bond platforms, whereby 6H2.1 was consistently stronger than SP218 or 138G6. Intra-tumoral cancer-associated fibroblasts served as internal positive control for H-score 300. All ETOP centers and the computer were capable of distinguishing the PTEN positive from the negative cases on both scanned webbook whole sections and TMA stainings. Comparing pathologist's scores with Image J analysis indicated that the computer scored low-positive PTEN areas 0.5-fold lower, but high positive immunoreactivity up to 2 fold lower. The computer calculated H-score variation coefficient among the ETOP TMAs staining was between 0.42 - 2.29.

Conclusion:
Computer-based image analysis of IHC stainings of tumor suppressors like PTEN, in which protein loss rather than overexpression needs to be assessed, may allow for more accurate and global measurement of immunoreactivity.

3542

O. Török[1], B. Schreiner[2], A. Keller[1]

The role of brain pericytes in the regulation of leukocyte trafficking and immune response under homeostatic and pathological conditions

Division of Neurosurgery, University Hospital Zurich, Zurich[1], Institute of Experimental Immunology, University of Zurich, Zurich[2]

Introduction:
In the central nervous system (CNS), brain endothelium limits the passage of plasma proteins, and the extravasation of immune cells under homeostatic condition, which is achieved by several special characteristics of brain endothelial cells. The blood-brain barrier (BBB) is a collective term for these CNS endothelial cell characteristics, which are not intrinsic to brain endothelial cells but are actively induced by neural tissue and other components of the neurovascular unit. It has been demonstrated that pericytes play a role in the development and regulation of the BBB at the level of endothelial transcytosis. In multiple sclerosis (MS), it is believed that immune control mechanisms fail such that aberrant leukocytes invade into the CNS and attack the body's own myelin sheath and nervous tissue. The entry of auto-immune leukocytes into the brain parenchyma of MS patients is crucial for the demyelinating pathology, and is accompanied by breakdown of the BBB. Thus there are convincing evidences that pericytes regulate several BBB characteristics, further studies are needed to better define the role of pericytes in immune cell invasion into the CNS in the steady-state and during autoimmune inflammation in vivo.

Methods:
During the course of this study, we use genetically modified, pericyte-deficient (Pdgfb ret/ret) mice. These animals show an approximately 85% reduction of pericyte numbers in the CNS compared to wild type animals. Experimental autoimmune encephalomyelitis (EAE) was induced, the animal disease model of MS. The following techniques were used: immunohistochemistry, histochemistry, confocal microscopy, flowcytometry.

Results:
The analysis of brains of adult Pdgfb ret/ret mice suggest that these animals show an increased extravasation of leukocytes into the CNS. Immunohistochemical analyses demonstrate an infiltration of $CD45^+$ cells in the brain parenchyma. These infiltrates were mostly found in the corpus callosum and in regions close to lateral ventricles. FACS analysis demonstrated that in particular the number of $CD45^{high}CD11b^+$ myeloid cells (4.1 fold, n=6-7, p=0.0117, two-tailed t-test) was increased in pericyte deficient CNS compared to control tissue. In contrast, $CD4^+$ T cells, $Ly6G^+$ neutrophils, and $CD45^{low}CD11b^+$ microglia cells were not significantly increased. Analysis of the leukocyte composition in blood showed no deviations in leukocyte populations in Pdgfb ret/ret mice compared to controls ($CD11b^+$ cells: 1.0 fold change, p=0.8504, two-tailed t-test) indicating that increased parenchymal infiltration of myeloid cells is not due to their increased number in the blood. The active immunization of Pdgfb ret/ret mice with myelin oligodendrocyte glycoprotein (MOG) peptide or adoptive transfer of MOG-specific, activated T cell blasts led to an early and strong atypical EAE phenotype.

Conclusion:
Based on these observations we hypothesize that pericytes act as inflammatory sentinels in the CNS by contributing to the non-permissive properties of the endothelium during homeostasis, and restrict leukocyte migration during EAE. We plan to further characterize the "leukocyte extravasation" phenotype in Pdgfb ret/ret brains and spinal cords under homeostasis, with a particular focus on the regional leukocyte distribution pattern and proportions of certain leukocyte cell subsets. Furthermore, we will investigate the aggravated atypical EAE that we observe after MOG-peptide immunization, and examine if myelin-reactive (unprimed) T cells in the periphery will be activated in Pdgfb ret/ret mice

3543

D. Shinde[2], H. Ademi[1], J. Vogel[1], T. Gorr[1]

Targeting vascularized and hypoxic compartments in solid malignancies: from basic research to dogs with cancer

Institute of Veterinary Physiology, Vetsuisse Faculty, University Zürich, Zürich[1], Institute of Oncology Research, Cantonal Hospital Bellinzona, Bellinzona [2]

Introduction:
Solid malignancies, one of the leading causes of morbidity and mortality worldwide, activate angiogenesis, the formation of new blood vessels from pre-existing capillaries. Angiogenesis is mainly driven by vascular endothelial growth factor (VEGF) that is highly abundant in many tumors. Consequently, VEGF became an attractive target for anti-cancer therapy and VEGF-blockers like the anti-VEGF monoclonal antibody Bevacizumab (Avastin®) raised big hope. However, blocking of VEGF alone frequently wasn't sufficient to prevent tumor progression. *In vivo* and in patients this therapeutic approach even induced resistance and increased metastatic rate and aggressiveness.

Since tumors can be heterogeneous in regard to oxygenated and hypoxic areas, they often consist of oxygenated cells that generate energy by oxidative phosphorylation whereas the cells in the hypoxic regions undergo a "glycolytic switch", by which glycolysis is uncoupled from respiration and yields lactate as end product. Lactate is not wasted but taken up by oxygenated cells through monocarboxylate transporter 1 (MCT1) and eventually oxidized to produce energy. This interaction between hypoxic and oxygenated cells is also known as the "metabolic symbiosis" that we aim to interrupt by treating tumors with the MCT inhibitor α-cyano-4-hydroxycinnamate (CHC) in combination with Avastin® to target simultaneously both, oxygenated and hypoxic cells.

Methods:
Human U87 glioblastoma and the MDA-MB-231 breast cancer cell lines as well as canine cancer cell lines K9 soft tissue sarcoma (STS), 17CM98 oral melanoma and hemangiosarcoma (HAS) were inoculated on d9 of development onto the chicken chorioallantoic membrane (CAM) of an *ex-ovo* preparation. Four different treatments, applied on the following day, included: topical administration of PBS as control, i.v. injection of Avastin® (10mg/kg) and topical CHC (60mg/kg) application either alone or in combination with Avastin®. Tumor growth was measured by digital imaging on d10, d12 and d14. Tumor perfusion was quantified by using Laser-Speckle perfusion imaging and tumor hypoxia by pimonidazole staining. For measuring cancer cell spreading a digital droplet PCR (ddPCR) technique was employed. For this purpose DNA was extracted from the tumor explant and in three adjacent zones of different distance from the tumor site. By terminating the CAM assay on d14 our comparative drug screening is an animal-testing-free set up.

Results:
Treatment of human cancer cells with Avastin® and CHC monotherapy arrested tumor growth but the combinatorial treatment of Avastin® with CHC was able to effectively shrink the neoplastic mass. Using Avastin® alone triggered a significant increase, rather than diminishment, of tumor hypoxia as well as cell spread. In contrast, combinatorial Avastin®+CHC treatment yielded a clear decrease of tumor hypoxia and cancer cell dissemination (manuscript in prep.). Preliminary data revealed growth of canine HAS cells to also be halted upon treatment with Avastin® or CHC monotherapy, and the combinatorial treatment increased the effect.

Conclusion:

Disrupting the metabolic symbiosis between the hypoxic and oxygenated tumor cells seems to be a promising approach to treat human or canine solid malignancies as well as to reduce metastasis and aggressiveness, the side-effects of anti-VEGF treatment. Moreover the *ex-ovo* CAM assay appears to be a promising and animal-testing-free drug screening approach for development of seminal anti-cancer therapies.

3544

Y. Valko[1], E. Werth[1], C. Baumann[1], D. Straumann[1], P. Valko[1], K. Weber[2]

Positional nystagmus from BPPV in polysomnography of PD patients

Department of Neurology, University Hospital Zurich, University of Zurich, Switzerland[1], Department of Ophthalmology, University Hospital Zurich, University of Zurich, Switzerland[2]

Introduction:
Patients with Parkinson Disease (PD) have an increased risk of falls due to postural instability, orthostatic dysregulation, or benign paroxysmal positional vertigo (BPPV). BPPV is common in PD, and BPPV often occurs during changes of head position in bed. We recently demonstrated that positional nystagmus can be discerned from other electrooculography (EOG) patterns. Since polysomnography is a commonly performed diagnostic test in PD, we aimed at elucidating the frequency of so-far undetected BPPV by analysis of EOG recordings.

Methods:
Retrospective analysis of whole-night polysomnography recordings of 30 PD patients. EOG recordings were manually inspected and screened for nystagmus-like patterns. Patient characterization included disease duration, UPDRS III, and disease type. In addition, the impact of polysomnography variables on BPPV frequency was assessed.

Results:
Twelve patients (40%) exhibited one or more nystagmus-like EOG episodes. Patients with and without nystagmus-like EOG episodes did not differ with respect to age (64±11y vs. 61±8y, p=0.32), UPDRS III (25±9 vs. 23±12, p=0.27), or disease duration (9±7y vs. 7±6y, p=0.42). Sleep efficiency was similar between PD patients with and without nystagmus-like EOG episodes (77±14% vs. 80±15%, p=0.53).

Conclusion:
Our preliminary findings indicate that BPPV may be more common in PD than appreciated so far, although the impact of nocturnal BPPV attacks on sleep quality remains unclear. The search for BPPV in polysomnography may be particularly meaningful in PD, as it has become a routine diagnostic tool in many specialized movement disorder units.

3545

S. Isringhausen[1], N. Kraeutler[2], D. Stoycheva[2], U. Suessbier[1], P. Helbling[1], L. Kovtonyuk[1], H. Wong[1], M. Manz[1], A. Oxenius[1], C. Nombela-Arrieta[1]

Dynamics of the bone-marrow microenvironment during viral infections

Experimental Hematology Division, University Hospital Zürich, Zürich[1], Microbiology, ETH Zürich, Zürich[2]

Introduction:
Hematopoiesis as the primary function of the bone marrow (BM) is a highly dynamic and tightly regulated process. It is sustained by a rare population of self-renewing, multipotent hematopoietic stem and progenitor cells (HSPCs), which reside in specialized nurturing microenvironments within BM cavities. The BM is extremely diverse, comprising all hematopoietic lineages as well as complex stromal cellular networks of mesenchymal, neural and vascular origin. Beyond providing a structural scaffold for hematopoietic cells, stromal cells are critically involved in the fine regulation of different stages of hematopoiesis. Yet, the functional interplay of stromal components with hematopoietic cells during both homeostasis as well as in inflammatory conditions is incompletely understood.
Viral infections trigger major stress in the hematopoietic system inducing an adaptive response in cellular output. Nonetheless, the effect of viral infections on BM stromal scaffolds remains poorly defined.

Methods:
Combining conventional in vitro and in vivo assays with 3D imaging technology, we are investigating the effect of acute and chronic viral infections on the microarchitectural and functional integrity of the BM.

Results:
Our results indicate that viral infections result in rapid vasodilation of BM sinusoids and disruption of extracellular matrix networks. Notably, chronic infections with LCMV strains induce a profound and sustained reduction in the number of HSCs, which correlate with a downsizing of the population of endothelial and mesenchymal stromal progenitor cells and a decrease in their capacity to produce HSPC-sustaining factors.

Conclusion:
We are currently investigating both the precise molecular and cellular mechanisms driving viral-induced BM tissue damage as well as the functionality of HSCs after viral infection.

3546

S. Freiberger[1], P. Cheng[1], R. Dummer[2], M. Levesque[1]

Transcriptome Analysis to investigate Melanoma Heterogeneity and Drug Resistance

Department of Dermatology, University of Zurich, Zurich[1], Department of Dermatology, University Hospital Zurich, Zurich[2]

Introduction:
Melanoma is the most fatal skin cancer with 5 year survival rates of 63% and 16% for patients diagnosed with Stage III and Stage IV, respectively. Targeted therapies have extended the progression free survival of melanoma patients by 6 months using BRAF inhibitors, and by 4 months using MEK inhibitors. Immunotherapies, such as anti-CTLA4 and anti-PD1 inhibitors have been successful extending overall survival of metastatic patients by 4 months and 17 months, respectively. Unfortunately most patients relapse to targeted therapy, and more than 70% relapse under immunotherapy. Thus, there is a large need to uncover resistance mechanisms to targeted therapy and immunotherapy. Furthermore, melanoma is a very heterogeneous tumor and the impact of this heterogeneity for drug resistance is poorly understood. Therefore, we are investigating the intra-patient and inter-patient diversity in terms of gene expression changes after targeted therapy or immunotherapy. In the current project, we have collected melanoma patient cell cultures from the URPP melanoma biobank under various targeted therapies and immunotherapies from during treatment and after relapse and performed RNA sequencing.

Methods:
Sample cohort: We have selected a number BRAF or NRAS mutated melanoma patients with multiple cell cultures established from the URPP melanoma biobank. This cohort of patients includes targeted therapy and immunotherapy treated patients that have relapsed. RNA was isolated from these melanoma cell cultures and submitted to the FGCZ for RNAseq.

Results:
Preliminary analysis of 40 melanoma cell lines from 18 patients shows that BRAF or NRAS mutation does not correlate with gene expression. Gene expression changes due to relapse of targeted therapy or immunotherapy are also highly variable but cluster into specific groups. This finding suggests that there are different mechanisms to resistance between the therapies but specific common mechanisms could be detected in small groups.

Conclusion:
Detecting gene expression changes after relapse have allowed us to detect several resistance mechanisms that could arise from relapse to targeted therapy or immunotherapy. There does not seem to be one common resistance mechanism for BRAF inhibitor, or MEK inhibitor, or anti-CTLA4 therapy. This result has high implications on the therapy that the patient will receive after. We are continuing collecting new relapse samples to increase our dataset for resistance mechanisms which will be useful for future development of new therapies.

3547

A. Franchini[1], M. Ender[1], L. Vazquez Rojo[1], D. Heuberger[1], R. Schuepbach[1]

Cleavage of protease activated receptor 2 (PAR2) by staphylococcal proteases

Division of Surgical Intensive Care, University Hospital Zurich, Zurich, Switzerland[1]

Introduction:
Protease activated receptors (PARs) sense for extracellular proteolytic activity. They are targets for clotting protease and regulate the platelet aggregation and the endothelial barrier function. PARs are activated by enzymatic removal of an N-terminus peptide uncovering a neo-N-terminus that serves as a tethered activation ligand. Bacterial proteases have been shown to cleave PARs, which might result in an activation of a shedding of the signaling. *Staphylococcus aureus* is a major human pathogen, which colonize 20-30% of the human population. The colonization by *S. aureus* may cause infections, ranging from mild skin infections to severe and life threatening infections, such as necrotizing fasciitis and infective endocarditis. *S. aureus* has a broad range of extracellular proteases and we hypothesize that these proteases cleave PARs and thus affect the strain's virulence by boosting abscess formation.

Methods:
Staphylococcus aureus strains were grown until stationary phase, the supernatant collected and applied to all the experiments. In addition, Recombinant proteases and supernatant collected from strains lacking one or more genes encoding proteases were tested for their activity in PARs cleavage. Alkaline phosphatase (AP) N-terminally tagged PARs were transiently overexpressed in HEK T293 cells. These cells were incubated with the proteases or the supernatant of the bacterial culture to assess the cleavage of PARs by the release of the N-terminal AP. The released N-terminal AP activity was recorded and use as proxy of protease activity in the cleavage of PARs.

Results:
Cleavage of PAR2 and, to a less extent, PAR4 was observed when PARs overexpressing cells were incubated with the supernatant of a *S. aureus* culture. The incubation of the supernatants with several protease inhibitors identified metalloproteases as the cleaving enzymes. Moreover, zymography was used to identify specific proteases in the supernatant. The serine protease SspA and the cysteine protease ScpA were identified as candidate enzymes responsible of the cleavage of PAR2. The protease(s) responsible of the PAR2 cleavage are under the transcriptional control of the global regulator *agr*. Although, single knock out mutant of the mentioned proteases demonstrated reduced cleavage of PAR2, no protease could be identified as single cleaving enzyme. Moreover, potential cleavage could be identified at residues E56 and E63 of PAR's N-terminus.

Conclusion:
S. aureus secretes proteases capable to cleave PAR2, potentially linked to host reactions allowing the formation of abscess formation. SspA and ScpA were identified as candidate proteases involved in PAR2 activation by *S. aureus*.

3548

C. Huber[1], J. Schneider[1], B. Mueller[3], M. Christ-Crain[2], M. Katan[1]

Mid-regional pro-adrenomedullin (MR-proADM) is an independent predictor of post stroke mortality

Neurology department, University Hospital Zurich, Switzerland[1], Departement of Endocrinology, University Hospital of Basel, Switzerland[2], Medical University Clinic, Cantonal Hospital Aarau, Switzerland[3]

Introduction:
Adrenomedullin – an immune modulating and vasoactive peptide- is associated with stroke outcome. However, little is known about the incremental prognostic role of mid-regional pro-adrenomedullin (MR-proADM) in the acute stroke setting. We hypothesize that MR-proADM improves risk-stratification beyond established vascular risk-factors.

Methods:
MR-proADM-levels were measured in 362 consecutively enrolled acute ischemic stroke patients. Patients were followed for 90 days and functional outcome and mortality was determined by structured telephone-interviews. Cox proportional hazard and logistic regression models were fitted to estimate hazard and odds ratios for the association of MR-proADM with functional outcome and mortality. The discriminatory value of MR-proADM was evaluated, by calculating the area under the receiver operating characteristic curve (AUC). The incremental value for risk-stratification was assessed by the net reclassification improvement (NRI) and integrated discrimination improvement (IDI).

Results:
After adjustment for traditional risk-factors MR-proADM levels remained independently associated with mortality (HR 6.65, 95%CI 3.63-12.16, p<0.001) but not with functional outcome (OR 0.80, 95%CI 0.33-1.95, p=0.64). Adding MR-proADM levels to the multivariate model improved the discriminatory accuracy of the model for mortality significantly (from AUC 0.90 to AUC 0.92, p-value<0.001). The continuous NRI of 0.721 (95%CI 0.302-1.145) and IDI of 0.060 (95%CI 0.006-0.151) suggests clinical meaningful improvement in risk classification, for the endpoint mortality.

Conclusion:
MR-proADM is a novel prognostic blood biomarker in the acute stroke setting, improving risk prediction for mortality beyond established risk factors, probably due to its pleotropic effects on the cerebral vasculature and immune response. Further validation studies are needed to confirm these results.

3549

A. Jöhl[2], M. Stäuble[2], M. Monn[2], M. Schmid Daners[2], S. Klöck[1], S. Lang[1]

Modeling of a Robotic Treatment Couch to Improve the Control Performance

USZ, Oncology, Zürich[1], ETH Zurich, Mechanical Engineering, Zurich[2]

Introduction:
In Radiation Therapy, the tumor may move due to respiration (e.g. lung tumors). This motion forces an increase of the irradiated volume to ensure the prescribed dose to the tumor. However, the volume increase also increases the dose to healthy tissue. Therefore, mitigation of the tumor motion during treatment decreases the dose to healthy tissue. One method for tumor motion mitigation is couch tracking, where a robotic treatment couch moves the patient such that the tumor motion is compensated. The robotic treatment couch considered here is the Perfect Pitch (Varian, Palo Alto, CA, USA). For couch tracking, the dynamic behavior of the Perfect Pitch is of high interest. The Perfect Pitch is part of the TrueBeam (Varian, Palo Alto, CA, USA) system, which offers couch tracking capabilities. These tracking capabilities were evaluated.

Methods:
The Perfect Pitch's internal position sensors were verified using external sensors. A numerical model of the Perfect Pitch was developed. The unknown parameters of the model were identified by letting the couch track known trajectories of a robot. The tracking performance was evaluated by using a tumor motion phantom that was tracked by the radio-frequency system Calypso (Varian, Palo Alto, CA, USA). The phantom moved according to a sinusoidal signal with a peak-to-peak amplitude of 20 mm and linearly increasing frequency from 0.01 Hz to 0.5 Hz over 100 s. This frequency range covers the variety of human respiration frequencies. The performance was evaluated by considering the differences between the phantom motion and the couch motion. For each measurement the differences were summarized to one value by taking their root mean square (RMS).

Results:
The differences between the internal and the external measurements were in the median 0.05 mm in the lateral direction, -0.003 mm in the longitudinal direction and -0.07 mm in the vertical direction, respectively. The RMS of the differences between the numerical model and the real couch using the same input signal was on average 1.04 mm in longitudinal, 0.10 mm in lateral and 0.11 mm in vertical direction. The RMS of the differences between the phantom motion and the couch motion was below 2 mm for velocities up to 20 mm/s for lateral and vertical motion.

Conclusion:
The internal sensors are reliable. The Perfect Pitch allows for couch tracking as long as the tumor motion speed does not exceed the speed limits of the Perfect Pitch. The model represents the real Perfect Pitch well and can be used for further investigations without the real Perfect Pitch, which is in clinical use and, therefore, not always available.

3550

N. Vital[1], J. Malamud[1], J. Taeymans[2], C. Mueller-Pfeiffer[1]

Functional impairment in posttraumatic stress disorder: a systematic review and meta-analysis

Department of Psychiatry and Psychotherapy, University Hospital Zurich, Zurich[1], Bern University of Applied Sciences – Health, Berne, Switzerland[2]

Introduction:
Posttraumatic Stress Disorder is a serious condition that is often associated with significant impairment in daily functioning. Empirically derived estimations for the magnitude of functional impairment in PTSD in distinct domains are essential e.g., for forensic evaluations in insurance medicine.

Methods:
A systematic literature search was conducted in Scopus, Pubmed, PsycINFO, Ovid, Embase, Medline, and clinicaltrials.gov using the keywords "PTSD" or "Posttraumatic stress disorder" combined with "Functioning" or "Disability". Inclusion criteria were observational studies including case-control, cohort and cross-sectional-studies; adults with a current (past month) categorical PTSD diagnosis assessed by a validated interview-based instrument; subjects recruited from a trauma-exposed population or from the general population; systematic diagnostic assessment of functioning and/or disability using a validated instrument at the time of diagnosing PTSD; successful assignment of outcome measures to categories of the WHO International Classification of Functioning, Disability and Health (ICF). Studies that investigated subjects drawn from a population characterized by a somatic disorder or specific mental disorder/syndrome other than PTSD were excluded. Random effects meta-analyses were conducted for the different functional areas according to the ICF and standardized mean difference statistic (d) and their corresponding 95% confidence intervals were calculated.

Results:
Forty-two studies were included in the meta-analysis. PTSD subjects, compared to healthy subjects, had higher impairment in the areas of general tasks and demands (d = 1.99, 95% CI [0.82, 3.14]), domestic life (d = 1.90, 95% CI [0.96, 2.84]), interpersonal interactions and relationships (d = 1.45, 95% CI [0.74, 2.16]), major life areas (d = 1.66, 95% CI [0.73, 2.60]), and community, social, and civic life (d = 1.70, 95% CI [1.01, 2.40]). PTSD subjects, compared to subjects with mental disorders other than PTSD, had higher impairment in self-care (d = 0.29, 95% CI [0.06, 0.52]), interpersonal interactions and relationships (d = 0.27, 95% CI [0.05, 0.49]), community, social, and civic life (d = 0.31, 95% CI [0.05, 0.57]). No differences between groups were found regarding impairment in mobility.

Conclusion:
Modest to large effect sizes were found for impairment in PTSD in many areas of daily functioning as conceptualized in the ICF of the WHO. These results suggest a significant impact of PTSD on public health and social insurance systems.

3551

H. Rodriguez Cetina Biefer[1], S. Sündermann[1], M. Emmert[1], H. Alkadhi[2], M. Genoni[1], F. Maisano[1], A. Plass[1]

Sternal healing in asymptomatic patients and potential influencing factors

Cardiovascular Surgery, University Hospital Zurich, Zurich[1], Institute of Diagnostic and Interventional Radiology, University Hospital Zurich[2]

Introduction:
Median sternotomy is the routinely access for multiple open heart surgeries. Sternal instability, dehiscence, wound infection and mediastinitis are feared complications. The cause is often not clearly comprehensible, inadequate sternal healing can be one of them. This might translate into certain number of asymptomatic patients showing sternal abnormalities (SAs). We assessed by multi-planar CT-scans (CTs) the sterna of asymptomatic patients with no postoperative complications. Potential related causes were analyzed with the goal to identify possibilities for more optimized sternal healing.

Methods:
We analysed CTs from 131 asymptomatic consecutive patients performed between 2007 and 2009 who underwent cardiac surgery at our institution via median sternotomy between 1989-2001**.** CTs were performed after an average of 11.9±4.5 years post sternotomy. Average age of the cohort was 59.5±11.2 years. Patients' selection was limited to CABG (*n*=83, 63%) and aortic valve (AV) procedures (*n*=48, 37%). Non of these patients presented sternal complains at the time the CTs were performed. To identify *SAs,* all CTs were analysed in axial view. Once *SAs* were identify, CTs were 3D reconstructed to perform detail measurements of *SAs* and distance of the first wire to proximal manubrial edge. Furthermore, the wire technique and number of used wires were analyzed. A chart review analysis for well-established risk factors for sternal complications was also performed.

Results:
32.1% of sterna showed abnormalities (*n*=42/131). 7 patients presented a combination of *SAs*: 5 gap/offset and 2 offset/impaction combination. A total of 49 *SAs* were identified: 24 offsets, 18 gaps and 7 impactions. 532 wires in total were implanted for sternal closure, averaging 4.2±0.5 wires per patient (*n*=125/131). 96.1% of implanted wires (*n*=511) were figure-of-8 wires, averaging 4.1±0.5 wires per sternum, while only 3.9% of implanted wires were single wires (*n*=21), averaging 0.2± 0.6 wires per sternum. Wire count in normal sterna (*M*=4.2±0.5) and abnormal sterna (*M*=4.3±0.6) were not statistically different (*t(123)*=1.3, *p*=>0.05, 95% CI [-0.3,0.1]). 65% *SAs* were found in the manubrium (*n*=32/49). Difference between the distance from the first wire to proximal edge of the manubrium in normal sterna (*n*=61/85, *M*=11.2±4.2mm) and the abnormal sterna (*n*=24/85, *M*=10.9±4.8mm) showed no statistical difference (*t(83)*=0.3, *p*=>0.05, 95% CI [-1.8,2.4]).CABG-patients presented a higher risk for *SAs* compared to AVR-patients (*OR*=2.4, **p*=≤0.05, 95% CI [1.2,4.9]). Furthermore, use of bilateral mammary (*OR*=4.4,**p*=≤0.05, 95% CI [1.1,17.9]) and BMI>31kg/m^2 (*OR*=3.4,***p*=≤0.01, 95% CI [1.4,8.3]) significantly increased the risk of *SAs*.

Conclusion:
Sternal healing after median sternotomy is a mayor problem. In our study, more than 30% of asymptomatic patients showed abnormalities of the sternum with a potential higher risk of complications in the initial postoperative period. We could confirm CABG, BIMA and BMI>30kg/m^2 as independent risk factors for *SAs.* Further, the area around the manubrium seems of higher risk for SAs, which could be also the potential starting point for larger problems. Of note, our analysis of sternal wiring is this area did not show any significant influence on the outcome of *SAs*. Different closure techniques in these risk groups as well specifically on the manubrium—such as osteosynthesis plate—should be considered.

3552

J. Günter[1], P. Wolint[1], J. Steiger[1], E. Cambria[1], A. Bopp[1], S. Hoerstrup[1], M. Emmert[1]

Biobanking of 3D microtissues for future off-the-shelf regenerative therapies

Swiss Centre for Regenerative Medicine, University of Zurich, Zurich[1]

Introduction:
Current available cardiac cell therapies performed with single cell suspensions show limited efficacy partially due to low retention rate. Pre-aggregation of cells into three dimensional microtissues (MTs) might improve cell retention by providing a unique microenvironment. For the off-the-shelf supply of MT-based cell therapies it is of utmost importance to cryopreserve MTs. Due to limited mass transfer within MT and to their complex structure, cryopreservation protocols of their single cell counterparts cannot be adopted. We investigate the efficiency of different cryopreservation media compositions and incubation times with respect to viability and cell membrane integrity.

Methods:
MTs of human adipose-derived mesenchymal stem cells (hADSCs) were produced by gravity enforcement in hanging drops. The MTs were collected after 3 days of hanging drop culture. Next, the culture medium was replaced by different cryopreservation media and incubated for different time periods before cooling them at 1°C/min until -80°C. After 8-24 hours the cryovials were transferred to liquid nitrogen and stored for at least 2 days. MTs were thawed in a water bath at 37°C and analyzed regarding their morphology, metabolic rate, ATP content and membrane integrity. Non-frozen MTs served as a control.

Results:
The morphology of thawed MTs after low incubation times in cryopreservation media was more diffuse than after longer incubation. This effect was slightly rescued by cryopreservation media composed of higher concentrated cryoprotective agent (CPA). The post-thawing metabolic activity was strongly influenced by the previous incubation time in the cryopreservation media. Indeed it rose with longer incubation times independent of the medium composition. However, the maximal metabolic activity of freshly thawed MTs was only about 50% compared to non-frozen MTs. The ATP content of thawed MTs was drastically reduced compared to their non-frozen counterparts and there was only a little variation between different freezing media. The prolongation of the incubation time influenced the ATP content positively. The membrane integrity of cells within thawed MTs was assessed by DNA quantification. It seemed to be influenced by both cryopreservation media composition and incubation time.

Conclusion:
The preliminary results of this ongoing project show that several parameters need to be optimized to achieve sufficient viability and functionality of MTs after cryopreservation for clinical applications. In addition to cryopreservation media composition and incubation time, cooling and thawing rates as well as nucleants and other additives might influence post-thaw viability.

3553

D. Keller[1], C. Eberhardt[2], M. Rottmar[2], D. Haralampieva[1], T. Sulser[1], D. Eberli[1], A. Boss[2]

Diffusion-Tensor-Imaging (DTI) for in vivo muscle regeneration after Cell therapy

Urology, University Hospital Zurich[1], Institute of Diagnostic and Interventional Radiology, University Hospital Zurich[2]

Introduction:
Urinary incontinence compromises a patient's quality of life and inflicts tremendous health care costs. Recent advances using cell therapy such as muscle precursor cells (MPC) show promising results towards correcting the underlying etiology, but evaluating the success of such treatments *in vivo* is difficult. In this study, we show that Magnetic Resonance Imaging (MRI) using novel sequences for alignment and complex macro molecules enables monitoring of adult stem cell myogenic differentiation in a mouse model.

Methods:
We have isolated, characterized and expanded human MPCs followed by injection into a tibialis anterior and quadriceps femoris muscle crush mouse model. We followed the *in situ* differentiation via MRI (4.7 T scanner) for 21 days focusing on Diffusion-Tensor Imaging (DTI) properties of the *de novo* tissue and confirmed the results by histology, immunohistochemistry, western blot and real time PCR.

Results:
DTI revealed that *de novo* generated muscle fibers are orientated in the same direction as the surrounding fibers which were not affected by the initial muscle crush injury. Cell differentiation and myofibers formation could be confirmed by increased expression of skeletal muscle-associated markers.

Conclusion:
Human MPCs form muscle tissue *in situ* DTI highlights the direction of the newly formed fibers. These results will be transferable to the clinical setting as a non-invasive biomarker for the assessment of muscle tissue regeneration in patients.

3554

C. Eberhardt[2], D. Keller[1], M. Rottmar[2], D. Haralampieva[1], T. Sulser[1], D. Eberli[1], A. Boss[2]

Magnetization transfer ratio (MTR) for in-vivo muscle regeneration after Cell therapy

Urology, University Hospital Zurich[1], Institute of Diagnostic and Interventional Radiology, University Hospital Zurich[2]

Introduction:
Urinary incontinence compromises a patient's quality of life and inflicts tremendous health care costs. Recent advances using cell therapy such as muscle precursor cells (MPC) show promising results towards correcting the underlying etiology, but evaluating the success of such treatments *in vivo* is difficult. In this study, we show that Magnetic Resonance Imaging (MRI) using novel sequences for alignment and complex macro molecules enables monitoring of adult stem cell myogenic differentiation in a mouse model.

Methods:
We have isolated, characterized and expanded human MPCs followed by injection into a tibialis anterior and quadriceps femoris muscle crush mouse model. We followed the *in situ* differentiation via MRI (4.7 T scanner) for 21 days focusing on Magnetization Transfer Ratio (MTR) properties of the *de novo* tissue and confirmed the results by histology, immunohistochemistry, western blot and real time PCR.

Results:
MT measurements showed an initial MTR decrease before increasing steadily and approximating the MTR values of reference skeletal muscle tissue. Cell differentiation and myofibers formation could be confirmed by increased expression of skeletal muscle-associated markers.

Conclusion:
Human MPCs form muscle tissue *in situ* and MT-MRI allows to directly assess muscle fiber formation as a measure of myogenic differentiation. These results will be transferable to the clinical setting as a non-invasive biomarker for the assessment of muscle tissue regeneration in patients.

3555

I. Simões[2], D. Keller[1], P. Vale[3], J. Cabral[2], C. Da Silva[2], P. Baptista[4], T. Sulser[1], D. Eberli[1]

Impact of solubilized muscle-specific urethral extracellular matrix on skeletal muscle differentiation for sphincter reconstruction

Urology, University Hospital Zurich[1], Department of Bioengineering and iBB - Institute for Bioengineering and Biosciences, Instituto Superior Técnico, Universidade de Lisboa, Portugal[2], Serviço Urologia, Hospital Garcia de Orta, Portugal[3], Instituto de Investigación Sanatria Aragón, CIBERehd, Spain[4]

Introduction:
Stress urinary incontinence is caused by muscle and nerve damage from natural childbirth, aging, obesity or cancer therapy. Current therapeutic options include surgical interventions and pelvic floor muscle training. The long-term efficacy of such approaches is often low. Cell therapy might offer an alternative with a cure. Currently, the complex interplay of Extracellular Matrix (ECM) and the stem cells are only poorly understood. In this research, we produced a tissue specific naturally derived ECM and evaluated the impact on cell adhesion and myoblast fusion yielding skeletal muscle for sphincter reconstruction.

Methods:
We have isolated, characterized and expanded Muscle Precursor Cells (MPCs) and cultured them on solubilized extracellular matrix (ECM) coatings derived from bioscaffolds of the rhabdosphincter (RBS) containing either skeletal muscle ECM (skECM) or smooth muscle ECM (smECM) proteins. Tissue formation was analyzed via fiber formation assay, morphological analysis and protein / gene expression. Collagen, polystyrene respectively FBS coatings were used as negative controls.

Results:
Myofibers from MPCs showed a significant longer morphology on skECM coatings (109 ± 4.9 µm) compared to all others coatings (70 ± 3.6 µm (p-value = 0.002), 75 ± 3.7 µm (p-value = 0.002), 50 ± 3.1 µm (p-value = 0.0001) and 80 ± 4.3 µm (p-value = 0.003) for collagen coating, non-coated polystyrene, FBS coating and smECM, respectively. Regarding cell circularity, there were no significant differences (p-value = 0.532). MPCs cultured on skECM and smECM revealed a similar cell proliferation profile compared to controls. After 14 days of differentiation, the cells fused into fibers expressing skeletal muscle-associated markers.

Conclusion:
Our results show the great potential of solubilized tissue specific ECM bioscafolds for skeletal muscle bioengineering. The differences in myofiber and tissue formation in both muscle-specific ECM substrates (i.e. smooth versus skeletal) might be explained by the impact of biochemical cues, cell-ECM interactions and growth factors.

3556

R. Schweizer[1], J. Schnider[2], W. Zhang[2], K. Marra[2], M. Solari[2], P. Rubin[2], V. Gorantla[2], J. Plock[1]

Timing and Frequency of Immunomodulatory Cytotherapy with Adipose-derived Stem Cells Influences Graft Survival and Immunological Outcome in Vascularized Composite Allotransplantation

Department of Plastic Surgery and Hand Surgery, University Hospital Zurich, Zurich[1], Department of Plastic Surgery, University of Pittsburgh, UPMC / USA[2]

Introduction:
The pursue for an alternative to life-long drug immunosuppression in vascularized composite allotransplantation (VCA) unveiled encouraging outcomes with cellular therapies. Clinical translation of these cytotherapies must consider collateral effects of immunosuppressive drugs. Therefore, we investigated the influence of timing and frequency of adipose-derived mesenchymal stem cell (AD-MSC) administration on allograft survival, immunological outcome and transplant vasculopathy.

Methods:
Rat AD-MSCs were assessed *in vitro* for proliferation/viability under immunosuppressive drug influence for 7 days, as well as for their immunosuppressive function in mixed lymphocyte reaction assays. White blood cells (WBCs) counts were assessed repetitively *in vivo* after ALS injection. Lewis rats received full-mismatched allogeneic limbs from Brown Norway rats (day 0). All animals received ALS conditioning on days -4 and +1 and immunosuppression with tacrolimus for the first 21 days. AD-MSCs ($1x10^6$ cells) were administered on either postoperative day (POD) 1, or POD 4 or repeatedly on PODs 4, 8, and 15. Microchimerism and regulatory T-cell function were investigated at 4 weeks and in long-term survivors. Graft arteries were assessed histologically for intimal thickness.

Results:
ALS and tacrolimus had detrimental effects on AD-MSC viability/proliferation *in vitro*. WBCs decreased within 24h after ALS injection ($p<0.01$) and recovered within 10 days *in vivo*. Single early (POD 1) and repetitive AD-MSC (POD 4, 8, 15) injection resulted in 50% long-term graft acceptance in transplant recipients, whereas single treatment on POD 4 resulted in rejection comparable to untreated controls. Chimerism levels were associated with induction of regulatory T-cells ($CD4^+CD25^{high}FoxP3^+$). The intimal thickness of graft arteries revealed significant differences between rejecting and AD-MSC-treated animals with long-term graft survival ($p<0.01$).

Conclusion:
Immunosuppressive drugs influence viability and immunosuppressive function of rodent AD-MSCs, therefore adjusted administration timing and frequency may determine the outcome of immunomodulatory cytotherapies. In addition, AD-MSC therapy shows potential for attenuation of graft vasculopathy.

3557

A. Plass[1], J. Barthelmes[1], K. Higashigaito[2], J. Sromicki[1], R. Manka[3], H. Rodriguez Cetina Biefer[1], H. Alkadhi[2], F. Maisano[1]

Noninvasive ultra-low dose CT-image guided postoperative Quality Control of Coronary Artery Bypass Grafting

Cardiovascular Surgery, University Hospital Zurich, Zurich[1], Institute of Diagnostic and Interventional Radiology, University Hospital Zurich[2], Cardiology, University Hospital Zurich, Zurich[3]

Introduction:
Latest Computer tomography (CT) enables non-invasive high quality imaging of coronary artery bypass grafts with supposed ultralow radiation dose and usage of minimal amount of contrast agent. In this study we assessed by CT for quality control asymptomatic patients after coronary artery bypass grafting (CABG) before hospital discharge next to routinely done examinations like ECG, chest x-ray and blood parameters.

Methods:
Bypass grafts of 104 patients (M 82/F 22, age 68±9 years) were examined by CT 5.8 ± 4.0 (*Median*=5, *Min*=2, *Max*=29) days after CABG. Scans were performed by 3rd generation 192-slice dual source CT machine (Somatom Force, Fa.Siemens, Erlangen). The assessment contains patency of anastomosis and positioning of grafts, differentiation of graft material – saphena venous graft (SVG), radial artery (RA), right/left internal mammary artery (RIMA/LIMA) - and on-/off-pump technique. Further for estimation of patient burden caused by CT scan volume CT dose index (CTDIvol), dose length product (DLP) and Contrast media (CM) were calculated.

Results:
74% (77/104) of coronary revascularization surgeries were performed off-pump, 26% (27/104) on-pump. 318 bypass grafts – 59% arterial (34.6% LIMA, 10.4% RIMA, 13.8% RA) and 41.2% venous (SVG) – were analyzed. 2.2% (7/318) bypass grafts were occluded in 5 patients (4.8%), 4 patients with 1 occluded and 1 patient with 3 occluded grafts. Of the 7 occluded grafts were 4 SVG, 1 RA and 2 LIMA. In all patients a further viability test confirmed no consequences of treatment because of the occluded grafts showing no pathology in stress/rest by ischemic testing or scars. Mean CTDIvol was 3.96±1.24 mGy, mean DLP was 130.6 ± 41.5 mGy cm mean amount of CM was 64.4±10.9 ml.

Conclusion:
Even if the study showed very good results of coronary revascularisation, it demonstrates the potential additional value of postoperative quality control in clinical routine before patient discharge by using latest CT imaging technology with amazingly ultralow radiation dose and volume of contrast agent.

3558

D. Inderbitzin[1], M. Taramasso[1], F. Maisano[1], F. Eckstein[2], O. Reuthebuch[2]

Magnetic Resonance Derived Blood-Flow Pattern after Off-Pump Aortic Valve Bypass Implantation

Department of Cardiac and Vascular Surgery, University Hospital Zurich, Zurich, Switzerland[1], Department of Cardiac Surgery, University Hospital Basel, Basel, Switzerland[2]

Introduction:
Off-pump aortic valve bypass (AVB) provides an extended surgical option in high-risk patients with aortic stenosis and perilous comorbidities when open or transcatheter valve replacement is contraindicated. We present a magnetic resonance based net flow pattern in the thoracic aorta, in the supra-aortic vessels as well as in the conduit after AVB.

Methods:
After off-pump AVB using the latest apico-aortic conduit in 12 patients (7 female, mean age 79.4 ± 5.8 years, mean logistic EuroSCORE 30.8 ± 28.6) 6 were alive at time of follow-up (day 904 ± 230). They were summoned to transthoracic echocardiographic (TTE) and magnetic resonance tomographic (MRI) screening. Left ventricular outflow-fractions via native and conduit valve, flow measurements in the proximal and distal AVB-conduit as well as at five different levels of the thoracic aorta (ascending aorta, proximal and distal to the left carotid artery and at level of AVB anastomosis) were analyzed. Levels of intra-aortic still-water-zones were evaluated.

Results:
Preoperative mean transvalvular gradient (dpmean) was 40.8 ± 10.4 mmHg, left ventricular ejection fraction (LVEF) 45 ± 11.9% and LV-massindex (LVMI) 195.5 ± 41.7. Postoperative dpmean of native valve decreased by 62.5 ± 8.5 %, LVMI by 22 ± 13% and LVEF increased by 7.4 ± 23%. Mean left ventricular outflow-fraction via conduit was 68.8 ± 6.3%. Ante-grade mean net flows were found in all patients at the level of the ascending aorta, the descending aorta distal to AVB insertion and in the conduit (n=6). Retrograde mean net flows were found in descending aorta proximal to AVB insertion (n=4), in aortic arch proximal to left subclavian artery (n=2) and distal to the brachiocephalic trunk (n=1). Partial retrograde perfusion was found in brachiocephalic trunk (n=1), left carotid artery (n=2) and left subclavian artery (n=4).

Conclusion:
Off-pump aortic valve bypass effectively relieves detrimental cardiac adaptions to severe aortic stenosis. Two-thirds of left ventricular outflow consistently pass the conduit, whereas antegrade and retrograde flow patterns in the analyzed segments are highly variable.

3559

D. Inderbitzin[1], D. Kalbermatten[3], M. Taramasso[1], F. Maisano[1], F. Eckstein[2], O. Reuthebuch[2]

Severe Impairment of Parasternal Skin Perfusion after Pediculized Compared to Skeletonized LIMA-Harvesting Measured by Transcutaneous Duplex Sonographic Flow Mapping

Department of Cardiac and Vascular Surgery, University Hospital Zurich, Zurich, Switzerland[1], Department of Cardiac Surgery, University Hospital Basel, Basel, Switzerland[2], Department of Plastic and Reconstructive Surgery, University Hospital Basel, Basel, Switzerland[3]

Introduction:
Impaired parasternal skin perfusion (PSSP) after left intern mammary artery (LIMA) harvesting in coronary arterial bypass surgery (CABG) reflects sternal hypo-perfusion with potential risk of surgical site infection (SSI). We present the impact of pediculized versus skeletonized LIMA-harvesting on PSSP by quantitative transcutaneous duplex sonographic flow mapping. (TDSFM).

Methods:
Bilateral TDSFM was performed before and after (postoperative day 5-7) CABG with LIMA-harvesting on 3 parasternal levels (manubrium (M), corpus (C), xyphoid (X)) at 2 cm from midline. Left-sided PSSP was evaluated as % of a right-sided PSSP reference (baseline-value). Data were prospectively collected and analyzed post-hoc.

Results:
5 patients received pediculized and 5 skeletonized LIMA-harvesting. Referring to the right-sided baseline, mean (± SD) pre- / postoperative left-sided PSSP was 92.6 ± 15.4/66.8 ± 6.4% (M), 95.6 ± 5.2/71.2 ± 5% (C) and 107 ± 13.8/76.4 ± 13.6% (X) after pediculized and 100 ± 3.4/100 ± 4.2% (M), 106 ± 14/99 ± 5.1% (C) and 106 ± 15.6/99.8 ± 5.2% (X) after skeletonized LIMA-harvesting. There was a significant difference between left-sided pre- and postoperative measures of 25.8%, 24.4% and 30.6% after pediculized LIMA-harvest on level M, C and X, respectively ($p = 0.043$ (M), $p = 0.043$ (C), $p = 0.043$ (X), by Wilcoxon matched-pairs signed-ranks test). Significant difference was absent after skeletonized LIMA-harvesting: 0%, 7% and 6.2% ($p > 0.05$ for all levels M, C and X, by Wilcoxon matched-pairs signed-ranks test). Mean pre- to postoperative PSSP decrease was 4.4% and 26.9% after skeletonized and pediculized LIMA-harvesting, respectively.

Conclusion:
A significant 26.9-% impairment on average in postoperative parasternal skin perfusion after pediculized compared to 4.4-% after skeletonized LIMA-harvest suggests to routinely consider skeletonized LIMA-harvesting especially in patients with increased risk for SSI. Further prospective randomized studies are needed to confirm this trend.

3560

U. Suessbier*[1], H. Wong*[1], A. Gomariz-Carillo[1], S. Isringhausen[1], T. Nagasawa[2], M. Manz[1], A. Müller[1], C. Nombela-Arrieta[1]

Destruction and recovery of the bone marrow microenvironment following myeloablative treatment

Hematology, University Hospital Zürich, Zurich [1], Immunobiology and Hematology, Kyoto University, Kyoto[2]

Introduction:
In adult individuals, the bone marrow (BM) is the primary site of continuous, lifelong production of blood cells. The BM microenvironment provides a critical regulatory milieu that is responsible for orchestrating the maintenance of hematopoietic stem and progenitor cells (HSPCs) and their differentiation into different hematopoietic lineages. Over the past decade it has become evident that beyond providing structural support, the vascular, mesenchymal and neural cells that form the non-hematopoietic stromal framework of the BM, function as master regulators of hematopoiesis and HSC homeostasis.
Hematopoietic cell transplantation after chemo/radiotherapy conditioning is the treatment of choice for various hematologic and non-hematologic malignancies. 5-fluorouracil (5-FU), an inhibitor of the thymidylate synthase and therefore DNA replication, is one of the most commonly used drugs for cancer treatment and for studies addressing the effect of myeloablative treatments. While the cytoreductive effects of irradiation and chemotherapy in hematopoietic cells are extensively described, the alterations induced by myeloablative therapies in the BM stromal scaffold remain underexplored.

Methods:
In our study we employ state of the art quantitative 3D microscopy techniques requiring whole mount immunostaining of thick slices of BM, tissue clearing protocols, confocal microscopy and computational tools, to visualize and quantify the structural rearrangements of the BM microenvironments in response to myeloablative treatments. Novel flow cytometric protocols enabling the study of stromal populations are additionally used to provide a comprehensive analysis of the quantitative and phenotypic effects of chemo/radiotherapies in mesenchymal and vascular populations.

Results:
As previously described, both lethal (950 cGy) and sublethal (475 cGy) doses of TBI induced a rapid and almost complete loss of HSPCs by day 4 post-irradiation. In mice subject to 5-FU treatment or sublethal TBI, HSPC numbers gradually started to recover by day 14. At early time points (day 3 and 4) loss of HSPCs correlated with distinct signs of destruction of the extracellular matrix and prominent vasodilation of BM sinusoidal vessels. By day 7-10, adipocytes appeared and gradually infiltrated the BM parenchyma and a complete loss of structural integrity of the mesenchymal stromal cell network was observed. Notably, the profound destructive effects derived from 5-FU treatment and sublethal TBI, were progressively reversed from day 14 post-treatment on through a remarkable regenerative process that culminated at day 60, when normal tissue microarchitecture integrity was fully regained.

Conclusion:
Our observations highlight the intrinsic regenerative and self-organizing capacity of BM tissues following 5-FU and non-myeloabative exposure.

3561

R. Romao[1], E. Tejera Puente[3], K. Nytko[4], U. Siler[2], C. Münz[1], R. Reichenbach[2]

Defective nuclear entry of hydrolases prevents NETosis in Chronic Granulomatous Disease

Viral Immunobiology, Institute of Experimental Immunology, University of Zurich, Zürich[1], Division of Immunology, University Children's Hospital Zurich and Children's Research Center, Zürich[2], Current affiliation: Molecular, Cellular and Developmental Neurobiology, Instituto Cajal, CSIC, Madrid[3], Current affiliation: Laboratory for Molecular Radiobiology, Department of Radiation Oncology, University Hospital Zürich, Zürich[4]

Introduction:
Neutrophils can trap pathogens in their released DNA in a process called NETosis. Apart from NADPH oxidase-dependent formation of reactive oxygen species (ROS), triggering NETosis, and from neutrophil elastase (NE) translocation into the nucleus for DNA decondensation, little is known about the mechanism of NETosis. We have previously shown that NETosis is absent in NADPH oxidase-deficient chronic granulomatous disease (CGD) patients. Macroautophagy is a cytoplasmic degradation pathway reshaping cellular membrane compartments and was recently suggested to contribute to NETosis. The mechanism responsible for defective NETosis in CGD is unclear and it is unknown if this deficiency is linked to a potential role of macroautophagy in NETosis.

Methods:
NETosis was induced by PMA or Candida together with classical macroautophagy modulators in human control and CGD neutrophils. NE translocation was followed immunohistochemically. Nuclear NE catalytic activity was analysed by histone degradation assay.

Results:
We demonstrate that NE accumulates in the perinuclear region in CGD neutrophils, but does not gain access to the nucleus. Absent NE nuclear access prevents histone 4 degradation and nuclear DNA decondensation for NETosis. Phosphatidylinositol-3 (PI3) kinase inhibitors, which block macroautophagy, had the same effects on NETosis, but at the same time reduced ROS formation, while only minimally affecting macroautophagy in human neutrophils.

Conclusion:
These findings suggest that the PI3-kinase dependency of NETosis mainly reflects PI3-phosphate involvement in NADPH oxidase-dependent ROS production, which permits access of NE to the nucleus for DNA decondensation and NETosis. We conclude that macroautophagy is intact and does not account for deficient NETosis in CGD.

3562

A. Rafiei[1], Y. Saito[2], M. Bühler[3], D. Soldini[3], M. Manz[1]

Establishment of a Langerhans Cell Histiocytosis Model in Humanized Mice

Division of Hematology, University and University Hospital Zurich, Switzerland[1], Division of Biochemistry and Molecular Biology, Kobe University of Graduate School of Medicine, Japan [2], Department of Pathology, University Hospital Zurich, Switzerland[3]

Introduction:
Langerhans cell histiocytosis (LCH) is the most common histiocytic disease in humans with a complex pathophysiology and unknown etiology. LCH has been recently reclassified from an inflammatory disease to a neoplastic disorder due to the high prevalence of BRAFV600E mutations. In recent studies we found that the expression of BRAFV600E in distinct hematopoietic compartments defines the stage and the clinical risk in LCH disease; Whereas the expression of BRAFV600E in differentiated dendritic cells (DC) resembled low risk disease, the expression of this mutant in DC precursors was associated with high risk disease (Berres et al. J Exp Med 2014). The aim of this study is to model LCH in a xenograft system and identify the blood-borne LCH-initiating cells. We recently generated MISTRG mice that express multiple human myeloid cytokines, supporting human myeloid cell development (Rongvaux et al. Nat Biotech 2014). Thus, these mice might also be suitable for the development and support of myeloid neoplasia and are used for the experiments.

Methods:
Human $CD34^+$ hematopoietic stem and progenitor cells (HSPCs) obtained from healthy donor cord blood samples were lentivirally transduced using a bidirectional promoter vector harboring BRAFV600E and GFP in the presence of supportive growth factors. For colony forming unit (CFU) assay $CD34^+$ cells were plated in M4230 medium in the presence of supportive growth factors and scored microscopically after 14 days for colony formation. The In vivo experiments were performed by the injection of transduced $CD34^+$ intrahepatically into newborn and adult MISTRG mice, which were sublethally irradiated previous to transplantation. Mice were analyzed subsequently for investigating the development of LCH-like disease.

Results:
We observed that mice transplanted with human $CD34^+$ HSPCs expressing BRAFV600E suffer from anemia and reduced WBC counts. BRAFV60E could be observed in different organs using immunohistochemistry staining. Further analysis of lymphoid and non-lymphoid organs demonstrated the accumulation of ''atypical'' dendritic cells expressing CD68, CD1a and CD207 markers, which were negative for CD20, the marker for hairy cell leukemia.

Conclusion:
Our results indicate that overexpression of BRAFV600E in $CD34^+$ HSPCs induce an aggressive histiocytosis disease in MISTRG mice with the ability to spread to lymphoid and non-lymphoid organs. Further characterization of the disease-associated cells will clarify the role of MAPK pathway on the differentiation potential of hematopoietic stem and progenitor cells and the effect of these cells on the pathogenesis of histiocytosis diseases. Our ongoing investigations aim to increase our understanding of the pathophysiology of histiocytic diseases, possibly leading to novel diagnostic and therapeutic strategies for patients.

3563

M. Schneider[1], D. Eshmuminov[1], R. Vonlanthen[1], P. Gertsch[1], K. Lehmann[1]

Survival and Patterns of Recurrence after Cytoreductive Surgery (CRS) and Hyperthermic Intraperitoneal Chemotherapy (HIPEC) for colorectal and appendicular peritoneal malignancy – results of a 5-year monocentric experience

Department of Visceral and Transplantation Surgery, University Hospital Zürich, Zürich[1]

Introduction:
Cytoreductive Surgery (CRS) and hyperthermic intraperitoneal chemotherapy (HIPEC) is a treatment option for well-selected patients with peritoneal carcinomatosis (PC). Despite an increasing number of centers, survival data from Switzerland is scarce.

Methods:
Data of 113 patients with colorectal or appendicular carcinomatosis treated from 2009 to 2014 at the university hospital of Zurich were prospectively collected and analyzed. Patients with malignant disease were selected (extent of PC, no extra-abdominal disease, performance status), and received standard perioperative chemotherapy. Patients with low-grade appendix tumors were directly operated. HIPEC was indicated after successful cytoreduction (CC-score 0, no visible tumor). Follow-up included a clinical exam, tumor markers and CT scan every six months.

Results:
Patients had carcinomatosis from appendix tumors in 63% (71/113), including low-grade (31/71) and high-grade (40/71) tumors, and colorectal cancer in 37% (42/113). Curative surgery was possible in 67% of patients, major morbidity and mortality were 8.1% and 2%, and median follow-up was 24 months. For colorectal PC, median overall (mOS) and disease free (DFS) survival were 40 and 12 months, and 3-year survival was 66% for patients with complete resection versus 17% for incompletely resected carcinomas. For low-grade appendix tumors, OS and DFS were 100% and 71% at 5y. For high-grade appendix tumors mOS was 44 months and DFS was 19 months. 32% were disease free and 37% alive at 5 years. Signet ring differentiation was a highly negative prognostic factor on survival for colorectal and appendix tumors ($p<0.001$).

Conclusion:
Outcomes after curative CRS/HIPEC are excellent for appendix tumors, and a majority of well-selected patients with PC from colorectal cancer have a survival benefit. Patients with signet ring differentiation have worse outcomes.

3564

L. Kovtonyuk[1], R. Ramin[1], H. Takizawa[1], M. Manz[1]

Aging-associated intrinsic and extrinsic factors control hematopoietic stem cell behavior

Division of Hematology, University Hospital and University of Zurich, Zurich, Switzerland[1]

Introduction:
Lifelong continuous blood production is sustained through stepwise differentiation program by a very limited number of self-renewing hematopoietic stem cells (HSCs) in bone marrow (BM). Hematopoietic cell development needs to be tightly controlled by both cell intrinsic and extrinsic factors, as its dysregulation potentially leads to neoplasia or aplasia. Upon aging, HSCs increase in number, reduce self-renewal capacity on per cell basis, skew towards myeloid differentiation, and show less efficient bone marrow (BM)–homing ability. Recently, we have demonstrated that at any given time young adult HSCs consist of actively cycling and dormant pools, and that aged HSCs tend to be dormant in a permissive environment, suggesting that a cell-intrinsic drive towards quiescence is imprinted on HSCs through increased proliferative history. Here we tackle the questions how extrinsic and intrinsic factors determine HSC behaviour and what their molecular signature and relative contribution are in HSC cell fate decision.

Methods:
We have established in vivo single HSC divisional tracking with CFSE (5(6)-carboxyfluorescein diacetate N-succinimidyl ester), and subsequent isolation of different divisional classes of HSC-containing cell fractions (LKS) based on CFSE dilution for in vivo HSC functional readout. CFSE-labeled young (8-12 week old), aged (>2 year old) and experimentally aged LKS were transferred into non-irradiated young or aged recipients, respectively. To test biological function of HSC with distinct divisional histories, quiescent (0-divided at 8 weeks) or cycling (>5-divided at 8 weeks) LKS were isolated and transplanted into lethally irradiated mice. The transplanted mice were monthly bled to follow long-term donor engraftment and lineage repopulation. To dissect aging-associated extrinsic factors, we performed antibody based protein arrays and transcriptome analysis with total BM of young versus aged animals, and bioinformatical analysis. The effect of identified candidates on HSC behavior was further tested in vivo by employing CFSE assay.

Results:
BM analysis at 8 weeks after tracking showed that young LKS proliferated faster than old LKS, while both young and aged LKS appear to be more dormant in an old environment. This indicates increased intrinsic and extrinsic drive towards quiescence during ageing. Young HSC, irrespective of environment and cycling activity, demonstrated balanced lineage repopulation. Dormant aged HSCs favor myelopoiesis independent of the environment. In contrast, cycling aged HSCs that had been exposed to a young environment showed balanced lineage repopulation as do young HSCs, indicating that the young external factors can modulate aging-associated lineage skewing in a cell cycle dependent manner. Similar biology as in aged HSCs was observed in HSCs with extensive divisions during serial transplantation. Expression levels of some inflammatory cytokines and myeloid differentiation factors were altered in aged BM. These factors drive young HSC towards proliferation and differentiation, while this effect is limited on aged HSCs, due to their increased quiescent state.

Conclusion:
These findings demonstrate that HSC proliferation and differentiation are controlled by cell-intrinsic and -extrinsic factors: extensive proliferative history imprints a quiescence program on HSCs that is associated with myeloid-biased differentiation; lineage skewing of HSC during aging can be modulated via environmental cues. This indicates a possibility for rejuvenation therapies.

3566

N. Parrinello[1], M. Balabanov[1], C. Nombela-Arrieta[1], S. Isringhausen[1], S. Balabanov[1]

Systems biology analysis of eIF5A function in eukaryotic cells

Department of Hematology, Universitätsspital, Zürich[1]

Introduction:
The eukaryotic initiation factor 5A (eIF5A) is emerging as a crucial regulator in cancer, infections and inflammation. Although its function in translational regulation has been sufficiently demonstrated, mostly in bacteria and low eukaryotes, its biological role and its contribution at gene expression level in higher eukaryotes remains poorly understood.

Methods:
To investigate the biological role of eIF5A in eukaryotic cells, we established an IPTG-inducible lentiviral eIF5A shRNA vector system in murine fibroblasts (NIH3T3) that allowed us to tightly regulate the expression of our protein of interest and obtain an eIF5A deficient cell culture model. Moreover, we overexpressed exogenous eIF5A and the isoform eIF5A2.

Results:
Successful knockdown of eIF5A expression affects cell proliferation in NIH3T3 cells after 6 days post-IPTG treatment and we could observe a significant increase of apoptosis in those cells compared to the control. As expected, polysome profile analysis revealed that loss of eIF5A leads to a defect in the elongation step of translation 4 days post-IPTG treatment. Furthermore, protein synthesis rate in eIF5A-deficient cells significantly decreased compared to the control at 2 and 4 days post-IPTG treatment, respectively.
In order to investigate candidates and pathways that are directly or indirectly regulated by eIF5A, we conducted a RNA-Seq analysis combined with sensitive proteomics approach of our model system, using different setting of data (transcriptome, polysomal RNA, proteome day 4 and day 6). The number of genes differentially regulated in the transcriptome was 437, with more than half upregulated; in the polysomal RNA there were 1354 differentially regulated genes, most of which were upregulated. The number of proteins differentially regulated at day 4 and 6 was 185 and 474, respectively. Only 14 genes were common between the four settings of data, the general trend of the differentially identified genes was heterogeneous molecular layer regulation. Comprehensive bioinformatics analysis of the generated data by algorithms and analytical tools unveiled that four pathways (inflammation and ECM) were common to the different settings of data considered in our study.
eIF5A is known to promote translation of polyproline motifs in yeast. To investigate whether in high eukaryotes there is a similar role for eIF5A in translation, we checked the content of polyproline motifs in our settings of data. Surprisingly, we could observe that the genes with more than 15 prolines in their sequence were affected, with an accumulation at polysome compartment, different scenario than the yeast translations.
Moreover, we examined whether exogenous expression of eIF5A and eIF5A2, isoform expressed only in certain tissues and cancer, can compensate for the loss of endogenous eIF5A, by overexpressing both isoforms in our model system. Interestingly, we could observe that exogenous eIF5A and eIF5A2 overexpression shown to: compensate for the endogenous eIF5A knockdown rescuing the cell growth, for the elongation defect in eIF5A depleted cells, at translation level and restore the protein synthesis comparable to the control levels.

Conclusion:
Our results provide a genome wide characterization of biological function of eIF5A in mammalian cells. Furthermore, bioinformatics analysis revealed inflammation and ECM signaling pathway activation in absence of eIF5A, and for the first time, we show that eIF5A is required for the elongation of long proline stretches in higher eukaryotes.

3567

N. Scherrer[1], Y. Devaux[2], F. Fays[3], O. Collignon[3], B. Mueller[4], A. Luft[1], M. Christ-Crain[5], M. Katan[1]

MicroRNA-150 Adds Prognostic Information After Acute Ischemic Stroke

Dep. of Neurology, University Hospital of Zurich, Switzerland[1], Dep. of Population Health, Luxembourg Institute of Health, Luxembourg[2], Competence Center in Methodology and Statistics, Luxembourg Institute of Health, Luxembourg[3], Medical University Clinic, Cantonal Hospital Aarau, Switzerland[4], Dep. of Endocrinology, University Hospital of Basel, Switzerland[5]

Introduction:
MicroRNAs (miRNAs) are involved in post-transcriptional gene regulation influencing disease progression and prognosis. MiR-150 regulates proinflammatory cytokines, mediators of cellular communication in the ischemic brain, as well as vessel integrity. We aimed at evaluating the incremental prognostic value of miR-150 after ischemic stroke.

Methods:
In a prospectively enrolled ischemic stroke cohort , levels of miR-150 were measured within 72 hours of symptom onset in 272 patients. The primary endpoint was functional outcome (modified Rankin Scale score <3 or 3–6), the secondary endpoint was mortality within 90 days. Logistic regression and cox proportional hazards models were fitted to estimate odds ratios (OR), respectively hazard ratios (HR) and 95% confidence intervals (CI) for the association between miR-150 and the primary and secondary endpoints. The discriminatory accuracy was assessed with the area under the receiver-operating-characteristic curve (AUC) and the incremental prognostic value was estimated with the net reclassification index (NRI).

Results:
After adjusting for demographic and vascular risk factors, lower miR-150 levels were independently associated with mortality (HR 0.16 [95% CI, 0.06–0.44], $p<0.001$) but not functional outcome (OR 1.33 [95% CI, 0.57–3.07], $p = 0.51$). Adding miR-150 to the multivariate model modestly improved the AUC from 0.89 [95% CI, 0.84–0.93] to 0.90 [95% CI, 0.85–0.95], likelihood ratio test -*p-value*<0.01), and resulted in a NRI of 26.3% ($p<0.0001$).

Conclusion:
In patients with ischemic stroke, miR-150 is a novel prognostic biomarker, improving risk classification beyond traditional risk factors.

3568

J. Steiger[1], E. Cambria[1], J. Günter, P. Wolint[1], A. Bopp[1], S. Hoerstrup[1], M. Emmert[1]

Generation of therapeutic multi-cellular three dimensional (3D) microtissues (MTs) for cardiac regeneration: Evaluation of the in vitro microenvironment of co-culture MTs

Swiss Center for Regenerative Medicine and Department of Surgical Research, University of Zurich, Zurich, Switzerland[1]

Introduction:
The highly-organized microenvironment in threedimensional (3D) stem cell-based microtissues (MTs) fills the gap between in vivo and *in vitro* applications and might be therapeutically beneficial for cardiac regeneration in the future. The regenerative properties of 3D MTs are comprised of the secretion of anti-inflammatory and angiogenic mediators, the so called paracrine effects, which may initiate cardiomyocyte survival, neoangiogenesis, stem cell engraftment, and possibly the recruitment of endogenous cardiac stem cells to the diseased area. In this ongoing project we investigate and characterize the *in vitro* generated stem cell-based 3D MTs formed by two different, complementary human stem cell sources to assess the principal feasibility of different patterns of co-culture and the impact on the extracellular matrix (ECM) microenvironment.

Methods:
3D MTs were generated from human adipose tissue-derived mesenchymal stem cells (hADSCs) and human endothelial colony forming cells (hECFCs) using a modified hanging-drop method. Cells were co-cultured in different ratios and seeding patterns to form uniform co-culture spheroids, containing 2000 cells per MT. 3D MT formation was directly seized under the microscope and by histology. Cell type location within the MTs was determined by cell membrane staining with either the cell tracker fluorescence probe CMFDA or CM-DiI, followed by DAPI staining and fluorescence microscopy. An alamar blue assay was performed to study the viability of co-culture and control MTs compared to 2D cell culture. To obtain tubular network formation, which gives insight into the potential angiogenic activity of hECFCs, a matrigel assay was performed.

Results:
Both hADSCs and hECFCs displayed the capacity to form 3D MTs in co-culture after 3 days of hanging drop culture under different formation conditions. Bulk formation of hADSCs and hECFCs into 3D MTs was already visible after 48h. 3D MTs have shown to be viable, holistic and showed intact micro-architecture. Morphological assessment via histology and fluorescence microscopy verified a compact and uniform cell formation of co-culture MTs. hECFCs exhibited tube formation activity in the matrigel, showing angiogenic potential.

Conclusion:
The *in vitro* generation and investigation of 3D MTs employing clinically-relevant human stem cell sources can be successfully achieved in hanging drop cell culture. Supported by successful *in vitro* assessment, these results facilitate further investigations towards a promising application-format for stem cell-based therapies for cardiac regeneration in the future. Further investigations of this project will comprise the impact of different patterns of 3D co-culture on the ECM microenvironment of therapeutic MTs, a secretome assay, followed by *in vivo* monitoring as well as post-mortem analysis of 3D MTs utilizing a murine infarction model.

3570

M. Kirschner[1], B. Vrugt[2], M. Friess[1], M. Meerang[1], P. Wild[2], N. Van Zandwijk[3], G. Reid[3], W. Weder[1], I. Schmitt-Opitz[1]

Evaluation of the novel prognostic miR-Score in a cohort of multimodality treated malignant pleural mesothelioma patients

Thoracic Surgery, University Hospital Zürich[1], Pathology, Institute of Surgical Pathology, University Hospital Zurich[2], Asbestos Diseases Research Institute, Sydney, Australia[3]

Introduction:
In a recent study, we have identified several microRNAs which expression in surgical specimes was found to be associated with survival outcomes following surgical intervention in patients with malignant pleural mesothelioma (MPM). A combination of six of these microRNAs, termed the miR-Score, provided the best predictive accuracy for identifying patients with a survival of >20 months following surgery. The purpose of the current study is to further evaluate these microRNAs in an independent cohort of both surgical and diagnostic tumor specimens obtained from multimodality treated MPM patients.

Methods:
We identified a cohort of 140 MPM patients who have undergone chemotherapy followed by extrapleural pneumonectomy (EPP) between 1999 and 2014 at the University Hospital Zurich. At present a subset of 30 EPP (chemo-treated) and 15 matching diagnostic (chemo-naïve) specimens is available for microRNA analysis. From these RNA was isolated on microdissected tumor tissue, and this RNA was then subjected to microRNA specific RT-QPCR for the six microRNAs of the miR-Score. Kaplan-Meier log rank analysis was performed to determine association of the microRNAs with survival. Related-samples Wilcoxon Signed Rank Test was employed to determine possible differences in microRNA expression between diagnostic and surgical specimens.

Results:
Of the 30 initial EPP specimens, 25 passed quality control (QC) and were included in subsequent analyses. All diagnostic specimens passed QC, resulting in 13 matched pairs of diagnostic and surgical specimens. For 5 of the 6 signature microRNAs Kaplan-Meier analysis in the EPP specimens showed comparable results to the previously published data. However, we surprisingly found that the microRNA previously most associated with prolonged survival, miR-21, did not reach statistical significance in the current subset ($p=0.764$). As expected based on the result from the individual microRNAs, the combined miR-Score was in both EPP and diagnostic specimens not significantly associated with survival in this subset of patients. To evaluate if chemotherapy might affect microRNA levels, we compared expression before and after chemotherapy in 13 matched sample pairs. While this analysis did not show significant differences between pre- and post-chemotherapy tissue for any of the microRNAs, on a sample-by-sample investigation, we observed in particular for miR-21 subtle reductions in expression levels after chemotherapy. For all other microRNAs, while individual samples did show strong differences between pre- and post-chemo expression, no conclusive trend regarding effect of chemotherapy could be observed.

Conclusion:
Preliminary data from an independent series of chemo-naïve and chemo-treated specimens show that while for the majority of investigated microRNAs associations with survival can be validated, a subset of microRNAs may indeed be affected by chemotherapy. If this observation is confirmed in a larger series of samples, the miR-Score may require further adjustment to take this effect of chemotherapy into account, and this is subject of ongoing investigations.

3571

M. Meerang[1], B. Karima[1], E. Felley-Bosco[2], O. Lauk[1], B. Vrugt[3], A. Boss[4], A. Broggini-Tenzer[6], D. Kenkel[4], R. Stahel[5], S. Arni[1], W. Weder[1], I. Schmitt-Opitz[1]

Antagonizing the Hedgehog Pathway with Vismodegib Impairs Malignant Pleural Mesothelioma Growth In Vivo by Affecting Stroma

Thoracic Surgery, University Hospital Zürich[1], Molecular Oncology, Clinic of Oncology, University Hospital Zurich, Switzerland[2], Surgical Pathology, University Hospital, Zurich[3], Institute of Diagnostic and Interventional Radiology, University Hospital Zurich[4], Oncology, University Hospital Zurich[5], Laboratory for Molecular Radiobiology, Radiation Oncology, University Hospital Zurich[6]

Introduction:
Upregulation of the Hedgehog (Hh) signaling pathway is associated with poor prognosis of malignant pleural mesothelioma (MPM) patients. An autocrine driven upregulation of the Hh pathway was described in MPM, in which the ligand, desert hedgehog (DHH), was produced from tumor cells. Paracrine activation of Hh signaling has been described in other solid tumors and our recent investigation revealed that the Hh pathway was activated in both tumor and stroma of human MPM specimens. In this study, we investigated the importance of paracrine Hh signaling in MPM progression in vivo.

Methods:
We employed an orthotopic immunocompetent rat MPM model. Sarcomatoid rat MPM cells transfected with luciferase (IL45-luc) were implanted subpleurally in Fischer rats. After tumors were formed, rats were treated orally with a FDA approved Hh antagonist, vismodegib, (once daily, 100 mg/kg; n=6) for 6 days while control group (n=6) received vehicle alone. Tumor load was monitored by bioluminescence, magnetic resonance imaging (MRI) and macroscopically. Tumors were harvested and evaluated for Hh target genes expression by quantitative real time PCR and immunohistochemistry. Tumor cells were isolated and cultured in medium without serum at 37°C, 5%CO_2 and 3%O_2. Tumor cell culture supernatant was collected freshly and applied to confluent mouse embryonic fibroblasts (NIH3T3). The expression of Hh pathway target genes in NIH3T3 cells were analysed at 72h afterwards by quantitative real time PCR.

Results:
Similar to that observed in human MPM specimens, positive immunohistochemical staining of Hh pathway components, Glioma associated oncogene 1 (GLI1) and Patched1 (PTCH1), were detected in both tumor and stromal fractions of the rat MPM model. Hh ligand, DHH, was predominantly expressed in the tumor fractions. Daily treatment with vismodegib in vivo efficiently downregulated Hh target genes, Gli1, Hedgehog Interacting Protein (Hhip) and Ptch1, and caused a significant reduction of tumor volume, and tumor growth delay. Tumor cell proliferation, Ki-67 and phospho-histoneH3 positive indices, were significantly reduced in the treated group. Immunohistochemical analyses revealed that vismodegib treatment primarily down regulated Hh target genes, GLI1 and HHIP, in the stromal compartment along with a reduced expression of previously described fibroblast Hh responsive genes such as Fibronectin (Fn1) and vascular endothelial growth factor (Vegf). Primary cells isolated from the rat tumors cultured in physiological O_2 level (3%) continued to express Dhh but did not respond to vismodegib treatment in vitro. However, culture supernatant from these cells stimulated Gli1, Ptch1, and Fn1 expression in mouse fibroblasts NIH3T3 which was suppressed by vismodegib treatment.

Conclusion:
MPM cells expressed ligand and induced Hh response in fibroblasts, implying the role of paracrine Hh signaling in MPM. Hh pathway activated fibroblasts in turn produced growth factors important for tumor progression. Hh pathway antagonization in MPM stroma efficiently delayed tumor cell growth, emphasizing the importance of Hh pathway as a treatment target for MPM. In addition, our study highlights the significant aspect of tumor-stroma crosstalk in promoting MPM progression.

3572

M. Meerang[1], B. Karima[1], M. Friess[1], B. Bitanihirwe[1], A. Soltermann[2], B. Vrugt[2], E. Felley-Bosco[5], R. Bueno[3], W. Richards[4], B. Seifert[4], R. Stahel[5], W. Weder[1], I. Schmitt-Opitz[1]

Low Merlin Expression and High Survivin Staining Index are Indicators for Poor Prognosis of Malignant Pleural Mesothelioma Patients

Thoracic Surgery, University Hospital Zürich[1], Surgical Pathology, University Hospital, Zurich[2], Thoracic Surgery, Harvard Medical Scool, Birgham and Woman's Hospital, Boston [3], Department of Biostatistics, Epidemiology, Biostatistics and Prevention Unit, University Zurich, Zurich[4], Laboratory of Molecular Oncology, University Hospital Zurich[5]

Introduction:
Alterations of the tumor suppressor Neurofibromatosis type II (NF2) have been reported in about 40% of Malignant pleural mesothelioma (MPM) patients. NF2 (Merlin) deficiency leads to alterations of the Hippo pathway; resulting in activation of the oncogenic Yes Associated Protein-1 (YAP1). Our aim was to investigate the association between these alterations and clinical outcomes.

Methods:
Tissue microarrays comprised of MPM tumors derived from 2 independent MPM cohorts were employed for this study. The expression of Merlin, YAP1 and its target genes, Survivin and connective tissue growth factor (CTGF) were assessed in both nuclear and cytoplasmic fractions. Cohort 1 was comprised of 145 patients intended to be treated with chemotherapy (CTX) followed by extrapleural pneumonectomy (EPP), thus both pre- and post-CTX tissues were available. Cohort 2 was comprised of 59 patients treated with EPP followed by intraoperative hyperthermic cisplatin and/or adjuvant CTX and/or radiotherapy. Marker expression was quantified by means of labeling index (%) for nuclear Survivin and by H-score for the other markers. The dichotomized marker expression was tested for the association with overall survival (OS) and progression free survival (PFS).

Results:
Kaplan-Meier survival curves revealed a significant association between low cytoplasmic Merlin expression in pre-induction CTX tissues of cohort 1 with shorter PFS (p=0.02) and OS (p=0.03). The same tendency was observed in the chemotherapy naïve tissues obtained during EPP of cohort 2. Low nuclear Merlin expression in post-CTX tissues (available from cohort 1 only) was associated with short PFS (p=0.04) and OS (p=0.05). High nuclear Survivin labeling indices in both pre- and post-CTX tissues of cohort 1 was associated with shorter PFS (p=0.02). In cohort 2, this was associated with both PFS and OS (p=0.046 and p=0.002, respectively). In multivariate analysis, low expression of cytoplasmic Merlin remained an independent prognosticator for short PFS of cohort 1 [HR (95% CI): 0.5 (0.3-0.9); p=0.001] and OS [HR (95% CI): 0.5 (0.3-1); p=0.04]. High Survivin labeling index was an independent prognostic factor for short PFS in patients from cohort 1 [HR (95% CI): 3.4 (1.7-6.8); p=0.006] and short OS in patients from cohort 2 [HR (95% CI): 2.35 (1.27-4.33); p=0.006].

Conclusion:
Our findings uncover the significance of Merlin protein expression and Survivin labeling index as prognosticators for poor clinical outcome in two independent MPM cohorts. If confirmed, these markers may be used to identify subgroups of patients benefitting from additional treatment.

3573

J. Jang[1], F. Janker[1], S. Arni[1], Y. Yamada[1], I. Gil-Bazo[2], I. De Meester[3], W. Weder[1], W. Jungraithmayr[1]

Suppression of lung cancer in mice by the CD26/DPP4 inhibitor Vildagliptin

Division of Thoracic Surgery, University Hospital Zurich[1], Oncology, Clinica Universidad de Nevarra, Pamplona/Spain[2], Medical Biochemistry, University of Antwerp, Antwerp/Belgium[3]

Introduction:
Lung cancer is the most prominent cause of death among cancers, accounting for 1.59 million deaths worldwide. In spite of improved treatment in surgery, chemo- and radiation therapy, the five year survival is poor. CD26/DPP4 (dipeptidyl peptidase 4) is a transmembrane glycoprotein, that is constitutively expressed on most of hematopoetic cells, also found on lung epithelial and endothelial cell surfaces. In our previous works, we found that the activity of CD26/DPP4 of lung cancer patients was 4 times higher than normal tissue from same patients (n=38) and we could show previously that the CD26/DPP4 inhibitor Vildagliptin has anti-tumor properties against lung metastases in mice. Recently it has been shown that the inhibition of CD26/DPP4 increases surfactant protein (SP) which acts pro-inflammatory via the activation of macrophages and natural killer (NK) cells. Here, we tested if pharmacological CD26/DPP4 inhibitor (Vildagliptin) regulates lung cancer growth in mice.

Methods:
An orthotopic tumor model was employed by sc. injections of mouse lung cancer cell line (Lewis Lung Carcinoma [LLC]) and human lung adenocarcinoma cell line (H460). These tumors were developed syngeneically (C57BL6: n=18) or xenogeneically (CD1-nude: n=20). Tumor growth was evaluated by wet weight of tumor mass at 4 weeks. Vildagliptin was given in drinking water of 50mg/kg day dose. Histological assessment included HE, TUNEL, immunohistochemistry (IHC) of CD31, Ki67, pH3, CD3, CD4, CD8, and F4/80. The expressions of SP and Nkp46 were detected by western blotting. TNF-alpha was measured by ELISA. In vitro, surfactant (Curosurf) was given on macrophage cell line (Raw 267.4) for measuring the activation marker of macrophage TNF-alpha.

Results:
Vildagliptin treatment significantly reduced the size of tumor developed by lung cancer cell line injection. Beside tumor weight, there was no difference in HE, TUNEL, and IHCs of CD31, CD3, CD4, and CD8, while Vildagliptin treatment decreased Ki67-pH3 ratio and increased the population of F4/80 positive macrophages. The activation marker of macrophage (TNF-alpha) and NK cell marker (Nkp46) were expressed higher in Vildagliptin treated tumors. In vitro, we confirmed significantly enhanced SP expression in lung cancer cell lines by Vildagliptin treatment and TNF-alpha expression in surfactant treated macrophage cell line.

Conclusion:
The Inhibition of CD26/DPP4 by Vildagliptin decreased lung cancer growth in models of mouse and human lung cancer cell lines and increased inflammatory macrophages and NK cells within the tumors. The increased expression of SP by Vildagliptin treatment in lung cancer cell lines suggests that surfactant production in lung cancer might activate macrophages to fight against lung cancer.

3574

I. Schmitt-Opitz[1], O. Lauk[1], M. Meerang[1], M. Friess[1], M. Kirschner[1], G. Wuilleret[1], C. Bommeli[1], A. Jetter[2], B. Aeschlimann[3], D. Günther[3], R. Stahel[4], W. Weder[1]

Intracavitary Cisplatin-Fibrin Application following Resection of Mesothelioma

Division of Thoracic Surgery, University Hospital Zurich[1], Department of Clinical Pharmacology and Toxicology, University Hospital Zurich[2], Department of Chemistry and Applied Biosciences and Laboratory of Inorganic Chemistry, ETH Zurich[3], Laboratory of Molecular Oncology, University Hospital Zurich, Zurich[4]

Introduction:
Early local tumor relapse is very common after resection of malignant pleural mesothelioma (MPM). Intracavitary chemotherapy after tumor resection is a possible approach to improve local tumor control. Here, we present the results (extended) pleurectomy/decortication ((e)P/D) followed by intracavitary cisplatin-fibrin application MPM patients.

Methods:
Twelve patients (75% IMIG stage III + IV) with a median age of 65 years underwent intracavitary cisplatin –fibrin application after (e)P/D at 4 different dose levels of cisplatin (11, 22, 33 and 44mg/m^2). Eight patients were previously treated with intravenous cisplatin/pemetrexed (100 mg/m^2).
To evaluate cisplatin concentration in serum and tissue, blood was taken at several time points. Tissue sampling was conducted before and at 90 minutes after the administration. Cisplatin levels were measured by inductively coupled plasma sector field mass spectrometry.
Besides adverse and serious adverse events, hematological and renal toxicity were measured before and at day 1, 2, 3, 4, 5, 7, 10 and 14 as well as 4 weeks and 2 months after treatment. Toxicity levels were assessed using CTCAE grading.
Quality of life was assessed with the SF36v2 questionnaire before and at 4 weeks, 2, 4, 8 and 12 months after application. Posttreatment physical component summary (PCS) score and mental component summary (MCS) score were compared to the pre-treatment values using the Wilcoxon signed rank test.

Results:
No dose limiting toxicity due to cisplatin was observed. Major morbidity was observed in 4 patients (33%). 30day- and 90day-mortality was 0%. Hemoglobin values dropped to a maximum low after 1 to 5 days, returned in nearly all cases to preoperative level and were primarily grade III anemias related to blood loss during surgery. Creatinine levels never exceeded CTCAE grade III in all but 1 patient who suffered from postoperative hypovolemic shock.
Serum cisplatin kinetics and $AUC_{0\text{-}120}$ are depicted in figure 1. Induction intravenous chemotherapy contributed to >50% of total serum cisplatin levels compared to cisplatin-fibrin (fig. 1A). The median $AUC_{0\text{-}24}$ in the highest dose level group including predoses from induction chemotherapy reached 23 h*µg/g, which is still below the suggested renal toxicity risk level, 25 h*µg/g [Royer 2008]. Serum cisplatin AUC levels also stayed far below levels reported after intrapleural perfusion. Local cisplatin concentration in tissues at 90 minutes varied from 12-133 (median: 36.5 µg/g). Serial chest wall biopsies of 2 patients revealed the presence of cisplatin at day 74 and 204 after application (fig. 1B).
PCS score was significantly decreased 4 weeks (p=0.008), 2 months (p=0.004) and 4 months (p=0.04) after treatment compared to the pretreatment value but returned to baseline values at 8 and 12 months after application. The MCS score was at all time points not significantly different from pretreatment evaluation. The median follow-up after surgery was 17 months (range 11 – 36 months).
Median freedom from recurrence (FFR) was 8 months (95% confidence interval (CI): 4-12 months). Median overall survival was 21 months (95% CI: 14-28).

Conclusion:
The administration of intracavitary cisplatin-fibrin as high as 44mg/m^{2}BSA is safe after (e)P/D, also in combination with induction chemotherapy. Tissue cisplatin concentration was high whereas no dose limiting toxicity due to systemic distribution was detected. A confirmation of the safety and efficacy of the highest dosage, 44 mg/m^{2}BSA, in a phase II trial is ongoing.

3575

I. Schmitt-Opitz[1], M. Friess[1], O. Lauk[1], T. Fraunfelder[3], T. Nguyen-Kim[3], I. Inci[1], S. Hillinger[1], D. Schneiter[1], B. Seifert[4], R. Stahel[2], W. Weder[1]

A new prognostic score for treatment allocation for multimodality therapy for malignant pleural mesothelioma - an update

Division of Thoracic Surgery, University Hospital Zurich[1], Laboratory of Molecular Oncology, University Hospital Zurich, Zurich[2], Institute of diagnostic and interventional Radiology, University Hospital Zurich[3], Department of Biostatistics, Epidemiology, Biostatistics and Prevention Unit, University Zurich[4]

Introduction:
We developed a Multimodality Prognostic Score (MMPS) in our patient cohort receiving induction chemotherapy followed by extrapleural pneumonectomy (EPP) or pleurectomy/decortication (P/D) to facilitate the decision for surgery after induction chemotherapy.

Methods:
A 4 variable MMPS was developed including pre-chemotherapy tumor volume (> 500ml), progressive disease (PD) after induction chemotherapy (according to modified RECIST criteria), pre-chemotherapy CRP (> 30mg/ml) and non-epithelioid histological subtype. Overall survival (OS) was calculated from the first cycle of induction chemotherapy until death, and association with the score was analyzed using Kaplan-Meier curve and log rank test.

Results:
Between 1999 and 2015, 253 patients were intended to be treated with induction chemotherapy plus EPP. In 63 undergoing EPP and 20 undergoing pleurectomy/decortication (P/D) all variables of MMPS were available. Median age at diagnosis was 61 years in the EPP group and 65 in the P/D group. Epithelioid type was diagnosed in 81% of the EPP and 95% of the P/D group. IMIG stage III in EPP group was 63% and 65% in the P/D group.
In the EPP cohort patients with score 0 survived significantly longer than patients with score 3 or higher (Figure 1). The median OS for patients of the EPP cohort was 34 months (95% CI, 18-50) for score 0, 15 months (9-21) for score 1, 12 months (8-16) for score 2 and 4 months (3-6) for score 3 and 4. In the P/D group the maximum score reached was 2 in only one patient. All the others had a score of 0 or 1. The median OS for score 1 was 30 months (95%CI: 25-36) and 17 months for score 2, but 70% percent of the cases were censored.

Conclusion:
Our Multimodality Prognostic Score considering clinical variables already available before surgery allows identification of mesothelioma patients who would not get any relevant benefit from an intensified therapy. The concept is currently under prospective evaluation

3576

I. Schmitt-Opitz[1], M. Friess[1], T. Nguyen-Kim[2], T. Fraunfelder[2], S. Hillinger[1], B. Seifert[3], I. Inci[1], W. Weder[1]

Correlation of CT Scan based tumor volume measurement to actual resected tumor weight in malignant pleural mesothelioma - a new T-Factor?

Division of Thoracic Surgery, University Hospital Zurich[1], Institute of diagnostic and interventional Radiology, University Hospital Zurich[2], Department of Biostatistics, Epidemiology, Biostatistics and Prevention Unit, University Zurich[3]

Introduction:
Tumor volume has been reported several times to be a valuable prognosticator for malignant pleural mesothelioma (MPM) survival (Pass 1998, Opitz 2015). We wanted to assess the precision of CT scan based preoperatively measured tumor volume when correlated to the actual resected tumor weight during macroscopic complete resection and their impact on overall survival.

Methods:
From October 2012 until November 2015 the tumor weight of surgery specimens was measured in 27 patients undergoing macroscopic complete resection. 26 patients were male (96%), 25 MPM showed epithelioid type (96%) and the median age at surgery was 66 years (range 41-77). Twenty-two patients underwent induction chemotherapy prior to surgery. In all 27 patients tumor volume was measured in the CT or PET-CT scans performed before surgery as described previously (Frauenfelder 2011). Tumor weight and volume were compared using the Pearson correlation. Tumor volume and tumor weight were also tested for association with pT stage using Mann-Whitney U test. Association with overall survival (OS) was evaluated with the Kaplan-Meier method.

Results:
The median tumor volume assessed by CT scan was 79 ml and the median tumor weight 520 g. The analysis revealed a correlation between tumor volume and weight ($r=0.529$, $p=0.005$). There was also a significant association of tumor volume ($p=0.016$) as well as tumor weight ($p=0.005$) with the pT-stage (Figure 1). Association of tumor volume and weight with OS could not be evaluated as 82% of the cases were censored.

Conclusion:
The preoperative assessed tumor volume in CT scan seems to be a valuable descriptor of actual tumor volume to be resected and might be a reliable future T-descriptor.

3577

I. Jelcic[1], P. Ojer[1], M. Foege[1], R. Stenger[2], M. Kayser[2], J. Kessler[3], A. Müller[4], U. Schanz[4], J. Dudler[5], M. Sospedra[1], R. Martin[1]

Individual Treatment Attempt of Progressive Multifocal Leukoencephalopathy (PML) with Adoptive Immunotherapy by Ex Vivo-Stimulated JC Polyoma Virus-Specific T cells

Neuroimmunology and MS Research, Department of Neurology, University Hospital Zurich and University Zurich (UZH)[1], Wyss Center for Translational Medicine, UZH, ETHZ, Zürich, Switzerland[2], Miltenyi Biotech, Bergisch Gladbach, Germany[3], Department of Hematology, University Hospital Zurich and University Zurich[4], Department of Internal Medicine, Cantonal Hospital Fribourg, Switzerland[5]

Introduction:
Progressive multifocal leukoencephalopathy (PML) is an opportunistic infection with the ubiquitous polyoma virus JC (JCV). PML occurs in situations of acquired or hereditary immunocompromise and involves viral mutations and lack or insufficient protective JCV-specific humoral and cellular immunity. There is currently no treatment, and the prognosis of PML is poor unless immune function is restored. In the recent past, we have successfully explored both active vaccination with JCV major capsid protein VP1 and also developed candidate antibodies for passive vaccination/treatment of PML. Since neither are currently available to treat PML patient, we have combined active vaccination with JCV peptides together with adoptive immunotherapy by ex vivo-stimulated JC polyoma virus-specific T cells. The individual treatment attempt of a patient, who suffered from systemic lupus (SLE) and developed PML after immunomodulation with Rituximab and hydrochloroquine, was approved by Swissmedic.

Methods:
The patient, who was diagnosed with PML following neurological deficits (ataxia, difficulties to walk) by magnetic resonance imaging (MRI) and demonstration of JCV cerebrospinal fluid (CSF) viral load of 28.000 copies in July 2015, received two subcutaneous immunizations with JCV peptides in combination with dermal application of an adjuvant (imiquimode) after testing her peripheral blood mononuclear cells by proliferative testing in vitro. 6 weeks after the first vaccination, the patient received an adoptive immunotherapy by ex vivo-stimulated JC polyoma virus-specific T cells. Briefly, 1x10e9 peripheral blood mononuclear cells were isolated by leukapheresis and stimulated ex vivo with a cocktail of JCV VP1 peptides including the major mutations of known PML strains of JCV. Quality control steps assured the presence and isolation of interferon gamma-expressing CD4+ and CD8+ JCV-specific T cells, which were reinfused to the patient after ex vivo stimulation using a ClinicaMacs Prodigy (Miltenyi) instrument. Virus-specific cells were then re-infused approximately 24 hours after isolation of cells.

Results:

Conclusion:
Besides active vaccination with JCV VP1 protein and passive vaccination/treatment of PML with broadly neutralizing JCV-specific antibodies, the combination of active vaccination with JCV VP1 peptides and subsequent adoptive immunotherapy with JCV-specific T cells represents an additional treatment option for PML.

3578

T. Brodie[1], P. Ojer[1], M. Sospedra[1], R. Martin[1], A. Lutterotti[1]

CD4+ T cell Reactivity to Myelin-Derived Autoantigens in the Cerebrospinal Fluid of Multiple Sclerosis Patients

Neuroimmunology and MS Research, Department of Neurology, University Hospital Zurich and University of Zurich[1]

Introduction:
CD4 T cells play a central role in orchestrating pathogenic immune responses in MS as supported by genetic studies as well as animal models. The target antigens of self-specific T cells causing inflammation in the brain of multiple sclerosis (MS) patients remain only partially understood. MS patients, as well as healthy individuals have peripheral T cells responding to myelin components such as myelin oligodendrocyte glycoprotein (MOG), myelin basic protein (MBP), proteolipid protein (PLP), 2',3'-cyclic nucleotide 3'-phosphodiesterase (CNPase) and myelin-associated glycoprotein (MAG) . In this study we will analyze CD4+ T cells expanded from the cerebrospinal fluid (CSF) of MS patients and controls for reactivity towards a comprehensive set of overlapping peptides from MOG, MBP, PLP; MAG and CNPase, their splice variants and know posttranslational modifications.

Methods:
CSF-derived CD4+ T cells will be expanded from MS patients and controls and stimulated with overlapping peptides of the five major myelin proteins listed above and novel antigens that exploit the pitfalls of thymic selection due to alternative promoter usage (Golli MBP), differential splicing and post-translational modification (citrullination) in the case of MBP. We will exploit T cell proliferation to identify the presence of antigen-specific cells in this compartment and compare these responses in donors with different stages/forms of MS.

Results:
This study is in the preliminary stages of data acquisition, and current results indicate that the methodological approach allows the detection of low frequency myelin-reactive T cells in the CSF. We aim to determine the antigen specificity of CD4+ T cells in the CSF in MS and Non-MS donors and characterize the function and phenotype of these cells.

Conclusion:
This information will expand our knowledge about the potential myelin-derived autoantigens in MS, which can then be used in antigen specific tolerization approaches.

The study is supported by a grant of the Swiss MS Society.

3579

A. Lutterotti[1], M. Foege[1], C. Blumer[1], A. Zinganell[2], T. Berger[2], W. Faigle[1], M. Inglese[3], M. Sormani[4], M. Sospedra[1], R. Martin[1]

Treatment of Clinically Isolated Syndrome and Relapsing Remitting Multiple Sclerosis with Sodium Chloride-based Nanoparticles (RNS60) Administered Intravenously – a Phase IIa Clinical Trial

Neuroimmunology and MS Research, Department of Neurology, University Hospital Zurich and University of Zurich[1], Department of Neurology, Medical University Innsbruck, Austria[2], Department of Neurology, Icahn School at Mount Sinai, New York, USA[3], Department of Health Sciences, University of Genoa, Italy[4]

Introduction:
Multiple sclerosis (MS) is a detrimental inflammatory disease of the central nervous system. RNS60 is composed of saline and oxygen, which is electrokinetically modified to produce charge-stabilized nanostructures. In cellular and animal studies, RNS60 has demonstrated beneficial anti-inflammatory effects, through modulation of cytokines and induction of regulatory T cells. The primary objective of the study is to investigate the efficacy, safety and tolerability of RNS60 administered intravenously in patients with clinically isolated syndrome (CIS) and relapsing-remitting (RRMS).

Methods:
We conduct a investigator-initiated, two-center, open-label, baseline-to-treatment, phase IIa trial. The primary outcome of the trial is the change in the mean number of contrast-enhancing lesions (CELs) during weeks 8 to16 compared to the three baseline MRIs. Patients included in the trial will have to show baseline disease activity to be eligible for the treatment phase. Further mechanistic studies aim to assess the mode of action of RNS60 in treated patients.

Results:
18 patients (as of January 2016) were included in the trial (13 at University Hospital Zurich, 5 at Medical University Innsbruck), and so far 4 patients with baseline disease activity were eligible for the treatment phase. Intravenous RNS60 was safe and well tolerated, the analysis of efficacy parameters is pending.

Conclusion:
Intravenous RNS60 is safe and well tolerated. Provided we can demonstrate preliminary signs of efficacy in an interim analysis, a phase IIa trial involving twice daily inhalation of RNS60 is planned.

3580

D. Pease[1], M. Emmenegger[1], E. Schaper[1], V. Chandrasekar[1], V. Eckhardt[1], A. Hartung[1], S. Hornemann[1], A. Aguzzi[1]

Discovery of Novel miRNA-Regulated PrPC Biosynthesis and PrPSc Conversion Pathways via a High-Throughput miRNA Screening Platform

Neuropathology, University Hospital of Zurich, Zurich[1]

Introduction:
Prion diseases are lethal transmissible neurodegenerative diseases afflicting a wide variety of species. Characterized by misfolding and aggregation of the cellular prion protein (PrP^{c}) into its pathogenic conformer, PrP^{Sc}, these infectious diseases have become the prototype for many proteopathies. Despite significant advances in elucidating the mechanisms underlying neurotoxicity, the cellular machinery controlling PrP^{c} biosynthesis and the means by which host PrP is converted into PrP^{Sc} remains poorly understood. The current project seeks to assess whether, and to what extent, the microRNAome may post-transcriptionally modify PrPc through direct or indirect pathways. To do so, our lab is developing a cell-based high-throughput human miRNA screen, exploiting a genome-wide library encompassing 2019 mimics and 2019 corresponding antagonists. While this exploratory approach is bound to yield novel potentially therapeutic hits, their validity will be contingent upon the robustness of this platform, the reproducibility of results and to what extent the cells will recapitulate a biological system.

Methods:
In order to assess potential effects of human miRNA on PrP^{C} levels, we utilize a reverse-transfection approach on a robotic screening platform in which miRNA mimics and antagonists were initially printed into 384-well plates in a randomized layout using an acoustic dispenser. Lipofectamine and cell suspensions as well as a real-time viability marker are added using robotic micro-dispensers in subsequent steps. Plates are then incubated for 48-72 hours, prior to content lysis and PrP^{C} quantification via TR-FRET. A combined screening of primary human myoblasts and fibroblasts as well as various cell lines is applied to select convergent hits for subsequent characterization. Comparison of FRET derived IC_{50} values with IC_{50} obtained from viability marker signals will yield information on the specificity of the observed effect. Following a secondary screening run, most promising hits will be further validated in iPSC-derived neurons and potentially in organoids. For the hit characterization, genetic and biochemical tools will be applied. Regulatory networks will be elucidated using bioinformatic enrichment analyses.

Results:
SH-SY5Y cells harboring murinized Prnp loci developed in-house as well as primary myoblasts were shown to contain high PrP^{c} levels, a cardinal prerequisite inferring suitability. Time-course experiments have revealed that a total incubation duration spanning 48 to 72 hours is appropriate to observe marked changes in PrP^{c} expression levels using less than 30 nM of Prnp-targeting RNA. Currently, we are in the process of optimizing volumes and concentrations as well as considering prime transfection reagent and optimal cell number to standardize the protocol and commence with the primary screen.

Conclusion:
A high-throughput platform has been established allowing the arrayed screening for effects of miRNA mimics and antagonists on PrP^{c} levels. Results gained during these experiments will not only help understand the regulatory role of miRNAs in the homeostasis of PrP^{c}, they may also prove to be therapeutically valuable: miRNAs, unlike siRNAs, are endogenously expressed in humans and act on multiple targets which may belong to the same pathway. This ordains miRNAs as potentially potent therapeutics for multigenic diseases involving complex pathways.

3581

C. Egger[1], T. Kepp[2], L. Spies[2], R. Opfer[2], S. Schippling1[1]

Validation of automated versus manual T2-lesion segmentation in Multiple Sclerosis patients applied on FLAIR sequences

Neuroimmunology and Multiple Sclerosis Research, Department of Neurology, University Hospital Zurich and University of Zurich[1], jung-diagnostics GmbH, Hamburg, Germany[2]

Introduction:
Magnetic resonance imaging (MRI) is key in the diagnostic process and disease monitoring of patients with multiple sclerosis (MS). T2 lesion load next to Gadolinium enhancing T1 lesions is a true surrogate of clinical disease activity and serves as an important endpoint in clinical trials in MS. Until to date, T2 lesion quantification – due to methodological constraints - is mostly performed manually although strong efforts have been made to allow automated segmentation. In 2012, Schmidt and co-workers published an algorithm to be applied on fluid-attenuated inversion recovery (FLAIR) sequences.
The aim of this study was to apply the Schmidt algorithm on an independent FLAIR data set and compare automated versus manual T2 lesion segmentation. Results were put in relation to inter-rater variability of manual segmentation by three independent raters.

Methods:
All MRIs have been performed on a 3.0T GE scanner (Discovery MR750, GE Healthcare, Great Britain) using an 8ch head coil. T2-lesion load was determined in 50 MS patients using open source software (MeVisLab, MeVis Solutions AG, Bremen, Germany) and three versions (LGA and LPA based on either SPM8 or SPM12) of an automated segmentation algorithm first described by Schmidt et al. (2012). Hyperintensities on 3D FLAIR images were automatically determined using lesion belief masks. Manual segmentation was performed by three independent raters. Interrater correlation coefficients (ICC) and dice coefficients (DC) have been calculated for all possible pairwise comparisons.

Results:
We found a strong correlation between manual and automated lesion segmentation based on LGA SPM8, regarding lesion volume (ICC=0.958 and DC=0.6) that was comparable to inter-rater correlation (ICC=0.97 and DC=0.66). Correlation between the other two algorithms and manual raters was weaker but still satisfying (ICC=0.927 and DC=0.53 for LGA SPM12 and ICC=0.949 and DC=0.57 for LPA SPM12). Performance of manual raters as well as automated algorithms was significantly weaker regarding lesion number detection.

Conclusion:
Automated lesion volume quantification can be applied on FLAIR data sets using the algorithm of Schmidt et al. and shows good agreement with manual segmentation.

3582

R. Higgins[1,2], M. Theiler[1,2], A. Smith[1,2], R. Wälchli[1,2], L. Weibel[1,2], A. Navarini[1]

Hunt for somatic mutations in Linear Localized Scleroderma

Department of Dermatology, University Hospital Zurich[1], Department of Dermatology, University Children's Hospital Zurich[2]

Introduction:
Multiple skin conditions have been shown to follow Blaschko's lines. Some of these diseases have been shown to be caused by a de novo somatic mutation causing a cutaneous mosaicism. Thus, genetic investigation of skin biopsies in affected areas and subsequent comparison to germline DNA may allow identification of underlying genetic risk factors. Linear localized scleroderma (LLS) could be one such mosaic disorder. It is a rare connective tissue disease characterized by chronic inflammation and fibrosis and subsequent atrophy. Our study investigates whether LLS is driven by protein-coding somatic mutations.
The most frequently available types of biopsies are formalin fixed and paraffin embedded (FFPE) samples that are suitable for immunohistology. During preservation the DNA in these samples is altered chemically, mainly by the deamination of cytosine to deoxyuracil. This process results in non-reproducible and misleading sequencing artefacts of C>T variants, therefore extra-stringent quality controls have to be in place to ensure accuracy.

Methods:
Patients included: 30 patients of Caucasian origin, clinical trial number NCT02222038.
We performed 2-5mm skin biopsies from affected regions, namely formalin fixed paraffin embedded (FFPE) and snap frozen. DNA extracted from 16 x 10µm slices of FFPE and 1-2mm of snap-frozen tissue and blood. Isolation of >0.5ug DNA, shearing with Covaris Ultrasonicator to 200bp fragments. Library preparation with Agilent SureSelectXT kits and capture performed using the Agilent SureSelectXT All exons V5 kit. Sequencing using Illumina HiSeq devices. Raw reads are processed by a quality control, filtering and annotation pipeline that interrogates all available public and several private databases to maximize the yield of valid information from patients. Genotype calling of somatic mutations was performed with VarScan v2.3.7 , Mutect 1.1.7 and Strelka 1.0.7. All are cancer variant callers utilized by comparing unaffected blood with affected skin.

Results:
From the first experiments FFPE and snap frozen skin samples were revealed to be comparable in terms of quality of sequences, therefore both sample types can be included in our study.
Affected skin and corresponding blood samples have been sequenced of the first 17 collected LLS patients. These samples were analyzed pair-wise per patient and then called variants were analyzed between patients. Analysis of somatic mutations called by Varscan, Mutect and Strelka found that no somatic rare variant was present in more than 9/17 patients with only one mutation which is both rare and predicted to be damaging (PolyPhen-2) found in 6/17 patients.
To account for sample heterogeneity causing the mutated cell to be present in low numbers and thus undetectable, deep sequencing to a read depth of >200 was performed on 4 phenotypically consistent patients. This increases the number of reads of tissue present in lower fraction of the tissue sample, allowing more sensitive detection.

Conclusion:
Analysis has revealed 1 possibly damaging mutation found in 6 patients (Called with Varscan). A gene-restricted analysis did not reveal a gene burdened significantly with rare mutations. The analysis was repeated for the deep sequencing data and did not reveal any novel or significant rare and protein-damaging mutations. The number of germline mutations common between patients is much higher than that of somatic indicating the possibility that the causative mutation could be germline.

3583

S. Lukas[1], I. Jelcic[1], J. Hanson[1,2], K. Weber[1,2], K. Landau[2], M. Pless[3], A. Valavanis[4], A. Lutterotti[1], S. Schippling[1]

Structural and functional outcomes in bilateral optic neuritis with MOG-antibodies

Neuroimmunology and Multiple Sclerosis Research, Department of Neurology, University Hospital Zurich and University of Zurich[1], Department of Ophthalmology, University Hospital Zurich[2], Department of Ophthalmology, Hospital of the Canton of Lucern[3], Department of Neuroradiology, University Hospital Zurich, [4]

Introduction:
Antibodies against myelin oligodendrocyte protein (MOG) have been described in juvenile acute disseminated encephalomyelitis (ADEM) and, more recently, in patients with Aquaporin4 (AQP4) seronegative neuromyelitis optica (NMO) or NMO spectrum disease (NMOSD). Optic neuritis (ON) patients with MOG antibodies have been characterized as experiencing a relatively benign disease course, with more favourable outcomes in comparison to AQP4-positive ON patients. We present clinical and imaging findings in two cases with MOG-positive, AQP4-negative recurrent bilateral ON.

Methods:
Two male patients P1 (age 44) and P2 (age 18) with a 7 year and 8 month history, respectively, of optic neuritis received magnetic resonance imaging (MRI), optical coherence tomography (OCT) and cerebrospinal fluid (CSF) investigations. High- and low-contrast visual acuity (VA, LCVA) was measured as were serological levels of AQP4- and MOG antibodies.

Results:
Both patients tested positive for MOG antibodies while repeatedly testing negative for antibodies against AQP4. OCT showed severe thinning of the circumpapillary retinal nerve fibre layer (RNFL) in both patients (mean thickness: P1 48µm OD, 52µm OS; P2 46µm OD, 84µm OS). On MRI, P1 exhibited no visible abnormalities whilst in P2 multiple T2- and gadolinium-enhancing lesions were found in the optic nerves, chiasm and corpus callosum. CSF tested negative for oligoclonal bands and showed no elevated cell counts or protein levels. Clinically, LCVA was unmeasurable (P1, OS; P2, OU). In addition, high contrast VA varied from normal (P1, OD) to reduced (P1, OS; P2, OD) or non-recordable (P2, OS).

Conclusion:
MOG-antibody seropositivity/AQP4-antibody seronegativity can be associated with aggressive, disabling disease in patients with recurrent bilateral ON similar to patients with ON and AQP4 antibodies. None of the cases fulfilled the diagnostic criteria for NMO, however, results of retinal neuronal atrophy (as quantified by OCT) and the severity of visual impairment closely resembled that typically observed in NMO and NMOSD. Testing for MOG antibodies may be helpful in cases of bilateral optic neuritis or suspected NMO/NMOSD, particularly in AQP4-negative patients. MOG-antibody positivity should lead to initiation of high efficacy immune treatment given the danger of severe clinical sequelae.

3584

L. Rigassi[1], E. Unterleutner[1], F. Barchiesi[1], B. Imthurn[1], R. Dubey[1]

Role of microRNA-193a in mediating the protective action of Estradiol in vascular cells

Department of Reproductive Endocrinology, University Hospital of Zürich[1]

Introduction:
Recent studies provide evidence that microRNAs (miRNAs) participate in many clinically relevant biological and pathophysiological processes. They regulate differentiation, proliferation, migration and apoptosis in many cell types, including the cardiovascular system. Vascular remodeling associated with cardiovascular disease involves endothelial cell (EC) damage/dysfunction and abnormal growth of smooth muscle cells (SMCs). Several miRNAs are known to influence both EC function and SMC growth. Estrogens are known to protect women against vasoocclusive disorders by promoting endothelial repair/recovery and inhibiting SMC growth. Thus, it is feasible that processes associated with vascular protection and repair are mediated by miRNA modulation. Hence, we hypothesize that the vasoprotective actions of estradiol (E2) may in part be mediated via modulation of miRNAs. In the present study we investigated the role of miR-193a on EC and SMC growth and its participation to the protective action of E2 in vascular cells.

Methods:
To investigate the expression of miR-193a, human coronary artery SMCs (HCASMCs) and human umbilical vein ECs (HUVECs) were treated with or without E2 (10nM-1uM) prior to small RNA extraction and RT-qPCR. Both cell types were then transfected with miR-193a mimics or antimirs, to assess the role of miR.193a using different functional assays. Cell counts, and BrdU ELISA were employed to study HCASMC growth. Matrigel microvessel formation and scratch assay were used to investigate the cell function of HUVECs. Western Blotting was performed to inspect protein expression.

Results:
Treatment of HUVECs with miR-193a mimic inhibited capillary formation and wound closure. Moreover, the expression of miR-193a was negatively regulated by E2 in HUVECs. This observation was further supported by the observation that downregulation of miR-193a by the antimir mimicked the protective effects of E2 by promoting the microvessel formation and the wound closure (scratch assay). In contrast, the overexpression of miR-193a by the mimic inhibited these processes. In HCASMCs, E2 decreased the PDGF-induced miR-193a levels in a concentration dependent manner. Similar to PDGF, the miR-193a mimic increased the cell number and the BrdU incorporation, as well as the expression of CyclinD1 protein. Surprisingly, the downregulation of miR-193a by the antimir did not significantly reduce the cell number. However, it inhibited the DNA synthesis and reduced CyclinD1 protein level, similar to the effects of E2 in these cells. Additionally, the inhibition of HCASMC proliferation and the induction of HUVEC function by E2 were reversed in the presence of the miR-193a mimic. These findings provide evidence which indicates an important role for miR-193a in mediating the protective actions of E2 on the cardiovascular system.

Conclusion:
Here, we demonstrate a differential role of miR-193a in regulating growth of endothelial and smooth muscle cells. Overexpression of miR-193a increased SMC proliferation and impaired EC-induced capillary formation and wound healing. We further show that E2 negatively modulates miR-193a expression in HCASMCs and HUVECs and that miR-193a downregulation by the antimir mimics the effects of E2. Interestingly, the miR-193a mimic was able to reverse the E2 effects in both cell types, suggesting that miR-193a modulation may represent a novel mechanism by which E2 mediates its protective actions on the cardiovascular system.

3585

B. Li[1], M. Emmenegger[1], E. Schaper[1], M. Zurbrügg[1], V. Eckhardt[1], C. Zhu[1], N. Guex[1], P. Gribbon[1], S. Hornemann[1], I. Xenarios[1], A. Aguzzi[1]

A genome-wide siRNA screen for genes controlling PrPC biosynthesis and prion propagation

Institut Neuropathologie, Universitätsspital Zürich[1]

Introduction:
Transmissible spongiform encephalopathies (TSEs) are characterized by spongiform changes in the neuronal tissue, astrogliosis and microglial activation, leading to death within a short time after disease onset. The causative agent of TSEs is called prion, which mainly consists of the scrapie prion protein (PrP^{sc}), a misfolded conformational variant of the cellular prion protein (PrP^{c}). Our lab currently develops a cell-based siRNA high-throughput screen (HTS) by which we aim at identifying genes implicated in biosynthesis of PrP^{c} and in the cellular machinery involved in the conversion of PrP^{c} into PrP^{sc}. We expect to identify novel genetic targets for the development of therapeutics to treat TSEs

Methods:
Primary screen. In order to assess the effect of siRNAs on PrP^{c} and PrP^{sc} levels, 384-well plates are printed with siRNAs with ultrasound dispensers following a randomized layout, lyophilized and then stored at -80 °C. On the day of experiment, transfection reagent and cell suspension as well as real-time viability markers are added with robotic microdispensers, and the plates are incubated for 48-72 hours. Subsequently, PrP^{c} and PrP^{sc} levels are measured in the cell lysates using HP-FRET. Secondary screen. Putative candidate siRNAs selected in the primary screen will be further analyzed for effect specificity by comparing the IC_{50} of the FRET signal with the IC_{50} of the viability signal for a range of siRNA concentrations. For the subsequent hit characterization, genetic and biochemical tools will be applied. Regulatory networks will be elucidated by enrichment analyses. Bioinformatics. Plate readouts are subjected to automated, unbiased quality control. Spatial readout gradients are attenuated with local control-based background normalization. For hit detection, owing to low target-specificity of some siRNAs, off-target effects are deconvoluted.

Results:
We are in the final stages of assay optimization before launching the Primary Screen. Recently, durations of the assay were adjusted to 48-72 hours assessed by multiple sandwich ELISAs. siRNA concentrations were shown to work constantly at 30 nM or lower. The stability of the readout was increased, and the variation decreased by altering the dispensing volumes of the FRET buffers. Cell dispensing has been improved using novel peristaltic multidispensing technologies. Preparations for a pilot run to quantify sensitivity and specificity of the current workflow are ongoing.

Conclusion:
With all experimental procedures implemented on the local HTS platform, and most optimization and validation steps completed, we are now close to realizing a genome-wide siRNA HTS. Starting from several sublibraries of particular interest to prion pathology (i.e., endocytome and chaperome), we aim to screen several genome-wide siRNA libraries. The explorative approach of RNA interference screens allows unveiling unbiased, unprecedented knowledge on key genetic players. Ultimately, by establishing analogous assays, we would like to transfer this untapped potential to local research on other neurodegenerative diseases such as Parkinson’s disease or Alzheimer’s disease.

3586

D. Heuberger[1], A. Franchini[1], J. Madon[1], R. Schuepbach[1]

Membrane-bound thrombomodulin mediates cleavage of protease-activated receptor 2 by thrombin

Surgical Intensive Care Medicine, University Hospital Zurich, Zurich, Switzerland[1]

Introduction:
Protease-activated receptors (PAR) are G-protein coupled receptors involved in a variety of biological processes ranging from platelet activation, vascular barrier regulation, chronic inflammation, cancer growth and apoptosis. Clotting proteases activate PARs by enzymatic removal of an N-terminal peptide, allowing the unmasked tethered ligand to activate PAR. For efficient cleavage of cell surface expressed PARs recruitment of proteases to the cell surface by direct receptor enzyme binding interaction or via cell bound co-receptor is required.
Thrombin can bind to the hirudin like domain of PAR1, cleaves and activates the receptor inducing pro-coagulant and pro-inflammatory signaling. In thrombomodulin (TM) expressing cells, this high affinity thrombin co-receptor preferentially mediates cell surface thrombin recruitment and enables an anti-inflammatory signaling. Contrary to PAR1, PAR2 lacking the thrombin recognition site is not cleaved by soluble thrombin. We wondered if PAR2 can be direct cleaved by thrombomodulin bound thrombin and whether the thrombin-thrombomodulin complex is interacting with PAR2 by protein-protein binding to mediate biological effects.

Methods:
To determine whether thrombin can cleave PAR2 in presence of the co-receptor thrombomodulin, pcDNA3.1 PAR2 constructs tagged with an N-terminal alkaline phosphatase (AP) and pcDNA3.1 thrombomodulin constructs were transfected by lipofection in the overexpression system of HEK 293T cells. Cell surface expression of PAR2 and thrombomodulin was measured by immunoassay. The cleavage of the AP-PAR2 construct was detected by an established alkaline phosphatase assay (SEAP) measuring alkaline phosphatase activity. 48hours after transfection the cells were incubated with thrombin and the cleavage efficiency of thrombin was measured by the cell bound and the released AP.

Results:
The results from the cleavage assay in our overexpression system showed that thrombin, if thrombomodulin is co-expressed, cleaves PAR2. Thrombin cleavage of PAR2 was blunted in presence of the specific thrombin inhibitor hirudin and in AP-PAR2 mutant construct lacking positively charged amino acids, the thrombin cleavage sites. Overexpression of thrombomodulin mutants showed that only EFG-like domain 5 and 6 are required for thrombomodulin mediated cleavage of PAR2 by thrombin.

Conclusion:
We showed in our overexpression system that PAR2 is directly cleaved by thrombin in a thrombomodulin-dependent manner. Thrombin is recruited to the cell membrane and binds on thrombomodulin EFG-like domain 5 and 6 to cleave PAR2. As none of the other thrombomodulin domains are required for PAR2 cleavage, we assume that thrombomodulin and PAR2 don't interact by protein-protein binding.

3587

K. Frontzek[1], M. Emmenegger[1], L. Saleh[2], R. Moos[1], E. Schaper[1], G. Meisl[3], D. Zimmermann[4], A. Von Eckardstein[3], H. Budka[1], S. Hornemann[1], A. Aguzzi[1]

Prevalence of human autoantibodies against the prion protein in unselected USZ patients and in PRNP mutation carriers

Institute of Neuropathology, University Hospital Zürich, Switzerland[1], Institute of Clinical Chemistry, University Hospital of Zurich[2], Department of Chemistry, University of Cambridge, UK[3], Department of Surgical Pathology, University Hospital Zurich, Zurich[4]

Introduction:
Prion diseases are fatal neurodegenerative diseases of the central nervous system relying on the seeded propagation of the “scrapie” conformer PrP^{Sc} onto its cellular counterpart PrP^{C}. Our lab was the first to report the protective action of systemic antibodies against prions. We recently found that protection is contingent on specific epitopes, with antibodies to the N-terminal "flexible tail" (FT) of PrP^{C} being protective and those against parts of the C-terminal "globular domain" (GD) being toxic. In around 30% of autoimmune brain diseases the underlying etiology cannot be identified. Detecting patients from the general population bearing toxic anti-PrP autoantibodies that can be held responsible for causing their autoimmune disease would provide immediate treatment options. Conversely, protective autoantibodies may be responsible for delaying the clinical manifestation of genetic prion disease (gPrD) in mutation carriers. Cloning of cognate memory B-cells from patients harboring protective anti-PrP autoantibodies may provide powerful therapeutics against so far incurable prion diseases.

Methods:
All blood samples from patients at the University Hospital of Zurich that underwent diagnostic laboratory work-up with positive research consent were chosen for the population screen, while blood from gPrD mutation carriers was collected in an international, collaborative approach. High-throughput antibody screens were performed through implementation of an enzyme-linked immunosorbent assay onto a liquid handling platform allowing testing capacities of up to ca. 1500 patient samples per day at microliter volumes. Humanized anti-PrP antibodies were generated for use as positive controls. Primary screens deliver information about blood anti-PrP reactivity and polyclonal affinities while epitope mapping and competition assays determine specificity and molecular targets of the autoantibodies. Clinical diagnoses are correlated with experimentally gathered antibody data.

Results:
Preliminary screens of ca. 2000 irreversibly anonymized plasma samples from an unselected patient cohort showed the majority of patients to harbor no anti-PrP autoantibodies while < 1% showed high anti-PrP reactivity. Competition experiments showed diminished anti-PrP reactivity of the samples upon addition of recombinant ligand. In gPrD patients primary screens showed some patients to harbor partially strongly reacting, anti-PrP autoantibodies as well. Epitope mapping showed the presence of specific autoantibodies binding to the FT of PrP^{C} in a clinically silent mutation carrier and autoantibodies binding both PrP^{C}-FT and PrP^{C}-GD in patients.

Conclusion:
We have found autoantibodies against the prion protein in both randomly selected patient blood samples from the University Hospital of Zurich and mutation carriers of genetic prion disease. The prevalence of anti-PrP autoantibodies is limited to ca. 0.1% of unselected USZ patients. The significance of these findings in terms of human disease etiology will be studied by clinical correlations. In genetic prion disease, certain patients harbor PrP^{C}-FT-directed, as shown before putatively protective autoantibodies that may be responsible for delaying clinical manifestation until high age. Cloning of these antibodies from memory B-cells could yield powerful new therapeutics against prion diseases.

3588

U. Nüesch[1], A. Mauracher[1], B. Volkmer[1], A. Urwyler[2], S. Vavassori[1], J. Pachlopnik Schmid[1]

The effect of dysfunctional mutation in Ttc7 on the haemtopoietic versus non-haemtopoietic system

University Children's Hospital Zürich, Division of pediatric Immunology[1], Cytolab, Regendsdorf[2]

Introduction:
Hereditary Multiple Intestinal Atresia (MINAT; OMIM 243150) is a rare congenital disorder characterized by a variable number of atresias throughout the small and large intestine. The disease has been linked to various mutations in the tetratricopeptide repeat domain 7A (TTC7A) gene and is associated with a combined immunodeficiency (CID).
Interestingly, one patient carrying mutation in TTC7A was described with a dendriform pulmonary ossification accompanied by CID and other patients developed an early-onset IBD associated with progressive immune deficiency, but not MINAT.
In our studies we employ the flaky skin mutant mouse ($Ttc7^{fsnfsn}$). This mouse carries a mutation in the mouse orthologue of human TTC7A (TTC7). $Ttc7^{fsn/fsn}$ mice show a complex phenotype including hyperinflammation, psoriasis-like skin disease, gastric forestomach papillomas, anemia and autoimmunity.
We want to investigate whether this phenotype is characteristic of the skin or caused by immune cells. Therefore, mice doubly homozygous for $Ttc7^{fsn/fsn}$ and for the severe combined immunodeficiency mutations were generated and bone marrow grafts experiments were performed.

Methods:
Mice. CByJ.A-Ttc7fsn/J ($Ttc7^{fsn/fsn}$) mice were purchased from the Jackson Laboratory. Heterozygous offsprings were used for breeding to obtain $Ttc7^{fsn/fsn}$ mice.
By.SJL(B6)-Ptprc<a>/J (Balb/c; CD45.1) mice were used as control for haematopoietic stem cell transfer (License No. 65/2014).
The C.129S7-Rag2<tm1Mom> ($Rag2^{-/-}$, Recombination-Activating Gene 2) mice and the Balb/c-IL2rg<tm1>B6.129S6-Rag2<tm1Fwa> ($IL2rg^{-/-}$ (Interleukin 2 receptor subunit gamma), $Rag2^{-/-}$) mice are used to generate double and triple mutant mice (gift from Prof. Burkhard Becher).
Histopathology. Skin, lymph nodes, spleens and thymi were collected and prepared for staining with H&E, anti-CD3 and anti-CD19.
Flow cytometry analysis. Spleen and peripheral lymph nodes were harvested, digested and stained. Flow cytometric analysis was performed using Gallios (Beckman&Coulter) and FlowJo software.
Graphical and Statistical analysis. Analysis were performed with FlowJo Version 10 and GraphPad Prism 6. Statistical data were expressed as mean ±S.EM.

Results:
Our first results after haemtopoietic stem cell transplantation showed a partly transferred phenotype with a mild splenomegaly and lymphadenopathy. The mice showed no sign of anemia, no gastric forestomach papillomas and no psoriasis-like skin. Interestingly, the double homozygous mutant mice ($Rag2^{-/-}Ttc7^{fsn/fsn}$) developed flaky skin, splenomegaly, slight lymphadenopathy, anemia and gastric forestomach papillomas. Flow cytometry anaylsis showed similar percentages of neutrophils, monocyte/macrophages in the spleen and lymph nodes compared to controls.

Conclusion:
So far, our first results from the HSCT and breedings indicate that the gastric forestomach papillomas and the flaky skin phenotype are not caused by defects in T lymphocytes nor B lymphocytes. The splenomegaly and lymphadenopathy remained, although in a mild form.
Altogether, we think that the flaky skin is caused by an epithelial dysfunction leading to an epithelial-stress syndrome that drives immunological responses.

3589

I. Jelcic[1], B. Combaluzier[2], Il. Jelcic[1], W. Faigle[1], L. Senn[2], B. Reinhart[1], L. Ströh[3], R. Nitsch[4], T. Stehle[3], M. Sospedra[1], J. Grimm[2], R. Martin[1]

Broadly Neutralizing Human Monoclonal JC Polyomavirus VP1-Specific Antibodies for the Treatment of Progressive Multifocal Leukoencephalopathy

Neuroimmunology and Multiple Sclerosis Research Section, Department of Neurology, University of Zurich, University Hospital Zurich, Switzerland[1], Neurimmune Holding AG, Schlieren, Switzerland[2], Interfaculty Institute of Biochemistry, University of Tübingen, Germany[3], Division of Psychiatry Research, University of Zurich, Switzerland[4]

Introduction:
In immunocompromised individuals, JC polyomavirus (JCPyV) may mutate and gain access to the central nervous system resulting in progressive multifocal leukoencephalopathy (PML), an often fatal opportunistic infection for which no treatments are currently available. Despite recent progress, the contribution of JCPyV-specific humoral immunity to controlling asymptomatic infection throughout life and to eliminating JCPyV from the brain is poorly understood.

Methods:
Here, we examined antibody responses against JCPyV major capsid protein VP1 variants in serum and cerebrospinal fluid (CSF) of healthy donors, JCPyV-positive multiple sclerosis (MS) patients treated with the anti-VLA-4 monoclonal antibody natalizumab, and patients with natalizumab-associated PML. Furthermore, we generated a series of memory B cell-derived JCPyV VP1-specific human monoclonal antibodies from healthy donors and a NAT-PML-IRIS patient, who recovered from PML.

Results:
Prior to and during PML, CSF antibody responses against JCPyV VP1 variants show "recognition holes"; however, upon immune reconstitution, CSF antibody titers rise, then recognize PML-associated JCPyV VP1 variants and eliminate the virus. We therefore reasoned that the memory B cell repertoire of individuals who recovered from PML could be a source for the molecular cloning of broadly neutralizing antibodies for passive immunization. These antibodies exhibited diverse binding affinity, cross-reactivity with the closely related BK polyomavirus, recognition of PML-causing VP1 variants, and JCPyV neutralization. Interestingly, almost all antibodies with exquisite specificity for JCPyV, neutralizing activity, recognition of all tested JCPyV PML variants and high affinity were derived from one patient, who had recovered from PML.

Conclusion:
Our findings provide insight about the role of the humoral immune responses during PML and lay the foundation for the development of targeted immunotherapy for PML with a newly identified class of broadly neutralizing human recombinant monoclonal antibodies.

3590

K. Nytko-Karouzakis[1,2], I. Grgic[1,2], M. Pruschy[1,2]

The combined treatment modality of a hypoxia-activated prodrug (Evofosfamide) with ionizing radiation

Laboratory for Applied Radiobiology, Department of Radiation Oncology, University Hospital Zürich[1], Clinical Research Priority Program "Tumor Oxygenation"[2]

Introduction:
Hypoxia is a hallmark of many solid malignancies and confers resistance to radiotherapy as well as other treatment regimens. We investigated the combined treatment modality of ionizing radiation (IR) with the clinical stage hypoxia-activated prodrug (HAP; evofosfamide) in vitro and in vivo using mechanistic and efficacy-oriented endpoints. The combined treatment modality of IR with this HAP might lead to complementary tumor cell killing. Ionizing radiation will primarily target well-oxygenated tumor cells, while the HAP will primarily kill hypoxic tumor cells. At the same time enhanced, supra-additive cytotoxicity will be expected by the diffusible activated prodrug leading to more complex DNA damage when used in combination with IR.

Methods:
We investigated the cytotoxic effects of evofosfamide on tumor cell (A549 lung carcinoma and UT-SCC-14 head&neck squamous cell carcinoma, HNSCC) proliferation and clonogenicity in normoxic (21% O_2) and hypoxic (0.2% O_2) conditions. For in vivo experiments, cells were subcutaneously injected on the back of athymic nude mice. Treatment was initiated when tumors reached volume of 300 mm^3 +/- 10%. Irradiation was performed with either a fractionated (3x2Gy) or a single high dose regimen (1x10Gy). Evofosfamide was administered i.p. Q3Dx5 (50 mg/kg in saline).

Results:
Lung carcinoma A549 cells were more sensitive to evofosfamide when incubated with the compound under hypoxic conditions in comparison to normoxic conditions in a dose- and time-dependent manner. We observed decreased clonogenicity of A549 cells with evofosfamide/IR co-treatment, which suggests that the evofosfamide has a radiosensitizing effect in vitro. Moreover, evofosfamide alone and in combination with IR induced a strong DNA-damage response and senescence (β-galactosidase staining) in A549 cells. We performed in vivo, efficacy- oriented experiments with lung A549 and HNSCC UT-SCC-14 xenografts to test different schedules of evofosfamide in combination with fractionated and single high-dose IR (neoadjuvant, concomitant, adjuvant). Combined treatment resulted in a strongly enhanced tumor growth delay when compared to the single treatment regimens in lung A549 xenografts applying the three different scheduling regimens in combination with fractionated and single high dose irradiation. Interestingly, evofosfamide did not reduce tumor growth of HNSCC UT-SCC-14 xenografts, most probably due to lack of P450 oxidoreductase, which might act as major predictive determinant of sensitivity to HAPs.

Conclusion:
Enhanced tumor growth delay of lung carcinoma xenografts in response to a combined treatment of evofosfamide with two different regimens of IR suggests a potent complementary effect with IR of this compound in vivo. Further studies to investigate DNA-damage related endpoints in response to evofosfamide alone and in combination with IR in a genetically defined background (BRCA1/2 deficient cells) are ongoing to further understand the mechanism of a combined treatment. These efficacy- and mechanistic-oriented experiments on the preclinical level are highly relevant to launch clinical phase I/II trials combining radiotherapy with this clinical stage HAP.

3591

R. Myburgh[1], A. Müller[1], M. Van den Broek[2], B. Becher[3], M. Manz[1]

Treatment of AML with CAR T cells

Hematology, University Hospital Zürich, Zurich [1], Experimantal Oncology, Institute of Experimental Immunology, University of Zurich, Zurich [2], Neuro and Tumor Immunobiology, Institute of Experimental Immunology, University of Zurich, Zurich[3]

Introduction:
Immunotherapies hold promise and have made major progress in the treatment of hematological malignancies in recent years. One particularly effective approach is the use of chimeric antigen receptor (CAR) T cells, consisting of high affinity single-chain monoclonal antibodies or single-chain variable fragments (scFv), linked to the signaling machinery of the T-cell receptor and costimulatory molecules. Recently, ground-breaking clinical responses to CAR T- cell therapy in CD19+ B-cell malignancies have been reported. Acute Myeloid Leukemia is a clonal disorder of the hematopoietic stem cell (HSC) and contains a subpopulation of leukemia-initiating cells (LIC) that can self-renew and give rise to the hierarchy of maturing blasts. While the proliferating mature blast pool is highly sensitive to chemotherapy, the more quiescent LICs are relatively resistant and can be a source of relapse. We postulate that the only way to lasting success in poor-risk disease is to radically eliminate LICs and accept collateral damage to HSCs that, subsequently, can be replaced by transplantation. We aim to create a platform for the generation of human CAR T-cells directed against leukemic and HSC antigens, the first of which will be c-Kit (CD117).

Methods:
We will use mouse AML models as well as humanized models carrying human AML cell lines and primary human leukemia to evaluate CAR T-cell safety and efficacy. The capacity to eliminate LICs as well as bystander effects on healthy hematopoiesis will be assessed.

Results:
For the mouse AML model, we have generated a murine FBL3 cell line expressing murine c-Kit (CD117), luciferase and GFP. For the humanized model, the human AML cell line (Kasumi-1) has been characterized and naturally expresses c-Kit. Additionally we have modified the Kasumi-1 cells to express human CXCR4 to facilitate in vivo homing and engraftment in immunodeficient mice, GFP and luciferase will be used as reporter genes. The design and synthesis of both fully murine and human CAR lentivector constructs consisting of an extracellular CD8α sequence linking the scFv to the intracellular 4-1BB co-stimulatory and CD3zeta stimulatory domains have been completed. The design allows for insertion of different antigen targeting scFvs' without modification of the rest of the CAR construct. To generate the first scFv targeting CD117 we used the ACK2 hybridoma which produces a depleting anti-mouse CD117 antibody. The ACK2 antibody was purified and binding to murine CD117 was verified on mouse bone marrow mononuclear cells as well as the c-Kit+ murine FBL3 cell line. The CD117 targeting scFv was produced by PCR amplifying and sequencing the VH and VL sequences of the ACK2 antibody and linking the VH and VL chains with a standard GGGGS pentapeptide linker. A dual purpose positive selection and negative selection gene called RQR8 will be co-expressed on the CAR T cells, characterization of which is underway. Expression of RQR8 on a CAR T cell will allow for magnetic selection of CAR T cells using an anti-human CD34 antibody prior to administration of the cells. RQR8 also acts as a safety gene since it binds the B cell depleting antibody Rituximab. Administration of Rituximab will allow for the in vivo depletion of CAR T cells.

Conclusion:
Our goal is to use these immunotherapies to radically eliminate both AML-LICs and HSCs by targeting non-tumor-selective HSC antigens and to subsequently deal with the life-threatening HSC depletion by allogeneic HSC transplantation.

3592

P. Manogaran[1], R. Opfer[1], R. Opfer[2], T. Kepp[2], P. Suppa[2], L. Spies[2], C. Egger[1], S. Schippling[1]

Assessing intra - and inter - scanner variability of automated brain volumetry using SPM12, SIENA, and SIENAX

Neuroimmunology and Multiple Sclerosis Research, Department of Neurology, University Hospital Zurich and University of Zurich[1], Jung Diagnostics GmbH, Hamburg, Germany[2]

Introduction:
Loss of global and regional brain volume are increasingly recognized biomarkers of neurodegeneration in multiple sclerosis. Statistical Parametric Mapping (SPM), Structural Image Evaluation using Normalization of Atrophy (SIENA) and its cross-sectional version SIENAX are well established tools for quantitative measurement of brain volume and brain volume changes. We compared intra- and inter-scanner variability of SPM12, SIENA, and SIENAX. The impact of measurement variability on longitudinal volumetric studies for each tissue compartment and each method was assessed. The minimum percent of volume difference necessary to detect a significant volume change between two measurements in the same subject was determined.

Methods:
Three-dimensional T1-weighted magnetization prepared rapid gradient echo (MPRAGE) scans of 51 healthy subjects were included into this study. All subjects had two scans performed for each scanner platform at 1.5 T and 3.0 T field strengths (total of 4 scans) within a period of a few weeks. In total, 204 images were downloaded from the Alzheimer's Disease Neuroimaging Initiative (ADNI) repository. The data was acquired at 50 different imaging centers. The two scans on each scanner platform were acquired back-to-back during a single imaging session. Since no atrophy is expected for back-to-back scans, the percentage of volume change between the two scans can be used as a measure of error. The intra-scanner (1.5 T vs. 1.5 T and 3.0 T vs. 3.0 T scan) and inter-scanner errors (first 1.5 T vs. first 3.0 T scan) were determined for each subject.

Results:
The 5, 50, and 95 percentiles of the absolute errors for intra-scanner total brain volume were [0.05, 0.24, 1.28] for SPM12, [0.16, 1.93, 14.38] for SIENAX, and [0.01, 0.15, 0.9] for SIENA. The minimum percent of volume difference necessary to detect a significant (p=0.05) volume change between two measurements in the same subject is therefore 1.28% for SPM12, 14.38% for SIENAX, and 0.9% for SIENA. The 5, 50, and 95 percentiles of the absolute errors for inter-scanner total brain volume were [0.21, 1.74, 5.44] for SPM 12, [0.61, 4.96, 19.67] for SIENAX, and [0.20, 1.57, 4.97] for SIENA.

Conclusion:
SIENA appears better suited than SPM12 for intra-scanner comparisons of longitudinal measurements. SPM12 has significantly lower variability compared to SIENAX, therefore, SPM12 might be better suited for cross-sectional measurements. Significantly higher variability was observed in all methods when baseline and follow-up scans were acquired on different devices with different field strengths.

3593

J. Hanson[1,2], S. Lukas[2], K. Landau[1], R. Martin[2], C. Gerth-Kahlert[1], S. Schippling[2]

Evidence of functional retinal impairment in the absence of sustained structural damage following MS-related optic neuritis

Department of Ophthalmology, University Hospital Zurich[1], Neuroimmunology and Multiple Sclerosis Research, Department of Neurology, University Hospital Zurich and University of Zurich[2]

Introduction:
Acute optic neuritis (ON) is an inflammation of the optic nerve typically accompanied by demyelination, and is a common finding in patients with multiple sclerosis (MS). Recent evidence suggests consecutive changes to retinal structure, with thinning of the retinal nerve fibre layer (RNFL) and ganglion cell-inner plexiform complex (GCIP), and mild thickening of the mid- and outer retina over a period of six months. At 12 months post-ON, RNFL and GCIP remain abnormally thinned; however, the status of more distal layers at this timepoint remains unknown. We have embarked on a detailed investigation of MS patients with and without a history of ON using multimodal imaging, electrophysiological and clinical measurements in order to characterise MS phenotypes. We analysed the data from a subset of patients in order to search for long-term structural and functional changes in the mid- and outer retina following ON.

Methods:
Six patients (mean 33.7 years; 5 females) were identified from our study group as having had a single, unilateral ON more than 12 months previously (mean time since ON: 20 months). All were examined using OCT, electrophysiology (visual evoked potential (VEP), electroretinography (ERG), multifocal ERG (MF-ERG), and high- and low-contrast visual acuity charts. 18 normal subjects (mean 31.7 years; 14 females) underwent OCT imaging in order to obtain normative data for the retinal layers distal to RNFL. All OCT scans were segmented in order to obtain measures for total macular volume (TMV), thickness of the full retina (FR), RNFL, GCIP, inner nuclear layer (INL), outer nuclear layer (ONL), outer plexiform layer (OPL), and photoreceptor complex (PR).

Results:
In MS eyes with a history of ON, TMV was reduced (3/6 eyes), and FR (3/6), RNFL (4/6) and GCIP (5/6) were thinned, whilst OPL thickness was increased in 1/6 eyes. No thinning of layers distal to GCIP was observed. All six patients had abnormal VEP, with 3/6 also having abnormal ERG and 2/5 abnormal MF-ERG suggestive of bipolar cell dysfunction. Abnormality in ERG and/or MF-ERG was associated with poorer clinical outcomes.

Conclusion:
Our study provides electrophysiological evidence of functional impairment of retinal layers that appear structurally normal on OCT following MS-related ON. ERG and/or MF-ERG indicative of bipolar cell dysfunction was recorded in three patients, in whom no corresponding structural changes in INL or other mid- or outer retinal layers were observed.

3594

C. Corro[1], A. Von Teichman[1], D. Vuong[1], C. Mittmann[1], H. Moch[1], M. Rechsteiner[1]

Tumor heterogeneity and cancer stem cell properties in renal cancer

Institute of Surgical Pathology, University Hospital Zürich, Zürich1.[1]

Introduction:
Clear cell renal cell carcinoma (ccRCC) is the most common type of renal cancer. Asymptomatic manifestation in early stage and a poor response to radiotherapy and chemotherapy in metastatic stage makes this tumor type very difficult to diagnose and to treat. Recent studies showed that ccRCC is a very heterogeneous tumor with multiple key driver mutations (VHL, PBRM1, BAP1,and SETD2). However, which tumor subpopulation and driver mutation regulates tumor spreading and initiation of metastasis remains unresolved. Additionally, evidence for a stem cell like ccRCC subpopulation opened the question about the role and the mutational landscape of these selfrenewing and chemotherapy resistant cells.

Methods:
To elucidate tumor heterogeneity in ccRCC, eleven primary ccRCC cultures were established for studying the mutational profile, the expression pattern on RNA and protein level in relation to proliferation, migration and invasion characteristics in in vitro and in vivo models. Furthermore, to investigate and further characterize genotype and phenotype of the cancer stem cell fraction, a sphere assay was set up.

Results:
So far, six ccRCC primary cells were analyzed genotypically to obtain information about their genetic identity compared to the primary tumor which they derived from. In all primary cultures the VHL mutation status was confirmed. Moreover, changes in the mutational profile in these primary cells while culturing were investigated in depth using next generation sequencing (NGS). NGS data showed a selection of ccRCC subpopulations in the earliest passages while a consistent heterogeneous population was maintained with increasing passage numbers. In addition, immunohistochemical markers such as PancK, BAP1, PBRM1, and the cancer stem cell marker CD105, revealed similar expression patterns in both primary cultures and primary tumor tissue. Furthermore, to investigate and characterize genotype and phenotype of the cancer stem cell (CSC) fraction, a sphere assay was set up. The presence of cancer cells with stem cell properties was first investigated in ten RCC cell lines. Only five of them showed sphere formation capability and self-renewal properties. No differences were observed in the protein expression of BAP1, PBRM1 and CD105 in the spheres compared to the corresponding monoadherent cells. In accordance with the observations obtained from RCC cell lines, two metastatic primary culture showed enhanced sphere formation capability compared to primary tumor-derived cultures, suggesting an increased CSC fraction in the metastatic sites compared to the primary tumors.

Conclusion:
Primary cultures represent a valuable tool to characterize and investigate the genotype and phenotype of RCC in vitro. The identification of such subpopulations with CSC properties in ccRCC giving rise to chemoresistance and metastatic potential may help to tailor more effective drugs and increase the response to treatment.

3595

R. Parrotta[1], A. Okonska[1], L. Penengo[2], E. Felley-Bosco[1]

Alternative splicing in BAP1: implications in DNA damage response and drug sensitivity in mesothelioma

Laboratory of Molecular Oncology, Thoracic Surgery, University Hospital Zürich[1], Institute of Molecular Cancer Research, University of Zurich[2]

Introduction:
BRCA1-associated protein-1, Bap1, is known as tumor suppressor involved in multiple cellular processes as transcriptional regulation, chromatin modification and DNA repair. BAP1 mutations are frequent in malignant pleural mesothelioma (MPM), a rare tumor characterized by a very poor prognosis, due to the difficulties of an early diagnosis and the poor response to current standard therapy. The human protein Bap1 includes a catalytic domain UCH, conferring deubiquitinase activity, two nuclear localization signal (NLS) domains and different binding domains for BARD1, HCF1 and BRCA1. Recently we have identified a novel alternative splice shorter isoform of Bap1 in MPM cells missing a part of the UCH domain and BARD1 binding domain. Our aim was to investigate whether expression of this short BAP1 isoform affects response to drugs impairing homologous recombination DNA repair.

Methods:
The expression of the short BAP1 transcript was analyzed by qPCR and RT-PCR in MPM cell lines and tumor samples from patients. The sensitivity of the MPM cells to Olaparib, a poly(ADP-ribose) polymerase 1 (PARP1) inhibitor, and to GDC0980, a dual PI3K-mTOR inhibitor, and their combination, was assessed by colony formation and spheroids assays using MPM cell lines expressing different levels of the short BAP1 transcript. DUB activity was determined after acid extraction of histones.

Results:
We have observed that the $BAP1^{-/-}$ MPM cells are very sensitive to Olaparib and we can rescue this effect by reconstituting $BAP^{-/-}$ cells with long BAP1 but not with short BAP1 variant. We confirmed that short BAP1 isoform is detectable at mRNA level by RT-PCR in both MPM cell lines and MPM tumours and that its abundance varies as indicated by qPCR results. MPM cell lines expressing higher level of endogenous short BAP1 isoform are more sensitive to Olaparib, compared to the cells with low expression. Moreover, this sensitivity is enhanced when Olaparib treatment is combined with GDC0980.

Conclusion:
These observations suggest that alternative isoforms of BAP1 may regulate DNA damage response and drug sensitivity. This might be relevant, at a clinical level, to define if patients with high expression of short Bap1 could be selected for treatment with PARP-inhibitors in combination with PI3K-mTOR inhibitors.

3596

P. Forny[1], M. Mustedanagic[1], P. Burda[1], T. Hornemann[1], M. Baumgartner[1]

A novel mouse model of methylmalonic aciduria circumvents neonatal lethality

Division of Metabolism and Children's Research Center, University Children's Hospital Zurich, Zurich, Switzerland[1]

Introduction:
Methylmalonic aciduria (MMAuria) is caused by de?ciency of the enzyme methylmalonyl-CoA mutase (MUT), which catalyzes the reversible isomerization of L-methylmalonyl-CoA to succinyl-CoA, requiring vitamin B_{12} (cobalamin) in the form of adenosylcobalamin as cofactor. This reaction represents an important step in propionate catabolism, funneling metabolites from the breakdown of valine, isoleucine, methionine and threonine, odd-chain fatty acids and the side chain of cholesterol into the tricarboxylic acid cycle. MMAuria is an autosomal recessive disorder that usually presents in the newborn period with metabolic crisis - including elevated levels of propionylcarnitine, methylmalonic acid and ammonia - leading to failure to thrive, coma or even death. Survivors often suffer severe long-term complications such as renal failure and neurological impairment. Since Mut knock-out (ko) mice display neonatal lethality, the study of the disease in the ko situation is not feasible.

Methods:
To create viable mouse models closely mimicking human MMAuria, we have generated a constitutive Mut knock-in (ki) based on the p.M700K patient mutation causing an intermediate MMAuria phenotype, which can be used homozygously (ki/ki) or combined with a ko allele (ko/ki).

Results:
Transgenic $Mut^{ki/ki}$ and $Mut^{ko/ki}$ mice survive post-weaning, show decreased weight gain, increased methylmalonic acid levels in blood, urine and tissues, increased blood propionylcarnitine, and increased odd-chain fatty acids and sphingoid bases, compared to littermate controls. Consistent with a genetic-dosage effect, $Mut^{ko/ki}$ show higher levels of metabolites, and less weight gain than $Mut^{ki/ki}$ mice. When fed a high-protein or precursor-enriched diet, $Mut^{ki/ki}$ and $Mut^{ko/ki}$ mice have further elevated metabolite levels, including plasma ammonia, and show catastrophic weight loss, which is partially rescued by pre-treatment with hydroxocobalamin in the homozygous ki/ki situation. Under normal diet, $Mut^{ko/ki}$ mice have elevated p62 and LCN2 in the kidney, and both genotypes demonstrate elevated p62, LC3 and Lcn2 in the brain, indicating activated autophagy in these vulnerable organs.

Conclusion:
Our study introduces two new mouse models which accurately reflect the MMAuria patient situation and for the first time enable studies on pathomechanisms, partly uncovered by this work. The better understanding of the molecular in-cell mechanisms responsible for the disease phenotype will help to develop novel therapeutics. Further evaluation of the classical cobalamin treatment and of novel therapeutic approaches, such as pharmacological chaperones and gene therapy, can be applied in the new models.

3597

V. Chandrasekar[1], M. Einsiedler[1], U. Herrmann[1], S. Erni[1], H. Budka[1], A. Aguzzi[1]

Elucidating the physiological function of cellular PrPC

Institute of Neuropathology, University Hospital of Zurich, Zurich, Switzerland[1]

Introduction:
PrP^C is a lipid-raft associated glycoprotein anchored to the cell membrane by GPI and is ubiquitously expressed. Misfolding of cellular PrP^C into the pathogenic PrP^{Sc} results in progressive and fatal neurodegenerative disorders. Prion induced neurotoxicity is preceded by impairment in metabolism of cholesterol and other lipids which are major component of lipid-rafts in affected neurons. Understanding the function of cellular PrP^C may shed light on such pathological mechanisms. Towards this goal, we utilize human induced pluripotent stem (iPS) cell as a model system.

Methods:
To establish the model system, we reprogrammed human primary fibroblasts with Yamanaka transcription factors to create iPS cells and derived human neurons. We designed sgRNAs targeting PRNP gene in human primary fibroblasts and using CRISPR/Cas9 gene editing system, we generated PrP-KO cells. Clones were selected and confirmed using Sanger gene sequencing and Western blot. In order to understand the function of PrP^C, we performed metabolomics and RNAseq on these PrP-KO cells to identify pathways which are altered upon PrP^C depletion. Using these cells we will generate PrP-KO-iPS cells and human neurons.

Results:
Analysis of metabolites from PrP-KO primary human cells showed alteration in glycerophospholipid and cholesterol metabolism. Cholesterol and phospholipids are major components of lipid rafts and play roles in cell signalling, neurite outgrowth in neurons. RNAseq data generated using these same cells corroborated in transcript levels of genes involved in glycerophospholipid and cholesterol metabolism in the PrP-KO cells.

Conclusion:
Our preliminary data suggests a role of cellular PrP^C in glycerophospholipid and cholesterol metabolism. We plan to perform proteomics analysis of the PrP-KO cells, the data from which will be combined in a system biological approach together with metabolomics and RNAseq in order to establish the functional network of cellular PrP^C.

3598

H. Leske[1], U. Herrmann[1], S. Hornemann[1], K. Wüthrich[1], A. Aguzzi[1]

Removal of a single oxygen atom from the prion protein leads to significant reduction of proteinase K resistant PrP

Neuropathology, University Hospital of Zurich, Zurich[1]

Introduction:
Transmissible spongiform encephalopathies are fatal neurodegenerative diseases caused by proteinaceous infectious particles (prions). Infectious prions (PrP^{Sc}) are misfolded aggregates of the cellular prion protein (PrP^{C}) resistant to proteolytic digestion. In fact, the C-terminal part of PrP^{Sc} can withstand up to 500µg/ml proteinase K (PK) treatment. Accordingly, PK resistant PrP as determined by western blot is considered among the gold standards for the diagnosis of these neurodegenerative diseases. Of note, entities such as variable protease sensitive prionopathy (VPsPr) in humans have recently been discovered, which show novel patterns after PK treatment.
In this study, we investigated the structural basis for the phenomenon of protease-sensitive prion infectivity by substituting the amino acid Y169F, which removes a single oxygen atom from the β2–α2 loop of the cellular prion protein.

Methods:
Transgenic mice expressing wild-type PrP with the substitution Y169F, Tg($MoPrP^{169F}$), and lacking wild-type PrP were generated.
Animals were intracerebrally inoculated with two prion strains, the mouse adapted rocky mountain laboratory (RML) or the hamster adapted (263K) prion strain. Brain homogenates from terminally sick mice were reinjected into mouse PrP overexpressing Tga20, and hamster PrP overexpressing Tg81 mice. Mouse brains were investigated by biochemical and immunohistochemical methods for signs of prion diseases and the physicochemical properties of PrP^{Sc}.

Results:
When infected with RML or the 263K strain of prions, transgenic mice lacking wild-type PrP^{C} but expressing $MoPrP^{169F}$ generated prion infectivity at levels comparable to wild-type mice. The newly generated $MoPrP^{169F}$ prions were biochemically indistinguishable from those recovered from wild-type mice infected with identical strains, and elicited similar histopathological patterns of disease. Surprisingly, $MoPrP^{169F}$ prions lack PK resistance.

Conclusion:
We conclude that a subtle structural variation in the β2-α2 loop of PrP^{C} affects the sensitivity of PrP^{Sc} to protease but does not impact prion replication and toxicity. These findings represent compelling evidence that a specific structural feature of PrP^{C} can be linked to a physicochemical property of the corresponding PrP^{Sc}

3600

G. Wanner-Seleznik[1], T. Reding[1], L. Peter[1], A. Zabel[1], M. Heikenwalder[2], S. Sonda1[1], R. Graf[1]

Absence of p21 attenuates pancreatic inflammation but does not modulate the development of autoimmune pancreatitis

Swiss HPB Centre, Visceral & Transplantation Surgery, University Hospital Zurich, Switzerland[1], Institute of Virology, Technische Universität München–Helmholtz Zentrum München, 81675 Munich, Germany[2]

Introduction:
Cyclin dependent kinase (cdk) inhibitors are known to play key roles in inflammatory cell differentiation, neutrophil function and can influence inflammatory signaling pathways. Additionally, they are involved in the regulation of apoptosis and gene transcription. Therefore, cdk inhibitors are critical regulators in inflammatory and autoimmune diseases. p21 - a member of the cip/kip family of endogenous cdk inhibitors - has been described as a mediator of inflammation and autoimmunity in various diseases such as atherosclerosis, lupus nephritis or arthritis. Autoimmune pancreatitis (AIP) is considered mostly a T-cell mediated disease; however, the macrophages play a relevant role as well. Since p21 is known to influence T-cell proliferation and macrophage activation, we set out to test how p21 deficiency affects the development of (1) pancreatic inflammation and (2) autoimmunity.

Methods:
Lymphotoxin (LT)-transgenic mice (*Tg(Ela1-LTa,b)*) - that develop pronounced pancreatic inflammation at three months of age and progress spontaneously to autoimmune pancreatitis between the age of 9-12 months – were crossed with p21 deficient mice ($p21^{-/-}$). To study chronic pancreatitis and AIP, we analyzed 3 and 12 months old mice respectively. The distribution of infiltrating inflammatory cells was visualized by immunohistochemistry, and quantified by gene expression analysis. Circulating autoantibodies, the presence and composition of tertiary lymphoid organs (TLOs) were analysed.

Results:
Deficiency of p21 (*LT;*$p21^{-/-}$*)* prevented pancreatic injury as evidenced by normal pancreatic amylase levels, reduced inflammatory cell influx and attenuated inflammatory gene signature. Pancreatitis in *LT* mice is accompanied by extensive acinar cell proliferation, and consequently by acinar-to-ductal metaplasia (ADM). However, no such proliferative response or ADM formation was observed in the pancreata of *LT;*$p21^{-/-}$ mice. In absence of p21 the activation of non-canonical NF-kB pathway was abrogated in pancreatic acinar cells. Concerning autoimmunity, *LT;*$p21^{-/-}$ mice developed less TLOs than *LT* animals, however, the organization of the follicles was comparable in presence and absence of p21. Autoantibodies and elevated serum IgG were detected in both *LT;*$p21^{-/-}$ and LT animals.

Conclusion:
Our findings indicate that absence of p21 reduces pancreatic inflammation in LT-driven injury. Chronic pancreatitis and AIP are characterized by different inflammatory processes. Early pancreatic damage is mediated by innate immune cells and acinar cell transdifferentiation, which is modulated by p21. However, humoral immune response, accountable for autoimmunity is not affected. Deletion of p21 does not rescue the development of autoimmune pancreatitis.

3601

K. Fritsch[1], P. Bourgine[2], P. Bourgine[3], S. Pigeot[2], T. Schröder[3], I. Martin[2], H. Takizawa[4], H. Takizawa[1], M. Manz[1]

Maintenance of human hematopoiesis in in vivo engineered bone organs

Division of Hematology, University Hospital Zurich and University of Zurich[1], Department of Biomedicine and Surgery, University Hospital Basel[2], Department of Biosystems Science and Engineering, ETH Zurich, Basel, Switzerland[3], International Research Center for Medical Sciences, Kumamoto University, Japan[4]

Introduction:
Hematopoiesis is regulated in a specialized microenvironment in the bone marrow (BM). Within this, hematopoietic stem cells (HSCs) are maintained in the so-called “HSC niche” that provides them with vital factors for self-renewal and differentiation. Thus far, little is known about the cellular and molecular components of the human BM niche.

Methods:
To study human BM niche homeostasis, we took a developmental tissue engineering approach that allows to ex vivo generate a human cartilage template with human adult BM-derived mesenchymal stromal cells (MSCs), and to in vivo develop human bone organs, so called “ossicles”, through endochondral ossification. SDF-1 overexpressing ossicles were generated by retroviral transfer of MSCs. Ex vivo developed ossicles were implantated into immunodeficient mice, and 4 weeks later, third party donor cord blood (CB)-derived human CD34+ cells were transplanted in order to reconstitute human hematopoiesis, following sub-lethal irradiation. The implanted ossicles were isolated 3 months post CB transplantation and analyzed by flowcytometry to immunophenotype human HSC and hematopoiesis. To test the functionality of human HSPC in the ossicle, colony-forming unit assays (CFU) were performed with human CD34+ cells. To identify the putative human niche factors that are expressed in the ossicle and thus might be responsible for human HSC maintenance, total RNA were isolated from in vitro-expanded MSCs, in vitro-differentiated ossicles and in vivo-developed ossicles, and subjected to quantitative PCR.

Results:
Histological analysis showed that human MSC-derived ossicles developed a vascular network and a mature trabecular bone-like structure. Flowcytometric analysis at 2 months post CB transplantation showed comparable development of human hematopoiesis with presence of phenotypic HSCs in the human ossicles as inmouse BM. The CFU assay showed a higher frequency of hematopoietic stem and progenitor cells maintained in human ossicles than in mouse BM. In addition SDF-1 overexpression seems to increase the number of HSPCs in the human ossicles compared to mouse BM. Gene expression profiling showed that in vivo-developed human ossicles express higher levels of CXCL12, Thrombopoietin and Wnt5b than the in vitro-expanded original MSCs and the in vitro-differentiated template, indicating in vivo human BM niche formation with pivotal HSC maintenance factors.

Conclusion:
Our findings indicate that adult BM MSC develop functional bone organs in vivo through an endochondral ossification process that can support engraftment and maintenance of allogenic human HSCs and hematopoiesis. Engineering of a heterotropic human niche that is transplantable and genetically re-engineerable will serve as a platform that allows to studying physiology and pathophysiology of human HSCs in their environment in vivo.

3602

M. Wulf[1], M. Nuvolone[1], A. Aguzzi[1]

Electrophysiological changes in prion protein ablated mice

Institute of Neuropathology, University Hospital Zürich, Switzerland[1]

Introduction:
Prion protein (PrP^C) is a highly conserved cell surface protein that has been implicated in several cellular functions based on studies carried out in different lines of PrP^C knockout mice. However, the mixed genetic background of most of those mouse lines renders the results of these studies hard to interpret. Therefore, a new coisogenic PrP^C knock out mouse line (ZH3) has been generated in a pure Black-6 (C57Bl6/J) genetic background using TALEN-technology. My project is aimed at investigating the validity of a published phenotype of PrP^C knockout mice; a reduction of the slow afterhyperpolarization (sAHP), in the ZH3 mouse.

Methods:
We analyzed 4-6 weeks old Prnp ablated and wild-type male littermates from heterozygous ZH3/C57Bl6/J breedings. Visually guided whole-cell patch clamp recordings in current clamp mode of pyramidal neurons in the CA1 area of the hippocampus of acute brain slices in vitro were performed. Medium (mAHP) and slow AHP were induced by a train of 50 short current injections either from a fixed membrane potential of -65mV or from the spontaneous resting membrane potential of the cell and the amplitude of the sAHP was measured 200ms after stimulus cessation. Additional parameters assessed were: amplitude of the medium AHP (mAHP), resting membrane potential, input resistance, cell capacitance, action potential (AP) threshold, AP amplitude, AP rise time, AP half-width and fast AHP. Statistical significance was assessed using Student's t-test and two-way ANOVA with Bonferroni post-hoc correction where appropriate. P-values < 0.05 were considered significant.

Results:
CA1 pyramidal neurons of ZH3 mice show a significant reduction of the sAHP at 50 and 100Hz train frequency ($p < 0.0001$, two-way ANOVA, Bonferroni corrected) when holding the cells at a fixed membrane potential of -65mV. Interestingly, this difference was not observed when sAHP was induced from spontaneous resting membrane potential of the cell ($p = 0.0395$, two-way ANOVA, ns after Bonferroni correction). There was no significant difference in the other parameters.

Conclusion:
Our results show that CA1 pyramidal neurons of PrP^C knockout mice have a significantly reduced sAHP when the recordings were controlled for the membrane potential. This result reproduces several studies that have shown a reduced sAHP in PrP^C knockout mice of different genetic backgrounds indicating that the reduction of sAHP arises from a loss of physiological function of PrP^C and not due to genetic polymorphisms of mouse models used. Various mechanisms have been proposed to underlie the sAHP reduction, however, the exact molecular role of PrP^C remains to be elucidated.

3603

Z. Song[1]

Exogenous Melatonin Promotes Graft Regeneration

Department of Visceral and Transplantation Surgery[1]

Introduction:
Live donor liver transplantation increases the liver donor pool, but it is impeded by small for size syndrome. Melatonin is an endogenous hormone regulating circadian rhythm, which also has strong antioxidant and liver protective effect in a pharmacological dose. The aim of the study is to investigate whether melatonin prevents small for size liver graft failure in model of mouse liver transplantation.

Methods:
Male C57BL6 mice were divided into 3 groups: (I) I/R+PH group: 60 min liver ischemia plus 2/3 hepatectomy; (II) I/R+exPH group: 60 min liver ischemia plus extended hepatectomy; (III) POLT group: 30% arterialized partial liver transplantation. Each group was subdivided into melatonin treated and control groups. Hepatic injury was determined by AST, ALT and histology. The cytokines and histological evidence of liver regeneration were examined by PCR and immunohistochemistry staining. Serum HMGB1 was measured by ELISA. Survival rate was monitored in I/R+exPH and POLT groups. In mouse primary hepatocytes culture model, hepatocytes were subjected to 4h hypoxia followed by 2h reoxygenation, AST and ALT from the supernatant as well as cytokines from hepatocytes mRNA were measured.

Results:
The group I disclosed less hepatic injury, more regenerating hepatocytes and higher levels of regenerative cytokines in melatonin treated group than controls. HMGB1 was reduced significantly in mice treated by melatonin. In group II, 7 day's survival rate was 0% in control mice in comparison with 50% in melatonin treated mice. In POLT group, the treatment of melatonin increased the survival rate of recipient mice from 0% to 57%. In vitro experiment demonstrated less injury and lower level of pro-inflammatory cytokines in melatonin treated hepatocytes.

Conclusion:
Melatonin rescues small for size liver graft failure by reducing ischemic reperfusion injury and promoting liver regeneration.

3604

E. Kachaylo[1], C. Tschuor[1], N. Borgeaud[1], N. Calo[2], P. Limani[1], M. Foti[2], R. Graf[1], B. Humar[1], P. Clavien[1]

The regulation of liver volume gain and regeneration-associated steatosis through Pten

Laboratory of the Swiss Hepato-Pancreatico-Biliary (HPB) Center, Department of Surgery, University Hospital Zurich, Switzerland[1], Département de Physiologie Cellulaire & Métabolisme, Faculté de Médecine, Centre Médical Universitaire, Genève, Suisse[2]

Introduction:
Successful liver regeneration is associated with the transient accumulation of lipids in hepatocytes, likely for the provision of energy to fuel the regenerative process. How this transient steatosis is regulated is ill-understood. The loss of Pten from liver induces rapid redistribution of peripheral fats into liver. Given that Pten also controls the growth-promoting Akt-mTORC1 pathway, Pten may act after resection to facilitate lipid metabolism and to drive liver volume gain. To explore this possibility, we are analysing inducible, hepatocyte-specific Pten knockout mice following hepatectomy.

Methods:
Pten levels were assessed in hepatectomized wild-type mice. AlbCre$^{tg/+}$PTEN$^{fl/fl}$ (Pten ko) and AlbCre$^{+/+}$PTEN$^{fl/fl}$ (control) mice were studied shortly after tamoxifen induction. Etomoxir (Sigma) was used as inhibitor of Cpt1a. Regeneration was monitored via weight gain, proliferative activity and cyclin levels. Lipid content was quantified through a sulpho-phospho-vanillin protocol.
In wild type mice, Pten levels dropped, coinciding with the peak of transient steatosis. In parallel, fatty acid import (Cd36) and β-oxidation (Cpt1a, Hadha/b) increased, whilst lipogenesis (Acc, Scd, Fasn) decreased. Inducing Pten loss In AlbCre$^{tg/+}$PTEN$^{fl/fl}$ mice resulted in slight lipid accumulation, which was considerably exceeded by peak of transient steatosis at 16h after hepatectomy. This coincided with increased level of Cpt1a and strongly activated Akt-mTORC pathway in Pten ko. However at 16h and three days after resection, lipid content was similar to controls, yet liver weight gain was accelerated. Notably, the increased liver weight gain was not accompanied by elevations in proliferative markers, suggesting an involvement of hypertrophy. When beta-oxidation was pharmacologically inhibited no accelerated regeneration was observed in Pten ko.

Results:
Our results demonstrate a growth-promoting function for Pten downregulation during liver regeneration. The reduction in Pten may aid liver growth through (i) the release of inhibition of the hypertrophic Akt-mTORC pathway, and through (ii) the provision of energy via facilitated lipid metabolism.

3605

P. Kron[1], A. Schlegel[1], O. De Rougemont[1], C. Oberkofler[1], P. Clavien[1], P. Dutkowski[1]

Short, cool and well oxygenated – HOPE for Kidney Transplantation in a Rodent Model

Department of Visceral and Transplantation Surgery, University Hospital, Zurich[1]

Introduction:
To investigate novel and easily applicable preservation perfusion techniques in kidney grafts obtained from donors after circulatory death (DCD).
Organs from DCD suffer from severe loss of function requiring development of innovative methods of preservation. A novel perfusion approach, hypothermic oxygenated perfusion (HOPE), used for DCD liver grafts, is based on cold perfusion for 1h by an oxygenated solution before implantation. Here, we aimed to test HOPE in a rodent model of kidney grafts associated with substantial warm ischemia.

Methods:
Rat kidneys were exposed to 30min in situ warm ischemia, without application of heparin. Kidneys were removed and cold stored for 4 and 18hrs, mimicking DCD organ procurement and conventional preservation. In additional experiments, kidneys were normothermically perfused with oxygenated blood for 1h after cold storage. In a third group, kidneys were perfused by HOPE for 1h after cold storage. In each group, orthotopic kidney transplantation was performed after recipient nephrectomy. Graft injury was assessed during storage, machine perfusion and after kidney transplantation.

Results:
HOPE treated DCD kidneys showed dramatically better function after transplantation, when compared to cold stored grafts in terms of nuclear injury, macrophage activation, endothelium activation, tubulus damage and graft function. A short period of warm oxygenated perfusion before implantation improved graft quality as compared to cold storage, but was significantly less effective in all endpoints than HOPE. The effect of HOPE was dependent on perfusate oxygenation in the cold.

Conclusion:
HOPE of DCD kidneys was superior to other clinically used preservation approaches, consistent to earlier results in livers. Based on this, we assume a strong and generalized effect on solid organ viability through mitochondrial pathways by HOPE before transplantation. These results justify a clinical trial.

3606

A. Vrana[1], K. Humphreys[1], M. Meier[1], S. Hotz-Boendermaker[1], F. Scholkmann[2]

Hemodynamic responses in cortical sensorimotor areas to mechanosensory stimulations of the lower back measured by fNIRS

Department of Chiropractic Medicine, Interdisciplinary Spinal Research (ISR), Balgrist, University Hospital Zurich[1], Biomedical Optics Research Laboratory, Division of Neonatology, University Hospital Zurich, University of Zurich[2]

Introduction:
The present study aimed to investigate whether cortical activation in sensorimotor areas due to mechanosensory pressure on the lumbar spine can be i) detected using functional near infra-red spectroscopy (fNIRS) and ii) if it is possible to distinguish between painful and non-painful pressure as well as a tactile brushing stimulus based on relative changes in [O2Hb] and [HHb]. FNIRS is a promising non-invasive method to study brain function because it is able to capture both, relative oxyhemoglobin [O2Hb] and deoxyhemoglobin [HHb] changes as a result of the neurovascular coupling mechanism. Furthermore, it is more robust to motion artifacts than other neuroimaging methods such as fMRI (1) enabling a greater field of application, especially when applying experimental stimuli on the lower back as it was done in the current investigation.

Methods:
Twenty healthy right-handed subjects (33.5 ± 10.7 years; range 18-61 years; 8 women) participated in the study. Pressure stimulation was exerted with a thumb grip perpendicularly to the spinous process of the L3, inducing a posterior-to-anterior intervertebral movement (PA). One PA was non-painful (pressure force of ~30 N) (PA30) while the other one was painful (PAPain) according to the individual pressure-pain-threshold (PPT). Tactile stimulation was realized by a one-finger brushing over the left musculus erector spinae. The supplementary motor area (SMA) and primary somatosensory cortex (S1) were measured bilaterally using a multi-channel continuous wave fNIRS imager (NIRSport, NIRx Medical Technologies LLC, 8 LED sources and 8 detectors).

Results:
Results yielded robust bilateral relative changes in [O2Hb] in the SMA and S1 (FDR-corrected, $q<0.05$) whereas [HHb] revealed only much weaker changes (uncorrected, $p<0.05$). Major differences between different stimulations were found in [O2Hb] between tactile and both pressure stimulations in the SMA as well as in S1. Moreover, painful pressure yielded the strongest [O2Hb] response compared to the other two stimuli.

Conclusion:
The results indicate that fNIRS is sensitive enough to detect varying hemodynamic responses to different types of mechanosensory stimulation. The acquired data will serve as a foundation for further investigations in chronic low back pain (CLBP) patients. The future aim is to disentangle possible maladaptive neuroplastic changes in sensorimotor areas during painful and non-painful low back stimulations.

References:
Boendermaker B, Meier ML, Luechinger R, Humphreys BK, Hotz-Boendermaker S. (2014): The cortical and cerebellar representation of the lumbar spine. Hum Brain Mapp 35(8):3962-71.

Coghill RC, Sang CN, Maisog JM, Iadarola MJ. (1999): Pain intensity processing within the human brain: a bilateral, distributed mechanism. J Neurophysiol 82(4):1934-43.

Ferrari M, Quaresima V. (2012): A brief review on the history of human functional near-infrared spectroscopy (fNIRS) development and fields of application. Neuroimage 63(2):921-35.

Gervain J, Mehler J, Werker JF, Nelson CA, Csibra G, Lloyd-Fox S, Shukla M, Aslin RN. (2011): Near-infrared spectroscopy: a report from the McDonnell infant methodology consortium. Dev Cogn Neurosci 1(1):22-46.

Lloyd-Fox S, Blasi A, Elwell CE. (2010): Illuminating the developing brain: the past, present and future of functional near infrared spectroscopy. Neurosci Biobehav Rev 34(3):269-84.

Scholkmann F, Kleiser S, Metz AJ, Zimmermann R, Mata Pavia J, Wolf U, Wolf M. (2014): A review on continuous wave functional near-infrared spectroscopy and imaging instrumentation and methodology. Neuroimage 85 Pt 1:6-27.

Villringer A, Chance B. (1997): Non-invasive optical spectroscopy and imaging of human brain function. Trends Neurosci 20(10):435-42.

Yucel MA, Aasted CM, Petkov MP, Borsook D, Boas DA, Becerra L. (2015): Specificity of hemodynamic brain responses to painful stimuli: a functional near-infrared spectroscopy study. Sci Rep 5:9469.

3607

Y. Yamada[1], I. Laube[1], J. Jang[1], J. Bonvini[2], I. Inci[1], B. Beck Schimmer[2], W. Weder[1], W. Jungraithmayr[1]

The impact of preconditioning by Sevoflurane after experimental mouse lung transplantation

Division of Thoracic Surgery, University Hospital Zurich, Zurich, Switzerland[1], Institute of Anesthesiology, University Hospital Zurich, Zurich, Switzerland[2]

Introduction:
Sevoflurane has been evaluated as a preconditioning measure for the amelioration of post-transplant injury in various organs; however, the data available seem inconsistent particularly for the lung. We therefore evaluated if preconditioning by sevoflurane could modulate innate and adaptive immune responses and potentially protects from primary graft dysfunction (PGD) or acute rejection (AR) after lung transplantation (Tx).

Methods:
Two experimental approaches employing the mouse single lung Tx model with 18 hours of graft cold storage were performed: syngeneic Tx (C57BL/6, Syn-Tx, n=12) to mimic PGD, and allogeneic Tx to mimic AR (BALB/c as donors and C57BL/6 as recipients, Allo-Tx, n=12). Before lung retrieval, donor animals were ventilated (preconditioned) for 2 hours with sevoflurane (Sevo group) or fentanyl (Control group). We analyzed Syn-Tx grafts on day 1 and Allo-Tx grafts on day 3 for histology, immunohistochemistry, oxygenation and cytokines (ELISA).

Results:
Syn-Tx showed significantly lower plasma levels of IL-6 ($p=0.01$) but higher levels of IL-10 in lung tissue ($p=0.001$). Also, relatively lower levels of lactate dehydrogenase ($p=0.35$) and monocyte chemoattractant protein-1 ($p=0.26$) were found; however, no histologic and oxygenation differences were observed when compared to control.
In Allo-Tx, grafts in the Sevo group showed pronounced attenuation of AR with significantly lower rejection scores in histology ($p=0.03$), fewer classical macrophages ($F4/80^+$) but increased numbers of alternative macrophages ($CD206^+$), ($p<0.01$, both). Also functionally, the Sevo group had improved oxygenation ($p=0.16$), but no differences in IL-6 or IL-10 levels could be observed.

Conclusion:
Sevoflurane preconditioning showed protective effects on lung transplants in PGD and AR. The observed amelioration could be attributed to alternatively activated macrophages. Sevoflurane should therefore be clinically evaluated for the protection of lung transplants.

3608

Y. Yamada[1], D. Kenkel[2], J. Jang[1], C. Opelz[1], I. Inci[1], A. Boss[2], W. Weder[1], W. Jungraithmayr[1]

Experimental chronic lung allograft rejection – which mouse model is reliable?

Division of Thoracic Surgery, University Hospital Zurich, Zurich, Switzerland[1], Institute of Diagnostic and Interventional Radiology at the University Hospital of Zurich, Switzerland[2]

Introduction:
Several protocols are currently proposed for the induction of chronic rejection (CR) in experimental mouse lung transplantation (Tx). However, there is significant heterogeneity in the development of CR models available. The aim of this study was therefore to investigate experimental mouse Tx combinations differing in their histocompatibility background and immunosuppressive treatment.

Methods:
Mouse lung Tx was performed using the following 3 protocols: minor histocompatibility antigen-mismatched Tx (MINOR, C57BL/10 as donor, C57BL/6 as recipient) analyzed on week 4 (n=15), 8 (n=10) and 12 (n=7), major histocompatibility antigen-mismatched Tx (MAJOR, BALB/c as donor, C57BL/6 as recipient) treated by low-dose cyclosporine and analyzed on week 8 (n=12), and syngeneic Tx (SYN, C57BL/6 as donor and recipient) analyzed on week 8 as controls. Blood gas analysis was performed at sacrifice. HE histology and immunohistochemistry were analyzed based on the guide lines of the international society for heart and lung Tx.

Results:
Chronic rejection lesions were most prominently induced in the MAJOR Tx group at 8 weeks (9/12 transplants, 75%), which was significantly more compared to all other groups ($p<0.05$). MINOR Tx did not have CR at 4 weeks, but at 8 weeks (2/10, 20%) and at 12 weeks (1/7, 14.3%) and SYN had no CR. Also, MAJOR Tx had significantly higher acute rejection score compared to all other groups ($p<0.05$). MAJOR Tx had significantly lower PaO_2/FiO_2 ratio than MINOR Tx at 4 and 8 weeks ($p<0.05$).

Conclusion:
Among experimental CR models, the Major histocompatibility mismatched combination treated by low-dose cyclosporine is the most reliable CR model. At the same time, this model reflects the best the clinical situation thus making it useful in the research for finding new therapeutics against CR in lung Tx.

3609

Y. Yamada[1], I. Iskender[1], S. Arni[1], S. Hillinger[1], T. Cosgun[1], W. Jungraithmayr[1], W. Weder[1], I. Inci[1]

Ex vivo treatment of donors with nebulized N-acetylcysteine partially improved post-transplant lung function

Division of Thoracic Surgery, University Hospital Zurich, Zurich, Switzerland[1]

Introduction:
We have shown the beneficial effects of N-acetylcysteine (NAC) on post-transplant lung function, when both donor and recipient were pretreated intravenously. However, systemic treatment of multi-organ donors may not be clinically relevant. Thus, we hypothesized that ex vivo treatment of donors with nebulized NAC would be adequate to protect allografts from ischemia-reperfusion injury after lung transplantation.

Methods:
Lungs were retrieved from domestic pigs and stored at 4°C for 24h. After 2h of ex vivo lung perfusion (EVLP) to administer 50 mg/kg of NAC via nebulization in the NAC group (n=6) or saline in the control group (n=5), the left lungs were transplanted. The right main bronchus and pulmonary artery were occluded at 1h of reperfusion, followed by 5h of observation. Physiological data during EVLP and after reperfusion were recorded. Inflammatory response and markers of oxidative stress were measured.

Results:
There was a trend toward higher oxygenation and glutathione levels after reperfusion in the NAC group ($p=0.06$ and $p=0.1$, respectively, Fig. A, B). Myeloperoxidase levels were significantly lower at the end of EVLP in the NAC group ($p<0.05$, Fig C). At the end of the experimental period, local inflammatory response (IL-8) and oxidative stress markers (nuclear factor-κB p50 subunit, carbonyl protein, and malonedialdehyde) were relatively lower in the treatment group.

Conclusion:
Ex vivo treatment of donor lungs with nebulized NAC partially improved post-transplant lung function possibly via reducing oxidative stress and inflammatory response. However, the limited observable effects indicate that treatment of donor lungs only might not sufficient in this setting.

Conference Location

University Hospital Zurich
Grosser Hörsaal Ost
Rämistrasse 100
8091 Zürich

Contact Address

Prof. Dr. med. Gregor Zünd
Direktor Forschung und Lehre
Managing Director ZKF
UniversitätsSpital Zürich
gregor.zuend@usz.ch
phone: +41 (0) 44 634 55 00
fax: +41 (0) 44 634 55 03
Secretary office: +41 (0) 44 634 55 33

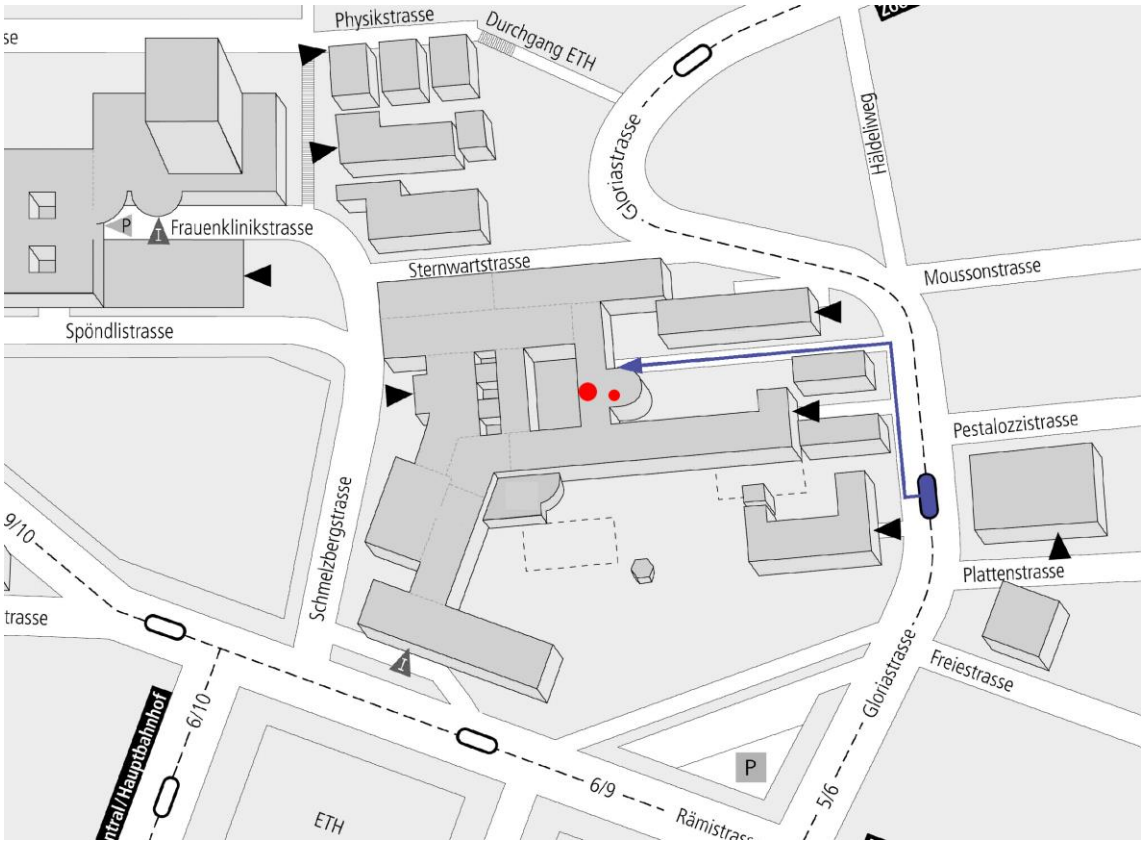

UniversitätsSpital Zürich

Universität Zürich[UZH]